



**HAL**  
open science

# Lagrangian stochastic modeling of turbulent gas-solid flows with two-way coupling in homogeneous isotropic turbulence

Zafer Zeren

► **To cite this version:**

Zafer Zeren. Lagrangian stochastic modeling of turbulent gas-solid flows with two-way coupling in homogeneous isotropic turbulence. Fluids mechanics [physics.class-ph]. Institut National Polytechnique de Toulouse - INPT, 2010. English. NNT : 2010INPT0106 . tel-04275874

**HAL Id: tel-04275874**

**<https://theses.hal.science/tel-04275874>**

Submitted on 8 Nov 2023

**HAL** is a multi-disciplinary open access archive for the deposit and dissemination of scientific research documents, whether they are published or not. The documents may come from teaching and research institutions in France or abroad, or from public or private research centers.

L'archive ouverte pluridisciplinaire **HAL**, est destinée au dépôt et à la diffusion de documents scientifiques de niveau recherche, publiés ou non, émanant des établissements d'enseignement et de recherche français ou étrangers, des laboratoires publics ou privés.



# THÈSE

En vue de l'obtention du

DOCTORAT DE L'UNIVERSITÉ DE TOULOUSE

Délivré par *Institut National Polytechnique de Toulouse*

Spécialité : *Dynamique des fluides*

---

Présentée et soutenue par Zafer ZEREN

le 29 Octobre 2010

Lagrangian stochastic modeling of  
turbulent gas-solid flows with two-way coupling  
in homogeneous isotropic turbulence

---

## JURY

Serge SIMOËNS  
Anne TANIÈRE  
Julien REVEILLON  
Benoît BÉDAT  
Olivier SIMONIN

Président  
Rapporteur  
Rapporteur  
Directeur de thèse  
Co-Directeur de thèse

---

École doctorale: Mécanique, Energétique, Génie Civil, Procédés (MEGeP)  
Unité de recherche: Institut de Mécanique des Fluides de Toulouse (IMFT)



*Dedicated to Tuğçe KUT, a lovely lady of Paris*



# *Abstract*

In this thesis, performed in IMFT, we are interested in the turbulent gas-solid flows and more specifically, in the phenomenon of turbulence modulation which is the modification of the structure of the turbulence due to the solid particles. This mechanism is crucial in flows with high particle mass-loadings. In this work, we considered a homogeneous isotropic turbulence without gravity kept stationary with stochastic type forcing. Discrete particles are tracked individually in Lagrangian manner. Turbulence of the carrier phase is obtained by using DNS. The particles are spherical, rigid and of a diameter smaller than the smallest scales of turbulence. Their density is very large in comparison to the density of the fluid. In this configuration the only force acting on the particles is the drag force. Volume fraction of particles is very small and inter-particle interactions are not considered.

To model this type of flow, a stochastic approach is used where the fluid element acceleration is modeled using stochastic Langevin equation. The originality in this work is an additional term in the stochastic equation which integrates the effect of the particles on the trajectory of fluid elements. To model this term, we proposed two types of modeling: a mean drag model which is defined using the mean velocities from the mean transport equations of the both phases and an instantaneous drag term which is written with the help of the Mesoscopic Eulerian Approach. The closure of the models is based on the Lagrangian auto-correlation function of the fluid velocity and on the transport equation of the fluid kinetic energies. The models are tested in terms of the fluid-particle correlations and fluid-particle turbulent drift velocity. The results show that the mean model, simple, takes into account the principal physical mechanism of turbulence modulation. However, practical closure problem is brought forward to the Lagrangian integral scale and the fluid kinetic energy of the fluid turbulence viewed by the particles.

Keywords: Lagrangian stochastic modeling, Gas-solid flows, Two-way coupling, Turbulence modulation, Langevin equation

# *Acknowledgements*

Well, after a long distance I performed which counts to almost 4 years, I really do not know who to thank to and how. Cause my feelings are at top momentarily and go down a second after. It would be really nice to start the thanks with my incredible adviser, Prof. Olivier SIMONIN, who is one of the greatest scientists in our century. Today, if I am capable of calling myself a doctor, it is thanks, from one-side, to his wide-open knowledge of fluid mechanical processes and his experience on directing a lost student to the final purpose of these painful years. I am totally overwhelmed that I worked with him.

I should not pass my second adviser, Mr. Benoit BEDAT. At the beginning, we were alone and we could not produce something, really shame on those pass-time activities. I cannot say the problem is me or him, but it was not working. Without the intervention of Prof. SIMONIN, I should frankly say that this project would not have seen the day. However, I am totally thankful to his sympathetic personality in my dire times, he was on my side. I appreciate his help.

I equally thank the members of the jury, Mme Taniere, M. Reveillon, M. Simoens for their times to read and to judge my writing, the philosophy of the modeling which is complicated to understand. I appreciate it very much.

I take the pleasure to thank my non-official adviser, M. Pascal Fede, who was attentive to my studies and made many valuable contributions to the writing of the thesis and to my point of view to science. Thank you, Pascal.

Well, the markers show my colleagues from IMFT and from CERFACS. You were lovely for all this time, I am really happy that I was with you all, I am happy for everything, "pot", "fest", etc... with you. It was a pleasure. I should thank at first to my dear turkish friend Ali, we passed, counting this year, like maybe 8 years of which the last 3 was completely together. I hope you were not bored when we were eating "pates" several times a week. If you count the number for a whole year, I am happy that we did not have any stomach problem :)). Mehdi Agam, well I should not say the total word but "vraiment, anani ...". I am sorry for the kids who are banned to read this. I thank you very much for your friendship, I'll never forget the discussions we did. It was a pleasure. I thank the other turkish from CERFACS, Kamer, Selime, Bora. Yanimda oldugunuz icin cok sansliyim, gercekten cok tesekkurler. I thank the king Arthur who left us along in IMFT. My king, you were and are a great king wherever you go. I thank you very much. Mr. Florian Moreau, good luck to you for your defense, it was you who say this but :), vive la greve :)). Florian (mon prof. de francais prefere), you were the nicest french for me, I am really happy to know you, I hope we'll be in contact for long long time. I thank the CERFACS team for recruiting me and giving me the

chance of being in these nice places in Toulouse. I specially thank Michelle CAMPASSENS. You are a great person, Michelle. Without you, I think Sarkozy would kick me out of France :). I thank equally Marie Labadens, Chantal Nasri, Lydia Otero, for their smiling faces. I also thank Mr. Thierry Poinot who was the first to inform me about the project, it is due to him that I am here. I also thank my project mates from CERFACS, Jean-Mathieu, Benedetta, Camilo, Felix, Davide, rugby guy Marco Maglio, spanish Vital Fernandez. It was a pleasure being with you.

The group EEC, or PSC is great place. I thank all alone to Florence who was patient with my wantings :). Merci Florence, J'espere que je t'ai pas embette beaucoup avec des papiers, papiers, papiers ... Bien sur, il faut continuer avec M. Gerard Couteau qui m'a reproche, Richelieu quand j'avais de la barbe :). Je vais jamais l'oublier. Well, I can count the nicest people in the world. I thank you very much, Enrica. You're special, I hope that you'll have a very nice life and career and we'll be in touch. Of course, we should count, Fabrizzio, when we count you, non?:). The ex-member of EEC, Dirk, I thank you very much for your kindness and being there during my defense. Thanks also goes to Toufik, my ex-roommate. Well in total, I can count, Laurent, Florent, Roel (I always mis-pronounce his name, sorry), Charlotte (nicest girl in France), Jean-Luc, Bernard (impressionant voix), Marion Perrodin, Nicolas G., Nicolas N., Guillaume, Aurelien, Daniel, Mos who charged me 50 euros for using his bureau for one day, Arthur (not the king), Marco Afonso, Marion Linkes, Eric, Olivier Praud. You were all sweet. If I did something wrong, I am sorry, guys.

Some friend from Paris also deserve a special paragraph here. I take the pleasure of thanking Thomas, Victoire (thanks for the dinner surprise you did for me, Vic), Samantha, Nadejda (Necla in turkish), Pauline, Azim, Barthelemy, Elois (quantum guy !!) et Anne-Virginie. I am thankful to the family of girlfriend, Zafer abi (koyu fenerbahce taraftari), Fatma abla, Tilbe (namideger kanki, benden cok dayak yedi ama olsun). Sizinle tanismak, zaman gecirmek size yakin olmak her zaman gurur kaynagi oldu. Cok tesekkur ederim degerli yardimlariniz icin. Fatma abla, sen olmasaydin, sanirim bogazimizdan (Ali'de dahil) sicak bir lokma gecmeyecekti (Emrah misali). Sen cok ozelsin ve umarim izin alabilirsem, sana anne diebilme imkani bulurum. Zafer abi, seninle sohbet etmek senin bakis acini bilmek hep hosuma gitti hep gidecek. Ve kanki, sen cok ozel birisin. Seni tanidigima icten mutluyum, yanimda oldugun icin tesekkur ederim sana. Hepinizi seviyorum.

I would like to give my special thanks to my family, my mother, my father, my two brothers. You are the special part of my life. I am truly indebted to you, preparing and writing of this manuscript and my career. There is always a special place in my heart for you. Annecim ve babacim, cok zor zamanlar gecirdik ama sonuna geldik ve bitti. Bugun artik doktor unvanini aldım. Bilmiyorum ben kucukken ne olacagimi dusunuyordunuz ama

bugunu herhalde biraz imkansiz buluyordunuz. Cok tesekkur ederim ikinizede, varliginiz ve desteginiz icin.

To finish my thanks, I am most grateful and most emotional with tears in my eyes to my lovely lady of Paris, Mlle Tugce KUT. We have met with a pure coincidence when you were in Montpellier and can I say the life is all about the coincidences? I do not know the exact answer but this one was truly the most superb of my life and I am specially thankful to Mr. President which handed you to me as a birthday present. I hope you will accept to become Mme Zeren when I propose to you, if not, merde !!! I love you with the deepest emotions from my heart and I'd like you to know that if you were not there, this would not be possible. Many bizooooos.

# Contents

<b>Abstract</b>	<b>iii</b>
<b>Acknowledgements</b>	<b>iv</b>
<b>Nomenclature</b>	<b>xii</b>
Latin Letters . . . . .	xii
Greek Letters . . . . .	xv
<b>1 Introduction</b>	<b>1</b>
1.1 About two-phase flows . . . . .	1
1.2 Importance of turbulence modulation and modeling of two-phase flows . . . . .	4
1.3 Aim of this study . . . . .	6
<b>2 Numerical simulation of fluid turbulence and solid particle trajectories</b>	<b>9</b>
2.1 Introduction . . . . .	9
2.2 Single particle motion in a turbulent flow field . . . . .	10
2.2.1 Dynamic equation of a single particle motion in a turbulent field . . . . .	10
2.2.1.1 Theoretical background . . . . .	11
2.2.1.2 General equation . . . . .	12
2.2.1.3 Hypotheses of the study and the equation retained . . . . .	14
2.2.1.4 Numerical solution of the equation of particle motion . . . . .	15
2.2.1.5 Ghost particle test . . . . .	16
2.2.1.6 Interpolation scheme . . . . .	17
2.3 Fluid turbulence simulation . . . . .	18
2.3.1 Introduction - General considerations . . . . .	18
2.3.2 Navier-Stokes equations and solution . . . . .	19
2.3.3 Numerical approach, description of the code NTMIX3D . . . . .	20
2.3.4 Turbulence forcing . . . . .	22
2.3.4.1 Spectral forcing . . . . .	23
2.3.4.2 Numerical implementation of stochastic forcing scheme . . . . .	26
2.3.4.3 Analysis of the turbulence characteristics . . . . .	27
2.4 Initiating the study of two-way coupling . . . . .	35
2.4.1 Force acting on the fluid . . . . .	37
2.4.2 Point source approximation . . . . .	38

2.4.3	Reference case for the study . . . . .	40
<b>3</b>	<b>Linear deterministic forcing scheme</b>	<b>43</b>
3.1	Introduction . . . . .	43
3.2	Physical forcing scheme . . . . .	44
3.2.1	Linear Forcing Scheme 1 . . . . .	44
3.2.2	Linear Forcing Scheme 2 . . . . .	44
3.3	Parametrization of simulations . . . . .	45
3.3.1	Initial condition with Passo-Pouquet spectrum . . . . .	45
3.3.2	Initial condition with stochastic forcing . . . . .	46
3.4	Results and comparison of the schemes . . . . .	46
3.4.1	Turbulent kinetic energy balance . . . . .	46
3.4.2	One-point correlations . . . . .	50
3.4.3	Two-point correlations . . . . .	53
3.4.4	Spectral analysis . . . . .	55
3.4.5	Conclusion . . . . .	57
<b>4</b>	<b>PDF modeling of gas-solid flows</b>	<b>59</b>
4.1	Introduction . . . . .	59
4.2	Statistical description of the particle phase using a probabilistic approach . . . . .	60
4.2.1	One-point probability density function $f_p$ . . . . .	60
4.2.2	Transport equation for $f_p$ . . . . .	61
4.2.3	Moment equations of the particle phase . . . . .	63
4.2.3.1	Particle number density balance equation, $\Psi = 1$ . . . . .	64
4.2.3.2	Mean momentum balance equation, $\Psi = u_{p,i}$ . . . . .	64
4.2.3.3	Particle kinetic stress tensor equation, $\Psi = \langle u'_{p,i} u'_{p,j} \rangle_p$ . . . . .	66
4.3	Statistical description of the system using a joint probabilistic approach . . . . .	67
4.3.1	One-point joint probability density function $f_{fp}$ . . . . .	67
4.3.2	Transport equation for $f_{fp}$ . . . . .	68
4.4	Conclusion . . . . .	69
<b>5</b>	<b>Lagrangian stochastic modeling of gas-solid flows with two-way coupling</b>	<b>71</b>
5.1	Introduction . . . . .	71
5.2	Lagrangian stochastic approach . . . . .	72
5.3	Trajectory and PDF point of views . . . . .	73
5.3.1	Trajectory point of view . . . . .	75
5.4	Langevin Equation for monophasic turbulent flows ( $Re_L \rightarrow \infty$ ) . . . . .	75
5.4.1	Drift and diffusion terms in Langevin equation . . . . .	77
5.5	Fluid velocity along the fluid element trajectories in two-way coupled flows . . . . .	79
5.5.1	Autocorrelation function . . . . .	81
5.5.2	Mean momentum equation . . . . .	81
5.5.3	Fluid Reynolds stresses transport equation . . . . .	82
5.6	Fluid velocity along the solid particle trajectories . . . . .	84
5.6.1	Closure to the Lagrangian derivative term along particle trajectory . . . . .	85
5.6.2	Closure by a Langevin type equation in one-way coupled flows . . . . .	87
5.6.3	Closure by a Langevin type equation in two-way coupled flows . . . . .	89
5.6.4	Fluid autocorrelation function seen by the particles, $R_L^{f@p}$ . . . . .	90

5.6.5	Drift velocity transport equation, $V_d$ . . . . .	90
5.6.6	Transport equation for fluid Reynolds stresses seen by the particles, $\langle u'_{f@p,i} u'_{f@p,j} \rangle_p$ . . . . .	91
5.6.7	Fluid-particle velocity correlation equation . . . . .	92
5.7	Modeling the two-way coupling term in homogeneous isotropic turbulence . . . . .	93
5.7.1	Modeling with the mean drag force . . . . .	95
5.7.1.1	Autocorrelation functions . . . . .	95
5.7.1.2	Mean momentum equation . . . . .	97
5.7.1.3	Turbulent kinetic energy equations . . . . .	97
5.7.1.4	Fluid-particle turbulent drift velocity prediction . . . . .	98
5.7.1.5	Fluid-particle velocity covariance prediction . . . . .	99
5.7.1.6	Interim conclusion on the mean drag model . . . . .	99
5.7.2	Modeling with the instantaneous drag force . . . . .	100
5.7.2.1	Application of Mesoscopic Eulerian Formalism to two-way coupled flows . . . . .	101
5.7.2.2	Autocorrelation functions . . . . .	108
5.7.2.3	Mean momentum equation . . . . .	112
5.7.2.4	Turbulent kinetic energy equations . . . . .	112
5.7.2.5	Fluid-particle turbulent drift velocity prediction . . . . .	114
5.7.2.6	Fluid-particle velocity correlation prediction . . . . .	114
5.8	Conclusion . . . . .	114
<b>6</b>	<b>Fluid statistics from DNS+DPS results</b> . . . . .	<b>117</b>
6.1	Introduction . . . . .	117
6.2	Description and parametrization of simulations . . . . .	118
6.3	Calculation of statistics . . . . .	120
6.3.1	Eulerian statistics . . . . .	120
6.3.2	Lagrangian statistics . . . . .	122
6.4	Modulation of the turbulent kinetic energy and the dissipation rate . . . . .	123
6.5	Modulation of 3D turbulent energy spectrum . . . . .	129
6.6	Modulation of the Eulerian and Lagrangian temporal correlations of turbulence . . . . .	131
6.6.1	Classical stochastic modeling for single phase flows . . . . .	134
6.6.2	Extension to the two-way coupled gas-solid flows . . . . .	136
6.7	Modulation of the Lagrangian structure function . . . . .	138
6.8	Conclusion . . . . .	142
<b>7</b>	<b>Simulation and modeling of fluid-particle correlations</b> . . . . .	<b>143</b>
7.1	Introduction . . . . .	143
7.2	Analysis of solid particle dispersion in turbulent flow field . . . . .	144
7.2.1	Fluid element diffusion . . . . .	144
7.2.2	Solid particle dispersion . . . . .	145
7.3	Theory of Tchen-Hinze for the particle dispersion . . . . .	148
7.3.1	Classical theory of Tchen-Hinze . . . . .	148
7.3.2	Extension of the theory of Tchen-Hinze . . . . .	149
7.3.2.1	Low Reynolds number effects . . . . .	153
7.3.3	Modification of the dispersion coefficient by the two-way coupling . . . . .	155

7.3.4	Effect of two-way coupling on the fluid statistics viewed by the particles	159
7.3.5	Effect of preferential concentration on the statistics viewed by the particles . . . . .	160
7.3.5.1	Methodology . . . . .	162
7.3.5.2	Results . . . . .	162
7.4	Lagrangian stochastic modeling results . . . . .	165
7.4.1	Mean drag model . . . . .	165
7.4.1.1	A practical closure . . . . .	168
7.4.2	Instantaneous drag model . . . . .	169
7.5	Analysis of fluid-particle turbulent drift velocity . . . . .	173
7.5.1	Methodology . . . . .	173
7.5.2	Theoretical study . . . . .	175
7.5.3	Modeling of the flux due to the mean red particle motion . . . . .	176
7.5.4	Modeling of the flux due to the fluid-particle turbulent drift velocity .	177
7.5.4.1	Mean drag model . . . . .	178
7.5.4.2	Instantaneous drag model . . . . .	178
7.6	Conclusion . . . . .	180
<b>8</b>	<b>Conclusion</b>	<b>183</b>
	<b>Bibliography</b>	<b>189</b>



# Nomenclature

## Latin Letters

$a_0$	Universal constant for fluid element acceleration modeling	Eq. 7.19
$a^F$	Turbulence forcing in spectral space	Eq. 2.34
$A(X(t))$	Drift coefficient of general stochastic equation	Eq. 5.1
$A_f, A_{f@p}$	Drift coefficient of Langevin equation	Eq. 5.17, 5.49
<b>b</b>	Stochastic forcing coefficient	Eq. 2.32
$B$	Linear forcing coefficient	Eq. 3.1
$c$	Scalar concentration	Eq. 7.1
$C$	Mean number of particles per subvolume	page 162
$C_0$	Kolmogorov constant	page 78
$C_D$	Drag coefficient	Eq. 4.20
$\mathbf{c}_f$	Realization of a fluid velocity	page 67
$\mathbf{c}_p$	Realization of a velocity of particle	page 61
$d_p$	Particle diameter	page 13
$D_f^t$	Dispersion coefficient of fluid elements	Eq. 7.3
$D_{fp}^t$	Binary dispersion coefficient	Eq. 7.59
$D_p^t$	Dispersion coefficient of particles	Eq. 7.8
$D_L$	Lagrangian structure function	Eq. 5.9
$D_m$	Molecular diffusion coefficient	page 144
<b>dW</b>	Markovien increase in Langevin equation	page 73
$E$	Total energy of turbulence	Eq. 2.22, 2.24
$E(k)$	3D spatial energy spectrum of turbulence	Eq. 2.57
$E_{f@p}(\omega)$	3D spatial energy spectrum of fluid phase viewed	page 149
$E_p(\omega)$	3D spatial energy spectrum of particle phase	page 149
$f_D$	Correction for drag coefficient	Eq. 2.10
$f_f(\mathbf{c}_f)$	One-point probability density function of fluid velocity	Eq. 4.28
$f_f(\mathbf{c}_f \mathbf{c}_p)$	One-point conditional probability density function of fluid velocity	Eq. 4.28
$f_{fp}$	Joint one-point probability density function of fluid and particle velocities	Eq. 4.28

$f_i$	Acceleration due to turbulence forcing in physical space	page 23
$f_{u_i}$	Acceleration of the fluid due to particle effects	Eq. 2.67
$F_p$	Drag force acting on a particle	Eq. 2.8
$f_p(\mathbf{c}_p)$	One-point probability density function of particle velocity	Eq. 4.6
$f_r$	Eulerian longitudinal two-point correlation of fluid velocity	Eq. 2.48
$F_{pp}$	Eulerian longitudinal two-point correlation of particle mesoscopic velocity	Eq. 5.92
$g_r$	Eulerian transversal two-point correlation of fluid velocity	Eq. 2.49
$\mathbf{g}$	Gravitational acceleration	page 13
$G_{fp,ij}$	Classical drift term in Langevin modeling	Eq. 5.43
$G_{pp}$	Eulerian transversal two-point correlation of particle mesoscopic velocity	Eq. 5.93
$\mathbf{k}$	Wavenumber of turbulent scales	page 24
$\mathbf{k}_{eff}$	Effective wavenumber for numerical resolution	Eq. 2.35
$\mathbf{k}_{\max, \min}$	Maximum and minimum wavenumber of forced turbulent scales	page 24
$\mathbf{k}_0$	The least wavenumber of the turbulence	page 24
$L_b$	Size of the domain's one side	Table. 2.2
$L_f$	Longitudinal integral length scale of turbulence	Eq. 2.51
$L_g$	Transversal integral length scale of turbulence	Eq. 2.52
$m_p$	Mass of a particle	page 13
$N_d$	Number of subvolumes covering flow domain	page 162
$N_{f\&p}$	Number of fluid-particle realizations	page 62
$n_p$	Particle number density	Eq. 4.3
$N_p$	Number of particles	page 62
$P$	Mean pressure	Eq. 5.5
$p$	Instantaneous fluid pressure	Eq. 2.25
$p'$	Fluctuating part of fluid pressure	page 83
$P_f$	Turbulence production term	page 26
$P(C)$	Spatial distribution function of particles	Eq. 7.23
$q_f^2$	Turbulent kinetic energy of fluid	Eq. 2.16
$q_{f@p}^2$	Turbulent fluid kinetic energy viewed by the particles	Eq. 5.59
$q_{fp}$	Fluid-particle covariance	Eq. 5.63
$q_p^2$	Total turbulent agitation of particles	Eq. 4.25
$\tilde{q}_p^2$	Mesoscopic kinetic energy of particles	Eq. 5.90
$Q(\omega)$	Transfer function	Eq. 7.12
$O_{ij}$	Oseen tensor	Eq. 2.65
$r$	Spatial separation for two-point correlations	page 29
$r_g$	Ideal Gas constant	Eq. 2.25
$R_{e,ij}$	Eulerian two-point correlation of fluid velocity	Eq. 2.47

$R_{E,ij}$	Eulerian one-point correlation of fluid velocity	Eq. 2.40
$R_{L,ij}^f$	Lagrangian one-point correlation of fluid element velocity	Eq. 2.43
$\tilde{R}_{pp,ij}$	Lagrangian two-point correlations of particle mesoscopic velocity	Eq. 5.91
$Re_L$	Turbulent Reynolds number	Eq. 2.14
$Re^*$	Lagrangian Reynolds number of fluid elements	Eq. 7.18
$Re_p$	Particle Reynolds number	Eq. 2.4
$Re_\lambda$	Reynolds number based on the Taylor length scale	Eq. 2.17
$s_{ij}$	Instantaneous deformation-rate tensor	Eq. 2.37
$S_k$	Skewness of the turbulent velocity distribution	Eq. 2.59
$St_0$	Initial Stokes number of particles	Eq. 6.4
$St_{f@p}$	Stokes number	Eq. 6.3
$t$	Time	
$T$	Temperature	Eq. 2.25
$T_e$	Eddy turnover time	Eq. 2.46
$T_E$	Eulerian timescale	Eq. 2.42
$T_F$	Characteristic timescale of stochastic forcing	Eq. 2.32
$T_k$	Flatness of the turbulent velocity distribution	Eq. 2.59
$T_L^{f*}$	Lagrangian timescale corresponding to infinite Reynolds number flow	Eq. 7.20
$T_L^f$	Lagrangian timescale	Eq. 2.45
$T_L^{f@p}$	Lagrangian timescale of the fluid velocity viewed by the particles	Eq. 6.13
$T_L^p$	Lagrangian timescale of the particle velocity	Eq. 6.14
$u'$	Characteristic velocity of turbulence	Eq. 2.15
$\mathbf{u}_f^*$	Velocity of a stochastic particle	page 76
$u'_{f,i}$	Fluctuating part of fluid velocity at one-point of the domain	page 18
$U_{f,i}$	Mean fluid velocity	page 81
$\mathbf{u}_{f@p}$	Instantaneous velocity vector of undisturbed fluid at the particle position	page 13
$\mathbf{u}_p$	Instantaneous velocity vector of a solid particle	Eq. 2.12
$\mathbf{U}_p$	Mean velocity vector of a solid particle	Eq. 4.4
$\mathbf{V}_d$	Turbulent drift velocity	Eq. 4.22
$\mathbf{V}_r$	Mean relative velocity	Eq. 4.22
$V_p$	Volume of a particle	Eq. 2.1
$\mathbf{v}_r$	Instantaneous relative velocity vector between particle and fluid	Eq. 2.5
$W_p$	Fine-grained distribution function	Eq. 4.7
$\mathbf{x}_f$	Position vector of a fluid element	Eq. 2.11
$\mathbf{x}_p$	Position vector of a solid particle	Eq. 2.12
$X$	Random number governed by general stochastic equation	Eq. 5.1

## Greek Letters

$\alpha_p$	particle phase volume fraction	Eq. 6.2
$\delta_{ij}$	Kronecker delta	
$\epsilon$	Dissipation of the turbulent kinetic energy	Eq. 2.36
$\rho_f$	Density of the fluid	page 13
$\rho_p$	Density of a particle	page 13
$\sigma$	Variance of the particle distribution	page 162
$\sigma_{Poisson}$	Variance of the particle distribution corresponding to Poisson distribution	page 162
$\Sigma_p$	Deviation of particle distribution from homogeneity	Eq. 7.25
$\eta$	Inverse of Stokes number $St_{f@p}$	Eq. 5.112
$\eta_K$	Kolmogorov scale of turbulence	Eq. 2.18
$\lambda$	Molecular mean free path	page 18
$\nu_f$	Kinematic viscosity of the fluid	page 18
$\Pi_{u_f,i}^*$	Two-way coupling term in Langevin equation for fluid element trajectory	Eq. 5.17
$\Pi_{u_f@p,i}^*$	Two-way coupling term in Langevin equation for particle trajectory	Eq. 5.49
$\Pi_{R_f,ij}$	Two-way coupling term in fluid kinetic energy transport equation	Eq. 5.29
$\Pi_{R_f@p,ij}^*$	Two-way coupling term in transport equation for fluid kinetic energy viewed	Eq. 5.55
$\tau$	Time separation for time correlations	page 28
$\tau_{ij}$	Viscous stress tensor	Eq. 2.23
$\tau_p$	Particle relaxation time	Eq. 2.9
$\tau_\eta$	Kolmogorov timescale	Eq. 2.19
$\phi$	Particle phase mass-loading	Eq. 6.1
$\omega$	Wavenumber of the energy spectrum for both phases	page 149

## Abbreviations and Symbols

BBO	Basset-Bousinesq-Oseen equation
DNS	Direct Numerical Simulation
DPS	Discrete Particles Simulation
PDF	Probability density function
PSIC	Particle Source In Cell
$\langle \cdot \rangle$	Ensemble mean operator
$\langle \cdot \rangle_p$	Mean operator on particle phase
$\langle \cdot   \cdot \rangle$	Conditioned mean operator





# Chapter 1

## Introduction

### 1.1 About two-phase flows

Multiphase flows are found in many technological devices and naturally occurring processes and in this regard they receive much attention from the researchers and scientists from many different kinds of scientific areas. Chemical engineers, mechanical engineers, those who work on molecular biology and genetics are thoroughly keen on the theoretical and physical aspects of these flows where diversity of matters moves together. Diversity is an indication to the fact that these matters can be any combination of solid, liquid and gas.

Many examples can be found where these flows are the main part of the system. For example, energy conversion as the flow proceeds through pipes, pumps and valves are the center of motivation for many industrial coworkers. Gas-solid flows in pneumatic conveying in circular channels (Soo, 1983), frictional losses or the pressure gradient in these flows are highly related to oil industry where a solid phase can be joined to the flow from a reservoir due to drilling the ground (Earls , 2005, Ayala, 2007) or due to the production conditions (natural wax and asphaltene formation in oil flow). Boiling flows where the liquid phase is in motion with a bubbly phase have many applications such as in electronic chip-cooling using microchannels, in heat exchangers etc... Bubble coalescence and growth in cavitations are some of the important physics occurring in these flows. Gas condensation in natural gas pipelines caused by the temperature and pressure differences attracts the attention of much study, as well. The condensation in these applications subject the pipe to two-phase transport. Apart from the electronic chip-cooling, all these examples given are of a macroscale type. An example for micro scale multiphase flows could be microfluidic devices for manufacturing and processing food. This application is an emerging area in multiphase flow community. Micro level flows have kindly different physics than their macroscale counterpart therefore approaches for the prediction of these are significantly different. One of the

advantages in these mechanisms is that in the past these devices were using a macroscale dispersion by applying energy to the bulk of a material. This was leading to the ice-crystals in ice-cream or fat droplets in mayonnaise (Skurtys and Aguilera, 2008), for instance. The conversion of a phase into another such as evaporation of liquid into fine droplets is another challenging problem where the identification and quantification of the each phase are needed. There are many methods to parametrize these kinds of flows such as electrical capacitance tomography (ECT).

Injection of droplets (spray) with a high initial velocity in a still air is very important in combustion of droplets of liquid fuel or pulverized coal such as in internal combustion engines, rocket engines etc... The objective is to control the air-particle mixture in order to obtain a clean and efficient combustion process. Usually dense jet of particles is injected into motionless air or even a turbulent flow in these applications where particles generate turbulence or highly interact with the turbulent flow. Then, significant mass, momentum and energy exchanges between the two phases take place.

Diverse physical phenomena such as thermodynamics, kinematics occurring in many applications mentioned above requires a careful attention according to a particular flow type and a solid understanding of the underlying physics.

A rigorous organization of flow types should be constituted in order to make the future improvements and developments easier to the researcher. Because of the difficulty and the considerations that will take place in this thesis, two-phase flows where only two interpenetrating media will be considered and flows with more than two phases will be left out of the discussion. Considering the general states of matter, the most encountered two-phase flow types are liquid-solid, liquid-liquid, gas-solid and liquid-gas. In this thesis, gas-solid flows are going to be considered, hence the term 'gas-solid' will be used throughout the study. A general classification to the gas-solid flows comes with the work of Elgobashi (1994) categorizing the gas-solid suspensions according to the physical phenomena appearing during the complex motion. Elgobashi draws attention to two dimensionless numbers, namely: volume loading  $\alpha_p$  and mass loading  $\phi$ . These values indicate the significance of certain physical interactions such as fluid-particle and particle-particle interactions Crowe et al. (1998). Volume loading  $\alpha_p$  is the ratio of the total volume of dispersed phase to the overall volume of the physical domain. Mass loading is, on the other hand, is the ratio of the total mass of the particles to the mass of the fluid.

For  $\alpha_p < 10^{-4}$  and  $\phi < 10^{-2}$ , particle phase is said to have a very dilute loading such that particle-particle interactions and the effect of particles on fluid turbulence can be neglected. Dispersed phase's motion is then fully controlled by the continuous phase. In this regime (also called as 'one-way coupling'), many studies have been performed to understand the spatial

dispersion of discrete particles in a turbulent flow field. Certain works showed the spatial clustering of the particles during their interactions with different flow scales. Fluid element diffusion and its extension to solid particle dispersion in homogeneous isotropic turbulent flow field are now well-documented by the well-known works of Taylor (1921), Tchen (1947), Batchelor (1949), Hinze (1975) and many others. Following this, the effect of gravity on the agitation of particles, effect of shear on the motion of particles are worked progressively. Basic question is still on the controlling parameter of the clustering of the particles.

For  $\alpha_p < 10^{-4}$  and  $\phi > 10^{-2}$ , the effects of particles on fluid flow become important and the spectral structure of the turbulence is influenced by the presence of solid particles. Turbulent scales interact with the inertial particles and do work to transport them leading to a dynamic transfer of energy between the turbulent scales and particles. This phenomenon is called 'turbulence modulation' and it lacks pure understanding of the mechanism. Literature indicates that these interactions occur differently according to the particle properties and turbulent spectrum is modified non-uniformly by low inertia particles. The diversity of the parameters playing role in different flow types (jets, channel flows etc...) is the primary reason for the lack of comprehension of this phenomenon (Crowe et al., 1998). Squires and Eaton (1990), Elgobashi and Truesdell (1993), Kulick et al. (1994), etc... are among many researchers having studied the modulation of turbulence. Some of the open questions are the parameters intervening the two-way coupling, the effect of initial conditions, the modification of the turbulent energy spectrum, dispersion of the particles in presence of two-way coupling etc...

For  $10^{-1} > \alpha_p > 10^{-4}$  and  $\phi < 10^{-2}$ , the particles' motion governed not only by the interactions with the underlying fluid motion but also by the inter-particle collisions that might induce significant physics such as transfer of momentum, heat during the shock and can significantly affect the spatial distribution of particles. One determining factor is the relative velocity between the two particles in collision. Relative velocity can be induced by laminar or turbulent shear, difference in the particle properties etc... Today, the collision mechanism is shown to be a very complex phenomenon initiated with the studies of mono- and bi-disperse particles in a turbulent flow field. However, studies showed clearly that a range of particle diameters exists in gas-solid flows leading to different physical phenomenon related to collision such as coalescence, agglomeration etc... Determination of a proper collision frequency is the center of motivation to well-predict the flows in which these kinds of interactions occur.

For  $\alpha_p > 10^{-1}$ , the flow is referred as dense flow (also named 'granular flow') where the interparticle collisions are significantly important. Mostly particle-particle interactions govern the dynamic motion in this regime.

A good comprehension of the nature of the disperse phase is needed in all of the areas mentioned above in order to understand, improve and develop new techniques, new devices or take necessary precautions against the natural phenomena in which gas-solid flows occur. The phenomena could exist simultaneously or separately in a flow according to a specific problem.

## 1.2 Importance of turbulence modulation and modeling of two-phase flows

In the course of this study, the turbulence modulation will only be considered out of all the possible interactions mentioned above. In Stanford University, end of 70s, during an experience performed on a vertical diffuser at the outlet section of a fluidized bed through which a gas-solid flow is let out, relatively dilute loading of particles are seen to have an important effect on the mean velocity field giving rise to the work of modulation of turbulence. Developing a code, assuming the particles as point sources affecting the turbulent flow field developed by Crowe et al. (1977) (will be explained in chapter 2 in detail), many experimental or numerical studies followed on understanding the two-way coupling mechanism and how to integrate it on numerical models.

In free turbulence, the studies of Maxey et al. (1997), Gore and Crowe (1989), Parthasarathy and Faeth (1990), Squires and Eaton (1990), Mizukami et al. (1994), Elgobashi and Truesdell (1993), Kenning and Crowe (1997), Boivin et al. (1998), Druzhinin and Elgobashi (1999), Ahmed and Elgobashi (2000), Sundaram and Collins (2000), Vermorel et al. (2003) have shown the importance of very small particles effecting the structure of the turbulent energy spectrum. There are also theoretical works of Yarin and Hetsroni (1994), Yuan and Michaelides (1992) investigating to incorporate the wake effect of particles with relatively high diameters into the turbulence models. Hwang and Eaton (2006a,b) studied experimentally the effect of particles on the fluid turbulence where they showed that when the high turbulence rates are required, the attenuation of the turbulent kinetic energy by the particles can cause serious problems. More recently, García (2001), Boivin et al. (2000) discusses the extension of modeling the two-way coupled flows using LES approach to capture the flow dynamics more in detail in numerics.

In wall-bounded turbulence, Fessler et al. (1994), Uijttewaal and Oliemans (1996) studied the dispersion and deposition of particles in vertical pipe flows experimentally. Portela and Oliemans (2003) studied the channel flow, Rani et al. (2004) studied the turbulent pipe flow laden with inertial particles. Nasr and Ahmadi (2007), Benavides and van Wachem (2008), Chan et al. (2005) are among the many researchers that investigated the fluid-particle

interactions in flows with wall bounded vertical or horizontal domains. They drew attention to the fact that the particles interact with turbulence differently in the center of the channel and in the near-wall region.

According to all these studies, it is clear that the real problem of two-way coupling is that the enhancement or the attenuation of the turbulence do not have a consensus on specific particle parameters and the modification of the turbulent spectrum is very difficult to explain, especially, due to non-uniform modulation by low-inertia particles. In this purpose, the theoretical work of Gore and Crowe (1989) related turbulent intensity modification to the ratio  $d_p/L_f$  where  $d_p$  is the particle diameter and  $L_f$  is the integral scale of turbulence. They observed that for small ratio of  $d_p/L_f$ , turbulent intensity attenuates and for high ratio of  $d_p/L_f$ , turbulent intensity increases. Experimental studies in the literature showed that the maximum of turbulence attenuation occurs when the particle size is close to the Kolmogorov scales of turbulence (Kulick et al., 1994). However, the material density of the particles were not included in this reasoning that saw many objections. Yarin and Hetsroni (1994) then proposed using the particle Reynolds number,  $Re_p$ , in order to explain the increases and decreases in turbulence intensities. With high particle Reynolds numbers, particles have higher relative velocities compared to their fluid environment and they start to shed vortices. Coherently in very low particle Reynolds number regime, the works of Squires and Eaton (1990), Elgobashi and Truesdell (1993) have put in evidence that the highly inertial particles tend to modify the turbulence spectrum uniformly at each turbulent scale whereas low-inertia particles tend to modify it more non-uniformly, e.g., enhancement in high wavenumbers and attenuation in low wavenumbers.

Modeling of gas-solid flows are based on two distinct approaches namely; Euler-Euler methods where each phase is regarded as a continuum and they are coupled through interfacial transfer terms and Euler-Lagrange methods where particle phase is discrete and each particle is tracked individually. Euler-Euler methods are described in detail in the works of Ishii (1975), Delhay (1981). The approach is basically to write the continuum transport equations of both phases where each equation has the transfer term accounting for the mean and turbulent transfer of quantities between the phases. These methods are difficult to formulate and require constants therefore showing uncertainties according to the problem considered. Nevertheless, Euler-Euler methods are now the center of attention for the industrial partners because of their capability to predict certain types of flows of practical interest without much cost and reliability. Euler-Lagrange methods can be referred in the works of Elgobashi and Truesdell (1993), Squires and Eaton (1990). Approach solves the dynamic equation of motion of each particle and advances them in time. In this regard, Euler-Lagrange methods are very costly and become prohibitive easily with increasing particle numbers but they are very precise in terms of extracting particle statistics for any flow type. Therefore

the interaction between the two methods can be seen as practical Euler-Euler models motivate many modeling studies using the informations obtained from Euler-Lagrange methods. Especially with the help of kinetic theory, Euler-Euler models advanced enormously in the last two decades and sure it will continue.

### 1.3 Aim of this study

This thesis stands at the continuation of these studies to improve the understanding the two-way coupled flows by using a Lagrangian approach for the particle phase. Basic reason to use a Lagrangian approach is that these interactions occur along the particle trajectories and are therefore very difficult to take into account in Eulerian models which are defined at fixed points. Newly emerging powerful numerical tool Lagrangian stochastic models are going to be used to model the fluid turbulent velocity along the particle and fluid element trajectories. The aim is not only to understand the underlying physics of modification to the turbulent energy spectrum, especially due to low-inertia particles, but also to settle the stochastic equations governing the turbulent motion in presence of two-way interactions. These equations in turn will be able to lead to the Eulerian continuum equations for the fluid phase.

From modeling point of view, interest in this study is to lie down the equations in the context of Lagrangian stochastic modeling that will imitate the equations written in the Navier-Stokes formalism which are assumed in microscopic level. The tendency to reduce the number of degrees of freedom which is well-established purpose in Lagrangian stochastic models is the main driving fact of this thesis. So the equations obtained should help the improvements and developments of not only the codes using the stochasticity which are pretty novel in the community, but also the codes largely used in industry as of  $k - \epsilon$  type.

On the numerical experiment side, the intention is to perform 3D time dependent simulations of gas-solid flows in order to analyze and to understand the Lagrangian characteristics of the solid particle dispersion in presence of two-way coupling. Main challenges reside in the difficulty and exhaustivity of the precise calculation of the variables related to the gas-solid flows such as correlations of any type. Direct Numerical Simulation (DNS) without ad-hoc modeling assumptions are going to be used in order to form a database and to compare the computations from the models. Fluid phase is assumed to be homogeneous isotropic stationary turbulence with periodic boundary conditions in a cubical domain far from any wall effects. No mean flow gradients exist then to complicate the problem. Indeed, it is a known fact that in presence of shear or mean gradients, the structural changes in the turbulent

kinetic energy spectrum are not separable from one another. As a last point, gravity is also neglected in order to simplify the problem.

Solid, spherical, indeformable monosize distribution of particles with dilute loading are used in this study. Their diameters are smaller than the Kolmogorov scales so as not to include any wake-induced effect on the structure of turbulence. Particles have much higher density than the fluid phase to exclude certain forces acting on them (details are in chapter 2). Interparticle collisions are negligible because of very low volume fractions. With these assumptions, particles should cover certain properties of more realistic particle or droplets encountered in real applications mentioned above. Therefore, the configuration considered in this thesis is much of a fundamental type which has to allow to analyze and to understand the basic mechanisms of two-way coupling in order to propose a model.

In the light of these facts, the thesis is going to flow in following way:

Chapter 2 will talk about the motion of single particle in a turbulent flow. Specifically, the definition of the forces acting on a single particle due to the underlying turbulent flow will take place after which the simplifying hypotheses concerning the study will be discussed. The notion from a single particle motion to the motion of a particle cloud will be discussed. This will follow with the discussion of the homogeneous isotropic turbulence and how to keep it stationary in time. Stochastic forcing scheme of Eswaran and Pope (1988) is going to be discussed and a reference flow field is going to be generated in order to be used for the one-way and two-way coupled simulations. It is going to be seen that the stochastic forcing is well capable of generating a proper turbulent flow field with proper statistics. However, due to its requirement of inverse Fourier Transform, it is costly and inverse FFT is problematic in parallel environment (the code used is parallel).

In chapter 3, linear forcing scheme is going to be implemented on different initial conditions, namely: one generated by the stochastic forcing and the other is the Passo-Pouquet type spectrum. The purpose is to use the advantages of linear forcing which is very rapid and easy to code to obtain proper statistics. However, it is going to be seen that the scheme is further attention due to its lack of producing good statistical properties.

Chapter 4 will initiate the modeling of gas-solid flows in the context of Euler-Euler models in the frame of the kinetic theory. The chapter is going to talk about the evolution of the Euler-Euler models and the incorporation of the probabilistic description to reformulate the equations. Statistical or probabilistic description of the particle phase is going to be followed by the modeling the fluid-particle correlations for which the classical Euler-Euler methods (also named 'two-fluid models') are not able to propose a model.

The problems of modeling fluid-particle turbulent drift velocity and particle phase high-order moments are going to be discussed in chapter 5 and Lagrangian stochastic models will follow. These models use stochasticity in differential equations to imitate the natural processes more realistically. Stochasticity covers the random forces perturbing the process in an infinitely small time separation. Two equations are going to be proposed, one for the fluid velocity along the fluid element trajectories and the other for the fluid velocity along the solid particle trajectories. Due to the modulation of the fluid statistics by the particles, the originality in these equations will be an additional two-way coupling term which is not known a priori and should be modeled. Two propositions will be used at this level one is a mean drag term using the mean velocities of the both phases from mean momentum transport equations and the other is an instantaneous drag term using the mesoscopic particle velocity written in the context of the mesoscopic Eulerian formalism (MEF) developed by Février et al. (2005). These two models should carry the importance of the spectral content of the two-way coupling term, e.g., the non-uniform effect of low-inertia particles on turbulent scales. The models will be the first and significant part of a proposed methodology to determine the unknown coefficients in stochastic equations.

Chapters 6 and 7 are about the measurement of fluid and particle statistics, energy spectrum of turbulence and the tests of the models with comparison to the Direct Numerical Simulation (DNS) of an ideal case corresponding to the stationary homogeneous isotropic turbulence without gravity. The modification of the turbulence characteristics such as integral time and length scales, turbulent Reynolds numbers will be reported in order to analyze the modification of the turbulent flow. In chapter 7, the statistics concerning the particle phase will be reported and analyzed in terms of particle Lagrangian correlations. Then the Lagrangian stochastic modeling results are going to be discussed in terms of the fluid-particle covariance and turbulent drift velocity in order to evaluate the models.

## Chapter 2

# Numerical simulation of fluid turbulence and solid particle trajectories

### 2.1 Introduction

In this chapter, the dynamic equation governing a single spherical particle's motion in interaction with a turbulent flow will be discussed. The equation corresponds to the dynamic equation of motion written in classical Newtonian mechanics as a force  $F$  applied on a particle is equal to the mass of the particle times the acceleration of the particle. Definition of the forces acting on a particle due to the interactions with the underlying turbulent flow will be discussed and necessary hypotheses will be made so as to reduce the difficulty of the problem. This thesis considers spherical, indeformable particles all with the same diameter. Their diameters are much smaller than the smallest scales of turbulence (Kolmogorov scale,  $\eta_K$ ),  $d_p \ll \eta_K$ , and particles have fairly larger density than the fluid,  $\rho_p \gg \rho_f$ , leading to neglect certain forces in the equation of particle motion. These assumptions are, nevertheless, not crucial considering the wide range of applications of small dense particles in many processes such as fluidized beds, sandstorms in deserts etc... The final equation will be composed of only the drag force written in the context of point particle sources.

In order to determine the forces acting on a particle in a turbulent flow, fluid velocity surrounding the particle has to be provided. This requires the solution of the governing equations of the fluid motion around a particle which becomes overly difficult with increasing number of particles. The complexity lying in the fact that infinite number of degrees of freedom, spatial and temporal structures of very large and very small space dimensions

and temporal scales, coexist and interact with each other, is increased with the additional particles. Navier-Stokes equations governing the fluid motion take into account properly all the interactions in the motion of the fluid. However, an analytical solution does not exist and requires the numerical methods and the high power capacity of today's computers. Today the most reliable method to solve these equations is Direct Numerical Simulation (DNS) using no modeling approach. They are used widely in order to observe time evolution of three dimensional turbulent flow fields and therefore regarded as a numerical experiment. Throughout this thesis, many numerical computations have been performed in order to simulate particle motion and dynamics of turbulence corresponding to Direct Numerical Simulations of 3D unsteady compressible Newtonian fluid equations of Navier-Stokes type and Lagrangian dynamic particle equation written in the frame of the Newton's second law of motion. Therefore DNS method will be the subject of the second part of this chapter.

To finish, the most important part in implementation of two-way coupling is the definition of the force acting on the fluid due to the particles. This force is difficult to define explicitly due to the long-range interactions between the particle disturbance and the flow field. The disturbance can be imagined in two different forms: the first is the direct perturbation to the eddies due to the presence of the particles and the second one is the hydrodynamic interactions due to the wake of particles. The back effect of the particles on the fluid can be written as the force applied by the fluid on the particle with an opposite sign (action-reaction principle). Further simplifications are proceeded for the particles considered in the context of this thesis. Very small particles can be regarded as the point sources perturbing the fluid motion and their wakes are negligible to interact indirectly with the turbulent scales. Method called particle source in cell (P.S.I.C.) can then be utilized in order to perform numerical experiments.

## 2.2 Single particle motion in a turbulent flow field

A single particle motion in a turbulent flow is going to be studied. Particles are considered spherical with the coordinates  $(\mathbf{x}^{(n)})$  of  $n^{th}$  particle's center defining its position in space and with the velocity vector  $(\mathbf{u}_p^{(n)})$ . Each particle has a density,  $\rho_p$ , and the diameter,  $d_p$ . In the context of the thesis, all the particles have the same density,  $\rho_p$ , and the same diameter,  $d_p$ , which is called a monodisperse distribution.

### 2.2.1 Dynamic equation of a single particle motion in a turbulent field

Forces acting on a spherical object in a laminar flow was first studied by Stokes (1851) considering the no-slip boundary conditions at the particle surface. Boussinesq (1885), Basset

(1888) et Oseen (1927) considered the same problem with taking into account the distortion of the streamlines around the sphere and writing an equation of motion dependent on the Reynolds number of the flow around the object. Therefore a reference formulation of the equation of particle motion called 'BBO equation' was formulated. This equation is still used today and it is the subject of many research.

Faxen (1924) worked on a more realistic configuration in which a fixed particle is let in a non-uniform unsteady fluid flow. The BBO equation is then extended by Tchen (1947) to the cases where the fluid phase is in turbulent motion. Tchen improved the equation by introducing the unsteady forces acting on the particle due to the acceleration of the surrounding fluid. Corrsin and Lumley (1956) points out some of the discrepancies of the Tchen's expression and takes into account the pressure gradient. Buyevich (1966), Riley (1971) works on Tchen's expression of fluid acceleration considering further the viscous stresses. Recent works of Maxey and Riley (1983) and Gatignol (1983) gave the form of the equation that is used currently.

### 2.2.1.1 Theoretical background

Following the works mentioned above, today, the forces acting on a particle or a droplet due to a turbulent flow can be written as:

- drag force
- gravitational force
- fluid acceleration
- added mass
- history force

More forces could be included in presence of large shear rates, rapid particle rotation due to the velocity gradients over the particle diameter (Saffman, 1965). However, in the context of this thesis, all the particle rotations will be negligible. The definition of the forces mentioned above except the gravity force is based on the integration of the viscous stress tensor  $\tau_{ij}$  and the pressure over the particle surface  $\int_S \tau_{ij} \cdot \vec{n} dS$  and  $\int_S -p \cdot \vec{n} dS$ , respectively, that should satisfy the governing equations of turbulence.

Coherently with the works mentioned, the forces acting on a particle are grouped under two categories. These categories are composed of a force acting on a fluid element that occupies the particle's position and undisturbed by the particle's presence and a force resulting

from the perturbation of the streamlines owing to the particle's presence. It can formally be written that:

$$\rho_p V_p \frac{du_{p,i}}{dt} = F_{1,i} + F_{2,i} \quad (2.1)$$

$$\frac{dx_{p,i}}{dt} = u_{p,i} \quad (2.2)$$

where  $F_1$  term is the force applied on the fluid element taking into account the local pressure gradient and gravity.  $F_2$  is the force by the perturbation due to the particle presence such as drag, added mass etc...

Another categorization of the forces is given by Crowe et al. (1998) as steady and unsteady forces. Steadiness characterizes the stationary time behavior of the relative velocity between the fluid and the particle. Steady-state drag force, pressure gradient fall into this category. Unsteady forces correspond to the acceleration of the relative velocity leading to a deviation between the fluid element and the particle trajectories. Added mass, Basset forces fall into this category. Crowe et al. (1998) also pay some attention to the definition of the force acting on not a single particle but on a cloud of particles. Lack of promising knowledge on this subject feels the need of more research. In the context of this thesis, many of the forces acting on the particle are going to be neglected due to the hypotheses of the study. Therefore, this categorization will not be considered more after this point.

### 2.2.1.2 General equation

For the particles used in this thesis;

$$d_p \leq \eta_K \quad (2.3)$$

$$Re_p = \frac{d_p \mathbf{v}_r}{\nu_f} < 1 \quad (2.4)$$

where the relative velocity  $\mathbf{v}_r$  is written as:

$$\mathbf{v}_r = \mathbf{u}_p - \mathbf{u}_{f@p} \quad (2.5)$$

The forces  $F_1$  and  $F_2$  are written as:

$$\mathbf{F}_1 = \rho_p V_p \frac{D\mathbf{u}_{f@p}}{Dt} + V_p (\rho_p - \rho_f) \mathbf{g} \quad (2.6)$$

$$\begin{aligned}
\mathbf{F}_2 = & V_p \frac{18\rho_f\nu_f}{d_p^2} (\mathbf{u}_{f@p} - \mathbf{u}_p + F_{Faxen}) \\
& + \frac{1}{2}\rho_f V_p \frac{d}{dt} (\mathbf{u}_{f@p} - \mathbf{u}_p + F_{Faxen}) \\
& + V_p \frac{9\rho_f}{d_p} \sqrt{\frac{\nu_f}{\pi}} \int_{-\infty}^t \frac{d}{d\tau} (\mathbf{u}_{f@p} - \mathbf{u}_p + F_{Faxen}) \frac{d\tau}{\sqrt{t-\tau}}
\end{aligned} \tag{2.7}$$

In this equation,  $\rho_p$  and  $\rho_f$  are the density of particle and fluid, respectively.  $V_p$  is the volume of a particle,  $\mathbf{g}$  is the gravitational acceleration,  $\mathbf{u}_{f@p}$  is the fluid velocity locally unperturbed by the particle's presence.  $F_{Faxen}$  terms are the terms to take into account the curvature of the streamlines perturbed by the particle presence (Faxen, 1924). Gatignol (1983) extends this equation to the particles with diameter of the order of Kolmogorov scales ( $d_p \approx \eta_K$ ) and introduces the notion of the fluid velocity integrated over the particle's volume and surface to derive the Faxen terms.

$F_1$  term takes into account the pressure gradient and gravity. The first term in  $F_1$  introduced by Tchen on intuitive bases, and the Archimede force obtained as a solution of Navier-Stokes equations.

$F_2$  is the force due to the particle perturbation to the fluid flow. The first term is drag force related to the viscosity of the fluid initially written by Stokes (1851). The second term is the added mass force induced by the relative acceleration of a fluid element and a particle. It is about the acceleration and deceleration of the particles causing the acceleration or deceleration of the fluid therefore causing a relative motion. The third term is the Basset force (Basset, 1888) taking into account the historical effects of the relative particle acceleration the boundary layer. Rivero (1991) showed that for bubbles, this force is negligible considering small Reynolds numbers  $Re_p \ll 300$ .

In equations 2.6 and 2.7,  $D/Dt$  and  $d/dt$  represent the time derivatives following the fluid element trajectory and solid particle trajectory, respectively. In gas-solid flows with particles smaller than the Kolmogorov scales of turbulence and for very low particle Reynolds numbers, Minier (1988) showed that these two derivatives are equal. In flows where the added mass force acts on the particles, these derivatives become different (Magnaudet, 1995).

#### The notion of the unperturbed fluid velocity:

All the formulations above require providing the fluid velocity at the position of the particle, which is symbolized as  $\mathbf{u}_{f@p}$ . It is important to note that this velocity does not exist. It is an imaginary variable of the fluid which should exist if there were no particle at a space point which belongs to a particle. However, the definition uses this velocity because it is the only information concerning the fluid at the particle position and it is an accessible value in numerical simulations. It will be seen later on that the rigorous solution of the

fluid requires the solution of the governing equations of turbulence on a domain from which particles are extracted, in other words, equations should be solved around each inclusion. Unfortunately, with the inclusion of large number of particles, it becomes unfeasible.

### 2.2.1.3 Hypotheses of the study and the equation retained

Simplifications considered in this study includes particles with

- Small particle diameter,  $d_p \leq \eta_K$
- Large density ratio,  $\rho_p \gg \rho_f$
- Small particle Reynolds number,  $Re_p < 1$
- only translational motion, no rotation of particles
- no gravity

In dilute turbulent flows, for large density ratios, such as considered in this study, of the order  $O(10^3)$ , pressure gradient and added mass forces are negligible. Desjonqueres et al. (1986) showed that in terms of particle dispersion and particle agitation, Basset force is also negligible. Following these simplifications, the forces on the inclusion are composed only of the drag force and the gravity. To further simplify the problem, the gravity is also not considered. Then the equation is written as:

$$\frac{F_p}{m_p} \frac{d\mathbf{u}_p}{dt} = \frac{\mathbf{u}_{f@p} - \mathbf{u}_p}{\tau_p} \quad (2.8)$$

where  $\tau_p$  is the particle relaxation time given as:

$$\tau_p = \frac{\rho_p d_p^2}{18\mu_f} \frac{1}{f_D} \quad (2.9)$$

$f_D$  is the correction factor which is written as:

$$f_D = (1 + 0.15Re_p^{0.687}) \quad (2.10)$$

given by Schiller and Nauman (1935).

The last point is that this equation is related to an isolated particle or a droplet interacting with the turbulent field. The dispersion, agitation of the particles and the effect on the turbulence are the main aims in this study. Therefore a lot of effects could be questioned in terms of negligibility. However, the forces acting on a cloud of particles are not well

understood today. Therefore to exclude the additional problems, the forces are restricted to the drag.

More profoundly, the following assumptions are considered in this thesis,

- No hydrodynamic interactions between neighboring particles (no wake of a particle effect another particle)
- No interparticle collisions (very low volumetric loading of particles)

These hypotheses allow to solve the equation of motion independently for each particle. However, the two-way coupling mechanism requires an expression of the backforce acting on the fluid. This detail is going to be discussed in the third section of this chapter. With the hypotheses and explanations performed so far, the particle phase simulations should be enough to produce reliable results along with the DNS simulations of the fluid phase. In any case, results will be compared either to an experimental measure or to a numerical calculation performed in the literature.

#### 2.2.1.4 Numerical solution of the equation of particle motion

In Euler-Lagrange simulations, the difficulty of the particle phase is the numerical solution of the equation of particle motion requiring the undisturbed velocity of the fluid at the particle position,  $\mathbf{u}_{f@p}$ . The fluid element trajectories are easier to solve so the first attention goes to the Lagrangian tracking of fluid elements. The required equation for this operation is:

$$\frac{d\mathbf{x}_f(t)}{dt} = \mathbf{u}_f(\mathbf{x}_f(t), t) \quad (2.11)$$

This equation is the governing equation for a fluid element, a non-inertial particle. Then basically the Lagrangian interpolation used for the trajectory of inertial particles could be used. This equation is then used, in the context of this study, to calculate the trajectories of fluid elements.

Solution of the equation of particle motion is more complicated and requires the integration of the equations:

$$\frac{d\mathbf{x}_p(t)}{dt} = \mathbf{u}_p(t) \quad (2.12)$$

$$\frac{d\mathbf{u}_p(t)}{dt} = \frac{\mathbf{u}_{f@p} - \mathbf{u}_p}{\tau_p} \quad (2.13)$$

As mentioned, this equation requires the locally unperturbed velocity of the fluid at the particle position. This velocity will be referred as,  $\mathbf{u}_{f@p}$ , @**p** symbol meaning at the position

of the particle considered. Unperturbed velocity of  $n^{\text{th}}$  particle is the velocity undisturbed by the  $n^{\text{th}}$  particle however it is disturbed by all the other  $N_p - 1$  particles of the system. Imprecise calculation of this velocity causes a deviation in the drag force calculation. As Boivin (1996) notes that in case of lack in calculation, the fluid velocity of the next time step will be affected leading to a miscalculation of the drag force.

Lagrangian tracking to the solid inertial particles is performed. In this context, the particle motion equation is solved for each particle by the Runge-Kutta scheme of  $3^{\text{rd}}$  order implemented in the code. This scheme requires the prediction and correction of the velocity for 3 substeps and as noted by Février (2000) increasing the number of steps (degree of the scheme) does not improve the results much. Therefore the time step  $dt$  for the equation of particle motion is taken as equal to the time step of turbulence.

Periodic boundary conditions are used for the particles (for the fluid as well) conceding a reference initial point to a particle whose position evolves periodically in space.

Fluid velocity is computed only at the discrete grid points so an interpolation scheme is needed in order to obtain the fluid velocity at the particle center which is the subject of next section.

### 2.2.1.5 Ghost particle test

The precise solution of the particle trajectories (also the trajectories of fluid elements) is dependent on the precision of the interpolation scheme which is used to obtain the undisturbed fluid velocity to calculate the force acting on the particle. In accordance with this force, particle is timestepped. When there is no two-way coupling, the moments of the particle phase depends on the calculation using this velocity. However, in the presence of two-way coupling, this velocity is also modified and an account should be provided in order to show that the fluid velocity seen by the particle is the same as the one of the turbulent field's non-perturbed fluid velocity. Therefore, this fluid velocity is very difficult to calculate and some tests are needed in presence of two-way coupling.

The local undisturbed fluid velocity  $\mathbf{u}_{f@p}$  is computed by interpolation of the simulated velocity at the grid points to the position of the particle. As noted by Boivin (1996), the projection of the force term to the grid node can affect the fluid velocity (solution of the Navier-Stokes equation) and can create unphysical oscillations. Therefore the drag term of the next time step would be affected. To test this, a simple test proposed by Vermorel et al. (2003) is performed. Two groups of particles introduced into the flow with random distribution without any correlation neither with the other particles nor with the fluid. One of the groups will be ghost particles, e.g., they are one-way coupled with the turbulent flow.

The other group is physical particles. If the PISC approximation is valid then the statistics of these two groups of particles should be in an acceptable margin. The statistical difference in the fluid-particle covariance  $q_{fp}$  of the two groups is shown in figure 2.1. As seen on the

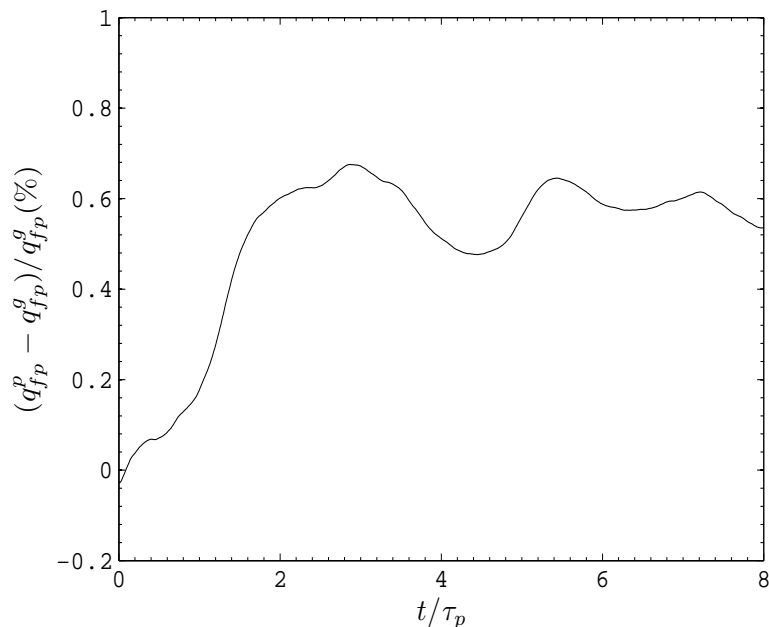


FIGURE 2.1: Statistical difference between the physical particles and ghost (one-way coupled) particles.

figure, the statistical difference between the two groups is less than 1% and this is verified in the totality of the simulations performed in this thesis.

### 2.2.1.6 Interpolation scheme

Different schemes exist in the literature for the interpolation procedure and they are usually classified according to their levels of order.  $3^d$  order Lagrangian polynomial interpolation scheme is used in this study requiring  $4^3$  grid variables surrounding the particle. Order 3 means that the second derivatives are precisely solved. The advantage of this scheme is that it takes into account all the flow scales precisely and it is largely discussed by Boivin (1996), Balachandar (1989) in terms of cost and feasibility. It is less costly than the sophisticated methods such as spectral interpolation as noted by Laviéville (1997).

## 2.3 Fluid turbulence simulation

### 2.3.1 Introduction - General considerations

Underlying flow field dispersing the particles is considered turbulent in this study. The fluid medium is characterized as a three-dimensional continuum implying that the smallest scale of motion  $\eta_K$  (also called Kolmogorov scale) is much larger than the molecular motion defined using the mean free path,  $\lambda$ . Therefore only the scales of equal to and larger than the Kolmogorov scales are of interest. This allows the definition of a fluid element that can be tracked in a Lagrangian manner as explained in the section of numerical solution of the equation of particle motion. Fluid elements are still very large in comparison to the molecular scales and much smaller than the Kolmogorov scales. This turbulent scales should then be solved in order to analyze the time evolution and characteristics of turbulence in order to extract information about the flow considered.

As explained in the introductory section of this chapter, turbulence is regarded as the superposition of many number of degrees of freedom (so-called 'scales' or 'structures' from now on) in time and in space interacting with each other. The smallest scales can be of a size that is not seen by a human eye (usually symbolized as  $\eta_K$ ), the largest scales can be of dimensions as big as several kilometers depending on the geometry (will be referred as  $L_f$  in this study). The quantity of the scales is characterized by a dimensionless number called Reynolds number,  $Re_L$ . It is defined as:

$$Re_L = \frac{u_{f,rms} L_f}{\nu_f} \quad (2.14)$$

where characteristic turbulent velocity is defined as:

$$u_{f,rms} = \sqrt{\frac{2}{3} q_f^2} \quad (2.15)$$

Fluid kinetic energy  $q_f^2$  is defined as:

$$q_f^2 = \frac{1}{2} \langle u'_{f,i} u'_{f,i} \rangle \quad (2.16)$$

To characterize the small scales, another Reynolds number is introduced:

$$Re_\lambda = \frac{u_{f,rms} \lambda_g}{\nu_f} \quad (2.17)$$

where  $\lambda_g$  is the Taylor length scale and it can be calculated using the two-point correlations, as will be seen later on.

At this level, the characteristic small scales are to be introduced to be used later on to further characterize turbulence. Small scale characteristics are obtained by dimensional analysis as:

$$\eta_K = (\nu_f^3/\epsilon)^{1/4} \quad (2.18)$$

$$\tau_\eta = (\nu_f/\epsilon)^{1/2} \quad (2.19)$$

where  $\eta_K$  is the Kolmogorov length scale and  $\tau_\eta$  is the characteristic timescale of Kolmogorov scales.

### 2.3.2 Navier-Stokes equations and solution

Navier-Stokes equations are a system of non-linear second order partial differential equations in four independent variables; position in three coordinates ( $\mathbf{x}$ ) and time ( $t$ ). They provide the evolution of the fluid velocity at a point in time. Classification of the partial differential equations helps to choose a particular method for the solution of a considered equation. However, a common property of Navier-Stokes equations is that they cannot be mathematically classified, nevertheless, they carry many of the characteristics of the partial differential equations which can be classified as hyperbolic, elliptic or parabolic (Ferziger and Péric, 2000).

No analytical solution exists for the general Navier-Stokes equations, except for some special cases such as inviscid flows, therefore numerical discretization in time and in space is widely used method of solution. All the fluid turbulent scales can be represented by numerical discretization. This discretization, however, requires sufficient computing power and resource to compute the each scale whose quantity increases rapidly with the Reynolds number,  $Re_L$ . This in turn restricts the maximum reachable  $Re$ . It is known that industrial application of DNS is impossible for many processes and it is regarded mostly as a numerical experiment tool and interesting for the academic studies. Use of DNS as a research tool and the new challenges for the recent and far future are summarized in the work of Nasr and Ahmadi (2007).

Foundations of DNS were laid at the National Center for Atmospheric Research laboratory by Fox and Lilly (1972). Orszag and Patterson (1972) simulated a  $32^3$  three dimensional turbulence flow with a Reynolds number based on the Taylor length scales  $Re_\lambda$  of 35. Rogallo (1981) extended the application to homogeneous turbulence subjected to mean strain in spectral space. First application to a plane channel flow was performed by Kim et al. (1987).

DNS method uses no model and is directly created for the purpose of solving the Navier-Stokes equations. Depending on the order of space and time discretization, it can capture all

of the flow scales for a low Reynolds number flow. The space discretization should be larger than the Kolmogorov scales. In the study conducted here, the space step is of the order of Kolmogorov scales or larger ( $\Delta x \approx \eta_K$ ). Time discretization should also be small enough to capture the birth and death of an Kolmogorov scale.

Dimensionless Navier-Stokes equations for a compressible Newtonian viscous fluid is written as:

$$\frac{\partial \rho_f}{\partial t} + \frac{\partial \rho_f u_{f,i}}{\partial x_i} = 0 \quad (2.20)$$

$$\frac{\partial \rho_f u_{f,i}}{\partial t} + \frac{\partial \rho_f u_{f,i} u_{f,j}}{\partial x_j} = -\frac{\partial p}{\partial x_i} + \frac{\partial \tau_{ij}}{\partial x_j} \quad (2.21)$$

$$\frac{\partial \rho_f E}{\partial t} + \frac{\partial (\rho_f E + p) u_j}{\partial x_j} = \frac{\partial u_i \tau_{ij}}{\partial x_i} - \frac{\partial q_i}{\partial x_i} \quad (2.22)$$

where the first equation is the conservation of mass and the second one is the conservation of momentum.  $E$  is the total energy,  $\mathbf{q}$  is the heat flux.  $\tau_{ij}$  is the visous stress tensor given as:

$$\tau_{ij} = \mu_f \left( \frac{\partial u_{f,i}}{\partial x_j} + \frac{\partial u_{f,j}}{\partial x_i} - \frac{2}{3} \delta_{ij} \frac{\partial u_{f,k}}{\partial x_k} \right) \quad (2.23)$$

The energy  $E$  is given by:

$$E = \frac{1}{2} \sum_{k=1}^3 u_{f,k}^2 + \frac{p}{\rho_f (\gamma - 1)} \quad (2.24)$$

$$p = \rho_f r_g T \quad (2.25)$$

where  $r_g$  is the universal gas constant,  $\gamma$  is the ratio of specific heats at constant pressure and constant volume.

### 2.3.3 Numerical approach, description of the code NTMIX3D

Numerical approach used in this thesis is DNS method solving directly the discretized Navier-Stokes equations at space grid points with  $\Delta x$  space step and  $dt$  time step. The code utilized is called NTMIX3D developed in collaboration with CERFACS, IFP (Institut Francais du Petrol), EM2C and IMFT initiated some 20 years ago. The code is intended primarily to solve the turbulent reactive flows then enhanced with a Lagrangian particle tracking routine in order to extend it to two-phase turbulent combustion problems. It is a compressible code and parallelized with MPI platform capable of simulating flow problems admitting high computer resources.

Spatial discretization:

6<sup>th</sup> order compact finite difference scheme for space discretization (Lele, 1992) and 3<sup>rd</sup> order Runge-Kutta scheme for time advancement of the equations, hence the high precision and more realistic simulation of turbulent flows. Space discretization for the first derivative  $u'_f = \frac{\partial u_f}{\partial x}$  for a point inside the domain is written as:

$$3u'_{f,i+1} + 9u'_{f,i} + 3u'_{f,i-1} = \frac{1}{\Delta x} \left( \frac{1}{4}u_{f,i+2} + 7u_{f,i+1} - 7u_{f,i-1} - \frac{1}{4}u_{f,i-2} \right) \quad (2.26)$$

where  $\Delta x_i$  is the space step in  $i^{\text{th}}$  direction. Because of the derivatives, the representation of the range of scales is very realistic. Compact schemes are known as quasi-spectral schemes called also of Padé type. They can handle different mesh geometries and admit different boundary conditions.

6<sup>th</sup> order discretization is not valid over the boundaries because it has a centered formulation. At the boundaries special scheme is considered by reducing the order of the approximation. At the boundary, this equation is written in 3<sup>rd</sup> order as:

$$2u'_{f,i} + 4u'_{f,i-1} = -\frac{1}{\Delta x} (-5u_{f,i} + 4u_{f,i-1} + u_{f,i-2}) \quad (2.27)$$

And for the points neighboring to the boundary points, 4<sup>th</sup> order scheme is written as:

$$u'_{f,i+1} + 4u'_{f,i} + u'_{f,i-1} = \frac{3}{\Delta x} (u_{f,i+1} - u_{f,i-1}) \quad (2.28)$$

For the second order derivatives, the derivation follows a similar procedure (for more details see Baum, 1994). The timestep is imposed using the CFL number of 0.35 due to the stability considerations in the code.

Temporal discretization:

3<sup>rd</sup> order (3 step) explicit Runge-Kutta schemes use the propagation of information over three intervals (Vichnevetsky and Bowles, 1982). Choice of the time integration effects also the space integration especially in the sense of allowable time step of the simulation. Spectral schemes have no numerical dissipation therefore the time integration should not induce any numerical dissipation, either. The following procedure can be written for the time integration of NTMIX3D:

$$\begin{aligned}
\mathbf{u}_f(t + \Delta t) &= \mathbf{u}_f(t) + \Delta t F(t, \mathbf{u}_f) \\
F(t, \mathbf{u}_f) &= \frac{1}{4}K_1 + \frac{3}{4}K_3 \\
K_1 &= F(t, \mathbf{u}_f) \\
K_2 &= F\left(t + \frac{\Delta t}{3}, y + \frac{\Delta t}{3}K_1\right) \\
K_3 &= F\left(t + \frac{2\Delta t}{3}, y + \frac{2\Delta t}{3}K_2\right)
\end{aligned} \tag{2.29}$$

where  $u$  is the function (velocity field) to be integrated,  $\Delta t$  is the time step,  $F$  is the time derivative of  $u$ . More detailed information can be found in (Hoffman, 2002, Press et al., 2001). The maximum time step  $dt$  corresponding is determined by the CFL number.

### 2.3.4 Turbulence forcing

Turbulence considered in this study was a fully developed turbulence far from any boundary. Moreover, homogeneity and isotropy were needed because of the fundamentality of the study. Homogeneity means that quantitatively mean quantities do not show variation in all points of the flow field. Isotropy, on the other hand, means that the statistics do not depend on a particular direction. Apart from being fundamental, the study considers the two-way coupling mechanism which is not well understood. Indeed, anisotropy, inhomogeneity need consideration of additional mechanisms such as mean gradients, correlations of higher order etc... These effects can induce an indirect effect on the flow and on the interactions with the particle phase and their neglecting is only possible with homogeneous, isotropic turbulence because no average shear and mean velocity gradient could occur in this kind of flow.

Homogeneous isotropic turbulence does not exist in nature, it can only be obtained by some special arrangements in experimental studies such as translational grid (Morize et al., 2007) or static grids (Comte-Bellot and Corrsin, 1971), jet flows in confined tubes (Risso and Fabre, 1997). In numerical environment, it is easier to obtain. There are two options: imposing an initial energy spectrum (Passot-Pouquet spectrum, for example) and leave it to decay in time exponentially, the other method is to start with an initial field and forcing it to an isotropic and homogeneous flow state. The latter choice is possible with artificial forcing which is the subject of the next section and has the advantage of achieving a stationary state for the turbulent statistics such as kinetic energy, dissipation etc... The former choice has a decaying (non-stationary) type turbulence making the statistics possible for certain time range whereas forced turbulence lends itself easily to statistical examination and statistics obtained are more robust with time and space averages.

Turbulence decays because of the viscous effects converting the kinetic energy of the turbulence into heat. Therefore turbulence has a dissipative nature and without the continuous feeding of energy from an external source, it decays. This continuous source of energy is artificially added as a divergence-free term to force the turbulent velocity in turbulence forcing. Artificial energy added has to be dissipated by the action of small scales, in other words, the level energy added to the system and the dissipation rate should be equal so that the energy could keep stationary level. Following section considers the stochastic method of calculation for this term, whereas in next chapter, another method, called Linear forcing, will be analyzed.

Turbulence forcing is not a new idea. Different deterministic methods have been already implemented by Siggia and Patterson (1978), Kerr (1981), Siggia (1981). A common method used in these studies is to keep the Fourier modes of the flow stationary in time. The common drawback of all these studies is that either they generate a turbulence that could not be modified by external effects such as particles, or they generate a turbulent state which is pretty far from reality.

Stochastic spectral forcing and a recently developed deterministic method will be considered in this study. Basic difference between them is that in stochastic methods coefficients are calculated in spectral space and transformed into physical space by inverse Fourier transform. The force is applied on the low wavenumber (large scales) of turbulence to assure the non-contamination of the small scales (large wavenumbers) in the dissipation range by the artificial algorithm. In deterministic method, forcing term is directly calculated in physical space using the statistics of turbulence. They are going to be compared in terms of the properties of turbulence and for the computational cost for the study of the gas-solid flows.

Navier-Stokes equation now is written with the turbulence forcing term  $f_i$  for an incompressible flow as:

$$\frac{\partial u_{f,i}}{\partial t} + \frac{\partial u_{f,i} u_{f,j}}{\partial x_j} = -\frac{1}{\rho_f} \frac{\partial p}{\partial x_i} + \nu_f \frac{\partial^2 u_{f,i}}{\partial x_j^2} + f_i \quad (2.30)$$

The forcing term by definition has zero mean;

$$\langle f_i \rangle = 0 \quad (2.31)$$

#### 2.3.4.1 Spectral forcing

Spectral forcing is developed initially by Eswaran and Pope (1988). The large scales are proposed to be forced by the term calculated with the help of stochastic Langevin equation

written as:

$$b_{i,m}(\mathbf{k}, t + \Delta t) = (1 - \Delta t/T_F)b_{i,m}(\mathbf{k}, t) + \sqrt{\frac{2\sigma_F^2\Delta t}{T_F}}\delta W \quad (2.32)$$

where  $m = 1, 2$  is real and imaginary part of the coefficient  $b_i$ ,  $i$  indicates a component.  $\Delta t$  is the time step of the process here equal to the time step of turbulence,  $T_F$  is the correlation time of the process and  $\sigma_F$  is the amplitude.  $\delta W$  is a Gaussian distributed random number with the mean 0 and variance 1. Using the random number, this second term produces the stochastic part of the process and it represents the fluctuations occurring due to an unknown source.

This equation is solved for the wavenumbers  $\mathbf{k}_{min} < \mathbf{k} < \mathbf{k}_{max}$  where  $\mathbf{k}_{min}$  is the minimum and  $\mathbf{k}_{max}$  is the maximum wavenumber. Exterior to this range, the coefficient  $b_{i,m}(\mathbf{k}, t)|_{\mathbf{k} < \mathbf{k}_{min}, \mathbf{k} > \mathbf{k}_{max}}$  is zero. Initially, Eswaran and Pope (1988) proposes to force in the range  $]0, 2k_0]$  and  $]0, 2\sqrt{2}k_0]$  where  $k_0$  is the base wavenumber of the domain defined as  $k_0 = \frac{2\pi}{L_b}$ ,  $L_b$  being the one side of the cubical domain. Février (2000) proposes to force the wavenumbers in the range  $[2k_0, 6k_0]$ . Such a forcing was demonstrated to give a turbulent field with a better statistical properties such as better isotropy and exponential correlations in time. Along with the work of Eswaran and Pope (1988), Eswaran and Pope (1988) showed that the small scales of turbulence are not modified by this modification of wavenumbers. Therefore in this study, the proposition of Février (2000) to use the range  $[2k_0, 6k_0]$  was followed. Therefore, the same method as Février's is going to be adapted to analyze the flow field in terms of homogeneity and isotropy.

The coefficients  $b_i$  do not necessarily satisfy the continuity (divergence-free field) of the velocity field, therefore, Eswaran and Pope (1988) proposes to perform a projection with the operator:

$$a_i^F = b_i - k_i \frac{k_j b_j}{\mathbf{k}^2} \quad (2.33)$$

Coefficients  $a_i^F$  is added to the Navier-Stokes equations in spectral space written as:

$$\frac{\partial u_{f,i}}{\partial t}(\mathbf{k}, t) = a_i(\mathbf{k}, t) + a_i^F(\mathbf{k}, t) \quad (2.34)$$

where  $a_i(\mathbf{k}, t)$  is the convection, diffusion, pressure gradient. Once the coefficient  $a_i^F(\mathbf{k}, t)$  is calculated, it can be converted to the physical space using inverse Fourier transform to calculate the forcing term  $f_i$ . To satisfy the continuity equation further in accordance with the numerical schemes implemented in the code, modified (effective) wavenumber  $\mathbf{k}_{eff}$  is used in order to reduce the differentiation errors. This wavenumber for the 6<sup>th</sup> order compact

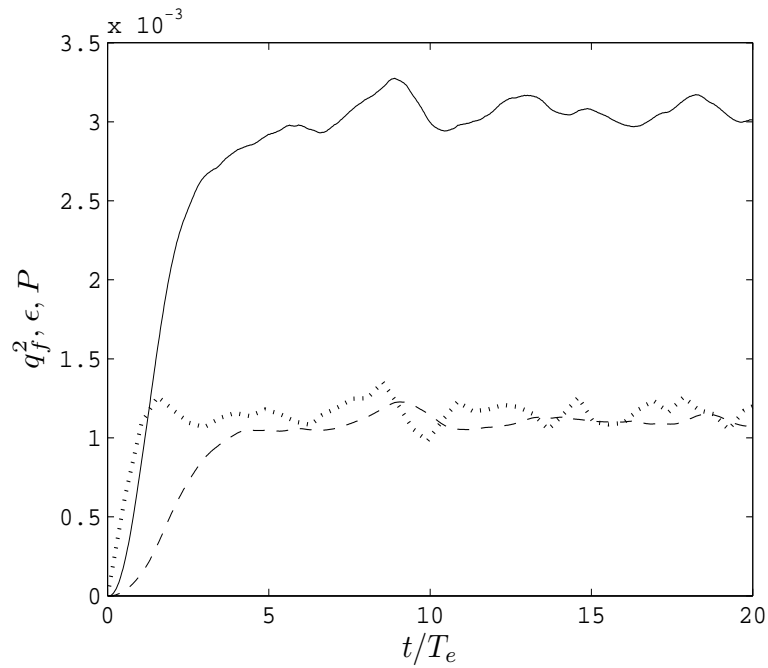


FIGURE 2.2: Turbulent kinetic energy balance. Solid line: turbulent kinetic energy,  $q_f^2$ , Dashed-line: energy dissipation rate,  $\epsilon$ , Dotted line: energy production,  $P$ .

scheme is defined as (Baum, 1994):

$$\mathbf{k}_{eff} = \frac{1}{\Delta \mathbf{x}} \frac{28 \sin(\mathbf{k}h) + \sin(2\mathbf{k}h)}{18 + 12 \cos(\mathbf{k}h)} \quad (2.35)$$

The wavenumber in the calculation of the projection operator has been replaced by  $\mathbf{k}_{eff}$  and this modification improved the divergence of the forcing term  $a_i^F$  significantly but the divergence of the final turbulent field is not observed to have much improvement. Therefore the use of the modified wavenumber is not considered in the simulations performed in this study.

Stationary level of turbulence statistics is reached after several eddy turnover time as seen on figure 2.2 after the balance is settled between the production of turbulence kinetic energy and its dissipation.

The dissipation rate  $\epsilon$  is defined as:

$$\epsilon = 2\nu_f \langle s'_{ij} s'_{ij} \rangle \quad (2.36)$$

where  $s'_{ij}$  is the fluctuating part of the deformation-rate tensor  $s_{ij}$  which is written as:

$$s_{ij} = \frac{1}{2} \left( \frac{\partial u_{f,i}}{\partial x_j} + \frac{\partial u_{f,j}}{\partial x_i} \right) \quad (2.37)$$

Production term  $P_f$  can be calculated by the formula:

$$P_f = \langle u'_{f,i} f_i \rangle \quad (2.38)$$

The oscillations around a mean value of each statistical value in the stationary period are remarkable (see figure 2.2). These oscillations are due to the stochastic term in the Langevin equation that does not produce the same kinetic energy from one timestep to another.

### 2.3.4.2 Numerical implementation of stochastic forcing scheme

In single phase flows:

As noted in preceding section, the implementation of stochastic forcing scheme requires the inverse Fourier transform of the forcing coefficients  $b_i$  calculated in spectral space. Due to the code NTMIX3D being in parallel platform, the implementation of inverse FFT is difficult. Therefore the calculation of the source term due to the turbulence forcing should be adapted to the parallel environment. To overcome the difficulty of parallel environment for the inverse FFT, an additional processor is considered to perform the inverse FFT and send the data to the processors solving the Navier-Stokes equations. Representation of the solution configuration is shown in figure 2.3. The extra processor  $n + 1$  performs the stochastic calculation of the force coefficients and inverse FFT. Then it sends the data (force coefficients) to the processors solving the Navier-Stokes equations.

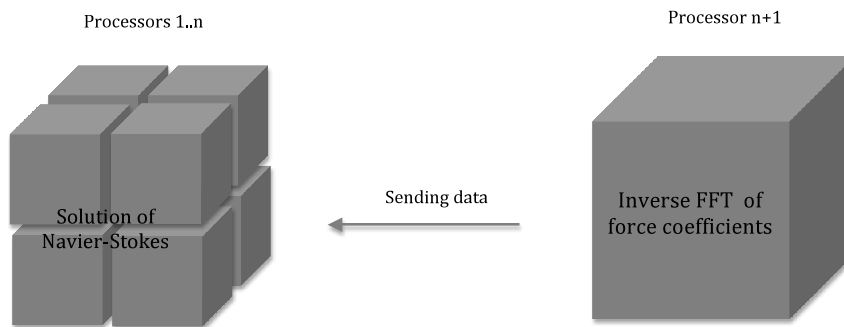


FIGURE 2.3: Representative figure showing the configuration of simulations to perform inverse FFT in parallel platform.

Due to the additional processor, the duration of the calculations are important in terms of synchronization between the processors, e.g., the additional processor only performs the inverse FFT whereas the other processors solve the Navier-Stokes equations. For a good

synchronization, the inverse FFT should be performed faster than the solution of the Navier-Stokes equations.

$$t_{Navier-Stokes} \geq t_{inverse\ FFT} \quad (2.39)$$

Time consumptions of the processors are compared in figure 2.4 for single phase flows. As seen, using more than 16 processors is not feasible due to the duration that processors must wait for the  $n + 1^{nd}$  processor finishes the inverse FFT and sends the data.

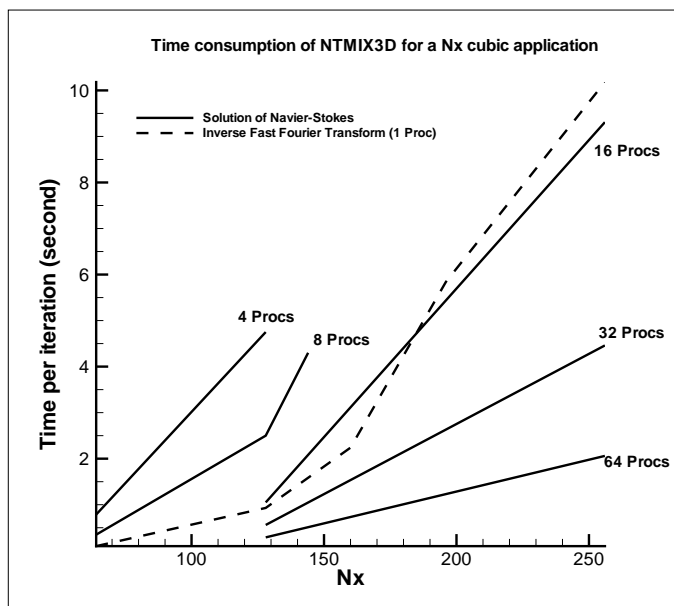


FIGURE 2.4: Time consumptions of NTMIX3D per step compared to the calculation of inverse FFT for  $N_x^3$  DNS application.

#### In gas-solid flows:

For gas-solid flows, the least number of particles used in this study is 262144 and to calculate the Lagrangian statistics of the fluid turbulence another 200000 fluid elements are used. In addition, the two-way coupling mechanism which requires the interpolation-projection of the fluid variables and backforce is also costly. With these additional computations, in the entirety of the simulations performed in this thesis, the condition  $t_{Navier-Stokes} \geq t_{inverse\ FFT}$  has always been satisfied. Thus, 64 + 1 processors are used for all the simulations.

#### 2.3.4.3 Analysis of the turbulence characteristics

The spatial and temporal dimensions of turbulent scales are important in terms of characterizing the turbulence, it can be noted, in passing, that they are the basic focus for the modeling of turbulent flows along with the viscosity. To calculate precisely the space and

time scales of turbulence, one-point and two-point statistics are used. The validation of the homogeneous isotropic stationary turbulence was already performed by Février (2000), therefore the same methodology will be followed. In the next subsections, the one-point and two-point correlations will be compared in terms of homogeneous isotropic turbulent flow field obtained by stochastic forcing scheme defined.

One-point correlations are used to determine the time scale (life time) of large or small eddies. They can be calculated in an Eulerian or in a Lagrangian frame.

Eulerian one-point correlations are defined as:

$$R_{E,ij}(\tau) = \langle u_{f,i}(\mathbf{x}, t) u_{f,j}(\mathbf{x}, t + \tau) \rangle \quad (2.40)$$

where  $\langle \cdot \rangle$  indicates an ensemble averaging operator. In isotropic turbulence, tensor descends to the diagonal components as:

$$R_E(\tau) = \frac{1}{3} \langle u_{f,i}(\mathbf{x}, t) u_{f,i}(\mathbf{x}, t + \tau) \rangle \quad (2.41)$$

Time scale related to the Eulerian correlations is defined as:

$$T_E = \frac{1}{R_E(0)} \int_0^\infty R_E(\tau) d\tau \quad (2.42)$$

$T_E$  is the timescale during which the fluctuating velocity decorrelates from itself. A practical calculation of Eulerian one-point correlations involves the evolution of the fluid velocity at a large number of arbitrarily distributed points in the flow domain and using the spatial averages. The fluid velocities are stored at the spatial grid points therefore a practical way of calculating the correlations is the consideration of the velocities at grid points. Using the stationarity in forced turbulence, the correlations can further be improved by using time averages for the correlations calculated for a certain number of realizations separated by a decorrelation time interval.

Lagrangian one-point correlations require marked fluid particles and are defined similarly as:

$$R_{L,ij}^f(\tau) = \langle u_{f,i}(\mathbf{x}_f(t), t) u_{f,j}(\mathbf{x}_f(t + \tau), t + \tau) \rangle \quad (2.43)$$

where fluid elements are followed during their motion. In isotropic turbulence, only the diagonal components are enough to calculate, then the correlation is written as:

$$R_L^f(\tau) = \frac{1}{3} \langle u_{f,i}(\mathbf{x}_f(t), t) u_{f,i}(\mathbf{x}_f(t + \tau), t + \tau) \rangle \quad (2.44)$$

Time scale related to the Lagrangian correlations is defined as:

$$T_L^f = \frac{1}{R_L^f(0)} \int_0^\infty R_L^f(\tau) d\tau \quad (2.45)$$

which is the timescale during which the eddy completes its rotation. Calculation of Lagrangian correlations faces the same difficulties as the calculation of Eulerian counterparts but in parallel codes, there is also an additional difficulty which is the particles changing the domain from one processor to another. Initial velocities of each particle should be communicated between the processors in order to accurately calculate the Lagrangian correlations.

These correlations need to be calculated using large number of points or fluid elements, arbitrarily located in the flow domain. Nevertheless, the grid points and 200000 fluid elements are used to calculate the Lagrangian and Eulerian properties of the fluid turbulence. Sequential simulations are used to average the correlations (and further statistics) in order to increase the precision of the calculations during  $10T_E$ .

Eulerian and Lagrangian correlations of the flow field obtained using the stochastic forcing are presented in figure 2.5. The Eulerian correlations follow the exponential curve, coherently with the postulate of Tennekes (1975) which supposes that the small scales are transported by the large ones. This, the Eulerian correlations have more rapid decay for small time separations. Therefore, Eulerian correlations take a form closer to the exponential curve than the Lagrangian counterparts. In turn these correlations confine with the Taylor frozen turbulence hypotheses where the Eulerian correlations are exponential and the large scales move with a characteristic velocity  $u'$  of turbulence.

Another time scale  $T_e$  can be associated to an Eulerian timescale during which a large eddy completes its passage with reference to a fix point. Formally it is written as:

$$T_e = \frac{L_f}{u'} \quad (2.46)$$

where  $L_f$  is the characteristic length of the large scales calculated using two-point correlations.

Eulerian two-point correlations in very general form are written as:

$$R_{e,ij}(\mathbf{r}, t) = \langle u_{f,i}(\mathbf{x}, t) u_{f,j}(\mathbf{x} + \mathbf{r}, t) \rangle \quad (2.47)$$

where  $r$  is the separation in any direction in space. In homogeneous stationary turbulence, statistics do not vary with position  $x$  or time  $t$  therefore spatial correlations are the function of separation  $r$  only. Using the isotropy, the two point correlations reduce to longitudinal

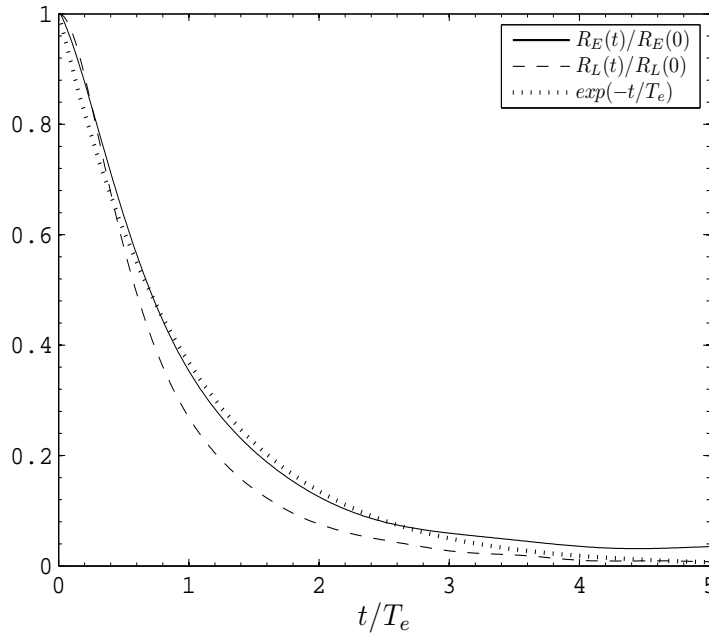


FIGURE 2.5: One-point correlations of the flows obtained with stochastic forcing.

and translational correlations which are written as:

$$f(r) = \frac{1}{3} \frac{\langle u_{f,i}(\mathbf{x}) u_{f,i}(\mathbf{x} + r e_i) \rangle}{u_{f,rms}^2} \quad (2.48)$$

$$g(r) = \frac{1}{3} \frac{\langle u_{f,i}(\mathbf{x}) u_{f,i}(\mathbf{x} + r e_j) \rangle}{u_{f,rms}^2} \quad (i \neq j) \quad (2.49)$$

Using the incompressibility, Karman and Howarth (1938) gives a relation connecting these two correlations. It is written:

$$g(r) = f(r) + \frac{r}{2} \frac{d}{dr} f(r) \quad (2.50)$$

Karman & Howarth relation is verified by the stochastic forcing as seen in figure 2.6. Consistently with the incompressibility condition, the transversal correlations have a negative region after 1 large length scale. Proper isotropy is obtained where the large scales are one-tenth of the length of the domain. Hence the effect of the boundary conditions on the flow field is negligibly small.

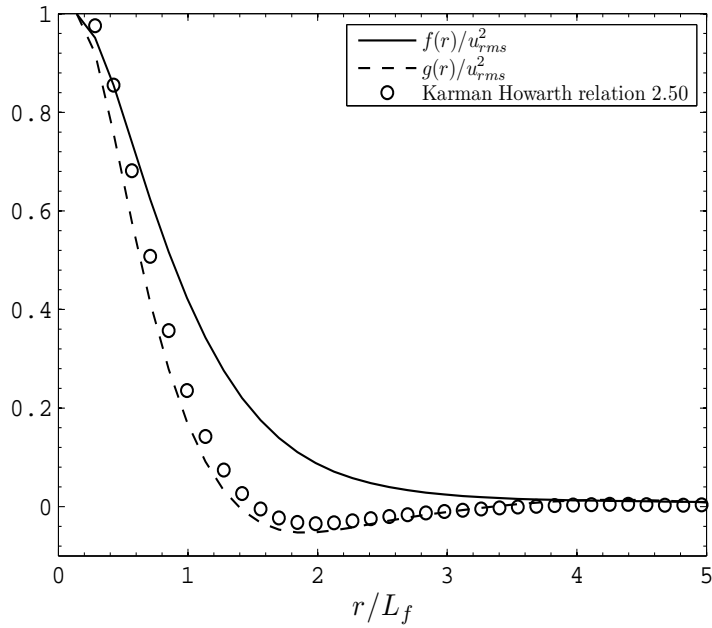


FIGURE 2.6: Two-point correlations of the flows obtained with stochastic forcing.

These two correlations allow the definition of two space scales, namely: longitudinal and transversal large scales. They can be calculated by:

$$L_f = \int_0^{\infty} f(r) dr \quad (2.51)$$

$$L_g = \int_0^{\infty} g(r) dr \quad (2.52)$$

According to the relation of Karman and Howarth, in homogeneous isotropic turbulence, the large scales are related to each other as:

$$\frac{L_f}{L_g} = 2 \quad (2.53)$$

Based on the two-point correlation functions, the Taylor length scale can be calculated as:

$$\lambda_f^2 = \left( -\frac{1}{2} \frac{d^2 f}{dr^2} \right)_{r=0}^{-1} \quad (2.54)$$

$$\lambda_g^2 = \left( -\frac{1}{2} \frac{d^2 g}{dr^2} \right)_{r=0}^{-1} \quad (2.55)$$

In practice, these scales can be calculated using the turbulent kinetic energy and dissipation rate as:

$$\lambda_g = \sqrt{15\nu_f u_{f,rms}^2 / \epsilon} \quad (2.56)$$

Three-dimensional energy spectrum  $E(k, t)$  of turbulence can be calculated from the two-point spatial correlations using the relation:

$$E(k) = \frac{1}{2} \int \int \int u_{f,i}^{TF}(k) u_{f,i}^{TF*}(k) dk \quad (2.57)$$

where  $TF$  is the Fourier transform operator and  $*$  symbol indicates a complex conjugate in complex plane. In forced homogeneous isotropic turbulence, turbulent kinetic energy is evolved by the action of viscosity and the artificial production by the forcing. Time evolution of the turbulent energy spectrum is given as:

$$\frac{\partial E(k, t)}{\partial t} = P(k, t) - 2\nu_f k^2 E(k) \quad (2.58)$$

where  $P(k, t)$  is the production of turbulent kinetic energy which is fulfilled by the forcing algorithm.

The spectrum of the turbulent flow generated by the stochastic forcing is presented in figure 2.7 compared with the experimental measurements in grid turbulence of Comte-Bellot and Corrsin (1971). At the high wavenumber end of the spectrum (small scales), kinetic energy follows concretely the experimental measurements.  $k\eta_K$  parameter is also superior to one which implies a good resolution of the smallest scales of turbulence (Eswaran and Pope, 1988). At the low wavenumber end, the DNS measures are sensibly different than the experimental measures which is related to the forcing scheme. Due to the low Reynolds number of the flow (restricted by DNS), there is no sensible inertial zone. Nevertheless, the stochastic forcing is capable of producing the low wavenumber curvature measured in experiments. This is attributed to the forcing range ( $[2k_0, 6k_0]$ ) which does not introduce any energy to the largest scale.

Further characterization of homogeneous isotropic turbulence is done by analyzing the probability density function (pdf) of the fluctuating velocity. Homogeneous isotropic turbulence is characterized by Gaussian distribution of velocity fluctuations in space. This property is satisfied in all simulations performed. For the sake of keeping place, only the results of the stochastic forcing field will be presented.

Probability distribution of the fluctuating fluid velocities in the flow field generated by the stochastic forcing is presented in figures 2.8 and 2.9. It is clear that the velocity field is

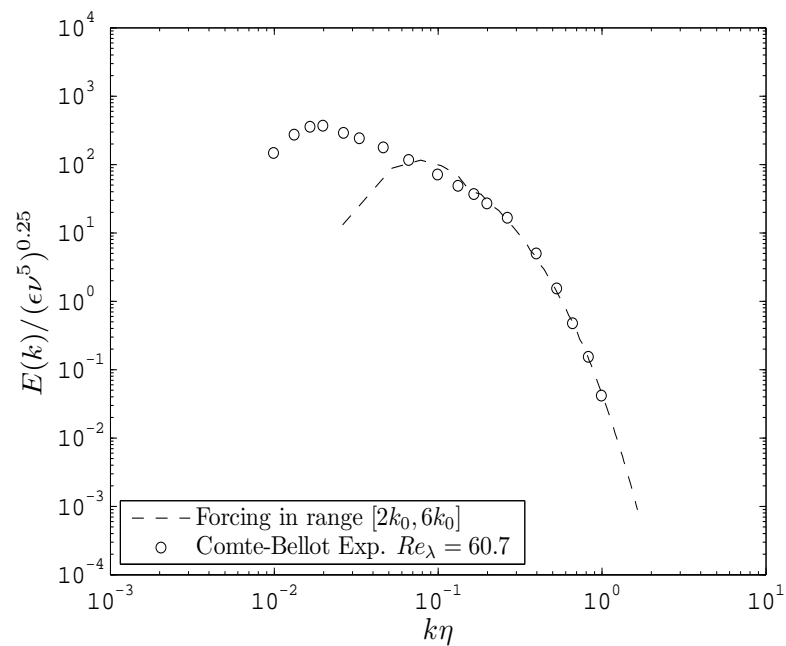


FIGURE 2.7: 3D kinetic energy spectrum of the flow field obtained using stochastic forcing.

characterized by the Gaussian distribution.

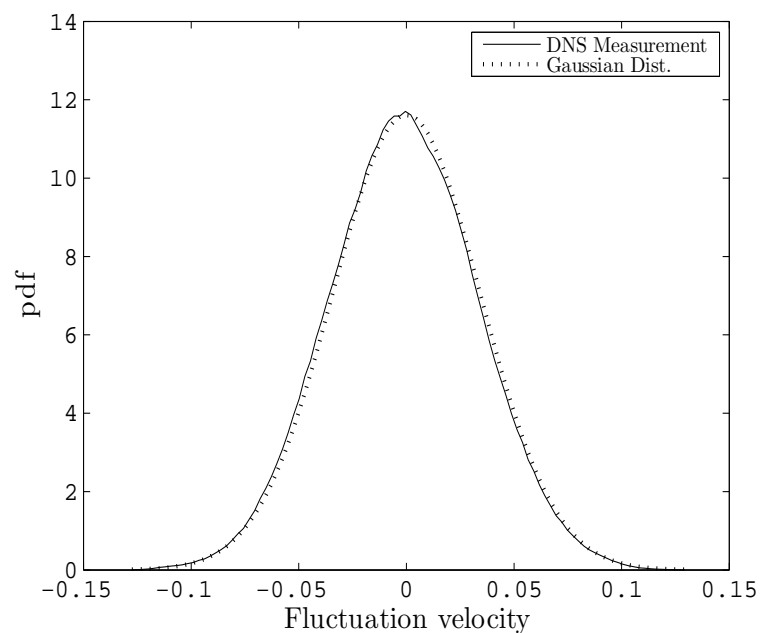


FIGURE 2.8: Probability distribution of the velocity fluctuations of the flow field obtained using stochastic forcing.

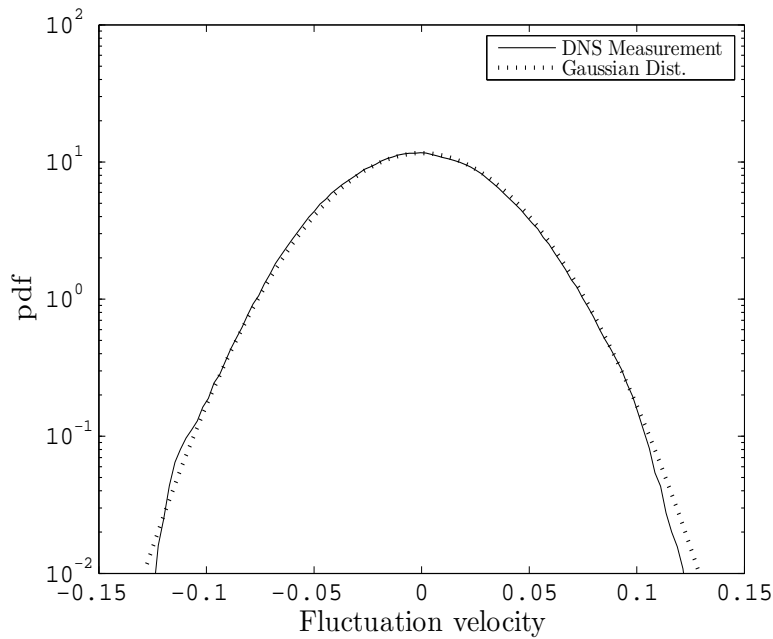


FIGURE 2.9: Probability distribution of the velocity fluctuations of the flow field obtained using stochastic forcing, in logscale.

It is a known fact, however, that the distribution of the longitudinal or transversal velocity gradients deviate from the normal distribution (Gaussian) as seen in figures 2.10, 2.11 and 2.12, 2.13. This deviation is measured using the two parameters; third and fourth order moment of the velocity gradients written as:

$$S_k = \frac{\left\langle \left( \frac{\partial u_{f,i}}{\partial x_i} \right)^3 \right\rangle}{\left\langle \left( \frac{\partial u_{f,i}}{\partial x_i} \right)^2 \right\rangle^{3/2}} \quad (2.59)$$

$$T_k = \frac{\left\langle \left( \frac{\partial u_{f,i}}{\partial x_i} \right)^4 \right\rangle}{\left\langle \left( \frac{\partial u_{f,i}}{\partial x_i} \right)^2 \right\rangle^2} \quad (2.60)$$

Third order moment  $S_k$  indicates the skewness of the pdf around a mean value and they are much encountered in flows with high gradients of turbulence intensity. Fourth order moment  $T_k$  measures the flatness of the pdf and they are encountered widely in turbulent/non-turbulent interface flows such as edge of a free turbulent flow. Skewness different from zero (like in non-gaussian distribution) is a known fact because in realistic turbulence cases, the skewness appears in the production term in the transport equation of vorticity. In order

to generate turbulence, the velocity gradients should be different from zero. This point is largely discussed in the book of Townsend (1956). Since these mechanisms do not exist in the work conducted here, the ordinary values for these variables should be obtained.

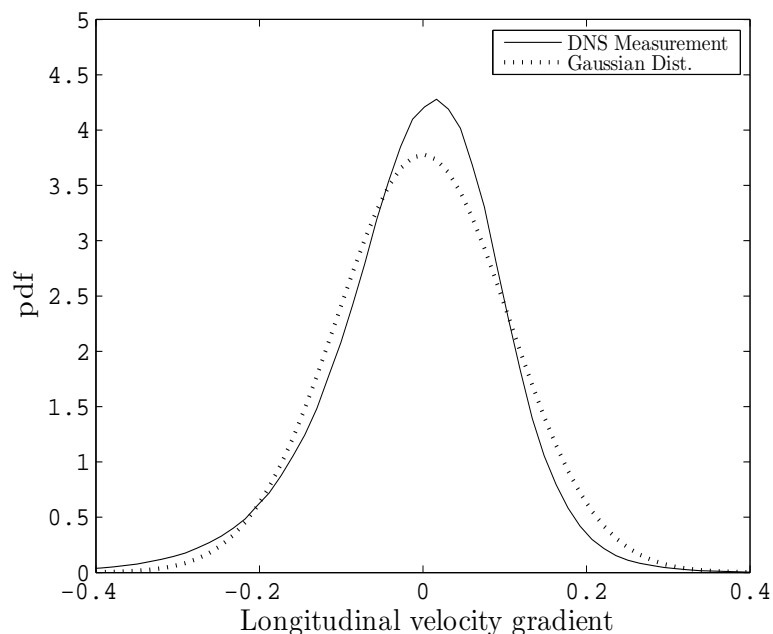


FIGURE 2.10: Probability distribution of the longitudinal derivative of velocity fluctuations of the flow field obtained using stochastic forcing.

As a last point, the values of  $S_k$  and  $T_k$  are well within the range of  $-0.3, -0.4$  and  $3.5, 4.0$ , respectively. Therefore, the stochastic forcing generates kindly good turbulent velocity fields with proper characteristics coherent to a homogeneous isotropic frozen turbulence.

Linear forcing scheme, on the other hand, will be discussed in next chapter.

## 2.4 Initiating the study of two-way coupling

So far, the governing equation for the motion of solid particles have been written under the effect of drag coefficient. The other forces are neglected because of the hypotheses conducted. Then the governing equations for the turbulent flow have been written and the turbulence has been characterized in terms of homogeneous isotropic stationary hypotheses.

As mentioned in the introductory chapter, in most industrial flows, the particles are highly inertial and their effect on the fluid turbulence can not be ignored. Therefore in this section, the study of two-way coupling will be initialized by defining the force acting on the fluid. As will be seen, this force is very difficult to write in exact form which is of many discussions.

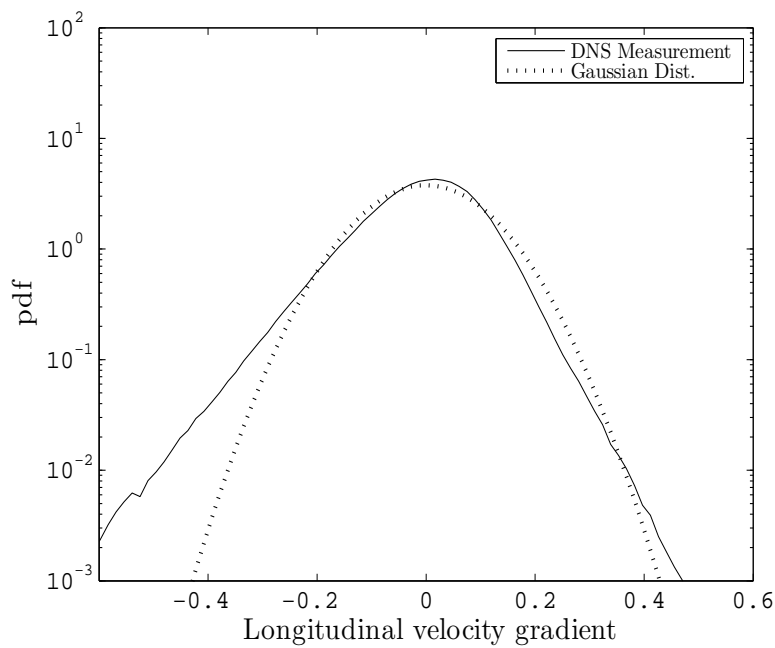


FIGURE 2.11: Probability distribution of the longitudinal derivative of velocity fluctuations of the flow field obtained using stochastic forcing.

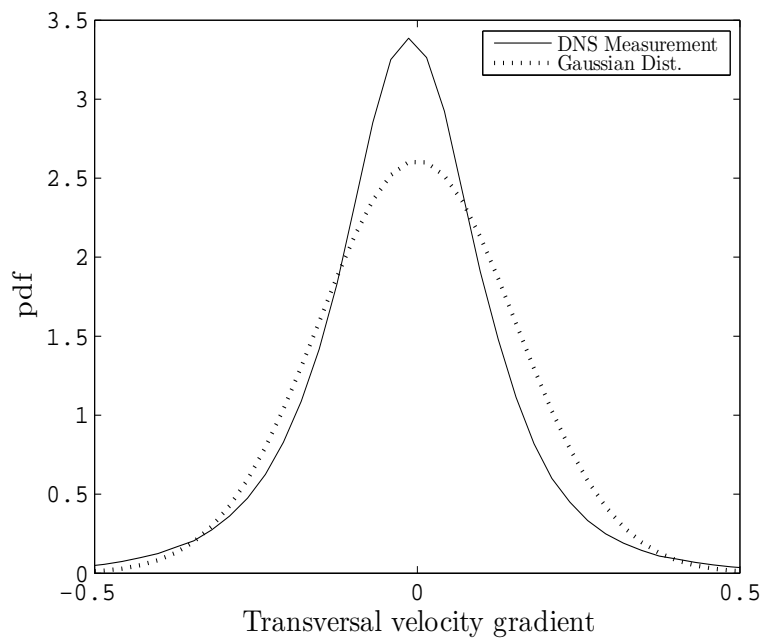


FIGURE 2.12: Probability distribution of the transversal derivative of velocity fluctuations of the flow field obtained using stochastic forcing.

The chapter will end by giving the reference case which is used throughout the thesis for gas-solid flow simulations which are of DNS+DPS type and they are mostly to calculate the

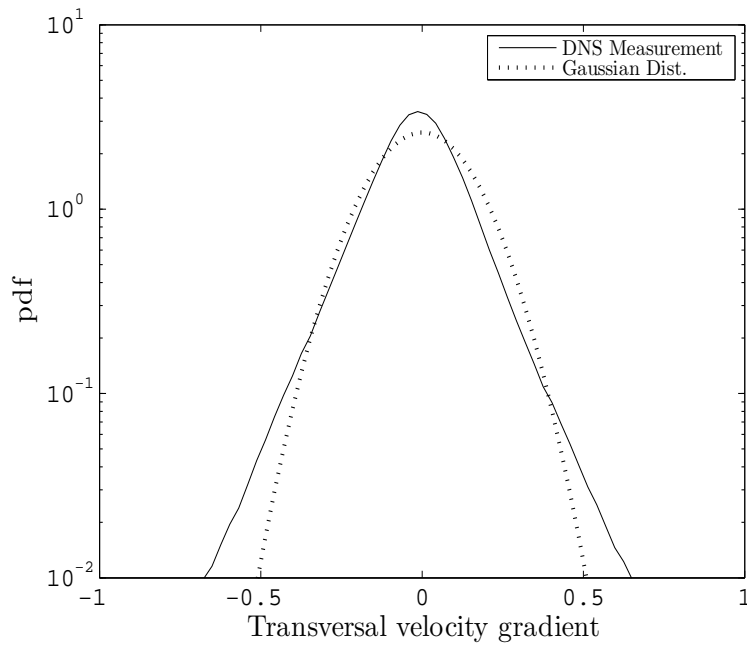


FIGURE 2.13: Probability distribution of the transversal derivative of velocity fluctuations of the flow field obtained using stochastic forcing.

time and spatial correlations of both phases. DNS restricts the highest Reynolds number reachable, nevertheless, the expectation is that the simulations performed should allow the analyze of the basic statistics and correlations and should allow the construction of a database to which models can be compared and tested.

#### 2.4.1 Force acting on the fluid

Turbulence effect on a particle is expressed as a source term in the equation of dynamic motion of particles (equation 2.12). Physically, turbulence sees the particles as sources therefore addition of a term representing this effect to the right hand side of the Navier-Stokes equation suffices. This idea first proposed by Migdal and Agosta (1967). The Navier-Stokes equations are then written as:

$$\frac{\partial u_{f,i}}{\partial t} + u_{f,j} \frac{\partial u_{f,i}}{\partial x_j} = -\frac{1}{\rho_f} \frac{\partial p}{\partial x_i} + \nu_f \frac{\partial^2 u_{f,i}}{\partial x_j^2} + f_i + f_{u_i} \quad (2.61)$$

where  $f_{u_i}$  is the force acting on the fluid in  $i^{th}$  direction due to the particles. In Euler-Lagrange simulations such as simulations conducted in this study, the definition of the back-effect of the particles on the fluid is relatively easy. On one hand, this is because the action-reaction principle of Newton can be used, e.g., the force acting on the particle due to the fluid acts on the fluid with an opposite sign. On the other hand, due to the low volumetric

loading of particles and ideal type turbulence field, no other phenomenon than the two-way coupling is not considered.

Mathematically, the force acting on the fluid is taken into account through the conditions on the surface of the particles where the fluid velocity is equal to the velocity of particle. Therefore a full account of particle's effect on the turbulence requires the resolution of the Navier-Stokes equations around each particle which becomes prohibitive rapidly with increasing particle number in the domain. However, for particles much smaller than Kolmogorov scales, velocity of the particle at its surface can be assumed equal to the velocity at its center. Based on this simplification for very small particles, Crowe et al. (1977) developed the point-source approach in which a punctual force defined at the position of each particle and projected onto the Eulerian grids.

### 2.4.2 Point source approximation

Point source method is based on multipole formulation of the drag force. In Stokes' flow, disturbance induced by inertial particles decays slowly with the distance  $\mathbf{r}$  ( $\mathbf{r} > d_p$ ). As noted by Climent and Maxey (2009), the source term due to the particles  $F_{p,i}$  can be written in multipole expansion as:

$$f_{u_i}(\mathbf{x}, t) = \sum_{n=1}^N \left[ \left( F_i^n + F_{ij}^n \frac{\partial}{\partial x_j} + F_{ijk}^n \frac{\partial}{\partial x_j \partial x_k} + \dots \right) \delta(\mathbf{x} - \mathbf{x}_p^n) \right] \quad (2.62)$$

where  $\delta(\mathbf{x} - \mathbf{x}_p^n)$  is the Dirac delta function and  $\mathbf{x}_p^n$  is the position of  $n^{th}$  particle.

The accuracy of the expression increases with the number of moments included inside the brackets,  $F_i^n$  monopole,  $F_{ij}^n$  dipole,  $F_{ijk}^n$  quadruple and so on (Saffman, 1973, Durlofsky et al., 1987). This expression of the force field was tested in a Stokes' flow with vanishing inertia (very low particle Reynolds number) which is given by the Navier-Stokes equations:

$$0 = -\frac{\partial p}{\partial x_i} + \mu \frac{\partial^2 u_{f,i}}{\partial x_j^2} + \sum_{n=1}^N \left[ \left( F_i^n + F_{ij}^n \frac{\partial}{\partial x_j} + F_{ijk}^n \frac{\partial}{\partial x_j \partial x_k} + \dots \right) \delta(\mathbf{x} - \mathbf{x}_p^n) \right] \quad (2.63)$$

Solution to this equation is given by:

$$u_{f,i}(\mathbf{x}) = u_{f,i}^\infty(\mathbf{x}) + \sum_{n=1}^N \left[ \left( F_i^n + F_{ij}^n \frac{\partial}{\partial x_j} + F_{ijk}^n \frac{\partial}{\partial x_j \partial x_k} + \dots \right) O_{ij}(\mathbf{x} - \mathbf{x}_p^n) \right] \quad (2.64)$$

where  $O_{ij}(\mathbf{x})$  is known as Oseen tensor or Stokeslet (Durlofsky et al., 1987) written as:

$$O_{ij}(\mathbf{x}) = \frac{1}{8\pi\mu} \left( \frac{\delta_{ij}}{\mathbf{r}} + \frac{x_i x_j}{\mathbf{r}^3} \right) \quad (2.65)$$

where  $\delta_{ij}$  is the Kronecker delta function.

Therefore the Oseen tensor indicates that the perturbation of a particle to the fluid field is composed of two terms: one proportional to  $1/\mathbf{r}$  and the other  $1/\mathbf{r}^3$ . The dipole term  $F_{ij}$  is zero because particles do not rotate around their axis. More details on the solution of the perturbation due to a moving body in a small Reynolds number flow can be found in the book of Batchelor (1967). As noted by Koch (1990), for the Stokes' flows and for very small particles in comparison to Kolmogorov scales, only the long range interactions are effective. Using this approximation, all the terms in the above relation except the first order term drop out. Therefore only the first order term which becomes equal to the force  $F_{p,i}$  rests to effect the turbulent field.

$$F_{p,i}^n = F_i^n \quad (2.66)$$

Therefore the force term in Navier-Stokes equation can be written as:

$$f_{u_i} = \left\langle \sum_{n=1}^{N_p} (F_{p,i}^{(n)} \delta(\mathbf{x} - \mathbf{x}^{(n)})) \right\rangle \quad (2.67)$$

In this relation, it is clear that the two-way coupling term is defined at the position of particles. The particles move in a arbitrary manner in the flow domain so that they can be close to the Eulerian nodes or not. To distribute the effect of the particle force on the Eulerian nodes, the PSIC method is going to be used. This scheme takes into account the fact that a particle situating close to a node will largely effect the fluid velocity at this node, but the nodes far will see an effect relatively weak. Therefore the force should be weighted by the distance between the particle and 8 nodes surrounding the particle.

As noted by (Boivin, 1996), this projection can be seen as a filter and can be written for any variable  $\psi$  as:

$$\hat{\psi}(\mathbf{x}, t) = \int_{\Delta} \psi(\mathbf{x}', t) H_{\Delta}(\mathbf{x} - \mathbf{x}') d\mathbf{x} \quad (2.68)$$

where  $H_\Delta$  is spatial low-pass filter which has a characteristic length equal to the grid spacing. The projection operator can be written as:

$$H_\Delta(\mathbf{x} - \mathbf{x}') = \begin{cases} \prod_{i=1}^3 (1 - \xi_i) & (x_i - x'_i) \leq \Delta x_i \\ 0 & (x_i - x'_i) > \Delta x_i \end{cases}$$

where  $\Delta x_i$  is the grid spacing in  $i^{\text{th}}$  direction and  $\xi_i = \left| \mathbf{x} - \mathbf{x}' \right| / \Delta x_i$

### 2.4.3 Reference case for the study

To finish the chapter, the reference flow case which is used in all gas-solid simulations in this work will be presented here. This case will be used as an initial condition for all of the simulations with varying particle properties such as mass-loading, particle material density etc. performed during this thesis. This should allow to observe the evolution of the turbulence properties due to different particle phase conditions such as inertia, number of particles etc... The parametrization of the stochastic forcing is presented in table 2.1. Briefly,  $\sigma_F$  determines the variance of the forcing. Turbulent kinetic energy of the flow generated is directly linked to this parameter. Considering the compressibility of the code used in this study, variance of forcing can not take very large values. Table 2.1 presents the maximum of this parameter with the  $128^3$  DNS simulation.  $T_F$  determines the Eulerian correlation time  $T_E$ . Prescription of this value requires couple of a priori simulations.  $T_F$  is taken equal to the Eulerian eddy passing time  $T_e$  which gives the ratio  $T_E/T_e \approx 1$ . The range of the forced wavenumbers determines directly the length of the large scales,  $L_f$ . Determination of the parameters explained in Février (2000) in more detail.

TABLE 2.1: Parametrization of stochastic forcing for NTMIX3D

Variable	Symbol	Value
Variance of forcing	$\sigma_F$	0,0003523
Characteristic timescale	$T_F$	6,54
Range of wavenumbers forced	–	$[2k_0, 6k_0]$

The characteristics of the reference flow field is given in table 2.2. It should be noted that DNS simulations were conducted for the study in a  $128^3$  cubic domain whose one side is considered  $2\pi$  to simplify the calculation of spatial wavenumbers. Reynolds number of 100 corresponds to sufficiently high turbulence achieved with the configuration. In any case, this flow should provide useful information in order to analyze the fluid-particle interactions in following chapters.

In conclusion, the stochastic forcing generates turbulent flows with more proper characteristics corresponding Taylor frozen turbulence which is homogeneous, isotropic and stationary.

TABLE 2.2: Statistics of the reference monophasic simulation (all numbers are non-dimensional).

Variable	Symbol	Value
Characteristic velocity	$u'$	0,088
Fluid kinetic energy	$q_f^2$	0,0118
Dissipation	$\epsilon$	$7,7 \cdot 10^{-4}$
Turbulent Reynolds number	$Re_L$	100
Taylor Reynolds number	$Re_\lambda$	48
Size of the box	$L_b$	$2\pi$
Longitudinal integral scale	$L_f/L_b$	0,0864
Transversal integral scale	$L_f/L_g$	1,9797
Taylor length scale	$\lambda_g/L_b$	0,0438
Kolmogorov length scale	$\eta_K/L_b$	0,0032
Maximum wavenumber	$k_{max}\eta_K$	1,2608
Eulerian integral timescale / eddy turnover time	$T_E/T_e$	1,02
Lagrangian integral timescale	$T_L^f/T_E$	0,8275
Kolmogorov timescale	$\tau_\eta/T_e$	0,131

The forcing scheme applied to the sufficiently large scales of turbulence is well verified in preceding sections in comparison to the work of Février (2000). Forcing in the range  $[2k_0, 6k_0]$  is already compared to different range of forced wavenumbers by Février (2000) therefore no further comparison will be considered in the following chapters.



## Chapter 3

# Linear deterministic forcing scheme

### 3.1 Introduction

It is stated that the stochastic forcing requires the transformation of the data from spectral space to the physical space which requires the inverse FFT. It is known that in parallel computing environment, the FFT is a delicate case. To overcome this difficulty, an additional processor is considered to perform only the inverse FFT and send the force data to the processors solving the motion of the fluid turbulence. It is direct to ask if any other method can serve faster than the stochastic forcing to force the turbulence with the proper characteristics.

To the purpose of accelerating the code, in this chapter, linear forcing is studied. The idea is to replace the stochastic forcing scheme with the linear forcing scheme which is known to be fast and easy to embed in a code (Rosales and Meneveau, 2005) and therefore to avoid the difficulties encountered in using the stochastic forcing. Then the question stays that, Is linear forcing scheme capable of generating a turbulent flow field with good homogeneity and isotropy?. This question is going to be answered in this chapter in comparison with the stochastic forcing scheme.

Two linear forcing schemes are going to be discussed, one is the initial idea of Lundgren (2003) and the other is the implementation of Toutant (2006). It is going to be seen that both schemes generate turbulent flows pretty far from the homogeneous isotropic turbulence. For the sake of the gas-solid flows in this thesis, the results of this section are going to be judged pragmatically. Therefore, the reasons why these schemes are successful or not will not be discussed in detail.

## 3.2 Physical forcing scheme

### 3.2.1 Linear Forcing Scheme 1

The initial idea of Lundgren (2003) was to use the properties of homogeneous isotropic turbulence, itself, e.g., the turbulence production term in the transport equation written for the fluid velocity fluctuation is indeed linearly proportional to the fluctuation velocity and therefore turbulence can be forced by a term proportional to the fluid fluctuation velocity.

The forcing term in the Navier-Stokes equations can then be written as:

$$f_i = B u_{f,rms} \quad (3.1)$$

where  $B$  is a constant calculated by the relation  $B = \epsilon/3u_{f,rms}^2$  where  $u_{f,rms}^2 = \langle \mathbf{u} \cdot \mathbf{u} \rangle / 3$  is the rms velocity of the turbulence. Prescription of the constant  $B$  and keeping it constant during the simulation impose an eddy turnover time (Rosales and Meneveau, 2005) to the flow. Very low Mach numbers considered in this study permits the calculation of the dissipation rate  $\epsilon$  by considering incompressibility.

### 3.2.2 Linear Forcing Scheme 2

Linear forcing can also be formulated by keeping the turbulent kinetic energy constant and letting the dissipation rate to oscillate. This scheme is implemented first by Toutant (2006) in his thesis. The procedure is to multiply the velocity with a coefficient calculated using the ratio of energy levels of two consecutive time steps. It is written as:

$$u_{f,final}(t) = u(f, t) \sqrt{\frac{q_f^{2^{t-1}}}{q_f^{2^t}}} \quad (3.2)$$

where  $u_{f,final}$  is the velocity at the time  $t$  as  $u_f(t)$ ,  $q_f^{2^t}$  is the fluid turbulent kinetic energy at time  $t$ . This scheme keeps the kinetic energy exactly at the same level.

One important point for the linear forcing is that it effects the entire scales of turbulence and it requires an initial velocity field. However, it is very easy to code and to embed into a numerical code and much less time consuming than spectral forcing.

### 3.3 Parametrization of simulations

Two types of forcing have been implemented in order to compare the results of the linear scheme to the results of spectral forcing scheme. Two initial conditions are considered as:

- Velocity field with Passo-Pouquet spectrum
- Velocity field forced with stochastic forcing

The intention in these tests is to keep the flow statistics obtained using stochastic forcing constant in time via a more feasible scheme. Then Passo-Pouquet scheme will be a test condition to observe the forcing scheme works properly.

#### 3.3.1 Initial condition with Passo-Pouquet spectrum

A solenoidal isotropic velocity field can be generated by the Passo-Pouquet (Passot and Pouquet, 1987) spectrum which is written as:

$$E(k) = \frac{16}{\sqrt{\pi/2}} \frac{u_0^2 k^4}{k_0^5} \exp\left(-\frac{2k^2}{k_0^2}\right) \quad (3.3)$$

where  $u_0^2$  is the initial input rms velocity and  $k_0$  is the wavenumber at which the maximum of  $E(k)$  occurs. These values are arbitrarily chosen as:

$$k_0 = 1 \quad (3.4)$$

$$u_0 = 0.03 \quad (3.5)$$

For this simulation, initial value of  $B$  is 0.011. The parametrization of the stochastic forcing is shown in table 3.1. Initial flow statistics of the flow field are presented in table 3.2.

TABLE 3.1: Parametrization of stochastic forcing to generate initial condition for linear forcing schemes

Variable	Symbol	Value
Variance of forcing	$\sigma_F$	0,000051
Characteristic timescale	$T_F$	20
Range of wavenumbers forced	—	$[2k_0, 6k_0]$

For more details about this spectrum function, interested reader may refer to Boughanem and Trouvé (1996), Vermorel et al. (2003), Rosales and Meneveau (2005).

TABLE 3.2: Statistics of the initial flow field with Passo-Pouquet spectrum

Variable	Symbol	Value
Characteristic velocity	$u'$	0,0294
Fluid kinetic energy	$q_f^2$	0,0013
Dissipation	$\epsilon$	$2,8516 \cdot 10^{-5}$

### 3.3.2 Initial condition with stochastic forcing

A similar flow field to the one for the Passo-Pouquet spectrum is generated with the stochastic forcing scheme. The parameter  $B$  has the value of 0.0135. The characteristics of the flow field are given in table 3.3.

TABLE 3.3: Statistics of the initial flow field with stochastic forcing

Variable	Symbol	Value
Characteristic velocity	$u'$	0,0351
Fluid kinetic energy	$q_f^2$	0,0019
Dissipation	$\epsilon$	$5,0 \cdot 10^{-5}$
Turbulent Reynolds number	$Re_L$	82
Taylor Reynolds number	$Re_\lambda$	40
Size of the box	$L_b$	$2\pi$
Longitudinal integral scale	$L_f/L_b$	0,1
Transversal integral scale	$L_f/L_g$	2,06
Taylor length scale	$\lambda_g/L_b$	0,0516
Kolmogorov length scale	$\eta_K/L_b$	0,0042
Maximum wavenumber	$k_{max}\eta_K$	1,64
Eulerian integral timescale / eddy turnover time	$T_E/T_e$	1,09
Lagrangian integral timescale	$T_L^f/T_E$	0,6816
Kolmogorov timescale	$\tau_\eta/T_e$	0,1257

## 3.4 Results and comparison of the schemes

Quantitative results obtained with the two schemes initialized by the two conditions are presented in tables 3.4 and 3.5. Qualitative analyses are presented in following sections.

### 3.4.1 Turbulent kinetic energy balance

Figure 3.1 presents the evolution of the turbulent kinetic energy for the application of the two linear forcing schemes to two different initial conditions. The initial increase of the

TABLE 3.4: Linear forcing applied to initial velocity field with Passo-Pouquet spectrum

Variable	Symbol	Scheme 1	Scheme 2
Characteristic velocity	$u'$	0,0417	0,0299
Fluid kinetic energy	$q_f^2$	0,0026	0,0013
Dissipation	$\epsilon$	$5,1 \cdot 10^{-5}$	$3,2 \cdot 10^{-5}$
Turbulent Reynolds number	$Re_L$	122	66
Taylor Reynolds number	$Re_\lambda$	55	35
Size of the box	$L_b$	$2\pi$	$2\pi$
Longitudinal macroscale	$L_f/L_b$	0,1339	0,1560
Transversal macroscale	$L_f/L_g$	1,13	2,134
Taylor length scale	$\lambda_g/L_b$	0,0608	0,0545
Kolmogorov length scale	$\eta_K/L_b$	0,0041	0,0046
Maximum wavenumber	$k_{max}\eta_K$	1,6387	1,83
Eulerian integral timescale / eddy turnover time	$T_E/T_e$	1,2865	1,7163
Lagrangian integral timescale	$T_L^f/T_E$	1,0463	0,7
Kolmogorov timescale	$\tau_\eta/T_e$	0,1173	0,1405

TABLE 3.5: Linear forcing applied to initial velocity field generated with stochastic forcing

Variable	Symbol	Scheme 1	Scheme 2
Characteristic velocity	$u'$	0,0552	0,0340
Fluid kinetic energy	$q_f^2$	0,0046	0,0017
Dissipation	$\epsilon$	$1,0 \cdot 10^{-4}$	$4,5 \cdot 10^{-5}$
Turbulent Reynolds number	$Re_L$	163	126
Taylor Reynolds number	$Re_\lambda$	66	40
Size of the box	$L_b$	$2\pi$	$2\pi$
Longitudinal macroscale	$L_f/L_b$	0,1345	0,1685
Transversal macroscale	$L_f/L_g$	1,1127	2,44
Taylor length scale	$\lambda_g/L_b$	0,0548	0,527
Kolmogorov length scale	$\eta_K/L_b$	0,0034	0,0043
Maximum wavenumber	$k_{max}\eta_K$	1,3512	1,6875
Eulerian integral timescale / eddy turnover time	$T_E/T_e$	1,6711	0,9831
Lagrangian integral timescale	$T_L^f/T_E$	0,4736	0,7191
Kolmogorov timescale	$\tau_\eta/T_e$	0,1051	0,0808

turbulent kinetic energy levels up to three times larger values is remarkable for the first scheme 'Linear forcing scheme 1'. High levels of fluctuations in the stationary period are also remarkable. These oscillations should be due to the forcing entire range of scales therefore an enhanced activity of all the scales of turbulence.  $B$  coefficient is calculated in order to control the equilibrium between the kinetic energy production and dissipation. In a settled equilibrium, this parameter prescribed at the beginning of a simulation should be equal to

its value calculated along the simulation. It is presented in figure 3.2 where it is clear that after 30 eddy turnover times, the coefficient recovers its initial fixed value after an initial sudden increase which states that the kinetic energy balance has been settled.

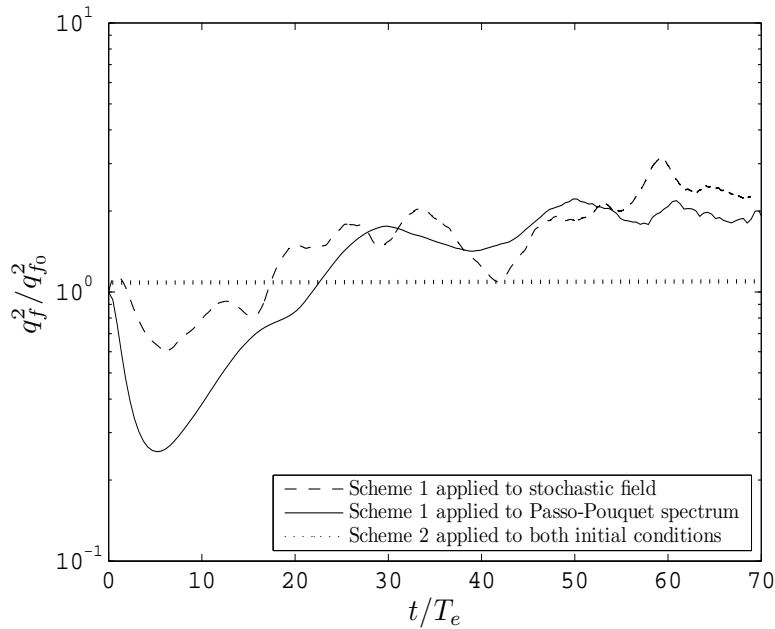


FIGURE 3.1: Turbulent kinetic energy of the flow simulations obtained by linear forcing applied to two initial conditions.

Second forcing scheme 'Linear forcing scheme 2' produces very weak oscillations, as seen on figure 3.1, that evolution of the kinetic energy is rather constant.

Dissipation levels for all the simulations are presented in figures 3.3 and 3.4. Coherently with the initial decrease in kinetic energy, dissipation rate increases initially for the first linear forcing scheme. The second scheme, on the other hand, generates initial increase in the dissipation rates which then return close to its initial value.

For both schemes, the oscillatory stationary periods are remarked which lengthens the necessary period to perform the statistics. For stochastic forcing, statistics performed during  $10T_e$  is enough whereas in first linear forcing scheme, it surely requires more than  $35T_e$ . Nevertheless, the second scheme generates very smooth kinetic energy evolution in time which results in small time period requirement for statistics.

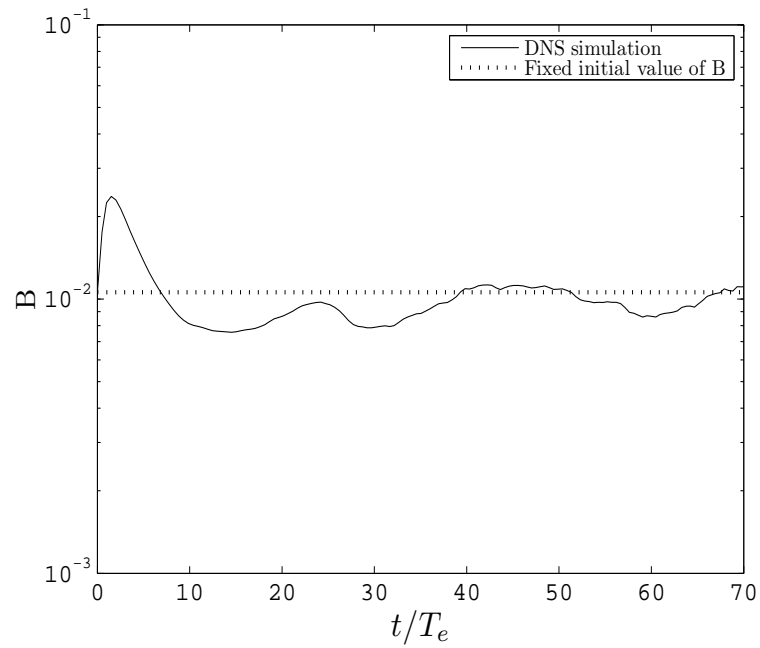


FIGURE 3.2: Coefficient  $B$  for the linear forcing indicating the balance of kinetic energy production and dissipation rates (**scheme 1**).

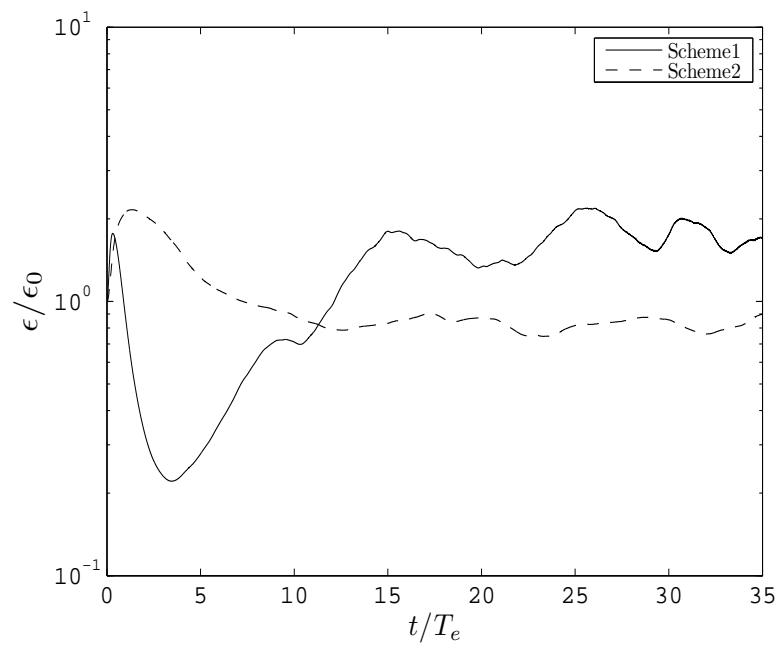


FIGURE 3.3: Turbulent kinetic energy dissipation rate for the flow simulations with **initial Passo-Pouquet** spectrum.

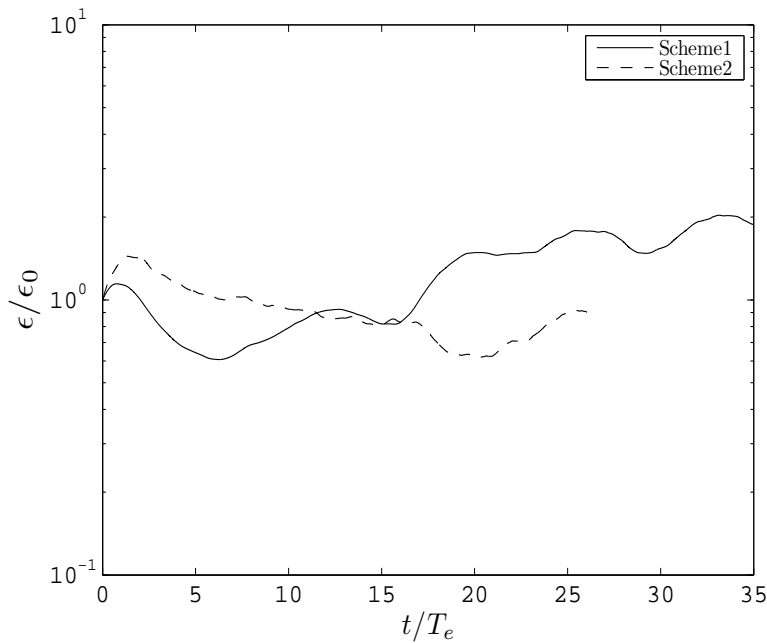


FIGURE 3.4: Turbulent kinetic energy dissipation rate for the flow simulations with **initial stochastic flow field** spectrum.

### 3.4.2 One-point correlations

Figures 3.5 up to 3.8 present the Eulerian and Lagrangian correlations of the simulations performed using the Linear forcing schemes applied to two different initial conditions.

Flow fields obtained using the first linear forcing scheme are seen to have the Eulerian and Lagrangian correlations highly oscillatory. These correlations are averaged over  $30T_E$  which should be large enough to precise calculation of the correlations. The oscillations are basically due to the high fluctuations of the kinetic energy from timestep to timestep (see figure 3.1) using the scheme applying energy to the entire range of eddies. Therefore, to obtain smooth correlation curves, even larger number of realizations is needed which becomes a consuming task.

From the other part, rapid descent of the Lagrangian correlations are well captured in the first scheme, however, the Eulerian correlations do not follow the exponential curve, especially, for the scheme applied to the stochastic field.

The correlation curves of the flows obtained using the second scheme are very smooth and they are converged (see figures 3.7 and 3.8). After a rapid decrease up to 1 or  $2T_e$ , the correlations decrease slowly until zero correlation. Lagrangian correlations are seen to be less dependent on the forcing scheme, however, Eulerian correlations are highly dependent.

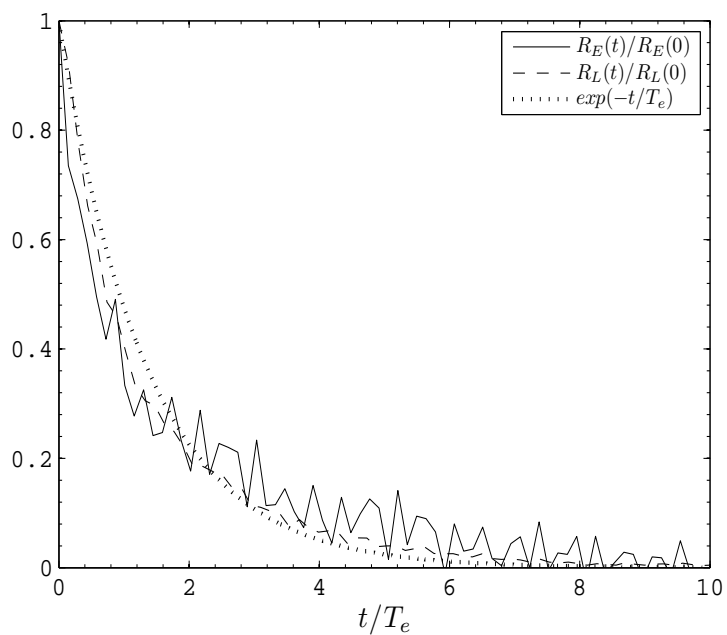


FIGURE 3.5: One-point correlations of the flows obtained with linear forcing, **scheme 1** applied to the **Passo-Pouquet** spectrum initial conditions.

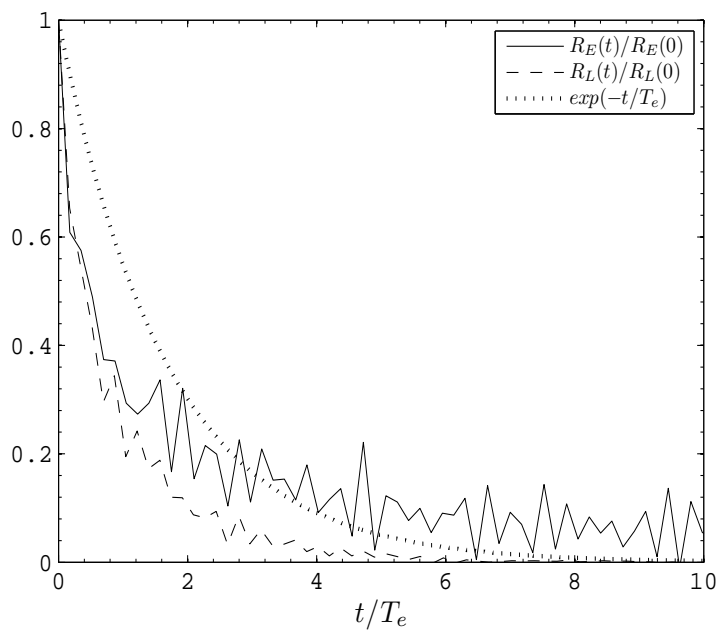


FIGURE 3.6: One-point correlations of the flows obtained with linear forcing, **scheme 1** applied to the **stochastic flow field** spectrum initial conditions.

This is in coherence with the hypothesis of Tennekes (1975) where the fluid elements follow the turbulence at small scales.

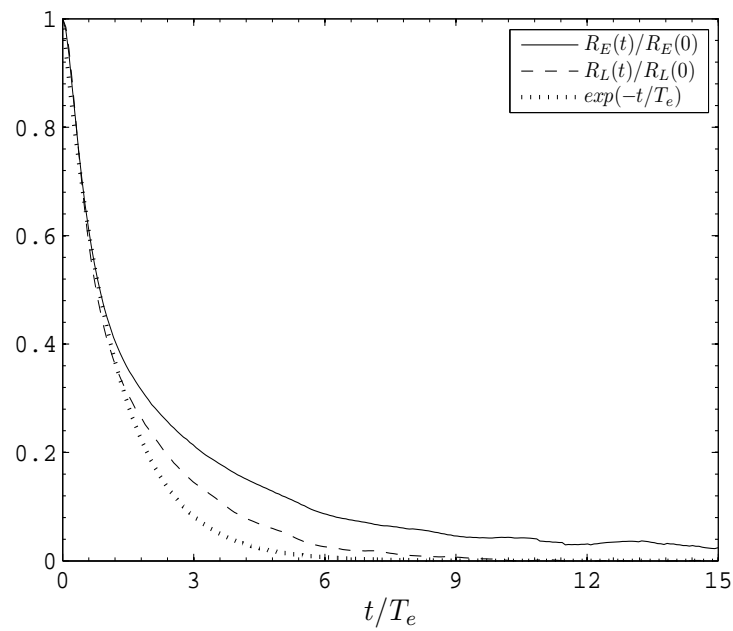


FIGURE 3.7: One-point correlations of the flows obtained with **scheme 2** applied to the **Passo-Pouquet** spectrum initial conditions.

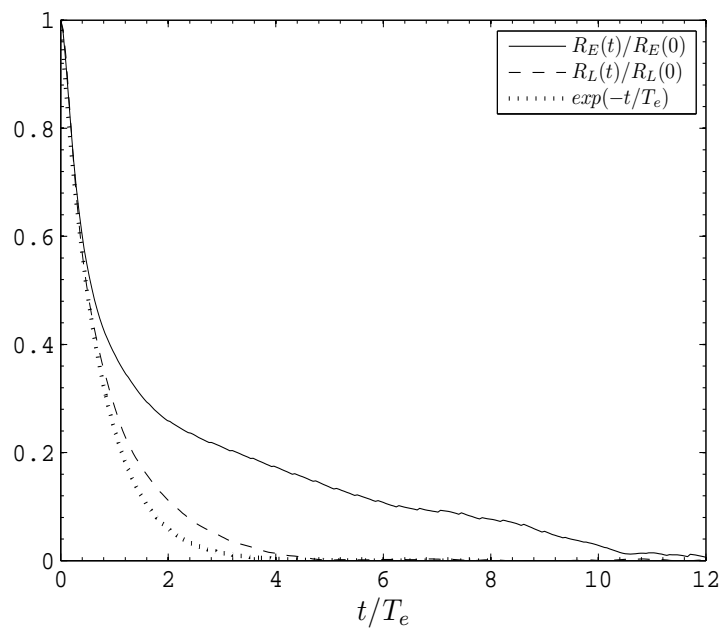


FIGURE 3.8: One-point correlations of the flows obtained with **scheme 2** applied to the **stochastic flow field** initial conditions.

Finally, the decrease in the correlation curves points out a turbulent field with wide range of different eddy sizes. The large scales will be reported at the end of the chapter where the

two-point correlations are analysed along with the spatial spectrum of the turbulent kinetic energy.

### 3.4.3 Two-point correlations

Linear forcing applied to the velocity field with Passo-Pouquet spectrum and to the velocity field obtained by stochastic forcing generates spatial correlations as shown in figures 3.9 and 3.10. It is immediately remarked the increase in the correlations which do not necessarily tend to zero. This increase results in the increase of the length of the longitudinal large scales. It is also to be noted that the longitudinal and transversal length scales tend to each other and the transversal correlation highly deviates from the Karman & Howarth relation by not having a negative region.

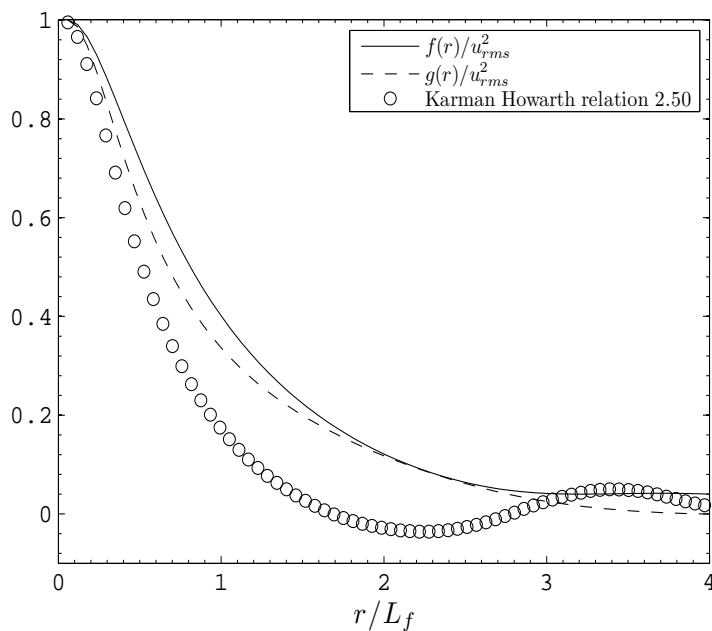


FIGURE 3.9: Two-point correlations of the flows obtained with **scheme 1** applied to **Passo-pouquet** spectrum.

Therefore the large scale in longitudinal and transversal direction become closer in length,  $L_f/L_g \approx 1$ . Isotropy in the domain also decays due to the increased eddy lengths.

The second linear forcing scheme also generates flow fields far from the frozen turbulence (figures 3.11 and 3.12). The longitudinal correlations do not tend to zero and the transversal correlations have a wide negative region therefore not satisfying the Karman & Howarth relation.

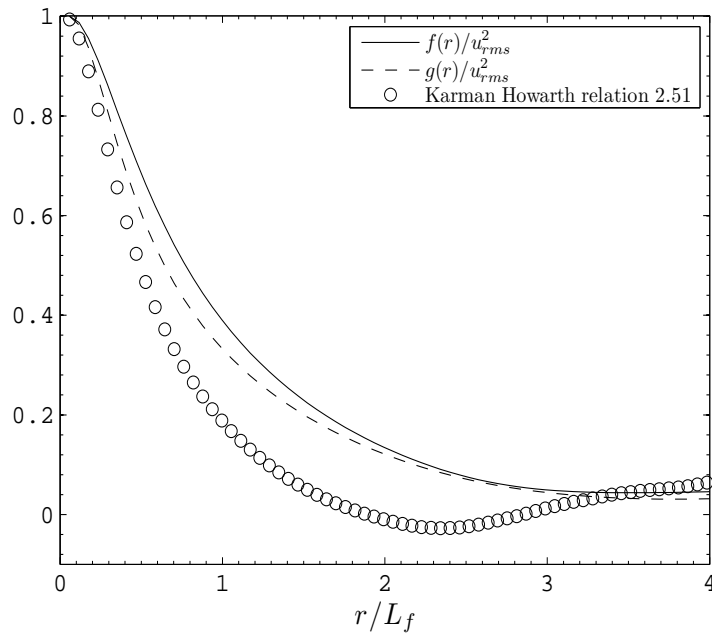


FIGURE 3.10: Two-point correlations of the flows obtained with **scheme 1** applied to **stochastic flow field spectrum**.

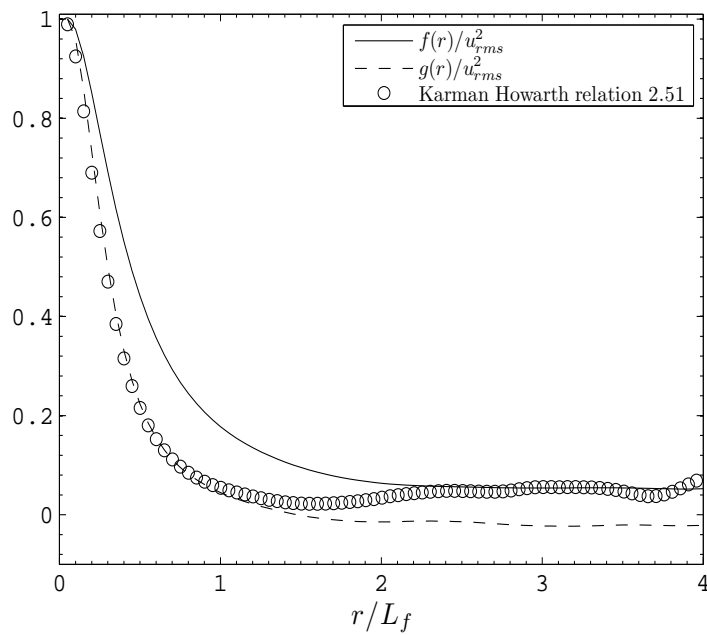


FIGURE 3.11: Two-point correlations of the flows obtained with **scheme 2** applied to **Passo-pouquet spectrum**.

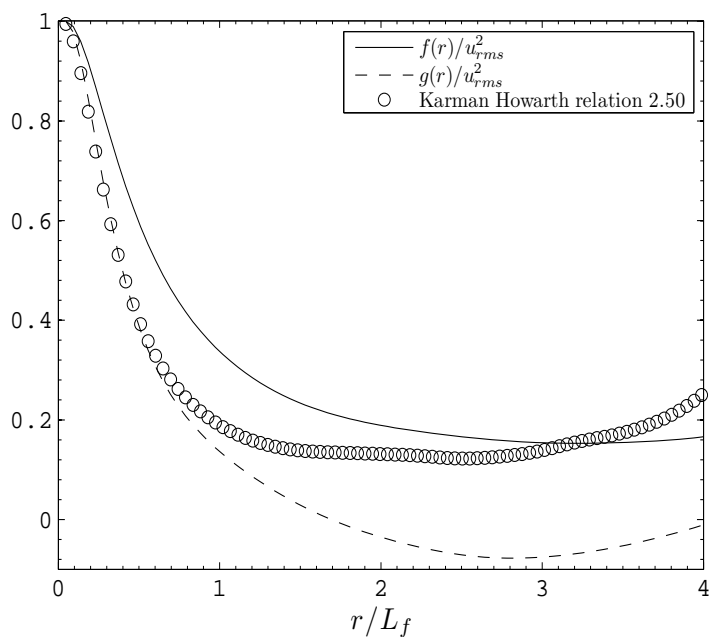


FIGURE 3.12: Two-point correlations of the flows obtained with **scheme 2** applied to **stochastic flow field spectrum**.

### 3.4.4 Spectral analysis

As a final point of the analyses of the turbulence characteristics of the two schemes, spectra of the flow fields obtained are presented in figures 3.13 and 3.14. Deviation from the experimental measurements are visible for the simulations with each initial condition using the first linear forcing scheme and at each wavenumber. First linear forcing scheme increases the turbulent kinetic energy of the flow and the length of the large scales therefore results in higher Reynolds numbers which become unrealistic beyond the capability of DNS simulations with the resolution used in this thesis. In accord with this, the spectra extends to higher values of  $k\eta_K$  parameter (more than 2).

Second linear forcing scheme, on the other hand, generates flow field with more realistic spatial spectra keeping the initial kinetic energy of the flow constant and it seems more advantageous than the first scheme which is highly oscillatory.

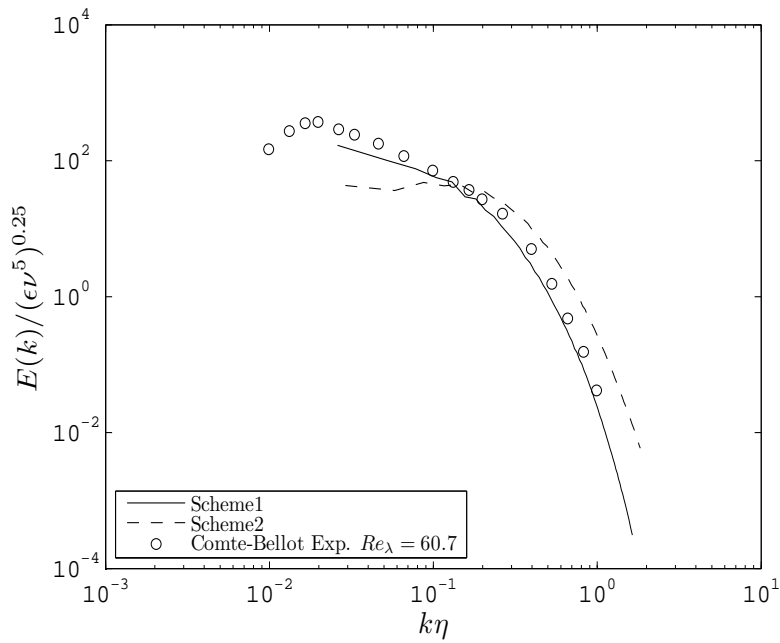


FIGURE 3.13: 3D kinetic energy spectrum of the flow field obtained using linear forcing schemes applied to **Passo-Pouquet** spectrum initial conditions.

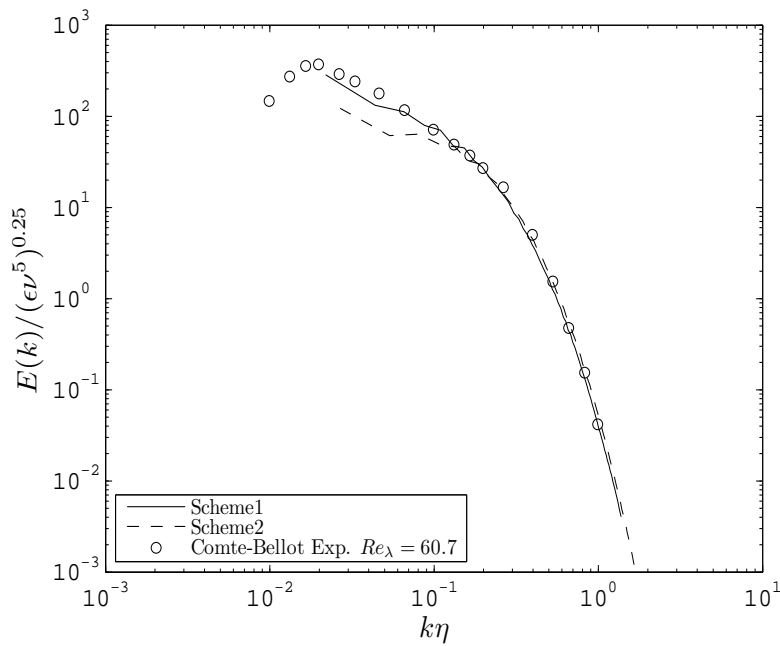


FIGURE 3.14: 3D kinetic energy spectrum of the flow field obtained using linear forcing schemes applied to **stochastic flow field** spectrum initial conditions.

### 3.4.5 Conclusion

Linear forcing scheme proposed by Lundgren (2003) is analyzed in this chapter in order to generate turbulent flow field with proper characteristics. It is shown with the DNS simulations that both linear forcing schemes are capable of generating stationary turbulent quantities, however, the statistical character of turbulence is far from the homogeneous isotropic turbulence. More study should be done in order to improve the schemes.

Due to the pragmatic results of this chapter, it seems that stochastic forcing is more advantageous in terms of turbulence characteristics. It is clear that good turbulent flow field would help analyze the complex effect of solid particles on the structure of the flow. Therefore, the gas-solid simulations are carried out with the turbulence generated by the stochastic forcing scheme.



## Chapter 4

# PDF modeling of gas-solid flows

### 4.1 Introduction

Modeling particulate flows has many interesting applications and one of the leading studies is the work of Prigogine and Herman (1971) who modeled successfully the urban vehicle traffic using the kinetic models. In this model, two phases are formed by the vehicles with rapid motion and the ones with slow motion. In gas-solid flows, the same principle holds and two-fluid models utilize the idea of continuum, which is used for gas or liquid turbulent motion for example, for the two phases of the system. Then a governing equation can be associated to each phase taking into account the principal physical phenomena. Intrinsic interactions between the each phase are taken into account through the interfacial transfer terms.

Two-fluid models are of the family of average models (constructed in Eulerian manner) where an infinitesimal volume, over which the averages are conducted, includes an homogeneous sample of the each phase. Therefore a Lagrangian fluid element in the sense used in monophasic turbulence cannot be defined in two-fluid models because there is not a strict distinction between the two phases. Two-fluid models are not without problems, they face the common drawbacks of the averaged models such as the requirement of universal constants and constitutive equations. Zhang and Roco (1993) notes that these models can describe the true physics of gas-solid flows only partially. Including nature of fluid-particle interactions occurring, which is the subject of this thesis, the nature of these flows is very complicated. Many details of the classical two-fluid models can be found in the book of Ishii (1975).

Buyevich (1971) initiated a probabilistic approach which takes into account different physically important phenomena and therefore avoiding much of the uncertainties of Eulerian modeling. Basically, similar set of equations to the two-fluid models were derived which

takes into account the phenomena such as particle dragging along the turbulence, particle-particle collisions, particle-wall collisions etc... Transport equations were derived for the first three moments of the particle distribution function and closure for the third order moments with a Boussinesq type approximation has been settled. The approach was enhanced by a stochastic Lagrangian equation which takes into account the fluid velocity along the trajectory of solid particles Simonin et al. (1993). Therefore the notion of fluid-particle interactions and turbulent drift velocity, which plays very important role in mean and turbulent momentum transfer between the two phases, were inherently modeled in Lagrangian frame with corresponding transport equations. This model has been shown to produce good results in two-phase jet flows Simonin (1991) and in boundary layer flows (He and Simonin, 1994) and the other works are Simonin et al. (1995), Laviéville (1997).

In this chapter, probabilistic approach will be explained with the derivation of the moment equations of the dispersed phase. First glance at the meaning of the probability functions is needed in this sense.

## 4.2 Statistical description of the particle phase using a probabilistic approach

In the context of this thesis, the mono disperse particles are distributed through the domain and their characterization is done with a probability distribution function in analogy to the kinetic theory of gases. The same idea is also possible polydisperse particles but it is beyond the scope of this thesis (Simonin, 2000). According to the formalism, each particle is represented by a velocity and a position which form the realizations of each particle. Once the particle realizations are settled, a distribution (or equally named probability density) function can be associated.

### 4.2.1 One-point probability density function $f_p$

Imagining a volume element  $dV$  in space inside which a number of particles exists with velocities in the range  $[u + du, v + dv, w + dw]$ , the number of particles within the volume  $dV$  will be proportional to  $dV du dv dw$  and a density function which is also a function  $u, v, w$  and  $t$  time. This density function is said to be the probability density function and it is defined with analogy to the kinetic theory of gases (Jeans, 1946, Chapman and Cowling, 1970, Peirano and Leckner, 1998). It measures the number of particles lying in the ranges of the variables on which the function depends.

More formally, a probability density function (pdf shortly)  $f_p(\mathbf{c}_p; \mathbf{x}, t)$  is introduced in order to characterize the spatial and temporal distribution of particles. It is a one-point, one-time Eulerian pdf of particle velocity  $\mathbf{c}_p$  in phase space and it provides the probability of finding a sphere with its center at  $\mathbf{x}$  and at time  $t$  and with the velocity  $\mathbf{c}_p$ . Accordingly, the number of particle centers at  $\mathbf{x} + d\mathbf{x}$  and with velocity  $\mathbf{c}_p + d\mathbf{c}_p$  is given by:

$$f_p(\mathbf{c}_p; \mathbf{x}, t) d\mathbf{x} d\mathbf{c}_p \quad (4.1)$$

The pdf function completely defines the random variable  $\mathbf{c}_p$  in terms of all the one-point statistics and can be used to calculate the average values of any function depending on the particle properties. This is written as:

$$\langle \Psi \rangle_p(\mathbf{x}, t) = \frac{1}{n_p(\mathbf{x}, t)} \int \Psi(\mathbf{c}_p) f_p(\mathbf{c}_p; \mathbf{x}, t) d\mathbf{c}_p \quad (4.2)$$

for a function  $\Psi$  depending on  $\mathbf{c}_p$ , for example. In this relation,  $n_p$  is the particle number density. As will be seen later on, more random variables are possible to add to this function in order to extend its range but all additional variables come with an extra term in the transport equation.

With analogy to the kinetic theory of gases, particle phase is macroscopically characterized with a number density function,  $n_p(\mathbf{x}, t)$ , which provides the average number of particles per unit volume, with a mean particle velocity  $\mathbf{U}_p(\mathbf{x}, t)$ , and with a kinetic stress tensor,  $\langle u'_{p,i} u'_{p,j} \rangle_p(\mathbf{x}, t)$  where ' symbol indicates a fluctuating variable. These averages can be calculated as:

$$n_p(\mathbf{x}, t) = \int f_p(\mathbf{c}_p; \mathbf{x}, t) d\mathbf{c}_p \quad (4.3)$$

$$\mathbf{U}_p(\mathbf{x}, t) = \frac{1}{n_p(\mathbf{x}, t)} \int \mathbf{c}_p f_p(\mathbf{c}_p; \mathbf{x}, t) d\mathbf{c}_p \quad (4.4)$$

$$\langle u'_{p,i} u'_{p,j} \rangle_p(\mathbf{x}, t) = \frac{1}{n_p(\mathbf{x}, t)} \int [c_{p,i} - U_{p,i}(\mathbf{x}, t)][c_{p,j} - U_{p,j}(\mathbf{x}, t)] f_p(\mathbf{c}_p; \mathbf{x}, t) d\mathbf{c}_p \quad (4.5)$$

Averages of higher order is possible but will not be considered here.

#### 4.2.2 Transport equation for $f_p$

It would not be complementary if this pdf function is not fulfilled with a transport equation which provides its evolution. The first three order moments of the transport equation will then correspond to the continuity  $n_p$ , mean momentum  $\mathbf{u}_p$  and kinetic energy  $\langle u_{p,i} u_{p,j} \rangle$  transport equations of the particle phase.

The pdf function  $f_p$  can be obtained by averaging over a large number  $N_{f\&p}$ , of gas-solid flow realizations,  $H_{f\&p}$ , (Reeks, 1980, Derevich and Zaichik, 1988, Reeks, 1991, Hyland, 1995), as:

$$f_p(\mathbf{c}_p; \mathbf{x}, t) = \lim_{N_{f\&p} \rightarrow \infty} \left[ \frac{1}{N_{f\&p}} \sum_{N_{f\&p}} \sum_{m=1}^{N_p} W_p^{(m)}(\mathbf{c}_p, \mathbf{x}, t, H_{f\&p}) \right] \quad (4.6)$$

where  $N_p$  is the number of particles and  $W_p^{(m)}$  is the fine-grained distribution function defined as:

$$W_p^{(m)}(\mathbf{c}_p, \mathbf{x}, t, H_{f\&p}) = \delta(\mathbf{x} - \mathbf{x}_p^{(m)}(t)) \delta(\mathbf{c}_p - \mathbf{u}_p^{(m)}(t)) \quad (4.7)$$

Here,  $\delta(\cdot)$  is the Dirac delta function. Considering this fine-grained pdf, a transport equation can be derived by taking the time derivative of the fine-grained pdf from equation 4.7 as:

$$\frac{\partial W_p^{(m)}}{\partial t} = - \frac{\partial W_p^{(m)}}{\partial x_i} \frac{dx_{p,i}^{(m)}}{dt} - \frac{\partial W_p^{(m)}}{\partial c_{p,i}} \frac{du_{p,i}^{(m)}}{dt} \quad (4.8)$$

where  $\frac{d}{dt}$  is the derivative following the trajectory of particles.

Let us introduce a conditional average of a Lagrangian particle quantity  $\Psi_p$  with respect to the particle velocity  $\mathbf{u}_p = \mathbf{c}_p$  as:

$$\langle \Psi_p | \mathbf{c}_p \rangle f_p = \lim_{N_{f\&p} \rightarrow \infty} \left[ \frac{1}{N_{f\&p}} \sum_{N_{f\&p}} \sum_{m=1}^{N_p} W_p^{(m)}(\mathbf{c}_p, \mathbf{x}, t, H_{f\&p}) \Psi_p^{(m)}(t) \right] \quad (4.9)$$

By taking the average of the two-sides of the equation 4.8, according to 4.9, it can be written that:

$$\frac{\partial f_p}{\partial t} = - \frac{\partial}{\partial x_j} \left[ f_p \left\langle \frac{dx_{p,j}}{dt} \middle| \mathbf{c}_p \right\rangle \right] - \frac{\partial}{\partial c_{p,j}} \left[ f_p \left\langle \frac{du_{p,j}}{dt} \middle| \mathbf{c}_p \right\rangle \right] \quad (4.10)$$

where the particle trajectory and velocity equations can be replaced by their forms written in Lagrangian frame for  $m^{th}$  particle as:

$$\frac{dx_{p,j}^{(m)}}{dt} = u_{p,j}^{(m)} \quad (4.11)$$

$$\frac{du_{p,j}^{(m)}}{dt} = \frac{F_{p,j}^{(m)}}{m_p^{(m)}} \quad (4.12)$$

This equation is referred as the kinetic pdf transport equation (also can be referred as the

Vlasov<sup>‡</sup> or Liouville<sup>†</sup> type equation) and using the discrete forms written above, it is usually written as:

$$\frac{\partial f_p}{\partial t} + \frac{\partial}{\partial x_j} [c_{p,j} f_p] + \frac{\partial}{\partial c_{p,j}} \left[ \left\langle \frac{F_{p,j}}{m_p} | \mathbf{c}_p \right\rangle f_p \right] = 0 \quad (4.13)$$

where the force term  $\frac{F_{p,j}}{m_p}$  which accounts for all the forces on the particle is averaged conditionally on  $\mathbf{c}_p$  which is shown by the notation  $\langle \cdot | \mathbf{c}_p \rangle$ . Instead of solving the kinetic pdf equation for each particle and averaging, such as the case would be with the equation written for a one-particle pdf in stead of the fine-grained pdf, this equation considers directly the mean terms and for gas-solid flow realizations constitutes a fundamental simplicity.

#### Closure of the kinetic transport equation for $f_p$ :

Equation of discrete particle motion was modeled in chapter 2. Using the equation 2.12, the force term in the equation 4.13 can be written as:

$$\frac{\partial}{\partial c_{p,j}} \left[ \left\langle \frac{du_{p,j}}{dt} | \mathbf{c}_p \right\rangle f_p \right] = \frac{\partial}{\partial c_{p,j}} \left[ \left\langle \frac{u_{f@p,j} - u_{p,j}}{\tau_p} | \mathbf{c}_p \right\rangle f_p \right] \quad (4.14)$$

As can be noted, the calculation of the instantaneous force acting on the particle due to the interactions with the fluid phase requires the Lagrangian temporal derivative of fluid velocity  $\mathbf{u}_{f@p}$  at particle position which is not available a priori. This leads to the requirement of a joint pdf which is handled later on.

The kinetic equation 4.13 can be enhanced by an additional term on the right-hand side accounting for the particle-particle interactions which is largely studied by Boltzmann<sup>\*</sup>.

### 4.2.3 Moment equations of the particle phase

Once the transport equation for the one-point one-time pdf  $f_p$  is given, it is possible to derive the spatially continuum equations of the high-order moments of the pdf function. The statistical moments  $n_p$ ,  $U_{p,i}$  and  $\langle u'_{p,i} u'_{p,j} \rangle_p$  are considered in this thesis. Higher orders are possible but they are very difficult to model.

The general procedure to obtain the mean  $\langle \Psi \rangle_p$  of a function over the particle phase of any function  $\Psi(\mathbf{c}_p)$ , which depends on  $\mathbf{c}_p$ , is composed of the multiplication of the kinetic

<sup>‡</sup>Anatoly Alexandrovich Vlasov, 1908-1975, was a Russian theoretical physicist prominent in the fields of statistical mechanics, kinetics, and especially in plasma physics. He obtained the same transport equation without collisions for a system where the external force is due to the electromagnetic force.

<sup>†</sup>Joseph Liouville, 1809-1882, was a French mathematician who first obtained a kinetic transport equation for a distribution function defined in phase space using a similar to the one presented in equation 4.9.

<sup>\*</sup>Ludwig Eduard Boltzmann, 1844-1906, worked largely on the closure of the collisional term. He committed suicide by hanging himself due to the fact that he was not sharing the same idea about the closure of this term as his contemporaries and this conflict was feeding his malady of rapid mood alternation.

PDF transport equation 4.13 with  $\Psi$  and integrating it over the entire phase space of  $\mathbf{c}_p$ . The pdf  $f_p$  is assumed to have zero value at infinity leading to the simplifications in the derivation procedure.

The general equation derived by the integration method of Enskog<sup>†</sup> and it is written as (Enskog and Sven, 1922, Chapman and Cowling, 1970):

$$\frac{\partial}{\partial t} (n_p \langle \Psi \rangle_p) + \frac{\partial}{\partial x_j} (n_p \langle c_{p,j} \Psi \rangle_p) = n_p \left\langle \frac{du_{p,j}}{dt} \frac{\partial \Psi}{\partial u_{p,i}} \right\rangle_p \quad (4.15)$$

for functions depending on the fluctuating quantities  $\Psi(\mathbf{c}_p - \mathbf{U}_p)$ , it is written as:

$$\begin{aligned} \frac{\partial}{\partial t} (n_p \langle \Psi \rangle_p) + \frac{\partial}{\partial x_j} (n_p \langle c_{p,j} \Psi \rangle_p) = & n_p \left\langle \frac{du_{p,j}}{dt} \frac{\partial \Psi}{\partial u_{p,i}} \right\rangle_p \\ & + n_p \left\langle \left[ \frac{\partial \Psi}{\partial t} + c_{p,j} \frac{\partial \Psi}{\partial x_j} \right] \right\rangle_p \end{aligned} \quad (4.16)$$

These two equations allow access to the moment equations of the dispersed phase and they will be used from now on.

#### 4.2.3.1 Particle number density balance equation, $\Psi = 1$

The particle number density balance equation is obtained by taking  $\Psi = 1$  in the equation 4.16. The equation is written as:

$$\frac{\partial}{\partial t} (n_p) + \frac{\partial}{\partial x_j} (n_p U_{p,j}) = 0 \quad (4.17)$$

In case of coalescence or agglomeration, the right hand side of this equation has additional terms. This equation is analog to the continuity equation written for monophasic fluid flows.

#### 4.2.3.2 Mean momentum balance equation, $\Psi = u_{p,i}$

Mean momentum equation of the particle phase is obtained by taking  $\Psi = u_{p,i}$ . The equation is written as:

$$\begin{aligned} n_p \frac{\partial}{\partial t} U_{p,i} + n_p U_{p,j} \frac{\partial U_{p,i}}{\partial x_j} = \\ \frac{\partial}{\partial x_j} \left[ -n_p \langle u'_{p,i} u'_{p,j} \rangle_p \right] + n_p \left\langle \frac{F_{p,i}}{m_p} \right\rangle_p \end{aligned} \quad (4.18)$$

---

<sup>†</sup>David Enskog, 1884-1947 is a Swedish mathematical physicist.

where the first term on the right hand side is the turbulent transport of mean momentum by the velocity fluctuations and the final term takes into account the exchange of mean momentum with the fluid phase due to the perturbations induced by the particle (due to the two-way coupling). The final term can explicitly be written using the general description of the drag force 2.8 as:

$$n_p \left\langle \frac{F_{p,i}}{m_p} \right\rangle_p = -n_p \left\langle \frac{\rho_f}{\rho_p} \frac{3}{4} \frac{C_D}{d_p} |\mathbf{v}_r| v_{r,i} \right\rangle_p \quad (4.19)$$

where  $C_D$  is the drag coefficient of the particle,  $v_{r,i} = u_{p,i} - u_{f@p,i}$  is the relative velocity between the two phases. The drag coefficient is written as (Schiller and Nauman, 1935):

$$C_D = \frac{24}{Re_p} (1 + 0.15 Re_p^{0.687}) \quad (4.20)$$

For gas-solid flows with uniform property particles in Stokes regime ( $Re_p < 1$ ), the relation 4.19 leads to the simple form:

$$n_p \left\langle \frac{F_{p,i}}{m_p} \right\rangle_p = -n_p \frac{1}{\tau_p} V_{r,i} \quad \frac{1}{\tau_p} = \frac{\rho_f}{\rho_p} \frac{18\nu_f}{d_p^2} \quad (4.21)$$

$V_{r,i} = \langle v_{r,i} \rangle_p$  is the mean relative velocity between the particle velocity and surrounding fluid velocity. The mean relative velocity can be written as:

$$V_{r,i} = [U_{p,i} - U_{f,i}] - V_{d,i} \quad V_{d,i} = \langle u_{f@p,i} - U_{f,i} \rangle_p \quad (4.22)$$

where  $V_{d,i}$  is the so-called fluid-particle turbulent drift velocity. It is measured as a conditional average of the undisturbed fluid velocity with reference to the particle distribution.

$V_{d,i}$  is important in gas-solid flows because it accounts for the turbulent dispersion of particles due to the transport by large turbulent scales (Simonin and Viollet, 1990). It is simply the correlation between the fluctuating fluid velocity field and the particle spatial distribution.

### 4.2.3.3 Particle kinetic stress tensor equation, $\Psi = \langle u'_{p,i} u'_{p,j} \rangle_p$

The final equation of this section concerns the kinetic stress tensor equation attributed to the particle phase which is written as:

$$\begin{aligned}
n_p \frac{\partial}{\partial t} \langle u'_{p,i} u'_{p,j} \rangle_p &+ n_p U_{p,m} \frac{\partial}{\partial x_m} \langle u'_{p,i} u'_{p,j} \rangle_p = \\
&- \frac{\partial}{\partial x_m} \left[ n_p \langle u'_{p,i} u'_{p,j} u'_{p,m} \rangle_p \right] \\
&- n_p \left[ \langle u'_{p,i} u'_{p,m} \rangle_p \frac{\partial U_{p,j}}{\partial x_m} + \langle u'_{p,j} u'_{p,m} \rangle_p \frac{\partial U_{p,i}}{\partial x_m} \right] \\
&+ n_p \left[ \langle \frac{F_{p,i}}{m_p} u'_{p,j} \rangle_p + \langle \frac{F_{p,j}}{m_p} u'_{p,i} \rangle_p \right]
\end{aligned} \tag{4.23}$$

The first term on the right hand side is the triple correlations which is the transport of the kinetic stress tensor by the turbulent particle velocities. It can be modeled using the Boussinesq approximation derived from the third order transport equation of the dispersed phase Simonin (1991).

The second term is the production term by the work of mean velocity gradients on the kinetic stresses.

The third term, on the third line, takes into account the interactions with the fluid phase.

The last term takes into account the turbulent interactions between the particle and fluid phase and it can create or destruct the particle agitation according to the fluid-particle covariance tensor  $\langle u'_{p,i} u'_{f@p,j} \rangle$ . Indeed, this term can be written more explicitly as:

$$\begin{aligned}
n_p \left[ \langle \frac{F_{p,i}}{m_p} u'_{p,j} \rangle_p + \langle \frac{F_{p,j}}{m_p} u'_{p,i} \rangle_p \right] = \\
- \frac{n_p}{\tau_p} \left[ 2 \langle u'_{p,i} u'_{p,j} \rangle_p - \langle u'_{f@p,i} u'_{p,j} \rangle_p - \langle u'_{p,i} u'_{f@p,j} \rangle_p \right]
\end{aligned} \tag{4.24}$$

The particle kinetic stress tensor can be contracted using the isotropy and the particle agitation can be defined as:

$$q_p^2 = \frac{1}{2} \langle u'_{p,i} u'_{p,i} \rangle_p \tag{4.25}$$

In the equation of mean momentum and particle kinetic stress tensor, it has been shown that the fluid statistics viewed by the particles  $\mathbf{u}_{f@p}$  are not present and should be modeled. In literature, different propositions exist for the closure of these quantities such as

the closure of Derevich and Zaichik (1988), Reeks (1991, 1993). Simonin et al. (1993) proposes a Langevin equation using the stochastic description of fluid turbulence to compute the Lagrangian statistics of the fluid phase encountered during the particle trajectories. This equation provides a closure to the fluid-particle joint probability density function (joint pdf) transport equation which will be the subject of the next section.

Once the transport equation is obtained for the joint pdf, the Eulerian continuum equations for the drift velocity  $\mathbf{V}_d$  and the fluid-particle covariance  $q_{fp}$  are possible to be derived.

### 4.3 Statistical description of the system using a joint probabilistic approach

The force acting on the particles can be written in the form:

$$\frac{F_{p,i}}{m_p} = -\frac{u_{p,i} - u_{f@p,i}}{\tau_p} \quad (4.26)$$

and it requires the fluid velocity at the particle position,  $\mathbf{u}_{f@p}$ . The acceleration term in the kinetic PDF transport equation 4.13 requires closure using a fluid velocity pdf conditioned on the particle's velocity,  $\mathbf{c}_p$ . This is formally written as:

$$\left\langle \frac{F_{p,i}}{m_p} | \mathbf{c}_p \right\rangle = \int -\frac{c_{p,i} - c_{f,i}}{\tau_p} f_f(\mathbf{c}_f | \mathbf{c}_p) d\mathbf{c}_f \quad (4.27)$$

where  $f_f(\mathbf{c}_f | \mathbf{c}_p; \mathbf{x}, t)$  is the probability that a particle with a velocity  $\mathbf{c}_p$  views a fluid velocity between the range  $(\mathbf{c}_f, \mathbf{c}_f + d\mathbf{c}_f)$ , at point  $\mathbf{x}$ , at time  $t$ .

#### 4.3.1 One-point joint probability density function $f_{fp}$

According to the probability theory, the conditional probability is classically written as:

$$f_f(\mathbf{c}_f | \mathbf{c}_p; \mathbf{x}, t) = \frac{f_{fp}(\mathbf{c}_f, \mathbf{c}_p; \mathbf{x}, t)}{f_p(\mathbf{c}_p; \mathbf{x}, t)} \quad (4.28)$$

where  $f_{fp}(\mathbf{c}_f, \mathbf{c}_p; \mathbf{x}, t)$  defines the probability density of a particle with a velocity  $\mathbf{c}_p$  and a fluid element with  $\mathbf{c}_f$  are at the position  $\mathbf{x}$  at time  $t$ . The conditional probability function verifies the condition:

$$\int_0^\infty f_f(\mathbf{c}_f | \mathbf{c}_p; \mathbf{x}, t) d\mathbf{c}_f = 1 \quad (4.29)$$

$f_{fp}(\mathbf{c}_f, \mathbf{c}_p; \mathbf{x}, t) d\mathbf{c}_p d\mathbf{c}_f$  gives the number of particles having the velocity in the range  $\mathbf{c}_p, \mathbf{c}_p + d\mathbf{c}_p$  in interaction with fluid elements having velocity in the range  $\mathbf{c}_f + d\mathbf{c}_f$ . This is called the fluid-particle joint probability density function and will open the way for the modeling of the source term in the kinetic transport equation of  $f_p$ . Indeed, the closure of  $f_p$  transport equation depends directly on the closure of  $f_{fp}$  transport equation. From the other part, joint pdf avoids the complicated use of a conditional pdf  $f_f(\mathbf{c}_f|\mathbf{c}_p; \mathbf{x}, t)$  due to the fact that this pdf is not equal to the standard pdf of the fluid velocity  $f_f(\mathbf{c}_f; \mathbf{x}, t)$ .

$$f_f(\mathbf{c}_f|\mathbf{c}_p; \mathbf{x}, t) \neq f_f(\mathbf{c}_f; \mathbf{x}, t) \quad (4.30)$$

Joint pdf can be integrated in the particle velocity space  $d\mathbf{c}_p$  as:

$$f_p(\mathbf{c}_p; \mathbf{x}, t) = \int f_{fp}(\mathbf{c}_f, \mathbf{c}_p; \mathbf{x}, t) d\mathbf{c}_f \quad (4.31)$$

It defines the conditional probability  $f_f(\mathbf{c}_f|\mathbf{c}_p)$  and particle probability function  $f_p$ , leading to the fact that the source term in the kinetic pdf transport equation can be written as:

$$n_p \left\langle \frac{F_{p,i}}{m_p} | \mathbf{c}_p \right\rangle = \int -\frac{c_{p,i} - c_{f,i}}{\tau_p} f_{fp}(\mathbf{c}_f, \mathbf{c}_p) d\mathbf{c}_f \quad (4.32)$$

More interested reader may refer to the thesis of Laviéville (1997).

### 4.3.2 Transport equation for $f_{fp}$

As explained in the previous section, the fluid velocity along the particle trajectory should be provided because it is not available a priori and requires modeling. In fact, in two-fluid models, an additional particle momentum flux occurs due to the fluctuating fluid velocity at the particle position. Two-fluid models are not capable of proposing new models for this flux. Simonin et al. (1993) then considers a stochastic equation in order to propose a Lagrangian model for the fluid velocity along the particle trajectories. Then the transport equation for the joint pdf  $f_{fp}$  could be written and closed with the help of stochastic processes.

The transport equation of  $f_{fp}$  can be derived in the same way as 4.13 written as:

$$\begin{aligned} \frac{\partial f_{fp}}{\partial t} + \frac{\partial}{\partial x_j} [c_{p,j} f_{fp}] + \frac{\partial}{\partial c_{p,j}} \left[ \left\langle \frac{du_{p,j}}{dt} | \mathbf{c}_f, \mathbf{c}_p \right\rangle f_{fp} \right] \\ + \frac{\partial}{\partial c_{f,j}} \left[ \left\langle \frac{du_{f@p,j}}{dt} | \mathbf{c}_f, \mathbf{c}_p \right\rangle f_{fp} \right] \\ = \left( \frac{\partial f_{fp}}{\partial t} \right)_{coll} \end{aligned} \quad (4.33)$$

where the third and the fourth terms on the left hand side are the acceleration terms. The fourth term has a derivative  $d/dt$  of the fluid velocity along the particle trajectory (fluid velocity viewed by the particles) taking into account the forces acting on the fluid element at the particle position. It is to be noted that this derivative is not, in a strict sense, the acceleration of the fluid element, it is the time derivative of the fluid velocity along the particle trajectory.

Along with the transport equation  $f_p$ , interparticle collisions are not considered here, either. Therefore:

$$\left( \frac{\partial f_{fp}}{\partial t} \right)_{coll} = 0 \quad (4.34)$$

The term with  $d\mathbf{u}_p/dt$  can be explicitly written in the same way as in the equation for  $f_p$ . For the term  $d\mathbf{u}_{f@p}/dt$ , stochastic approach of Simonin et al. (1993), Simonin (2000) will be used in this study consistent with the stochastic definition of a turbulent field (Haworth and Pope, 1986). This equation will be extended to the gas-solid flows where the carrier phase is modified by the existence of point particles. In the primitif approach of Simonin et al. (1993), the equation does not hold a term for the two-way coupling effect, e.g., the effect of particles on the fluid viewed. Therefore this effect will be represented by an additional term which is to be modeled.

Once the stochastic equation is closed, the pdf transport equation allows to write the continuum transport equations for the fluid-particle turbulent drift velocity  $\mathbf{V}_d$  appearing in mean momentum equation and fluid-particle velocity covariance  $\langle u'_{p,i} u'_{f@p,j} \rangle$  appearing in the particle kinetic stress tensor transport equation using the moment methods as:

$$n_p \mathbf{V}_d = \int [\mathbf{u}_{f@p} - \mathbf{U}_f] f_{fp}(\mathbf{c}_p, \mathbf{c}_f; \mathbf{x}, t) d\mathbf{c}_f d\mathbf{c}_p \quad (4.35)$$

$$n_p \langle \mathbf{u}'_{f@p} \mathbf{u}'_p \rangle_p = \int [\mathbf{u}_{f@p} - \mathbf{U}_f] [\mathbf{u}_p - \mathbf{U}_p] f_{fp}(\mathbf{c}_p, \mathbf{c}_f; \mathbf{x}, t) d\mathbf{c}_f d\mathbf{c}_p \quad (4.36)$$

## 4.4 Conclusion

In this chapter, no development is performed but only the classical Euler-Euler and probabilistic approach of Simonin et al. (1993) are briely explained. Coherently with the literature, the equations generate terms for the turbulent drift velocity and fluid-particle fluctuation velocity correlation which are not known and should be modeled. In next chapter, Lagrangian stochastic approach is going to be extended to the gas-solid flow cases where the carrier fluid phase is modified by the effect of particles.



## Chapter 5

# Lagrangian stochastic modeling of gas-solid flows with two-way coupling

### 5.1 Introduction

Basic difficulty lying in modeling gas-solid flows is the large turbulence scales' contribution to the particle transport by turbulent drift velocity and the interactions between the two phases giving rise to the fluid-particle velocity covariance (Simonin, 1991). It has been noted that the probabilistic approach closed using the stochastic Lagrangian equation for the fluid velocity along the solid particle trajectory handles naturally these characteristics particularly in gas-solid flows.

The fluid velocity viewed by a particle along its trajectory is the local velocity  $u_{f@p}$  non-perturbed by presence of the particle as if the particle were not at its position (Gatignol, 1983, Maxey and Riley, 1983). However, it is modified by all the surrounding  $N_p - 1$  particles of the system leading to the turbulence modification. Nevertheless, stochastic Langevin equation is modeled neglecting this modification which can lead to discrepancies in flows where the particle phase have large effect on the carrier phase statistics. In this chapter, a compensating term will be added for this effect to the Langevin equation. Such a study was initially performed by Boivin (1996) but with some discrepancies. In this thesis, the two-way coupling term will be modeled with two different approaches with different physical meanings and they will be compared in terms of accounting for turbulent particle dispersion and fluid-particle correlation statistics in the following chapters.

Initially, the basic approach of stochastic Lagrangian type will be introduced and discussed in terms of turbulence modeling (the approach of Haworth and Pope, 1986). It is a statistical method representing a turbulent flow with large number of stochastic elements in Lagrangian manner and it will play a primary role in the developments performed in this thesis which treats discrete solid particles moving in a random Lagrangian manner. From one part, the necessary parameters and topics will be defined and discussed in relation to the stochastic modeling which can treat stochastic processes in two different formulations, a probability distribution point of view and a trajectory point of view. Trajectory point of view will be chosen in this study. From the other part, modeling of the two-way coupling term will be performed and practical relations will be derived from the transport equations of turbulent drift velocity and fluid-particle covariance tensor. The proper modeling should then correspond to the fundamental physical mechanisms in two-way coupled flows.

## 5.2 Lagrangian stochastic approach

Because the turbulence is regarded as superposition of many degrees of freedom, direct numerical computation (DNS) of all the scales is feasible only for ideal and small Reynolds number flows. Thus, as in statistical physics, one is not interested in modeling of the entire range of scales in turbulent flow field but desires some limited information included in a reduced description. From modeling point of view, Lagrangian stochastic approach is based on the probabilistic description of the flow field leading to this purpose. The levels of modeling can be resumed as (Minier and Peirano, 2001):

Navier-Stokes equations: microscopic description

↓

Stochastic equations: mesoscopic description

↓

Mean Reynolds equations: macroscopic description

where the down arrows indicate going to less detailed information about the flow field. Navier-Stokes equations are assumed at the microscopic level containing all the relevant scales of turbulence. However, this level should not be confused with the molecular microscopic approach to turbulent flows where the simple equations define the fluid molecule's kinetic motion. Mean Reynolds equations such as the equation of mean velocity or second

order tensor have a macroscopic (the least detailed) information about the system. Consequently, model equations, which will be improved in this thesis, enter the modeling from the mesoscopic level.

Probabilistic description primarily requires the notion of particles and fields (Minier and Peirano, 2001). Primitively, positions and velocities of all the elements can be collected in a distribution function for which a transport equation is written or another way is to formulate a stochastic equation which defines the trajectory of each particle in the system. Then one can move to derivation of the macroscopic field equations which is generally the final interest of turbulence modeling.

These two possible probabilistic visions of the turbulence field is called the pdf point of view and trajectory point of view, respectively.

### 5.3 Trajectory and PDF point of views

Before going into the detail of the stochastic modeling, some preliminary subjects should be revised briefly.

#### Stochastic process:

A stochastic process, also called random process, is defined as the series of random variables usually indexed by time  $t$ . Randomness is represented by a noise term which would appear in an equation governing the process. A rather general equation in differential form can be given as (Pope, 2002):

$$dX(t) = A(X(t), t)dt + B(X(t), t)dW(t) \quad (5.1)$$

where  $A$  is the drift coefficient and  $B$  is the diffusion coefficient. These coefficients generally depend on the independent variable,  $t$  in this case, and the random variable  $X(t)$ . These coefficients can also be taken as vectors, tensors, etc... Drift term is a deterministic term which is correlated for successive timesteps.  $W(t)$  is the isotropic Wiener process representing the rapid fluctuations or random noise. It is a stochastic term which has zero autocorrelation in time and it gives the equation 5.1 undetermined character. According to this equation, the time evolution of  $X(t)$  is represented by a correlated  $A$  term which determines the propagation of information and an uncorrelated  $BdW$  term which represents the undetermined diffusion of information in probability space.

Solution to the equation 5.1 can be found by integration to find a relation for  $X$  but this is not possible with classical calculus because the stochasticity needs to be treated. Indeed, the

calculus in which the random character is dealt coherently is called stochastic calculus (also called Itô calculus) whose basics were founded by Kiyoshi Itô. Due to the Wiener process, the evolution of  $X(t)$  has infinite variability even for very small time increments which makes  $X(t)$  indifferentially. Therefore Riemann sums are not applicable such as used in classical calculus for the numerical integrals. In the context of stochastic calculus, different limiting process should be applied in order to perform the integration. This will not be discussed here more than this, interested reader can refer to the books of Lemons (2003) and Oksendal (2003).

The basic advantage of the stochastic processes is that the noise term corresponds to introduction of arbitrariness to the evolution of  $X(t)$  which is inherent to many natural phenomena. Deterministic modeling of physical mechanisms can not treat the uncertainty generated by this arbitrariness. To better comprehend the subject, in figure 5.1 an example solution of an ordinary differential equation is given and in figure 5.2, an example solution to a stochastic differential equation is shown where the small rapid oscillations (due to the stochastic term  $W(t)$ ) perturb the evolution (Evans, 2006).

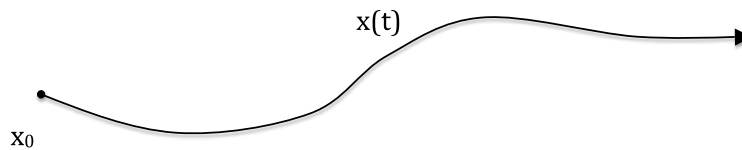


FIGURE 5.1: Solution of an ordinary differential equation follows a smooth line.

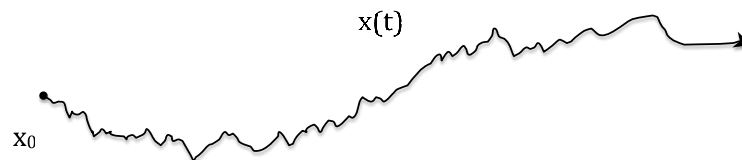


FIGURE 5.2: Solution of a stochastic differential equation is enhanced by random perturbations during very small time separations.

As noted above, the stochastic processes can be realized in two different manners which consider the trajectories of the particles performing random motion and the time evolution of the distribution function of these particles (a pdf function). Consider a random variable  $X(w, t)$  where  $w$  indexes the spatial position, for example, and its sample space is the range  $[x_a, x_b]$ .  $t$  represents time. Two point of views can be imagined as;

- For a fixed time  $t$ , a distribution function  $p(x, t)$  can be associated to the random variable  $X(w)$ ,
- For a fixed  $w$ ,  $X(t)$  is a function in time and represents the trajectory of the process.

In the first option, a governing equation is required in order to obtain the time evolution of the pdf  $p(x, t)$ . This is called pdf point of view and there exists a couple of equations for this task such as forward or backward Kolmogorov equations, Liouville equation and Fokker-Planck equation. In the second option, a particle is tracked in Lagrangian manner and this view is widely used in turbulent fluid element or solid particle dispersion studies (Minier and Peirano, 2001).

### 5.3.1 Trajectory point of view

In trajectory point of view, large number of stochastic particles is introduced into the domain and each is individually tracked by a stochastic equation. The equation imitates the Navier-Stokes equations which are regarded as expressing the trajectory of fluid elements by the relation:

$$dx_i^* = u_{f,i}^* dt \quad (5.2)$$

$$du_{f,i}^* = \left( \frac{1}{\rho_f} \frac{\partial p}{\partial x_i} + \nu_f \frac{\partial^2 u_{f,i}}{\partial x_j^2} \right)^* dt \quad (5.3)$$

The sign \* is to separate the real velocity and the velocity of a stochastic particle. Navier-Stokes equations are accepted at the microscopic level, as explained above, and the method is to write a stochastic trajectory equation for the velocity of a fluid element which should provide the same statistics as the reference equations but with a reduced description.

In contrast to the pdf view in which the purpose is to directly determine the Eulerian and Lagrangian pdfs, in trajectory view, the turbulent statistics are assumed known in order to specify the coefficients of the stochastic equation 5.1. Once these coefficients are determined, one can obtain the Lagrangian pdf using the stochastic equation.

## 5.4 Langevin Equation for monophasic turbulent flows ( $Re_L \rightarrow \infty$ )

Langevin equation is a prototype stochastic differential equation which is used widely for fluid element dispersion in turbulent flows. It models the chaotic motion of a fluid element analogous to Brownian motion observed in molecular movements in rarefied gases as described by kinetic theory. A primary concern for the Langevin equation is the Brownian motion which is first formulated by Einstein and later by Smoluchowski. Paul Langevin in 1908 takes another point of view by considering the same problem and treats the velocity of a fluid element as a stochastic process instead of its position. The common point of view of

these great researchers was that the motion of the particle was pretty far from the inclusion in Newtonian dynamics.

Langevin's insight is that the forces acting on a particle due to the underlying turbulent flow were basically of two types; first a viscous drag which particle experiences during its motion and second a very rapid instantaneous force due to the effect of many collisions of the particle with the other fluid elements (Lemons, 2003).

A rather general form of Langevin equation defining the trajectory of a Lagrangian fluid element is written by Pope and Haworth (1986). The Navier-Stokes equations can be written in Lagrangian form as:

$$\begin{aligned} du_{f,i}(t) = & \left[ -\frac{1}{\rho_f} \frac{\partial P}{\partial x_i} + \nu_f \nabla^2 U_{f,i} \right] dt \\ & + \left[ -\frac{1}{\rho_f} \frac{\partial p'}{\partial x_i} + \nu_f \nabla^2 u'_{f,i} \right] dt \end{aligned} \quad (5.4)$$

and the corresponding Langevin equation is written as:

$$\begin{aligned} du_{f,i}^*(t) \hookrightarrow & \left[ -\frac{1}{\rho_f} \frac{\partial P}{\partial x_i} + \nu_f \nabla^2 U_{f,i} \right] \delta t \\ & + Au'_{f,i} \delta t + B \delta W_i(t) \end{aligned} \quad (5.5)$$

The two last terms of drift and diffusion in Langevin equation are directly recognized analogously to the general stochastic equation 5.1.  $u'_{f,i}$  is the fluctuating velocity of the fluid,  $U_{f,i}$  is the mean velocity,  $P$  is the mean and  $p'$  is the fluctuating pressure. The coefficients  $A$  and  $B$  of the Langevin equation are out of the question for the moment, the stochastic term will be discussed.

$W_i(t)$  is the term corresponding to Wiener process, in honor of Norbert Wiener (1894-1964), which is continuous in time but indifferentiable stochastic process. As shown in figure 5.2, even on very small  $dt$ , the stochastic process  $X_t$  fluctuates enormously and for small increments, Wiener process models the Brownian motion. It is constructed as a random walk model under the family of Markov chains or Markov processes (Andrey Markov, 1856-1922). Markov processes model a memoryless process where the status of the system at the time step  $t + dt$  depends only and only on time step  $t$ , not previous time steps. As a useful detail, the stochastic Langevin equation used in this thesis is appropriate only if the Markov process is continuous in time. There are also dispersion models constructed with discrete Markov chains, however, it is shown by Borgas and Sawford (2000) that they are inconsistent with Kolmogorov hypothesis in homogeneous turbulence.

Wiener process forms the base on which many stochastic differential equations and diffusion processes are constructed. The general properties are given as:

$$\langle \delta W_i \rangle = 0 \quad (5.6)$$

$$\langle \delta W_i \delta W_j \rangle = \delta_{ij} \delta t \quad (5.7)$$

where the process is characterized by zero mean and by  $\delta t$  covariance.

In turbulent flows, use of the Langevin equation has two basic advantages:

- Lagrangian point of view is more adapted to the fluid element turbulent motion.
- Stochasticity adds to the numerical signal representing a certain variable (such as velocity fluctuation at a fix point) a random character which is closer to the real processes observed in nature.

As will be seen later on, these characteristics are also valid for gas-solid flows. Before, it is better to mention about the physical meanings of the terms in Langevin equation.

#### 5.4.1 Drift and diffusion terms in Langevin equation

The first term in Langevin equation  $Au'_f dt$  is the drift term and it is linear in the independent variable  $\mathbf{u}$ . This is why it is called a linear Markov model. The anisotropic deterministic drift tensor  $A$  forms basically the closure for the second order moment models also for the pdf evolution equation (Pope, 1994). Haworth and Pope (1986) notes that this tensor should be modeled in terms of mean quantities such as  $\langle u'_{f,i} u'_{f,j} \rangle$ ,  $\partial U_{f,i} / \partial x_j$ ,  $\epsilon$ . A dimensional analysis indicates that this term has the unit of inverse of time [1/second]. The characteristic time scales can be found using the large scales of turbulent flow and the dissipation time scale. However, Haworth and Pope (1986) notes that no timescale can be extracted from this one point closure therefore  $\epsilon$  is assumed known a priori and they descend to a model of type  $A = f(\partial U_{f,i} / \partial x_j, \langle u'_{f,i} u'_{f,j} \rangle)$ . For statistically stationary, homogeneous isotropic turbulence, the choice of  $A$  is only one which is written as:

$$A = -\frac{1}{T_L^f} \quad (5.8)$$

where the consistency with the exponential decay of the correlation function derived from the Langevin equation is satisfied.

The second term  $B\delta W_i$  models the inertial zone scales, however, not the smallest Kolmogorov scales because Langevin equation is quantitatively incorrect for very small time

separations. As noted by Haworth and Pope (1986), this term is consistent with Kolmogorov first hypothesis and validated using the Lagrangian structure function defined as:

$$D_{L,ij}(s) = \langle [u_{f,i}(t+s) - u_{f,i}(t)][u_{f,j}(t+s) - u_{f,j}(t)] \rangle \quad (5.9)$$

where  $s$  is the time separation. In isotropic turbulence, only the diagonal components are enough to calculate, therefore, the function can be contracted as:

$$D_L(s) = \frac{1}{3} D_{L,ij}(s) \delta_{ij} \quad (5.10)$$

For sufficiently large  $Re_L$  flow, Kolmogorov hypothesis predict for  $T_L^f \gg s \gg \tau_K$  that the Lagrangian structure function is written as:

$$D_L(s) = C_0 \langle \epsilon \rangle s \quad (5.11)$$

where  $C_0$  is the universal Kolmogorov constant and  $\langle \epsilon \rangle$  is the mean dissipation rate of the turbulent kinetic energy. The derivation of the Lagrangian structure function from the Langevin equation 5.5 results in

$$D_L^*(s) = B^2 s \quad (5.12)$$

By comparing the two structure functions, the coefficient  $B$  is obtained as:

$$B = \sqrt{C_0 \epsilon} \quad (5.13)$$

Due to the accepted validity of the Kolmogorov hypothesis for the all kinds of turbulence, this relation should be independent of the flow conditions in sufficiently large  $Re_L$  turbulent flows. However, it has been shown by Pope (2002) that in homogeneous shear flows, the stochastic term,  $B$ , is not locally isotropic and requires modification. It is noted that this could be due to the low Reynolds number of the flow considered in the study. High Reynolds number DNS simulations are needed in order to extract information and conclude on the subject.

To compare the Langevin modeling to the second-order turbulence modeling, the turbulent kinetic energy transport equation derived from the Langevin equation 5.5 should be matched with the transport equation derived from the Navier-Stokes equations. In stationary, homogeneous isotropic turbulence, this matching is written as:

$$\frac{dq_f^2}{dt} = 2Aq_f^2 + \frac{3}{2}C_0\epsilon = 0 \quad (5.14)$$

Using the isotropic form for the closure of  $A$  as  $A = -1/T_L^f$ , the Lagrangian timescale is obtained as:

$$T_L^f = \frac{4}{3C_0} \frac{q_f^2}{\epsilon} \quad (5.15)$$

Thus, the model is valid for the scales of inertial range for a high Reynolds number flow. Extension to the low Reynolds number flows was proposed by Sawford (1991) and will not be considered here (see chapter 7).

It is not possible to separate the drift and diffusion terms to treat them. For example, for very high Reynolds number flows, the molecular diffusion term in Navier-Stokes equation can be assumed equal to zero. Therefore, the pressure gradient will be modeled in both drift and diffusion terms of Langevin equation. Then, it is more proper to note that they model the turbulent spectrum in ensemble.

In the light of all these modeling issues of the two-way coupling terms in Langevin equations, it is fundamental to note that one-to-one matching between the Langevin equation and the Navier-Stokes equations is not possible. It is to say that  $A\mathbf{u}'_f dt$  term can not be referred to model the fluctuating pressure gradients and consequently  $B\delta W_i$  does not model only the viscous effects. They model these effects jointly. As will be more clear in the following sections, this restricts the fact that an additional term, which is supposed to take into account the two-way coupling effect of the particles, needs a rigorous modeling in the sense that effect of particles on what range of fluid scales is not known precisely. This modeling is the subject of the last section of this chapter.

Langevin equation can now be extended to include the particle effects on the fluid element trajectories.

## 5.5 Fluid velocity along the fluid element trajectories in two-way coupled flows

Having explained the basic advantages, Langevin equation will be extended to gas-solid flows where the two-way coupling is significant. As explained in section 5.4, Langevin equation should model the fluid element trajectory as the Navier-Stokes equations which have an additional term for the effect of the particles (see chapter 2). Therefore it is straightforward to add an implicit term to the Langevin equation. The Navier-Stokes equations 2.61 can be

written in Lagrangian form as:

$$\begin{aligned} du_{f,i}(t) = & \left[ -\frac{1}{\rho_f} \frac{\partial P}{\partial x_i} + \nu_f \nabla^2 U_{f,i} \right] dt \\ & + \left[ -\frac{1}{\rho_f} \frac{\partial p'}{\partial x_i} + \nu_f \nabla^2 u'_{f,i} \right] dt + f_{u_i} dt + f_i dt \end{aligned} \quad (5.16)$$

Langevin equation is written as:

$$\begin{aligned} du_{f,i}^*(t) \hookrightarrow & \left[ -\frac{1}{\rho_f} \frac{\partial P}{\partial x_i} + \nu_f \nabla^2 U_{f,i} \right] \delta t \\ & + A_{f,ij} \left( u_{f,j}^*(t) - U_{f,j} \right) \delta t + B_{f,ij} \delta W_j - \Pi_{u_{f,i}}^* \delta t \end{aligned} \quad (5.17)$$

where  $\Pi_{u_{f,i}}^*$  is the two-way coupling term. Form of this term will be kept implicit, for the moment, and will be modeled in the last section. The definition of the problem is that as noted in previous section,  $A_f$  and  $B_f$  models the turbulent spectrum, simultaneously. However, the effect of the particles on the scales of turbulence is known to be very complex and therefore the two-way coupling term should be properly modeled in order to take into account properly the physics of the flow.

The turbulence forcing is taken into account with the  $f_i$  term in Navier-Stokes equations. \* symbol in the Langevin equation is used to separate the stochastic particle's velocity from the real particle's one.

The equations above are for a very general gas-solid flow. The studied flow configuration in this thesis is the forced stationary turbulence which should be represented by one more additional term to the Langevin equation. Nevertheless, this term will not be used to simplify the problem because it also requires modeling which is not obvious a priori. Thus the turbulence forcing effect would be imposed to the drift and diffusion terms of the Langevin equation.

The tensors  $A_{f,ij}$  and  $B_{f,ij}$  is going to be simplified as  $A_f \delta_{ij}$  and  $B_f \delta_{ij}$  because of the isotropy of the flow field. In representing turbulent flows,  $B_f$  is accepted as a coefficient therefore dependance on independent or dependent variables is omitted. As mentioned above, this term has already been validated against the data produced from Lagrangian structure function in the context of Kolmogorov's first hypothesis (Yeung and Pope, 1989).

Thus, the Langevin equation will completely be determined by the coefficients  $A_f$ ,  $B_f$  and the two-way coupling term  $\Pi_{u_{f,i}}^*$ .  $A_f$  and  $B_f$  will be modeled in terms of fluid one-point statistics using the two-way coupling term closed.

### 5.5.1 Autocorrelation function

In homogeneous isotropic turbulence, only one component of the correlations is enough to be calculated. The Lagrangian autocorrelation function of the fluid velocity is defined as:

$$R_{L,ij}^f(t) = \langle u_{f,i}^*(t_0) u_{f,j}^*(t_0 + t) \rangle \quad (5.18)$$

With the assumption of isotropy of the fluid turbulence, only the diagonal components are enough to be calculated, then the correlation function can be written as:

$$R_L^f(t) = \frac{1}{3} R_{L,ij}^f(t) \delta_{ij} \quad (5.19)$$

The differential equation is obtained by performing a change of variables and multiplying the equation 5.17 by  $u_{f,i}^*(t_0)$  and following by an ensemble averaging. It is written as:

$$\frac{dR_L^f(t)}{dt} = A_f R_L^f(t) - \frac{1}{3} \langle u_{f,i}^*(t_0) \Pi_{u_{f,i}}^*(t_0 + t) \rangle \quad (5.20)$$

and the Lagrangian time scale is defined as the integration of  $R_f(t)$ :

$$T_L^f = \frac{1}{R_L^f(0)} \int_0^\infty R_L^f(t) dt \quad (5.21)$$

### 5.5.2 Mean momentum equation

Gas-solid flows with negligible solid particle volumetric fraction ( $\alpha_p \ll 1$ ) are considered in this study. The corresponding mean momentum equation derived from the Navier-Stokes equations 2.61 is written as:

$$\frac{\partial U_{f,i}}{\partial t} + U_{f,j} \frac{\partial U_{f,i}}{\partial x_j} = -\frac{1}{\rho_f} \frac{\partial P}{\partial x_i} + \nu_f \nabla^2 U_{f,i} + D_i + \langle f_{u_i} \rangle \quad (5.22)$$

The term  $D_i$  on the right hand side takes into account the turbulent transport and is written as:

$$D_i = -\frac{\partial}{\partial x_j} \langle u'_{f,i} u'_{f,j} \rangle \quad (5.23)$$

The fourth term represents the two-way coupling effect. It is written in the point-particle approximation as:

$$\langle f_{u_i} \rangle = -\frac{1}{\rho_f} \left\langle \sum_n^{N_p} F_{p,i}^{(n)} \delta(x - x_p^{(n)}) \right\rangle \quad (5.24)$$

where  $F_{p,i}$  is the force exerted by the fluid on a single particle and  $\rho_f$  is the fluid density.  $F_{p,i}$  is written as:

$$F_{p,i} = -m_p \frac{u_{p,i} - u_{f@p,i}}{\tau_p} \quad (5.25)$$

where  $m_p$  is the mass and  $\tau_p$  is the relaxation time of the particles. Inserting the expression (5.25) into the mean drag term, the term  $\langle f_{u_i} \rangle$  can be written as:

$$\langle f_{u_i} \rangle = -\frac{n_p m_p}{\rho_f \tau_p} V_{r,i} \quad (5.26)$$

where  $V_{r,i}$  is the mean relative velocity defined as  $V_{r,i} = U_{p,i} - U_{f,i} - V_{d,i}$ . The last term is the mean of the turbulence forcing effect which is zero due to the stochastic forcing configuration.

The model mean momentum equation corresponding to the Langevin equation 5.17, may be derived in general form as:

$$\frac{\partial U_{f,i}}{\partial t} + U_{f,j} \frac{\partial U_{f,i}}{\partial x_j} = -\frac{1}{\rho_f} \frac{\partial P}{\partial x_i} + \nu_f \nabla^2 U_{f,i} + D_i - \langle \Pi_{u_{f,i}}^* \rangle \quad (5.27)$$

As can be noted, drift and diffusion terms do not appear in the mean flow equations. The second necessary condition for the Langevin equation modeling to be a good approximation is then:

$$\langle \Pi_{u_{f,i}}^* \rangle = -\langle f_{u_i} \rangle \quad (5.28)$$

### 5.5.3 Fluid Reynolds stresses transport equation

It has been noted that the Langevin equation provides closure to the second order moments and the third condition 5.7 relates the second order Reynolds stress equations derived from Navier-Stokes using classical methods and derived from Langevin equation using stochastic calculus. The exact second order Reynolds stress tensor equation derived from the Navier-Stokes equations 2.61 is written as:

$$\frac{\partial \langle u'_{f,i} u'_{f,j} \rangle}{\partial t} + U_{f,m} \frac{\partial \langle u'_{f,i} u'_{f,j} \rangle}{\partial x_m} = D_{f,ij} + P_{f,ij} - \epsilon_{f,ij} + \Pi_{R_{f,ij}} + \langle F_i \rangle \quad (5.29)$$

The first term,  $D_{f,ij}$ , is the turbulent transport of the Reynolds stress by the fluctuating velocity. The second term,  $P_{f,ij}$  is the production term. They are given as:

$$D_{f,ij} = -\frac{\partial}{\partial x_m} \left[ \langle u'_{f,m} u'_{f,i} u'_{f,j} \rangle + \frac{1}{\rho_f} \left( \langle u'_{f,i} p' \delta_{jm} \rangle + \langle u'_{f,j} p' \delta_{im} \rangle \right) \right] \quad (5.30)$$

$$P_{f,ij} = -\langle u'_{f,i} u'_{f,m} \rangle \frac{\partial U_{f,j}}{\partial x_m} - \langle u'_{f,j} u'_{f,m} \rangle \frac{\partial U_{f,i}}{\partial x_m} \quad (5.31)$$

$\epsilon_{f,ij}$  is the dissipation rate and  $\Pi_{R_{f,ij}}$  term is the one taking into account the two-way coupling and it is written as  $\Pi_{R_{f,ij}} = \langle u'_{f,j} f_{u_i} \rangle + \langle u'_{f,i} f_{u_j} \rangle$ .  $\langle F_i \rangle$  is the turbulence forcing term and it can be written as  $\langle F_i \rangle = \langle u'_{f,i} f_j \rangle + \langle u'_{f,j} f_i \rangle$ .

Formally, the last two contributions to the turbulent transport term  $D_{f,ij}$  are separated to form a different term usually symbolized as  $\Phi_{f,ij}$ . They indicate the correlation between the fluid fluctuating velocity and the fluctuating pressure field. The term is written as:

$$\Phi_{f,ij} = -\frac{1}{\rho_f} \left[ \left\langle p' \frac{\partial u'_{f,i}}{\partial x_j} \right\rangle + \left\langle p' \frac{\partial u'_{f,j}}{\partial x_i} \right\rangle \right] \quad (5.32)$$

Physically this term corresponds to the redistribution of the turbulent stresses between the different components of the Reynolds tensor. For the modeling of this term, the reader is referred to the work of Gibson and Launder (1978).

The Reynolds stress tensor equation corresponding to the Langevin model, equation 5.17, is obtained by multiplying the equations written for  $i$  and  $j$  by cross-indexed velocity and then averaging over the fluid phase. It is written as:

$$\begin{aligned} \frac{\partial \langle u'_{f,i} u'_{f,j} \rangle}{\partial t} + U_{f,m} \frac{\partial \langle u'_{f,i} u'_{f,j} \rangle}{\partial x_m} = & D_{f,ij} + P_{f,ij} \\ & + A_f \delta_{im} \langle u'_{f,j} u'_{f,m} \rangle \\ & + A_f \delta_{jm} \langle u'_{f,i} u'_{f,m} \rangle \\ & + B_f^2 \delta_{ij} + \Pi_{R_{f,ij}}^* \end{aligned} \quad (5.33)$$

where  $\Pi_{R_{f,ij}}^* = -\langle u'_{f,j} \Pi_{u_{f,i}}^* \rangle - \langle u'_{f,i} \Pi_{u_{f,j}}^* \rangle$  is the coupling term. It is to be noted that the production term  $P_{f,ij}$  does not include the pressure-velocity correlations.

It should be noted that the symbol  $*$  in  $\mathbf{u}'_f$  is omitted except for the two-way coupling terms, from now on, to impose the fact that the statistics obtained from stochastic modeling should be the same as the ones obtained from Navier-Stokes.

To connect the terms Langevin equation for the fluid element trajectory to the second order closure models, it is fundamental to match the equations 5.29 and 5.33 (Haworth and Pope, 1986). With the necessary simplifications, this matching is written as:

$$0 = \Phi_{f,ij} - \epsilon_{f,ij} + \Pi_{R_f,ij} + \langle F_i \rangle = A_f \delta_{im} \langle u'_{f,j} u'_{f,m} \rangle + A_f \delta_{jm} \langle u'_{f,i} u'_{f,m} \rangle + B_f^2 \delta_{ij} + \Pi_{R_f,ij}^* \quad (5.34)$$

In second order modeling, the triple correlations and all the terms on the right hand side of the equation 5.29 needs to be modeled. However, in the Langevin model, the triple correlation term does not require modeling because it is already determined by the pdf function. In the configuration considered, the relation equals to zero due to the turbulence forcing term, as recognized in the relation 5.34.

This general relation is the one to be satisfied by the stochastic modeling for any kind of turbulent gas-solid flow. Forced turbulence corresponds to the homogeneous and isotropic steady turbulence where the convective, unsteady, turbulent transport and turbulent production terms are zero. It can be inferred that the right hand side of this equation models the fluctuating pressure-velocity correlations, dissipation rate of the turbulent kinetic energy, two-way coupling and the turbulence forcing effect. The necessary condition that the stochastic model has to satisfy is simply written by taking the right hand side of the preceding relation and contracting the indices for isotropic turbulence:

$$2A_f q_f^2 + \frac{3}{2} B_f^2 + \Pi_{q_f^2}^* = 0 \quad (5.35)$$

Here, the last term  $\Pi_{q_f^2}^*$  is the fluid-particle interaction term contracted using the hypothesis isotropy from its general form in equation 5.34. This term is an unknown and should be modeled.

## 5.6 Fluid velocity along the solid particle trajectories

In previous chapter, a transport equation for the fluid-particle joint pdf is written. The equation holds the force terms acting on the particle and on the fluid velocity at the position of the particles. The latter is an unknown and should be modeled in order to close the transport equation.

### 5.6.1 Closure to the Lagrangian derivative term along particle trajectory

In the last two decades, there were some attempts to close the fluid velocity viewed by the particles. Some of them are explained briefly in next paragraph.

Assuming a Gaussian velocity field, Derevich and Zaichik (1988) proposed a model for the net acceleration of a fluid element through the turbulent scales. However, Simonin et al. (1995) points out that this scheme is not consistent when there is shear in the flow considered. Koch (1990) defined an algebraic model assuming isotropic particle motion. This model is restricted to the particle Reynolds numbers ( $Re_p$ ) very small and Stokes numbers very large. Reeks (1992, 1993) derived a closure model taking into account the Lagrangian history effects as described by Kraichnan (1965). All these models are derived without considering a transport equation for the quantity considered and all should be tested against a rigorous experimental data.

Writing a complete transport equation for the fluid-particle turbulent drift velocity and the fluid-particle covariance was first conceived by Simonin et al. (1993). The idea was to write the equations which includes all the possible phenomena such as anisotropy, inhomogeneity, shear etc... Formally, the time derivative of the fluid velocity along the particle trajectory can be written as:

$$\frac{du_{f@p,i}}{dt} \approx \frac{u_{f@p,i}(\mathbf{x} + \mathbf{u}_{p,i}\delta t, t + \delta t) - u_{f@p,i}(\mathbf{x}, t)}{\delta t} \quad \text{with} \quad \tau_\eta \ll \delta t \ll \tau_p \quad (5.36)$$

where  $\tau_\eta$  is the Kolmogorov time scale. The increase of the fluid velocity along the trajectory of a particle can be written with reference to an initial point at  $(\mathbf{x}, t)$ . It is better to relate this velocity first to fluid element motion at time  $t + \delta t$ , first, because the velocity at the fluid element position exists and can be obtained using Navier-Stokes equations whereas fluid velocity at the particle position do not exist. A schematic motion of a fluid element  $f$  and a particle  $p$  is shown in figure 5.3. The velocity of the fluid element at  $(\mathbf{x} + \mathbf{u}_f dt, t + dt)$  can

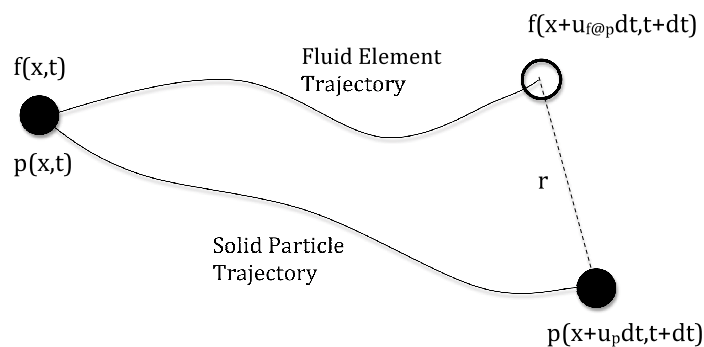


FIGURE 5.3: Deviation of the trajectory of a particle with finite inertia from the trajectory of a fluid element

be written as:

$$\mathbf{u}_{f@p}(\mathbf{x} + \mathbf{u}_p dt, t + \delta t) = \mathbf{u}_{f@p}(\mathbf{x} + \mathbf{u}_{f@p} \delta t, t + \delta t) + \delta \mathbf{u}_{f@p} \quad (5.37)$$

where  $\delta \mathbf{u}_{f@p}$  is the difference between the fluid velocities at time  $t + \delta t$ , at positions of the particle and the fluid element (see the figure). It can be written as:

$$\begin{aligned} \delta \mathbf{u}_{f@p} &= \mathbf{u}_{f@p}(\mathbf{x} + \mathbf{u}_p \delta t, t + \delta t) - \mathbf{u}_{f@p}(\mathbf{x} + \mathbf{u}_{f@p} \delta t, t + \delta t) \\ \delta \mathbf{u}_{f@p} &= \mathbf{U}_f(\mathbf{x} + \mathbf{u}_p \delta t, t + \delta t) + \mathbf{u}'_{f@p}(\mathbf{x} + \mathbf{u}_p \delta t, t + \delta t) \\ &\quad - \mathbf{U}_f(\mathbf{x} + \mathbf{u}_{f@p} \delta t, t + \delta t) - \mathbf{u}'_{f@p}(\mathbf{x} + \mathbf{u}_{f@p} \delta t, t + \delta t) \end{aligned} \quad (5.38)$$

Term  $\mathbf{u}_{f@p}(\mathbf{x} + \mathbf{u}_{f@p} \delta t, t + \delta t)$  in relation 5.38 can be written with reference to the initial value at time  $t$ , e.g., therefore letting the  $\mathbf{u}_{f@p}$  following the particle trajectory to be written with reference to the initial value. With some algebra the final relation is written as:

$$\begin{aligned} \mathbf{u}_{f@p}(\mathbf{x} + \mathbf{u}_p \delta t, t + \delta t) &= \mathbf{u}_{f@p}(\mathbf{x}, t) \\ &\quad + [\mathbf{u}_{f@p}(\mathbf{x} + \mathbf{u}_{f@p} \delta t, t + \delta t) - \mathbf{u}_{f@p}(\mathbf{x}, t)] \\ &\quad + [\mathbf{U}_f(\mathbf{x} + \mathbf{u}_p \delta t, t + \delta t) - \mathbf{U}_f(\mathbf{x} + \mathbf{u}_{f@p} \delta t, t + \delta t)] \\ &\quad + [\mathbf{u}'_{f@p}(\mathbf{x} + \mathbf{u}_p \delta t, t + \delta t) - \mathbf{u}'_{f@p}(\mathbf{x} + \mathbf{u}_{f@p} \delta t, t + \delta t)] \end{aligned} \quad (5.39)$$

This is the classical writing of the increment of the fluid velocity seen by the particle phase (Simonin, 1996, Laviéville, 1997, Peirano and Leckner, 1998).

The first contribution  $[\mathbf{u}_{f@p}(\mathbf{x} + \mathbf{u}_{f@p} \delta t, t + \delta t) - \mathbf{u}_{f@p}(\mathbf{x}, t)]$  is the Lagrangian increment of fluid velocity along the trajectory of a fluid element and can be obtained using the Navier-Stokes equations.  $u_{@p}$  should not be confused here because this contribution follow the motion of the fluid element and the element moves with the velocity  $\mathbf{u}_{f@p}(\mathbf{x}, t)$  to reach its position at  $t + \delta t$ . Formally, Lagrangian increment of the fluid velocity can be written as:

$$[u_{f@p,i}(\mathbf{x} + \mathbf{u}_{f@p} \delta t, t + \delta t) - u_{f@p,i}(\mathbf{x}, t)] = \left[ -\frac{1}{\rho_f} \frac{\partial p}{\partial x_i} + \nu_f \nabla^2 u_{f@p,i}(\mathbf{x}, t) \right] \delta t \quad (5.40)$$

The second contribution  $[\mathbf{U}_f(\mathbf{x} + \mathbf{u}_p \delta t, t + \delta t) - \mathbf{U}_f(\mathbf{x} + \mathbf{u}_{f@p} \delta t, t + \delta t)]$  is the Eulerian increment of the velocity due to the mean velocity difference following the fluid element and the particle. It is usually modeled, by neglecting the spatial gradients of the fluid-particle

turbulent drift velocity  $\partial \mathbf{V}_d / \partial \mathbf{x}$ , as:

$$[\mathbf{U}_f(\mathbf{x} + \mathbf{u}_p \delta t, t + \delta t) - \mathbf{U}_f(\mathbf{x} + \mathbf{u}_{f@p} \delta t, t + \delta t)] = [u_{p,j} - u_{f@p,j}] \frac{\partial U_{f,i}}{\partial x_j} \delta t \quad (5.41)$$

It is to be noted that this term is very important, since the sketch presented above does not consider clearly the effect of the particle inertia or mean drift. Indeed, particle inertia tending to zero  $\tau_p \rightarrow 0$ , the two trajectories become the same. Particles become tracers following perfectly the streamlines. In literature, different decomposition of the fluid and particle velocities in this relation has been performed such as in the studies of Pozorski and Minier (1998), Minier and Peirano (2001). With particles and flow configuration considered in this thesis, the coherence with the past works will be used and the relation 5.41 is chosen for further development.

The third contribution  $[\mathbf{u}'_{f@p}(\mathbf{x} + \mathbf{u}_p \delta t, t + \delta t) - \mathbf{u}'_{f@p}(\mathbf{x} + \mathbf{u}_{f@p} \delta t, t + \delta t)]$  is the Eulerian increment of the fluctuating fluid velocity seen by the particles due to the relative motion between the particle and the fluid element. It takes into account the effect of crossing trajectories effect in presence of mean drift and it requires modeling.

### 5.6.2 Closure by a Langevin type equation in one-way coupled flows

In contrast to the Langevin model for the fluid velocity along the fluid element trajectory, Langevin model for the fluid velocity along the discrete particle trajectory is not founded rigorously. The latter phenomenon is surrounded by difficulties such as relative motion between the two phases which is mentioned in previous section. As demonstrated by the works of Simonin et al. (1993), the relative motion, which occurs under the effect of gravity for example, influences the one-point correlations of fluid velocity seen by the particles. The effect is mentioned under the name of 'crossing trajectories effect'.

Taking into account the relative motion, Simonin et al. (1993) proposed a general Langevin equation which models the contributions  $[\mathbf{u}'_{f@p}(\mathbf{x} + \mathbf{u}_{f@p} \delta t, t + \delta t) - \mathbf{u}'_{f@p}(\mathbf{x}, t)]$  and  $[\mathbf{u}'_{f@p}(\mathbf{x} + \mathbf{u}_p \delta t, t + \delta t) - \mathbf{u}'_{f@p}(\mathbf{x} + \mathbf{u}_{f@p} \delta t, t + \delta t)]$ , simultaneously. The model is written in general form as:

$$\begin{aligned} u_{f@p,i}(\mathbf{x} + u_{p,i} \delta t, t + \delta t) = & u_{f@p,i}(\mathbf{x}, t) \\ & \left[ -\frac{1}{\rho_f} \frac{\partial P}{\partial x_i} + \nu_f \nabla^2 U_{f,i} \right] \delta t \\ & + [u_{p,j} - u_{f@p,j}] \frac{\partial U_{f,i}}{\partial x_j} \delta t \\ & + G_{fp,ij} [u_{f@p,j} - U_{f,j}] \delta t + B_{fp} \delta W_{fp,i} \end{aligned} \quad (5.42)$$

where the second line is the Navier-Stokes equation for the mean fluid velocity but **without two-way coupling term**. The third line is the Eulerian increment in mean fluid velocity due to the relative motion as modeled in section 5.6.1. The last line terms are the basic terms of the Langevin equation which models the increase in the Eulerian and Lagrangian fluctuation velocities together.

$G_{fp,ij}$  is the second order tensor which is modeled in terms of the mean one-point statistics (Haworth and Pope, 1986). Basically,  $G_{fp,ij}$  should be the function of Reynolds stress tensor, mean velocity gradients. The closure for this term can be derived using the monophasic approach.

Following the work of Haworth and Pope (1986), it can be proposed an isotropic form as:

$$G_{fp,ij} = -\frac{1}{T_L^{f@p}}\delta_{ij} \quad (5.43)$$

where  $T_L^{f@p}$  is the Lagrangian timescale of the fluid seen by the particles and  $\delta_{ij}$  is the Kronecker delta function. Simonin et al. (1993) integrates the anisotropy to this relation and proposes the form:

$$G_{fp,ij} = -\frac{1}{T_{L,\perp}^{f@p}}\delta_{ij} - \left[ \frac{1}{T_{L,//}^{f@p}} - \frac{1}{T_{L,\perp}^{f@p}} \right] \beta \quad (5.44)$$

$$\beta = \frac{V_{r,i} V_{r,j}}{|\mathbf{V}_r| |\mathbf{V}_r|} \quad (5.45)$$

where the symbols  $\perp$  and  $//$  indicate timescales in perpendicular and parallel direction to the direction of the relative velocity, respectively. More details can be found in Simonin et al. (1993), Laviéville (1997).

The second term in the third line of the Langevin equation 5.42  $B_{fp}\delta W_{fp,i}$  is the noise term which represents sudden, random effects perturbing the fluid velocity. To be coherent with the Kolmogorov similarity hypothesis, an isotropic model for this term can be written as:

$$B_{fp} = \sqrt{C_0\epsilon} \quad (5.46)$$

According to Haworth and Pope (1986), the general form of the fluid velocity increment along the particle trajectory can be written as:

$$\delta u_{f@p,i} = H_{fp,i}(\mathbf{u}_{f@p}, \mathbf{u}_p)\delta t + B_{fp}\delta W_{fp,i} \quad (5.47)$$

and the Lagrangian derivative of fluid velocity along a particle trajectory can be issued from a general transport equation of Fokker-Planck type. Therefore the source in the joint pdf transport equation 4.33 can be written as:

$$\begin{aligned} \frac{\partial}{\partial c_{f,j}} \left[ \left\langle \frac{du_{f@p,i}}{dt} \middle| \mathbf{c}_f, \mathbf{c}_p \right\rangle f_{fp} \right] &= \frac{\partial}{\partial c_{f,j}} [\langle H_{fp,i}(\mathbf{u}_{f@p}, \mathbf{u}_p) | \mathbf{c}_f, \mathbf{c}_p \rangle f_{fp}] \\ &\quad - \frac{\partial}{\partial c_{f,j}} \left[ \frac{\partial}{\partial c_{f,j}} \left( \frac{1}{2} B_{fp} f_{fp} \right) \right] \end{aligned} \quad (5.48)$$

The joint pdf transport equation can then be used for the derivation of the continuum moment equations. But for the flows that are considered in this thesis, as noted, this equation is going to be extended to the two-way coupling cases which is the subject of next section.

### 5.6.3 Closure by a Langevin type equation in two-way coupled flows

As noted by Peirano and Leckner (1998), the Langevin equation proposed by Simonin et al. (1993) written above is for dilute flows. For the flows where the carrier phase is modified by the particles, the equation should pose an additional term for the effect of particles on the fluid velocity viewed. Using the same reasoning as in section 5.5, a two-way coupling term can equally be added to this equation. The general form of the Langevin model is then written as:

$$\begin{aligned} du_{f@p,i}^*(t) &= \left[ -\frac{1}{\rho_f} \frac{\partial P}{\partial x_i} + \nu_f \nabla^2 U_{f,i} \right] \delta t \\ &\quad + A_{f@p} \delta_{ij} \left( u_{f@p,j}^* - U_{f,j} \right) \delta t + B_{f@p} \delta_{ij} \delta W_j - \Pi_{u_{f@p,i}}^* \delta t \\ &\quad + (u_{p,j} - u_{f@p,j}^*) \frac{\partial U_{f,i}}{\partial x_j} \delta t \end{aligned} \quad (5.49)$$

where  $f@p$  denotes the quantity of fluid at the position of the particle. Apart from the terms already explained above for the fluid element equation, the last term in this equation accounts for the deviation of the particle trajectory from the fluid element trajectory.

For a recapitulation, it must be said that the  $u_{f@p}$  is the unperturbed fluid velocity at the particle position but it is perturbed by the effect of all the other particles of the system, especially by particles surrounding the particle in question. The same form could be considered for the two-way coupling term in this equation as the one in the equation 5.17 for the fluid velocity along fluid element trajectories by analogy.

This equation is going to serve to derive the turbulent drift velocity transport equation and the fluid-particle fluctuating velocity covariance equation. Equally, it provides a comprehensive closure for the source term in the joint pdf transport equation. However, because the

trajectory point of view has been adapted in this study (see section 5.3), the first and second moment equations will be derived from this stochastic equation using stochastic calculus.

#### 5.6.4 Fluid autocorrelation function seen by the particles, $R_L^{f@p}$

Differential equation governing the autocorrelation function of the fluid fluctuating velocity along the solid particle trajectories can be derived using the equation 5.49. The autocorrelation is defined as:

$$R_{L,ij}^{f@p}(t) = \left\langle u_{f@p,i}^{*'}(t_0) u_{f@p,ij}^{*'}(t_0 + t) \right\rangle_p \quad (5.50)$$

For homogeneous isotropic turbulence, it can be written:

$$R_L^{f@p} = \frac{1}{3} R_{L,ij}^{f@p} \delta_{ij} \quad (5.51)$$

Contracting the equation 5.49,  $i = j$ , and multiplying it by  $u_{f@p,i}^*(t + t_0)$ , the differential equation can be written as:

$$\frac{dR_L^{f@p}(t)}{dt} = A_{f@p} R_L^{f@p}(t) - \frac{1}{3} \left\langle u_{f@p,i}^{*'}(t_0) \Pi_{u_{f@p,i}}^*(t_0 + t) \right\rangle_p \quad (5.52)$$

The integration of this autocorrelation function will give the Lagrangian timescale of the fluid seen by the particles as:

$$T_L^{f@p} = \frac{1}{R_L^{f@p}(0)} \int_0^\infty R_L^{f@p}(t) dt \quad (5.53)$$

#### 5.6.5 Drift velocity transport equation, $V_d$

Fluid-particle turbulent drift velocity is defined as the mean fluid fluctuation velocity seen by the particles, written as  $V_{d,i} = \left\langle \left( u_{f@p,i}^* - U_{f,i} \right) \right\rangle_p$ . Written in the two-fluid formalism, this mean fluctuation velocity is not zero because of the existence of a correlation between the fluid fluctuation velocity field and the spatial distribution of particles. The transport equation governing the turbulent drift velocity is derived by the subtraction of the exact mean fluid velocity equation 5.22 obtained from the Navier-Stokes equations, the transport equation for the mean fluid velocity seen by the particles obtained from the Langevin equation 5.49, and

it is written as:

$$\begin{aligned}
n_p \frac{\partial V_{d,i}}{\partial t} + n_p U_{p,j} \frac{\partial V_{d,i}}{\partial x_j} = & -n_p \frac{\partial \langle u'_{f@p,i} u'_{p,j} \rangle_p}{\partial x_j} + n_p \frac{\partial \langle u'_{f,i} u'_{f,j} \rangle}{\partial x_j} \\
& - \langle u'_{f@p,i} u'_{p,j} \rangle_p \frac{\partial n_p}{\partial x_j} - n_p V_{d,j} \frac{\partial U_{f,i}}{\partial x_j} \\
& + n_p A_{f@p} V_{d,i} - n_p \langle \Pi_{u_{f@p,i}}^* \rangle_p - n_p \langle f_{u_i} \rangle
\end{aligned} \tag{5.54}$$

First two terms on the right hand side of the equation take into account the turbulent transport. The third and fourth terms are the production terms due to the particle density gradients and the mean fluid velocity gradients, respectively. The fifth and sixth terms originate in the Langevin equation 5.49 and take into account the fluid acceleration at the particle position and two-way coupling effects, respectively. The final term is the two-way coupling term originating from the mean momentum equation 5.22.

### 5.6.6 Transport equation for fluid Reynolds stresses seen by the particles,

$$\langle u'_{f@p,i} u'_{f@p,j} \rangle_p$$

A transport equation for the Reynolds stresses seen by the particles can be derived from the Langevin model, equation 5.49, it is obtained by multiplying the equations written for  $i$  and  $j$  by cross-indexed velocity and then averaging over the particle phase. It is written as:

$$\begin{aligned}
n_p \frac{\partial \langle u'_{f@p,i} u'_{f@p,j} \rangle_p}{\partial t} + n_p U_{p,m} \frac{\partial \langle u'_{f@p,i} u'_{f@p,j} \rangle_p}{\partial x_m} = & D_{f@p,ij} + P_{f@p,ij} \\
& + n_p A_{f@p} \langle u'_{f@p,j} u'_{f@p,i} \rangle_p \\
& + n_p A_{f@p} \langle u'_{f@p,i} u'_{f@p,j} \rangle_p \\
& + n_p B_{f@p}^2 \delta_{ij} + \Pi_{R_{f@p,ij}}^*
\end{aligned} \tag{5.55}$$

where the two-way coupling term is given as:

$$\Pi_{R_{f@p,ij}}^* = -n_p \langle u'_{f@p,j} \Pi_{u_{f@p,i}}^* \rangle_p - n_p \langle u'_{f@p,i} \Pi_{u_{f@p,j}}^* \rangle_p \tag{5.56}$$

and the turbulent dispersion and production terms are given as:

$$D_{f@p,ij} = -\frac{\partial}{\partial x_m} n_p \langle u'_{f@p,m} u'_{f@p,i} u'_{f@p,j} \rangle_p \tag{5.57}$$

$$P_{f@p,ij} = -n_p \langle u'_{f@p,i} u'_{f@p,m} \rangle_p \frac{\partial U_{f,j}}{\partial x_m} - n_p \langle u'_{f@p,j} u'_{f@p,m} \rangle_p \frac{\partial U_{f,i}}{\partial x_m} \tag{5.58}$$

By contracting the indices of this tensor, we can define the fluid turbulent kinetic energy seen by the particles as:

$$q_{f@p}^2 = \frac{1}{2} \left\langle u'_{f@p,i} u'_{f@p,i} \right\rangle_p \quad (5.59)$$

and contracting the indices for the homogeneous isotropic stationary turbulence, it is obtained that:

$$2A_{f@p} q_{f@p}^2 + \frac{3}{2} B_{f@p}^2 + \Pi_{q_{f@p}^2}^* = 0 \quad (5.60)$$

### 5.6.7 Fluid-particle velocity correlation equation

The fluid-particle correlation equation is obtained from the particle dynamic equation (relation 5.25) and Langevin equation (equation 5.49) by cross multiplication with the velocity fluctuations and averaging. It is written as:

$$\begin{aligned} n_p \frac{\partial \left\langle u'_{f@p,i} u'_{p,j} \right\rangle_p}{\partial t} + n_p U_{p,m} \frac{\partial \left\langle u'_{f@p,i} u'_{p,j} \right\rangle_p}{\partial x_m} = & D_{fp,ij} + P_{fp,ij} \\ & + n_p \left\langle u'_{f@p,i} \frac{F_{p,j}}{m_p} \right\rangle_p \\ & + n_p A_{f@p} \left\langle u'_{f@p,m} u'_{p,i} \right\rangle_p \\ & - n_p \left\langle u'_{p,j} \Pi_{u_{f@p,i}}^* \right\rangle_p \end{aligned} \quad (5.61)$$

The first term on the right hand side,  $D_{fp,ij}$ , is the turbulent transport. The second term,  $P_{fp,ij}$  is the production term. They are given as:

$$\begin{aligned} D_{fp,ij} = & -\frac{\partial}{\partial x_m} n_p \left\langle u'_{f@p,i} u'_{p,j} u'_{p,m} \right\rangle_p \\ P_{fp,ij} = & -n_p \left\langle u'_{f@p,i} u'_{p,m} \right\rangle_p \frac{\partial U_{p,j}}{\partial x_m} \\ & -n_p \left\langle u'_{p,j} u'_{p,m} \right\rangle_p \frac{\partial V_{d,i}}{\partial x_m} \\ & -n_p \left\langle u'_{p,j} u'_{f@p,m} \right\rangle_p \frac{\partial U_{f,i}}{\partial x_m} \end{aligned} \quad (5.62)$$

By contracting the indices of the tensor for the isotropic turbulence, fluid-particle covariance can be defined as:

$$q_{fp} = \left\langle u'_{f@p,i} u'_{p,i} \right\rangle_p \quad (5.63)$$

It is now to model the coupling terms,  $\Pi_{u_f,i}^*$  and  $\Pi_{u_f@p,i}^*$ , to obtain a general form for the constants  $A_f$ ,  $A_{f@p}$ ,  $B_f$  and  $B_{f@p}$  for closure of the Langevin equation and reformulate the moment equations.

## 5.7 Modeling the two-way coupling term in homogeneous isotropic turbulence

The drift term in the Langevin equation corresponds to a memory effect on the trajectory of the fluid element, in addition, the diffusion coefficient corresponds to the random effects. In the classical methodology, for homogeneous isotropic turbulence, Pope (1994) considered the drift and diffusion terms in terms of the Lagrangian timescale of the fluid elements. Then the model parameters do not leave a choice, they are determined using the consistency of the Langevin model with the Kolmogorov hypothesis. This model agrees well with the DNS measurements (Yeung and Pope, 1989) for large Reynolds number flows where the diffusion at the molecular level is negligible for the large scales of turbulence. For more realistic flows, the generalized Langevin model is written with modified drift term to include anisotropy or inhomogeneity, however, the diffusion effect is still determined by the Kolmogorov hypothesis (Haworth and Pope, 1986). Then the drift term may be imposed using the consistence of the Langevin approach with the second-order transport equation (see equation 5.34). The methodology can be written as:

- Determination of the coefficient  $B_f$  using the Kolmogorov hypothesis
- Determination of the tensor  $A_{f,ij}$  using the fluid Reynolds stress transport equation

In homogeneous shear flows, Pope (2002) further proposed not to consider the Kolmogorov hypothesis for the determination of the diffusion term but to determine it from the consistence with the Reynolds stress transport equation. The drift term is assumed to be determined from the Lagrangian correlation function. He changed the above methodology as follows:

- Determination of the tensor  $A_{f,ij}$  using the fluid Lagrangian autocorrelation function
- Determination of the tensor  $B_{f,ij}$  using the fluid Reynolds stress transport equation

In this thesis, even though the flow we consider is homogeneous and isotropic, we will follow this methodology. Indeed, in gas-solid flows, the Langevin equations 5.5 and 5.42 are modified by the two-way coupling effect. In the preceding sections, it has been shown that the Langevin equations, 5.17 and 5.49, proposed are completely determined by the coefficients  $A_f, B_f, A_{f@p}, B_{f@p}$  and the two-way coupling terms,  $\Pi_{u_f,i}^*, \Pi_{u_f@p,i}^*$ .

Once these coefficients and the two-way coupling terms are given, closed Langevin equations should lead to:

1. the same fluid Lagrangian time scales,  $T_L^f$  and  $T_L^{f@p}$ , as the ones calculated by the autocorrelation function from the DNS experiments
2. the same two-way coupling terms as the one derived from the Navier-Stokes equation (the term 5.26)
3. the same kinetic energy transport equation ( $q_f^2$ ) as the one derived from the Navier-Stokes equations (only for the Langevin equation for fluid elements, equation 5.17).

In addition, in homogeneous isotropic turbulence, the fluid-particle correlations derived from the closed Langevin equations should be consistent with the Tchen-Hinze theory of particle dispersion which is found to be verified from the simulations performed in this thesis (as will be shown in chapter 7).

It is important to understand that, in this thesis, the closure for the terms  $A_f$ ,  $A_{f@p}$  and  $B_f$ ,  $B_{f@p}$  will be determined by the closure of the two-way coupling terms. Therefore the steps to determine the coefficients of the Langevin equation consistent with the above conditions will be as follows:

- A priori modeling of  $\Pi_{u_{f,i}}^*$  and  $\Pi_{u_{f@p,i}}^*$  satisfying the condition 2
- Derivation of the Lagrangian autocorrelation functions and kinetic energy transport equations in the frame of the Langevin model approach
- Determination of  $A_f$ ,  $A_{f@p}$  and  $B_f$ ,  $B_{f@p}$  in terms of the gas and particle properties to satisfy the conditions 1 and 3
- Model predictions of the drift velocity and fluid-particle covariance and comparison with DNS+DPS results

The general equations serving for the three conditions mentioned above will be derived in the next section. Afterwards, the chapter will end with the modeling of the two-way coupling term.

Two spatially continuous type of drag forces have been used in this study. They are of mean and instantaneous type, respectively. Following sections are dedicated to these subjects. For simplification of the problem at this stage, it is to be noted that the separation

of the two terms,  $\Pi_{u_{f,i}}^*$  and  $\Pi_{u_{f@p,i}}^*$ , will not be performed here. Therefore it will be written that:

$$\Pi_{u_{f@p,i}}^* = \Pi_{u_{f,i}}^* \quad (5.64)$$

This assumption is reasonable considering the forces acting on a fluid element and a fluid element at the position of a particle due to the surrounding solid particles. In case of a solid particle, the fluid element will be disturbed due to the surrounding particles but not due to the particle in question.

### 5.7.1 Modeling with the mean drag force

Following the reasoning of Haworth and Pope (1986), the two-way coupling term in the instantaneous Navier-Stokes equation 2.61 can also be decomposed into mean and fluctuating parts.

$$f_{u_i} = \langle f_{u_i} \rangle + f'_{u_i} \quad (5.65)$$

Then the first proposition is to model the two-way coupling terms  $\Pi_{u_{f,i}}^*$ ,  $\Pi_{u_{f@p,i}}^*$  in Langevin equations 5.17 and 5.49 using the mean force  $\langle f_{u_i} \rangle$ . It can be formally written as:

$$\Pi_{u_{f@p,i}}^* = \Pi_{u_{f,i}}^* = \frac{n_p}{\rho_p} \langle F_{p,i} \rangle = -\frac{n_p m_p}{\rho_f \tau_p} (U_{p,i} - U_{f,i} - V_{d,i}) \quad (5.66)$$

where  $V_d$  is the drift velocity appearing with the averaging operator.

Important consideration in this modeling is that the fluctuating part of the two-way coupling term  $f_{u_i}$  is assumed in the drift and diffusion terms,  $A_f, A_{f@p}, B_f, B_{f@p}$ , of the Langevin equations. Therefore turbulent interactions between the fluctuating velocities of the particle and the fluid phase are not effected by the mean two-way coupling term in stochastic modeling. Thus, using this modeling, the direct two-way coupling effects on the statistical quantities of the fluid such as Lagrangian temporal correlations, fluid kinetic energies, fluid-particle covariance and the drift velocity are absent, as will be seen in the equations derived.

#### 5.7.1.1 Autocorrelation functions

The general form of the differential equation (equation 5.20) can be rewritten as:

$$\frac{dR_L^f(t)}{dt} = A_f R_L^f(t) \quad (5.67)$$

The second term in the equation drops out because of the averaging. Solving this differential equation, Lagrangian autocorrelation is written as:

$$R_L^f(t) = R_L^f(0)e^{A_f t} \quad (5.68)$$

e.g., the same expression as in the one-way coupled flows is obtained. Integrating the autocorrelation function, the Lagrangian timescale  $T_L^f$  is related to the coefficient  $A_f$  as:

$$A_f = -\frac{1}{T_L^f} \quad (5.69)$$

where  $T_L^f = \frac{1}{R_L^f(0)} \int_0^\infty R_L^f(t) dt$ .

Similarly, the general form of the differential equation for  $R_L^{f@p}$  is written as:

$$\frac{dR_L^{f@p}(t)}{dt} = A_{f@p} R_L^{f@p}(t) \quad (5.70)$$

and the solution is written as:

$$R_L^{f@p}(t) = R_L^{f@p}(0)e^{A_{f@p} t} \quad (5.71)$$

The integration results in the Lagrangian timescale of the fluid along particle trajectories  $T_L^{f@p}$  related to the coefficient  $A_{f@p}$  as:

$$A_{f@p} = -\frac{1}{T_L^{f@p}} \quad (5.72)$$

The model 5.71 is compared to the DNS measurements, in figure 5.4, for two simulations (not all presented for convenience), for different mass-loadings,  $\phi$ , which is defined as  $\phi = \rho_p \alpha_p / \rho_f$  where  $\alpha_p$  is the volumetric loading of particles written  $\alpha_p = (N_p \pi d_p^3 / 6) / L_b^3$ . As seen, for low mass loading, exponential modeling takes better account of the small time separations with reference to the high mass loadings for which the turbulent Reynolds numbers are much smaller. Nevertheless, for both simulations, exponential curve does not predict well the correlation behavior for small time separations due to the small turbulent Reynolds numbers of the flows.

In one-way coupled flows without gravity without any mean flow, it has been shown by Deutsch (1992) that the Lagrangian timescale  $T_L^f$  along the fluid element trajectories and along the solid particle trajectories  $T_L^{f@p}$  can be equal up to some percentage. Then the classical assumption can be written as:

$$T_L^{f@p} = T_L^f \quad (5.73)$$

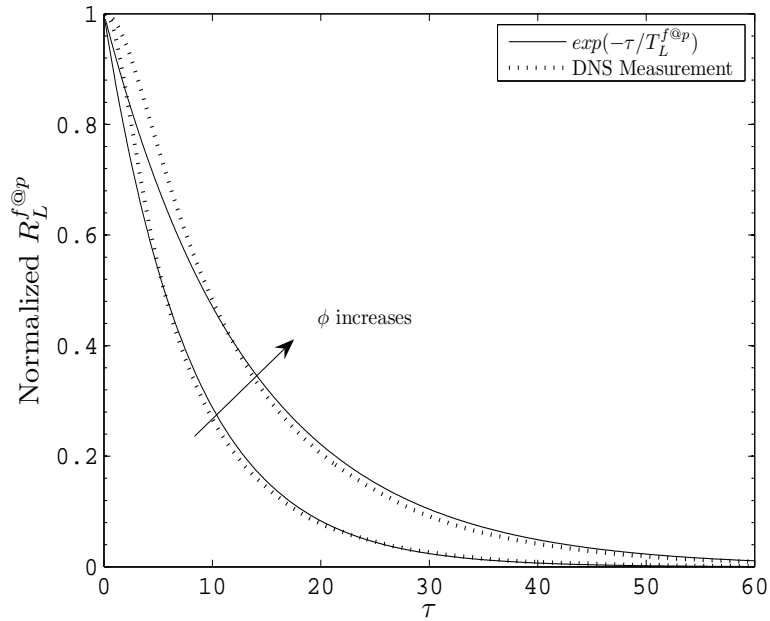


FIGURE 5.4: Comparison of the correlation of the fluid velocity viewed by the particles measured from DNS to the exponential form obtained with the mean drag model,  $St_0 = 0.25$

Using this assumption, the mean drag model leads to the equivalence of the coefficients  $A_f$  and  $A_{f@p}$ :

$$A_{f@p} = A_f \quad (5.74)$$

### 5.7.1.2 Mean momentum equation

Mean of the two-way coupling term in Langevin equations is written as:

$$\langle \Pi_{u_{f,i}}^* \rangle = -\frac{n_p m_p}{\rho_f \tau_p} (U_{p,i} - U_{f,i} - V_{d,i}) = -\frac{n_p m_p}{\rho_f \tau_p} V_{r,i} \quad (5.75)$$

As the relation implies, the first model satisfies the condition given by relation 5.28. Therefore the model is consistent with the mean fluid velocity transport equation.

### 5.7.1.3 Turbulent kinetic energy equations

To remind the general relation obtained at the end of the section 5.5.3, for stationary homogeneous isotropic turbulence, it was written that:

$$2A_f q_f^2 + \frac{3}{2} B_f^2 + \Pi_{q_f}^* = 0 \quad (5.76)$$

Given the form of the term  $\Pi_{u_{f,i}}^*$  (relation 5.66), the source term in the kinetic stress equation due to interactions with particles is zero,  $\Pi_{q_f^2}^* = 0$ .

It is important to note at this point that the terms with constants  $A_f$  and  $B_f$  takes into account turbulence forcing, the particle effects, viscous dissipation, pressure-velocity correlations and implicitly the fluctuating part of the drag term  $f_{u_i}$ . It is direct to obtain a relation for the Lagrangian time scale from this last relation. As a result, it can be written:

$$B_f = \sqrt{-\frac{4}{3}A_f q_f^2} \quad (5.77)$$

Similarly, the transport equation for the fluid kinetic energy seen by the particles is simplified as:

$$2A_{f@p} q_{f@p}^2 + \frac{3}{2}B_{f@p}^2 + \Pi_{q_{f@p}^2}^* = 0 \quad (5.78)$$

Given the form of the drag force  $\Pi_{u_{f@p}}^*$ , the two-way coupling term  $\Pi_{q_{f@p}^2}^* = 0$ . The relation leads then to the coefficient  $B_{f@p}$  as:

$$B_{f@p} = \sqrt{-\frac{4}{3}A_{f@p} q_{f@p}^2} \quad (5.79)$$

It has been shown by Deutsch (1992), Boivin (1996) that the fluid second order tensor along fluid element trajectory and solid particle trajectory for very large density ratios ( $\rho_p \gg \rho_f$ ) have negligible bias in one-way coupled gas-solid flows without mean flow and without gravity.

$$q_{f@p}^2 = q_f^2 \quad (5.80)$$

then using the assumption 5.74, this leads to:

$$B_{f@p} = B_f \quad (5.81)$$

#### 5.7.1.4 Fluid-particle turbulent drift velocity prediction

Simplifying the transport equation of turbulent drift velocity ( equation 5.54) for stationary homogeneous isotropic turbulence, following relation is obtained:

$$0 = - \left\langle u'_{p,i} u'_{f@p,j} \right\rangle_p \frac{\partial n_p}{\partial x_j} + n_p A_{f@p} V_{d,j} \quad (5.82)$$

The number density flux of particles due to the fluid-particle turbulent drift velocity is obtained as:

$$n_p V_{d,i} = \frac{\langle u'_{p,i} u'_{f@p,j} \rangle_p}{A_{f@p}} \frac{\partial n_p}{\partial x_j} \quad (5.83)$$

It is to be noted that the term of the particle dynamic equation cancels out with the two-way coupling term coming from the Langevin equation along the particle trajectory. Therefore the same equation as in the case of one-way coupled flows is obtained e.g., there is no direct effect of two-way coupling on the drift velocity. However, it will be shown in chapters 6 and 7 that  $A_{f@p}$  and  $A_f$  are modified by two-way coupling effects therefore leading to indirect modification of the turbulent drift velocity.

### 5.7.1.5 Fluid-particle velocity covariance prediction

Simplifying the general form of the fluid-particle covariance equation (equation 5.61) for the same conditions as above, it is written as:

$$n_p \left\langle u'_{f@p,i} \frac{F_{p,j}}{m_p} \right\rangle_p + n_p A_{f@p} \delta_{ij} \langle u'_{f@p,i} u'_{p,j} \rangle_p = 0 \quad (5.84)$$

As can be noted, the two-way coupling term coming from the Langevin equation for  $u_{f@p,i}$  disappears because of the averaging operator. Contracting the indices  $i$  and  $j$ , this equation leads to:

$$q_{fp} = \left( \frac{1}{1 - A_{f@p} \tau_p} \right) 2q_{f@p}^2 \quad (5.85)$$

where  $q_{fp} = \langle u'_{f@p,i} u'_{p,i} \rangle_p$  is the fluid-particle covariance and  $q_{f@p}^2 = \frac{1}{2} \langle u'_{f@p,i} u'_{f@p,i} \rangle_p$  is the fluid turbulent kinetic energy seen by the particle phase. By this derivation, it can be concluded that with the mean drag model, two-way coupling does not directly effect the fluid-particle correlations but the effect could occur through the modulation of  $A_{f@p}$  or  $q_{f@p}^2$ .

### 5.7.1.6 Interim conclusion on the mean drag model

The mean drag model considers a mean force acting on the fluid due to the particles. Physically, this model considers that the particles do not directly effect the fluid statistics; the fluid-particle turbulent drift velocity, fluid kinetic energy viewed by the fluid elements and solid particles and fluid-particle covariance. Therefore, for these statistics, the same set of equations as in the one-way coupled flows are obtained. The model is hence practical and

considers that the particle dispersion in a two-way coupled flow can be analyzed as in one-way coupled flows.

### 5.7.2 Modeling with the instantaneous drag force

Two-way coupling term  $f_{u_i}$  in the Navier-Stokes equation 5.16 can be written as the instantaneous force term as:

$$f_{u_i} = -\frac{1}{\rho_f} \sum_{n=1}^{N_p} -m_p \frac{u_{p,i}^{(n)} - u_{f@p,i}^{(n)}}{\tau_p} \delta(x - x_p^{(n)}) \quad (5.86)$$

In fact, the calculation of this term at the particle position requires the interpolation of the velocities of the surrounding particles to the position of the particle in question. In an Eulerian grid, this process is performed in two steps, first by interpolation of the particle velocities onto the Eulerian grid nodes, and then interpolation to the position of the particle in question. Février (2000) refers to this velocity as the mesoscopic particle velocity symbolized by  $\tilde{u}_p$  in the frame of the Mesoscopic Eulerian Formalism. Therefore instead of using the instantaneous particle velocity  $u_p$ , using mesoscopic particle velocity would be more proper to define the backforce of particles. As will be explained a few paragraphs later, this velocity is a kind of average velocity calculated by dividing the domain into small subdomains and performing the average of the particle velocities in each subvolume.

This model will take into account the interaction between the fluid and the cumulative effect of particles in local regions. It is written as:

$$\Pi_{u_{f@p,i}}^* = \Pi_{u_{f,i}}^* = -\frac{\tilde{n}_p m_p}{\rho_f \tau_p} (\tilde{u}_{p,i} - u_{f@p,i}) \quad (5.87)$$

where  $\tilde{n}_p$  is the particle number density defined in the context of mesoscopic Eulerian formalism. It is related to the total particle number density as  $\langle \tilde{n}_p \rangle = n_p$  where  $\langle \cdot \rangle$  is the averaging operator over the large number of two-phase flow realizations. The average of a particle property, say  $\psi$ , in the frame of the mesoscopic Eulerian formalism is then related to the particle number density-weighted average as  $\langle \tilde{n}_p \psi \rangle = n_p \langle \psi \rangle_p$ .

Using of mesoscopic velocity is not direct in gas-solid flows where the turbulence is modified by the particles and requires some comments.

### 5.7.2.1 Application of Mesoscopic Eulerian Formalism to two-way coupled flows

#### Base of Mesoscopic Eulerian Formalism

It is known that the spatial distributions of particles can cause significant changes in the physics of the both phases. For example, Sundaram and Collins (2000) showed that the spatially concentrated particle distribution modifies the collision frequency of particles. Parallel to this, Elgobashi and Truesdell (1993) demonstrated that the particle spatial distributions can modify the energy spectrum of turbulence non-uniformly.

Février et al. (2005) develops an Eulerian formalism in which the effect of spatial particle distributions are taken into account in gas-solid flows where the both inter-particle collisions and turbulence modification are not considered. According to the formalism, two particles in a turbulent flow field can be very close to each other but can have uncorrelated velocities due to their inertia. Therefore, the formalism considers the particles placed in the same fluid realization where the difference in initial conditions of particles, either in inertia or in position for large number of particle realizations, is quickly magnified by the fluid-particle one-way interactions. After a time range long enough, particles forget the initial conditions and they are fully controlled by the turbulence.

These fluid-particle interactions lead to different particle-particle and particle-fluid correlations according to the inertia and allow the particle velocity to be divided into two contributions; a correlated part and an uncorrelated part. Thus the total particle velocity can be written as:

$$u_p^{(n)}(t) = \tilde{u}_p(x_p^{(n)}(t), t) + \delta u_p^{(n)}(t) \quad (5.88)$$

where  $\delta u_p$  is referred to as the residual velocity of a particle which has higher portion of the total particle velocity for high inertia particles. It is of a Lagrangian character, proper to the particle, and is spatially uncorrelated particle velocity giving tendency to a quasi-Brownian motion.  $\tilde{u}_p$  is spatially correlated velocity and as Février (2000) notes it is shared by all the particles of the system. It corresponds to an Eulerian continuous particle velocity which tends to follow the fluctuations of the fluid velocity.

#### One-point statistics defined with the mesoscopic velocity

The mean velocity is defined as:

$$n_p \tilde{\mathbf{U}}_p = \langle n_p \tilde{\mathbf{u}}_p \rangle_p \quad (5.89)$$

Mean mesoscopic kinetic energy is defined as:

$$n_p \tilde{q}_p^2 = \frac{1}{2} \left\langle \tilde{n}_p \tilde{u}_{p,i}' \tilde{u}_{p,i}' \right\rangle \quad (5.90)$$

In this thesis, the most required quantity is the mesoscopic kinetic energy of particles due to the derivations of the second order quantities from the Langevin equations, when the two-way coupling term is modeled with mesoscopic velocity. The mesoscopic energy of the particle mesoscopic velocity is calculated using the two-point correlations due to the number of particle restrictions in the study. Therefore, the next section is dedicated to the definition and the computation of the particle mesoscopic kinetic energy.

### Two-point correlations of the mesoscopic velocity

Mesoscopic particle kinetic energy  $\tilde{q}_p^2$  is calculated in DNS simulations using the Lagrangian two-point correlations of two particles  $m$  and  $n$  of the system written as:

$$\tilde{R}_{pp,ij}(x, x+r, t) = \langle u_{p,i}'^{(m)}(x, t) u_{p,j}'^{(n)}(x+r, t) | x = x_p^{(m)}(t); x+r = x_p^{(n)}(t) \rangle \quad (5.91)$$

with  $m \neq n$ . In homogeneous isotropic turbulence, the two-point correlations can be written in terms of the longitudinal and transversal components. Longitudinal component is written as:

$$F_{pp}(r, t) = \frac{1}{3} \langle u_{p,i}'(x, t) u_{p,i}'(x+re_i, t) | x = x_p^{(m)}(t); x+re_i = x_p^{(n)}(t) \rangle \quad (5.92)$$

and transversal component is written as:

$$G_{pp}(r, t) = \frac{1}{3} \langle u_{p,i}'(x, t) u_{p,i}'(x+re_j, t) | x = x_p^{(m)}(t); x+re_j = x_p^{(n)}(t) \rangle \quad (5.93)$$

with  $m \neq n$ . As seen in figure 5.5 (taken from the work of Février, 2005), as the inertia increases, the spatial correlation normalized by the total agitation of particles  $\tilde{q}_p^2$  decreases as the space separation  $r$  tends to zero ( $r \rightarrow 0$ ). This is in coherence with the inertial particle motion where two particles could be close enough to each other having velocities completely uncorrelated. Then it can be concluded that as the space separation tends to zero, the correlations tend to the mesoscopic particle kinetic energy:

$$\lim_{r \rightarrow 0} F_{pp}(r) = 2\tilde{q}_p^2/3 \quad (5.94)$$

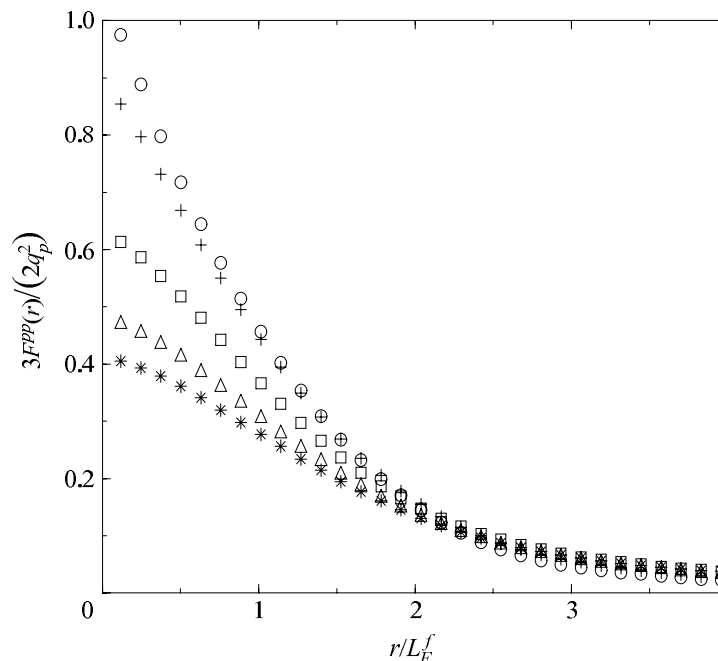


FIGURE 5.5: Two-point correlations of particle velocities, image taken from the work of Février et al., 2005. Circles: smallest inertia, stars: highest inertia.

TABLE 5.1: Particle Characteristics

$\rho_p/\rho_f$	$d_p/\eta_K$	$N_{p_{total}}$
12000	0.0751	$4 \times 128^3$

### Application to two-way coupled gas-solid flows

The application to two-way coupled gas-solid flows is not obvious due to the fact that a single fluid realization can not be defined in this kind of flows. Indeed, the fluid realization is the one imposed to the effects of particles and different particle initial conditions correspond to different fluid realizations.

To search on the existence of a time range during which the fluid realization rests the same for different particle initial conditions, two populations of particles are introduced into the same fluid realization all with the same properties except their initial positions. The properties of the populations are summarized in table 5.1. Characteristics of turbulent field is summarized at the end of chapter 2. Two populations were time-stepped without two-way coupling so that they settle to an equilibrium with the turbulent flow. The statistics of the particle phase and the fluid phase seen by the particles were settled to the similar levels for both classes. This final field was referred as at time  $t/T_e = 0$ . The spatial distributions of both phases are shown in figure 5.6. Once two populations were obtained with very similar initial characteristics in the same fluid realization, they were separated into two simulations

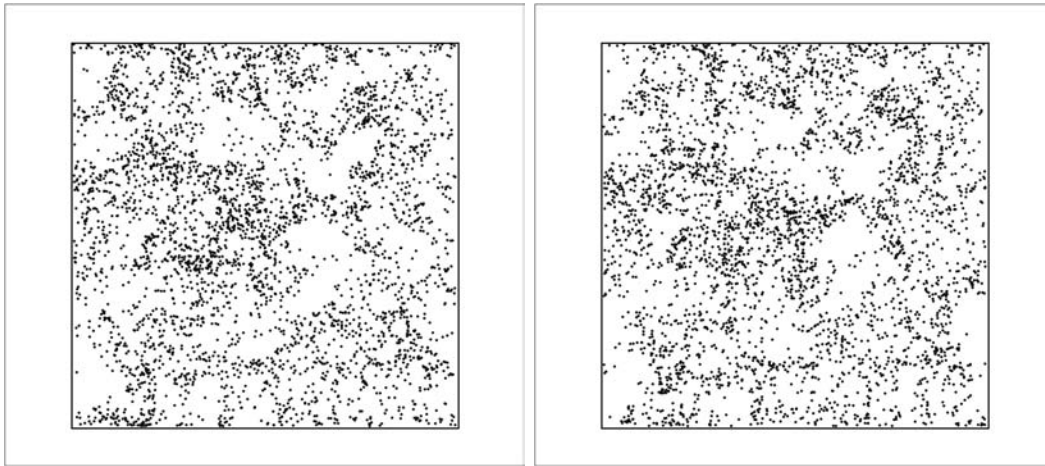


FIGURE 5.6: Initial particle distributions at reference time  $t/T_e = 0$  of group A on the left, of group B on the right. These distributions are then two-way coupled to modify the turbulence.

and time-stepped with two-way coupling. The difference between the turbulent fields in these two simulations was observed and calculated by the normalized relation:

$$D = \left( \frac{\langle (u_A - u_B)^2 \rangle}{u_A^{rms} u_B^{rms}} \right)^{1/2} \quad (5.95)$$

where  $u_A$  signifies the velocity of the fluid at a grid point in the first simulation with group A particles and  $u_B$  is the one of the fluid in the second simulation with group B particles.  $\langle \cdot \rangle$  indicates volume averaging.

Time behavior of  $D$  is shown in figure 5.7. As seen, the difference is more than %10 and it increases in time. The deviation of the fluid velocity field of the group A from the one of the group B is due to the minute initial differences of particle positions which is amplified due to the non-linear chaotic nature of turbulence. This is called in the turbulence community as 'butterfly effect'. Consequently, the definition of a single fluid realization seems not possible.

It should be noted in passing that the simulations use the same stochastic series to generate the turbulence forcing effect. So it can be concluded that the differences represented in the figure 5.7 are due to the two-way coupling, there is no disturbance coming from the turbulence forcing.

To overcome the chaotic nature of turbulence, two populations were introduced into the same fluid realization but only one of the populations was two-way coupled with the turbulence. The other group is ghost particles as explained in chapter 2 (section 2.4.2). Then the source terms  $f_{u_i}$  of the two group particles in the Navier-Stokes equation were compared to

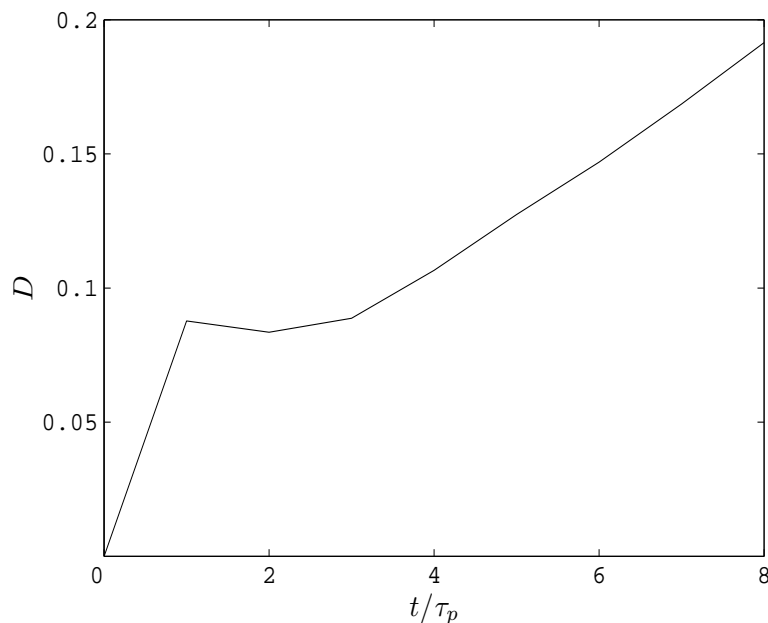


FIGURE 5.7: Statistical difference measured by the factor  $D$  (relation 5.95) between the flow fields in two simulations in which group A and group B particles are two-way coupled, respectively.

each other. Two simulations were performed in which groups  $A$  and  $B$  are active, respectively. The difference between the source terms were expected to depend on the number of particles per cell. Fundamentality here is that the two groups of particles in the same fluid realization form different particle initial conditions and the ghost particles, being not coupled with the flow, increase only the precision of the calculation of mesoscopic variables.

One-point statistics of the two groups in the same fluid realization are shown in figure 5.8 and for both phases, as seen, they are the same. This means that the particles hold the same mesoscopic field whether they are coupled to the flow or not. Turbulent velocity field responding to these different particle initial conditions are shown in figures 5.9. Topology of the field looks the same. Analyzing closely the field, the regions in the dashed-lines are shown in figures 5.10. The dots in the figure shows the approximative centers of the vortices and it is seen that these vortices have slight deviations.

Quantification of the difference was performed using the normalized parameter  $D$  and the trace in time is shown in figure 5.11 normalized by the initial value. As seen, the difference stays constant for more than one eddy turnover time. The initial peak in the trace is due to the transition of both fluid and particles to arrive at a new equilibrium. It can also be inferred that the changing the active group from  $A$  to  $B$  has the same effect on the difference which is found to depend largely on the number of particles, e.g., increasing the number of

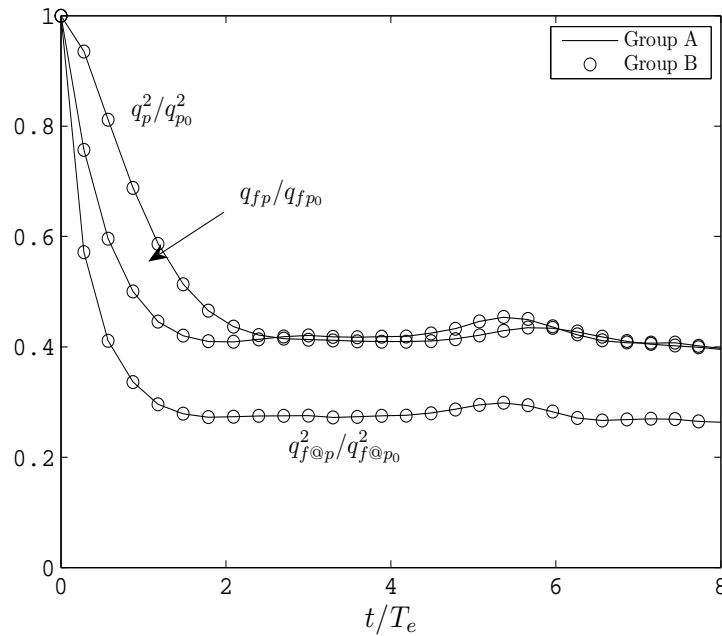


FIGURE 5.8: The evolution of statistics of the two groups of particles,  $A, B$ , in the same fluid realization, in time after the two-way coupling is turned on, group  $A$  is active and  $B$  is ghost particles.

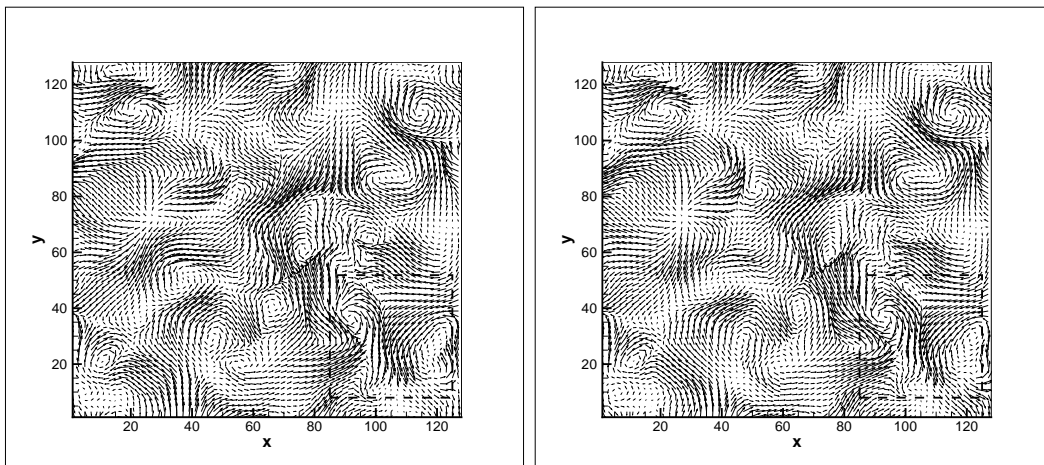


FIGURE 5.9: Vector fields of the flow simulation at time  $t/T_e = 8$  with two groups of particles in the same realization. On the left the flow with group  $A$  is active (two-way coupled) and  $B$  is ghost, on the right, the inverse.

particles reduces the difference. This behavior of the parameter  $D$  allows one to be able to change the particle initial conditions and with large enough number of particles, the same fluid realization is obtainable. Therefore using the mesoscopic velocity in the definition of the drag force relation is possible.

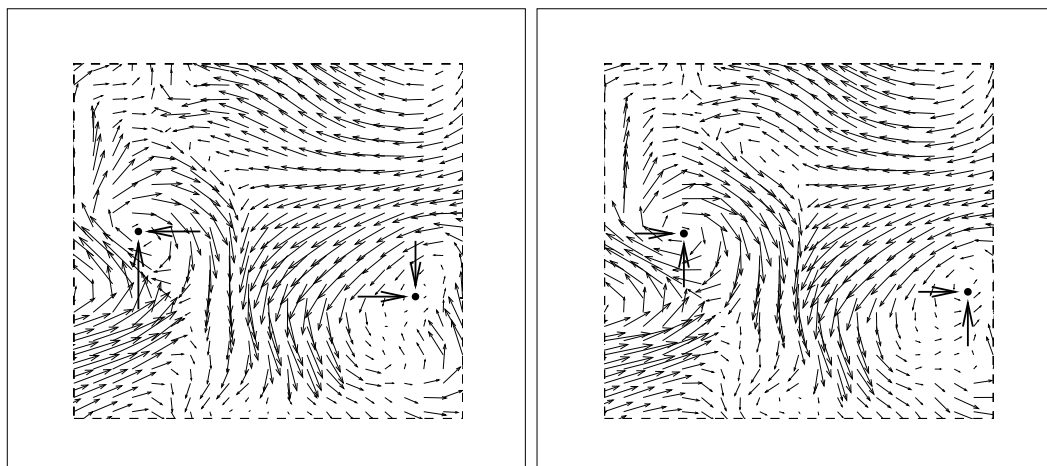


FIGURE 5.10: Dashed regions in figure 5.9

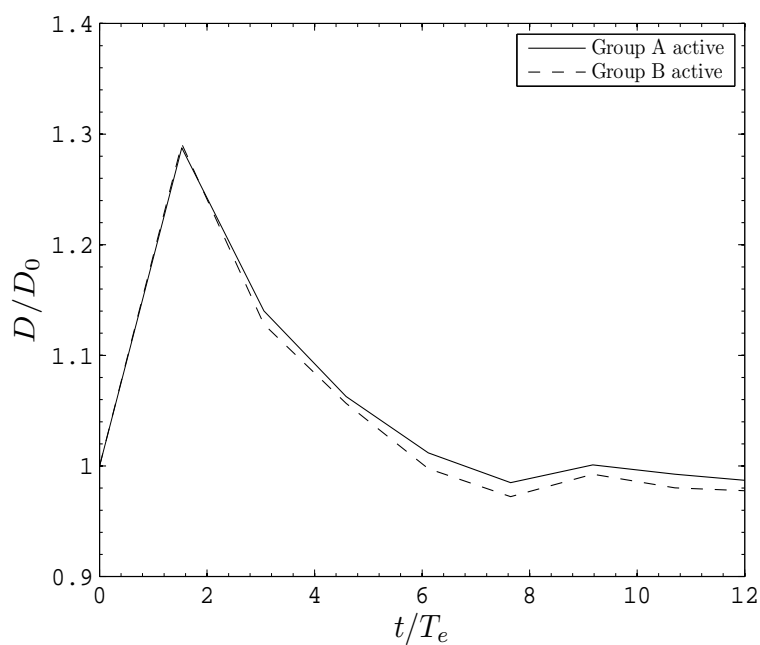


FIGURE 5.11: Statistical difference between the particle source terms  $f_{u_i}$  of the two groups  $A, B$  introduced into the same fluid realization; solid line: group  $A$  is active,  $B$  is ghost, dashed line: group  $B$  is active,  $A$  is ghost.

#### Calculation of the mesoscopic kinetic energy in two-way coupled flows:

As noted in section for two-point statistics of the mesoscopic particle velocity, the particle mesoscopic kinetic energy is calculated from the Eulerian two-point correlations of the particle phase (relation 5.92). To compare the measurements in two-way coupled flow simulations to the one-way coupled simulation measurements of Février (2000), the empirical model for

$\tilde{q}_p^2$  written as:

$$\frac{\tilde{q}_p^2}{q_{f@p}^2} = \left( \frac{q_p^2}{q_{f@p}^2} \right)^{1.5} \quad (5.96)$$

This relation is tested in DNS+DPS measurements and the results are plotted in figure 5.12. The particle mesoscopic energy follows remarkably the line  $\left( q_p^2/q_{f@p}^2 \right)^{1.5}$  for each mass-loading and each inertia.

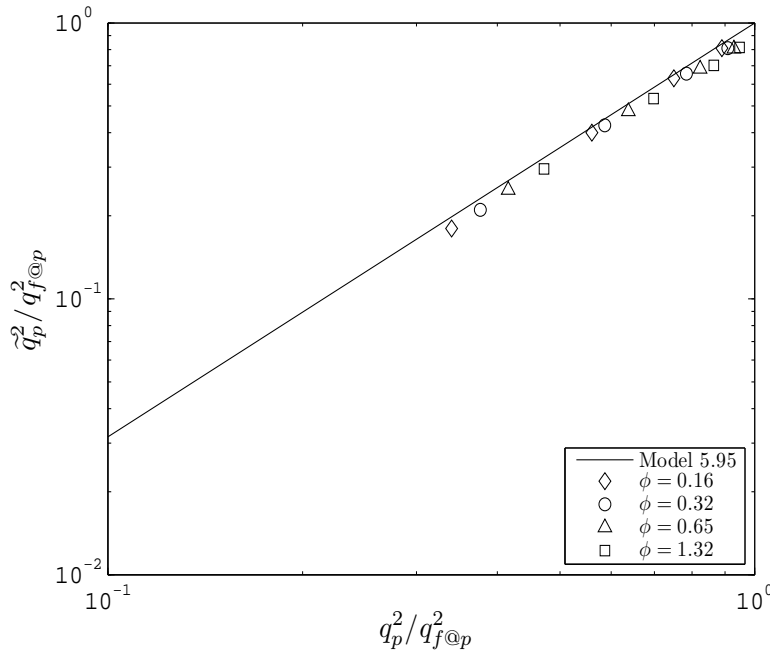


FIGURE 5.12: Relation 5.96 to calculate the mesoscopic particle energy.

### 5.7.2.2 Autocorrelation functions

Differential equation governing the Lagrangian autocorrelation of the fluid can be derived from the Langevin equation 5.17 and it is written as:

$$\frac{dR_L^f(t)}{dt} = A_f R_L^f(t) - \frac{1}{3} \left\langle u'_{f,i}(t_0) \Pi_{u_{f,i}}^*(t_0 + t) \right\rangle_p \quad (5.97)$$

$$\frac{dR_L^f(t)}{dt} = A_f R_L^f(t) + \frac{\phi}{\tau_p} \left( R_L^{fp}(t) - R_L^{f@p}(t) \right) \quad (5.98)$$

where  $R_L^{fp}(t)$  is the correlation between the particle velocity fluctuation and the local fluctuations of the fluid velocity viewed by the particle, it is written as:

$$R_{L,ij}^{fp}(t) = \left\langle u'_{f@p,i} u'_{p,j} \right\rangle_p \quad (5.99)$$

Using the homogeneity and isotropy, it can be rewritten as:

$$R_L^{fp} = \frac{1}{3} R_{L,ij}^{fp} \delta_{ij} \quad (5.100)$$

This equation cannot be solved directly due to the co-existence of non-perturbed velocity  $\mathbf{u}_{f@p}$  in the definition of  $\Pi_{u_{f,i}}^*$  (see general equation 5.87) and of the perturbed fluctuating velocity  $\mathbf{u}'_f$  in the equation.

Differential equation governing the Lagrangian autocorrelation of the fluid  $R_L^{f@p}$  is written as:

$$\frac{dR_L^{f@p}(t)}{dt} = A_{f@p} R_L^{f@p}(t) - \frac{1}{3} \left\langle u'_{f@p,i}(t_0) \Pi_{u_{f@p,i}}^*(t_0 + t) \right\rangle_p \quad (5.101)$$

$$\frac{dR_L^{f@p}(t)}{dt} = A_{f@p} R_L^{f@p}(t) + \frac{\phi}{\tau_p} \left( R_L^{fp}(t) - R_L^{f@p}(t) \right) \quad (5.102)$$

To solve this equation, the differential equation is derived for the  $R_L^{fp}$  as:

$$\frac{dR_L^{fp}(t)}{dt} = \frac{1}{\tau_p} R_L^{f@p}(t) - \frac{1}{\tau_p} R_L^{fp}(t) \quad (5.103)$$

The solution of the differential equations 5.101 and 5.103 is possible with matrix methods.  $R_L^{f@p}$  is written as:

$$\frac{R_L^{f@p}(t)}{2q_{f@p}^2} = \frac{(a - c) + \frac{\phi}{\tau_p} \frac{q_{fp}}{q_{f@p}^2}}{2a} e^{d_1 t} + \frac{(a + c) - \frac{\phi}{\tau_p} \frac{q_{fp}}{q_{f@p}^2}}{2a} e^{d_2 t} \quad (5.104)$$

where the coefficients a, b, c, and  $d_1$  and  $d_2$  are written as:

$$a = \sqrt{A_{f@p}^2 + \left( \frac{\phi}{\tau_p} \right)^2 + \left( \frac{1}{\tau_p} \right)^2} - 2 \left( A_{f@p} \frac{\phi}{\tau_p} - A_{f@p} \frac{1}{\tau_p} - \frac{\phi}{\tau_p} \frac{1}{\tau_p} \right) \quad (5.105)$$

$$c = -A_{f@p} - \frac{1}{\tau_p} + \frac{\phi}{\tau_p} \quad (5.106)$$

$$d_1 = -0.5 \left( -A_{f@p} + \frac{\phi}{\tau_p} + \frac{1}{\tau_p} - a \right) \quad (5.107)$$

$$d_2 = -0.5 \left( -A_{f@p} + \frac{\phi}{\tau_p} + \frac{1}{\tau_p} + a \right) \quad (5.108)$$

and for  $R_L^{fp}$ :

$$R_L^{fp}(t) = \frac{-2q_{f@p}^2 + q_{fp} \left(1 - \frac{\tau_p}{2}(x - a)\right)}{\tau a} e^{d_1 t} + \frac{2q_{f@p}^2 - q_{fp} \left(1 - \frac{\tau_p}{2}(x + a)\right)}{\tau a} e^{d_2 t} \quad (5.109)$$

where  $x$  is written as:

$$x = -A_{f@p} + \frac{1}{\tau_p} + \frac{\phi}{\tau_p} \quad (5.110)$$

Integration of the function 5.104 gives the Lagrangian time scale,  $T_L^{f@p}$ , and the coefficient  $A_{f@p}$  is derived as:

$$A_{f@p} = -\frac{1}{T_L^{f@p}} \left[ 1 + \phi \frac{q_{fp}}{2q_{f@p}^2} \right] \quad (5.111)$$

The correlation function 5.104 is compared to the DNS measurements and plotted in figure 5.13, for the smallest inertia  $St_0 = 0.25$  and for the smallest and the largest mass-loading. Qualitatively, the model does not reproduce the measured correlation function where the deviations are visible for small time separations, small  $\tau$ . Nevertheless, the area under the curves are similar meaning that the model recovers correctly the Lagrangian timescale viewed by the particles. From the other part, the deviations for small time separations could be associated to the model being formulated for turbulent flows with infinite Reynolds number.

In section 5.7, an hypothesis corresponding the Tchen-Hinze theory of particle dispersion has been made. Tchen-Hinze relation basically relates the fluid kinetic energy and fluid-particle covariance as:

$$\frac{q_{fp}}{2q_{f@p}^2} = \frac{\eta}{\eta + 1} \quad (5.112)$$

$$\eta = \frac{T_L^{f@p}}{\tau_p} \quad (5.113)$$

Then, the expression of the correlation function  $R_L^{f@p}(t)$  can be rewritten as:

$$\frac{R_L^{f@p}(t)}{2q_{f@p}^2} = \frac{(a - c) + \frac{\phi}{\tau_p} \frac{2\eta}{\eta + 1}}{2a} e^{d_1 t} + \frac{(a + c) - \frac{\phi}{\tau_p} \frac{2\eta}{\eta + 1}}{2a} e^{d_2 t} \quad (5.114)$$

and the coefficient  $A_{f@p}$  can be rewritten as:

$$A_{f@p} = -\frac{1}{T_L^{f@p}} \left[ 1 + \phi \frac{\eta}{\eta + 1} \right] \quad (5.115)$$

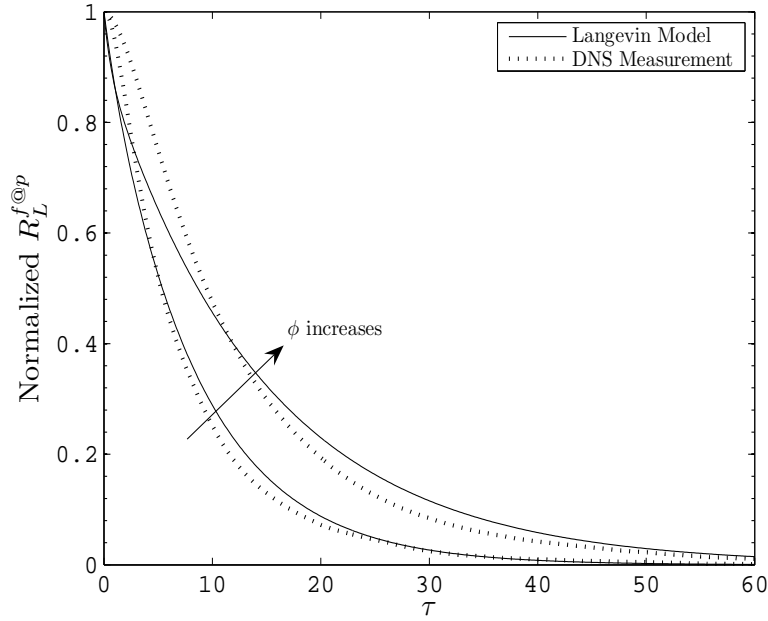


FIGURE 5.13: Comparison of the Langevin model 5.104 for the correlation of the fluid velocity viewed by the particles to the DNS measurements,  $St_0 = 0.25$

Using the solution for  $R_L^{f@p}(t)$  and the solution for  $R_L^{fp}(t)$ , the differential equation for  $R_L^f(t)$  can be solved by simple means of ordinary linear differential equations. The solution for  $R_L^f(t)$  is written as:

$$R_L^f(t) = \frac{f_1 \frac{1}{-A_f + d_1} e^{(-A_f + d_1)t} + f_2 \frac{1}{-A_f + d_2} e^{(-A_f + d_2)t} + C}{e^{-A_f t}} \quad (5.116)$$

where  $C$  is the constant determined with the initial conditions. It is written:

$$C = q_f^2 - f_1 \frac{1}{-A_f + d_1} + f_2 \frac{1}{-A_f + d_2} \quad (5.117)$$

where  $f_1$  and  $f_2$  are written as:

$$f_1 = -\frac{\phi}{\tau_p} \frac{2q_{f@p}^2 + q_{fp}(1 - \frac{\tau_p}{2}(x - a))}{\tau_p a} - \frac{1}{a} \left( q_{f@p}^2(a + c) - q_{fp} \frac{\phi}{\tau_p} \right) \quad (5.118)$$

$$f_2 = \frac{\phi}{\tau_p} \frac{2q_{f@p}^2 - q_{fp}(1 - \frac{\tau_p}{2}(x + a))}{\tau_p a} - \frac{1}{a} \left( q_{f@p}^2(a - c) + q_{fp} \frac{\phi}{\tau_p} \right) \quad (5.119)$$

with

$$x = \frac{1}{T_L^{f@p}} + \frac{\phi}{\tau_p} + \frac{1}{\tau_p} \quad (5.120)$$

Integrating the solution 5.116,  $T_L^f$  can be obtained as:

$$T_L^f = \frac{1}{2q_f^2} \left[ -f_1 \frac{1}{(A_f + d_1)d_1} + f_2 \frac{1}{(A_f + d_2)d_2} + \frac{C}{A_f} \right] \quad (5.121)$$

From this relation  $A_f$  could be determined in general form as:

$$A_f = \frac{1}{T_L^f} g(\eta, \phi, q_{fp}, q_{f@p}^2, q_f^2) \quad (5.122)$$

where it should be noted that the fluid statistics viewed by the particles and the fluid elements appear simultaneously. In two-way coupled flows, there is no a priori intuition for the evolution of these statistics in contrast to the one-way coupled flows where  $q_{f@p}^2 = q_f^2$  and  $T_L^{f@p} = T_L^f$ . Nevertheless, the coefficient  $A_f$  and the Lagrangian timescale of fluid element  $T_L^f$  will not be used on the continuation of the thesis because our aim here is to model the fluid statistics viewed by the particles. Therefore, we don't proceed further for these coefficients.

### 5.7.2.3 Mean momentum equation

The two-way coupling term with the mesoscopic drag modeling is written as:

$$\langle \Pi_{u_{f,i}}^* \rangle = -\frac{m_p}{\rho_p \tau_p} (\langle \tilde{n}_p \tilde{u}_{p,i} \rangle - \langle \tilde{n}_p u_{f@p,i} \rangle) \quad (5.123)$$

where:

$$\langle \tilde{n}_p \tilde{u}_{p,i} \rangle = n_p U_{p,i} \quad (5.124)$$

$$\langle \tilde{n}_p u_{f@p,i} \rangle = n_p (U_{f,i} + V_{d,i}) \quad (5.125)$$

so it can be written as:

$$\langle \Pi_{u_{f,i}}^* \rangle = -\frac{n_p m_p}{\rho_f \tau_p} V_{r,i} \quad (5.126)$$

As the relation implies, model using mesoscopic drag force also satisfies the condition given by relation 5.28.

### 5.7.2.4 Turbulent kinetic energy equations

Let us recall the general relation obtained at the end of the section 5.5.3, for stationary homogeneous isotropic turbulence:

$$2A_f q_f^2 + \frac{3}{2} B_f^2 + \Pi_{q_f^2}^* = 0 \quad (5.127)$$

It is important to note that the terms with  $A_f$  and  $B_f$  takes into account turbulence forcing, viscous dissipation, pressure-velocity correlations. Particle effects are taken into account using the mesoscopic drag force term. The term is written as:

$$\Pi_{q_f^2}^* = n_p m_p \left\langle u'_{f,i} \frac{F_{p,i}}{m_p} \right\rangle_p = -\frac{\phi}{\tau_p} (2q_{f@p}^2 - q_{fp}) \quad (5.128)$$

where  $\tilde{q}_{fp} = q_{fp}$ .

To obtain  $B_f$  from relation 5.127,  $A_f$  could be derived from the relation 5.121.  $B_f$  coefficient will be derived as a general form from the relation 5.127 as:

$$B_f = \sqrt{\frac{2}{3} \left[ 2A_f q_f^2 - \Pi_{q_f^2}^* \right]} \quad (5.129)$$

$B_f$  coefficient will not be considered due to the fact that our aim in this thesis is the modeling of the fluid statistics viewed by the particles, like  $A_f$ . Therefore, we leave the discussion at this level.

Transport equation for the turbulent kinetic energy viewed by the particles derived from the equation 5.55 leads to the following relation with necessary simplifications:

$$2A_{f@p} q_{f@p}^2 + \frac{3}{2} B_{f@p}^2 + \Pi_{q_{f@p}^2}^* = 0 \quad (5.130)$$

The explicit form of the term  $\Pi_{q_{f@p}^2}^*$  includes the average of the local instantaneous particle number density  $\langle \tilde{n}_p \psi \rangle_p$ , which can be written as  $\langle \tilde{n}_p \tilde{n}_p \psi \rangle / n_p$  (using the transformation  $\langle \tilde{n}_p \psi \rangle = n_p \langle \psi \rangle_p$ ). Neglecting the preferential concentration effects, the term will be simply equal to  $n_p \langle \psi \rangle_p$ . Then the two-way coupling term can be written as:

$$\Pi_{q_{f@p}^2}^* = -\frac{\phi}{\tau_p} (2q_{f@p}^2 - q_{fp}) \quad (5.131)$$

using the relation  $\phi = n_p m_p / \rho_f$ .

To determine  $B_{f@p}$  from equation 5.130, the expression of  $A_{f@p}$  given in 5.115 is used:

$$B_{f@p}^2 = \frac{4}{3} \frac{q_{f@p}^2}{T_L^{f@p}} g(\eta, \phi) \quad (5.132)$$

where  $g$  is written with the help of the Tchen-Hinze relation 5.112 as:

$$g(\eta, \phi) = 1 + 2\phi \frac{\eta}{\eta + 1} \quad (5.133)$$

with  $\eta = \frac{T_L^{f@p}}{\tau_p}$ .

### 5.7.2.5 Fluid-particle turbulent drift velocity prediction

Simplifying the transport equation of drift velocity for stationary homogeneous isotropic turbulence, following relation is obtained:

$$0 = -\langle u_{p,i} u_{f@p,j} \rangle_p \frac{\partial n_p}{\partial x_j} + n_p A_{f@p} V_{d,i} - n_p \langle \Pi_{u_{f@p,i}}^* \rangle_p - n_p \langle f_{u_i} \rangle \quad (5.134)$$

At this point, it is worth saying that the two-way coupling has a contribution to the turbulent drift velocity transport equation. Using the second condition of the modeling, which is  $\langle \Pi_{u_{f@p,i}}^* \rangle = -\langle f_{u_i} \rangle$ , and decomposing the particle number density as  $\tilde{n}_p = n_p + \tilde{n}'_p$ , this term can then be written as:

$$n_p V_{d,i} = \frac{\langle u_{p,i} u_{f@p,j} \rangle_p}{A_{f@p}} \frac{\partial n_p}{\partial x_j} + \frac{1}{A_{f@p}} \frac{m_p}{\rho_f \tau_p} \left( \langle \tilde{n}'_p \tilde{n}'_p \tilde{u}_{p,i} \rangle_p - \langle \tilde{n}'_p \tilde{n}'_p u_{f@p,i} \rangle_p \right) \quad (5.135)$$

The second term on the right-hand side of this equation shows the importance of the spatial segregation of the particles. As seen, in the case of an instantaneous drag effect, the transport equation for the drift velocity is different from the equation in one-way coupled flows.

### 5.7.2.6 Fluid-particle velocity correlation prediction

Using the hypotheses of stationary homogeneous isotropic turbulence, the fluid-particle covariance equation is written as:

$$\begin{aligned} \left\langle u'_{f@p,i} \frac{F_{p,j}}{m_p} \right\rangle_p + A_{f@p} \langle u'_{f@p,i} u'_{p,j} \rangle_p = \\ -\frac{\phi}{\tau_p} \left( \langle u'_{f@p,i} u'_{p,j} \rangle_p - \langle \tilde{u}_{p,i} u'_{p,j} \rangle_p \right) \end{aligned} \quad (5.136)$$

Contracting the indices  $i$  and  $j$ , this equation leads to the relation:

$$q_{fp} = 2 (q_{f@p}^2 + \phi \tilde{q}_p^2) \frac{1}{1 + \phi - A_{f@p} \tau_p} \quad (5.137)$$

where  $\tilde{q}_p^2 = \frac{1}{2} \langle \tilde{u}'_{p,i} \tilde{u}'_{p,i} \rangle$  is the mesoscopic energy of particles. In this relation, the mesoscopic particle kinetic energy is the unknown and should be modeled.

## 5.8 Conclusion

In this chapter, the Lagrangian stochastic modeling of the gas-solid flows for homogeneous isotropic stationary turbulence with point particles is extended to the cases where the fluid

phase is modified by the existence of the solid particles. The extension is reflected in an additional term in the trajectory equations for the fluid velocity seen by the fluid elements and solid particles. This additional term is to be modeled due to the lack of information on the spectral content of the drift and diffusion terms of the Langevin equation. Two models are proposed for the closure of this term, namely: a mean drag force using the mean velocities of the both phases from the mean transport equations, and the other an instantaneous drag force written with the help of the mesoscopic particle velocity defined in the frame of the mesoscopic Eulerian formalism.

The principal idea of using the Langevin equation for the trajectory of fluid elements, equation 5.17 is that this equation imitates the Navier-Stokes equations written in Lagrangian form. The advantage is that this stochastic equation uses the reduced description of the flow field and models a real physical phenomenon. The Langevin equation for the fluid velocity along the particle trajectories is to predict the fluid statistics viewed by the particles during their motions to precisely calculate the drag force acting on the particles. In this regard, the mean drag model results in the mean fluid transport equation coherent with the one derived from the Navier-Stokes equations. On the second order equations, this model assumes that the two-way coupling does not induce a direct effect on the second order quantities, e.g., the fluid kinetic energies,  $q_f^2$ ,  $q_{f@p}^2$  and the fluid-particle covariance  $q_{fp}$ , e.g., the model predicts that the two-way coupling does not produce or destroy these quantities directly. This effect is taken into account in the drift and diffusion coefficient terms of the Langevin equation.

The instantaneous model proposed takes into account the effect of the particles on the fluid turbulence structure more properly due to the mesoscopic particle velocity defined with the local averages. Physically, this force considers the collective effect of the particles on the turbulent preferential scales. In this sense, it is already known that particles can extract energy from some of the turbulent scales and inject it to the preferential scales of turbulence (see the section 6.5 for the modulation of the spectra), especially for the small inertia particles which are more sensible to the turbulent scales than the high inertia particles. The model eventually results in more complex first and second order equations for the particle-turbulence statistics and there are extra terms to be modeled such as the particle mesoscopic energy and an additional term in the fluid-particle turbulent drift velocity transport equation due to the segregation of non-inertial particles.

In chapter 7, these models' results will be compared to the measurements from the DNS+DPS experiments to test their validity. For validation, the Tchen-Hinze theory for the particle dispersion (based on the fluid-particle covariance) and the particle flux due to the drift velocity will be used.



## Chapter 6

# Fluid statistics from DNS+DPS results

### 6.1 Introduction

In this chapter, dynamic state in macroscopic level of turbulence interacting with a cloud containing  $N_p$  particles will be studied. The particles are in motion due to the underlying interactions with the continuum phase and due to their finite inertia, they modify the structure of turbulence. The carrier continuum phase is homogeneous isotropic turbulent gas forced with the stochastic forcing scheme developed by Eswaran and Pope (1988), to keep both phases' statistics in stationary level. The range of the turbulent scales forced is chosen as  $[2k_0, 6k_0]$  following the advices of Février (2000) (see chapter 2 for details). The domain involving the gas-particle motion is a cube whose one side is of length  $L_b = 2\pi$  and is far from any wall effects. It has periodic boundary conditions on borders which creates infinite space for particles' spatial dispersion. Gas phase is treated in Eulerian manner requiring definition of fixed points to create a grid and solving the time evolution equation of the fluid velocity at these points. This equation corresponds to Navier-Stokes equation which impose the balance of momentum in an elementary volume equal to the volume of cells covering the domain.

Discrete particles in motion are of very small diameter  $d_p$ , specifically, smaller than the Kolmogorov scales  $\eta_K$  of turbulence. The density ratio of the particles to the gas is of the  $3^{rd}$  order of magnitude which allows to neglect most of the forces effecting the discrete particle's trajectory. Finally, only the Stokes' drag force will be taken into account (see chapter 2 for more details). Throughout the chapter, two distinct limits for particle properties will be considered:

- Very large inertia ( $\tau_p \gg T_{fluid}$ ) particles where the particles respond none of the fluid scales and perform a pure random motion (Abrahamson, 1975). Because the inter-particle collisions are not treated in this thesis, this motion is referred rather as random uncorrelated motion.
- Very small inertia ( $\tau_p \ll T_{fluid}$ ) particles where the particles follow perfectly all the oscillations in the fluid motion, e.g., they act like fluid elements. This limit is also called 'passive scalar' limit.

Between the two limits, particles respond more or less different scales of turbulence which constitutes the basic difficulty for modeling discrete motion of particle with finite inertia. Therefore in this thesis, the particle inertia is imposed by modifying the particle density  $\rho_p$  of the particles (this will be discussed in parametrization of simulations). It could also be modified by varying the particle diameter  $d_p$  which leads to polydispersity but this is not the purpose in this thesis (see the definition of  $\tau_p$  given by relation 2.9).

Fluid-particle simulations will be presented in this section. For the fluid phase, the simulations are of DNS type and for the particles they are of DPS type. First, the effect of the particles on the fluid phase turbulent kinetic energy and the rate of energy dissipation will be discussed with reference to the literature. Finally, the distribution of the turbulent kinetic energy among the spatial wavenumbers will be discussed taking the 3D energy spectrum of the fluid into consideration. Next, the effect of two-way coupling on the Lagrangian correlations of the fluid phase will be discussed. Then Lagrangian structure function for all simulations will be presented. In fact, these correlations and structure functions help understanding of the spatial dispersion of the particles which will be analyzed using the models proposed in the following chapter.

Basically, the purpose here is to understand the underlying mechanisms occurring in two-way coupled gas-solid flows. Specifically, the effect of the particles on the turbulent statistics, such as fluid Lagrangian timescales, turbulent kinetic energy etc., will be reported. Wherever necessary, the results will be embedded into the literature survey of this kind of gas-solid flows.

## 6.2 Description and parametrization of simulations

16 simulations were performed with different mass-loadings  $\phi$  and different particle inertia  $\tau_p$ . For each simulation, particles were introduced into the reference turbulent flow of which characteristics are summarized in table 2.2. Reynolds number of the flow based on the large scales' length  $L_f$  is around 100. Therefore the inertial zone of the turbulence is very limited

TABLE 6.1: Parametrization of simulations. Values in the table show the number of particles  $N_p$ ,  $St_0 = \left(\tau_p/T_L^f\right)_{\phi=0}$  is the initial Stokes number of particles.

$\phi, St_0$	0.25	0.5	1.0	2.0
0.16	$1 \times 128^3$	$0.5 \times 128^3$	$0.25 \times 128^3$	$0.125 \times 128^3$
0.32	$2 \times 128^3$	$1 \times 128^3$	$0.5 \times 128^3$	$0.25 \times 128^3$
0.65	$4 \times 128^3$	$2 \times 128^3$	$1 \times 128^3$	$0.5 \times 128^3$
1.32	$8 \times 128^3$	$4 \times 128^3$	$2 \times 128^3$	$1 \times 128^3$

TABLE 6.2: Particle physical properties (all numbers are non-dimensional).

$St_0$	0.25	0.5	1.0	2.0
$\rho_p/\rho_f$	2000	4000	8000	16000
$(d_p/\eta_K)_{\phi=0}$	0.1323	0.1323	0.1323	0.1323

(see spectra in figure 2.7). Number of particles  $N_p$  in each simulations is presented in table 6.1. Particle parameters to impose different particle relaxation times are presented in table 6.2.

It is to be noted that the turbulence modulation is a physical process which is characterized by two parameters, namely; the mass-loading  $\phi$  and Stokes number  $St_{f@p}$  after the Irish mathematician George Gabriel Stokes (1819-1903). Mass loading of the particle phase is defined as:

$$\phi = \frac{\rho_p}{\rho_f} \alpha_p \quad (6.1)$$

where  $\alpha_p$  is the volumetric loading of particles written as:

$$\alpha_p = \frac{N_p \pi d_p^3 / 6}{L_b^3} \quad (6.2)$$

Stokes number  $St$  serves to characterize the inertia of the particles and it is, in this thesis, defined as:

$$St_{f@p} = \frac{\tau_p}{T_L^{f@p}} \quad (6.3)$$

where  $T_L^{f@p}$  is the fluid Lagrangian time scale measured along the particle trajectory. The definition of Stokes number is so chosen in this study due to the importance of  $T_L^{f@p}$  in turbulence modulation. Indeed the fluid velocity at the position of  $n^{th}$  particle is not modified by the  $n^{th}$  particle in question but it is modified by all the  $N_p - 1$  particles surrounding the particle  $n$ . Therefore,  $T_L^{f@p}$  will be the one modified primarily by the particles and its value

in two-way coupled simulations is not known a priori depending on the one-way coupled simulations. Therefore to characterize the simulations, the relaxation time  $\tau_p$ , normalized by the Lagrangian timescale  $T_L^f$  of one-way coupled simulations:

$$St_0 = \left( \frac{\tau_p}{T_L^f} \right)_{\phi=0} \quad (6.4)$$

and mass-loading  $\phi$  were used (see the table 6.1). Simulations correspond to investigate the response of turbulence, from one part, to a fixed loading of particles with different inertia, from the other part, to a fixed particle inertia with different mass loadings. A representative 2D field view of turbulence with particles is shown in figure 6.1.

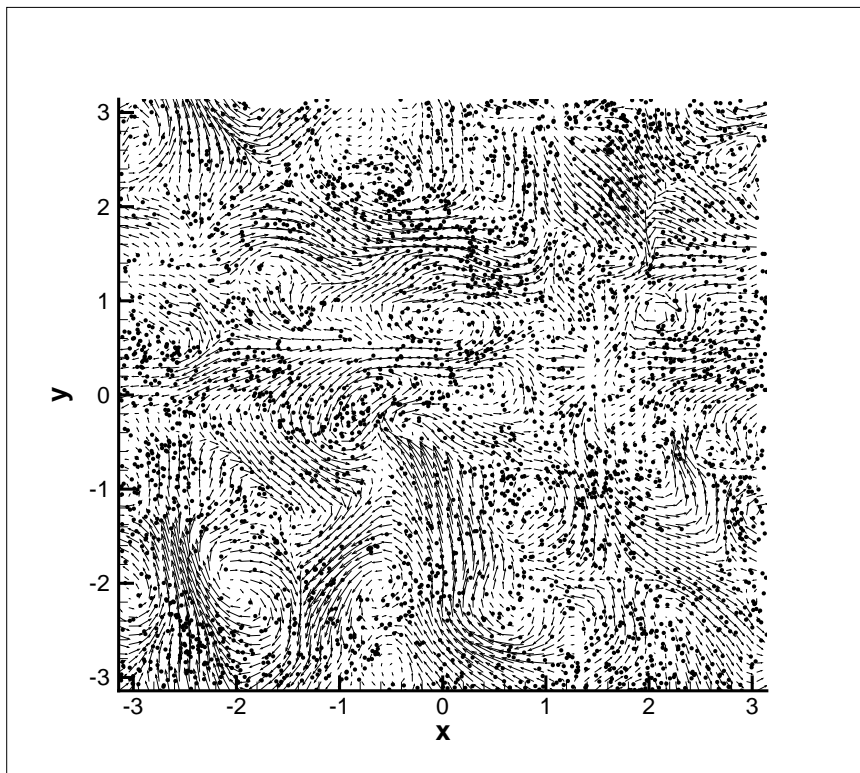


FIGURE 6.1: Fluid 2D velocity vector field with representative particle positions (particle dimensions are not realistic).

## 6.3 Calculation of statistics

### 6.3.1 Eulerian statistics

The Eulerian statistics concerning the fluid phase were all calculated using the spatial grid points. Due to the forced turbulence, the statistics were improved using time averages, as

well. Statistical operator  $\langle . \rangle$  is defined as the arithmetical average over large number of realizations of the phenomenon to be averaged. A representative graph 6.2 shows the periods during which the statistics, either Eulerian or Lagrangian, were calculated. Initially,

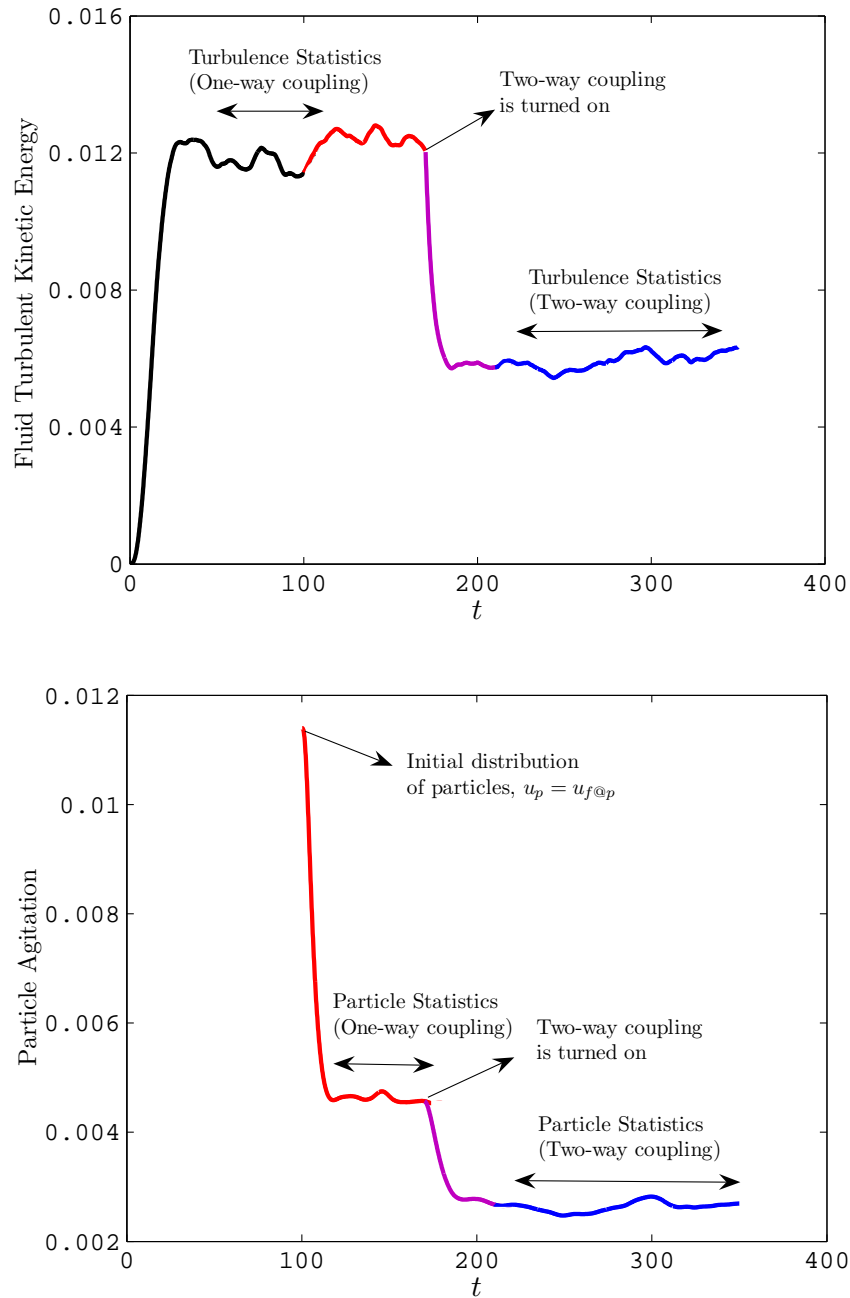


FIGURE 6.2: Representative figures showing the making of statistics for one-way and two-way coupled flows, for particles and turbulence

monophase turbulence was forced to a stationary level during which the statistics of turbulence have then been calculated (top figure). The statistics of the turbulence were calculated

at least for a time period of  $10T_e$ . In principle, this length of the calculation of the statistics provides the sufficient precision (Février, 2000).

Particles were introduced into the reference turbulent flow field at the end of  $10T_e$  (In graph, it corresponds to  $t = 100$ ). Particle initial velocities were put equal to the fluid velocity at their positions ( $u_p^{(n)} = u_{f@p}^{(n)}$ ) and their distribution was fairly homogeneous throughout the domain. They were then time-stepped with the turbulent flow field without two-way coupling. According to the results of Wang and Maxey (1993), particles put 3 to  $5\tau_p$  to arrive at the equilibrium which is well verified in our simulations. All the statistics reported in this chapter concerning the one-way coupled simulations were performed during this stationary period. Around  $10T_e$  or  $4,5T_L^p$  period were used to obtain precise statistics. For particles with increasing inertia  $\tau_p$ , this calculation becomes exhaustive due to  $T_L^p$  increasing.

Finally, afterwards, two-way coupling was put on ( $t = 170$  on the graph) and another equilibrium was waited for the fluid and particle phases. Statistics concerning the two-way coupled flows were calculated in this range again for another  $10T_e$ .

### 6.3.2 Lagrangian statistics

The statistics concerning the particles were calculated by performing the averages over the particle phase and profiting from the stationarity of the forced turbulence. One-point and two-point statistics were calculated using arithmetic averaging over the number of particles  $N_p$  with the operator defined as:

$$\langle \Psi \rangle_p = \frac{1}{N_p} \sum_{N_p} \Psi \quad (6.5)$$

where  $p$  symbol indicates the averaging over the particle phase.

#### Lagrangian correlations:

Lagrangian one-point correlations were calculated using the quantities along the particle trajectories such as  $u_f$ ,  $u_{f@p}$  or  $u_p$ . In each simulation, two clouds of particles were simulated one of which is the solid particles and the other one is the fluid elements which are both treated in Lagrangian manner. Lagrangian correlations are defined in isotropic turbulence as:

$$R_L^f(\tau) = \frac{1}{3} \langle u_{f,i}(x_{f,i}(t), t) u_{f,i}(x_{f,i}(t + \tau), t + \tau) \rangle \quad (6.6)$$

$$R_L^{f@p}(\tau) = \frac{1}{3} \langle u_{f,i}(x_{p,i}(t), t) u_{f,i}(x_{p,i}(t + \tau), t + \tau) \rangle_p \quad (6.7)$$

$$R_L^p(\tau) = \frac{1}{3} \langle u_{p,i}(x_{p,i}(t), t) u_{p,i}(x_{p,i}(t + \tau), t + \tau) \rangle_p \quad (6.8)$$

where  $f$  denotes a fluid variable and  $p$  denotes a particle variable.  $f@p$  indicates a fluid variable at the position of a particle. The indices are omitted due to the isotropic turbulence in which only the diagonal components are enough to be calculated. It can be noted that these correlations should tend to the second order statistical quantities of the phases in the limit as:

$$\lim_{\tau \rightarrow 0} R_L^f(\tau) = \frac{2}{3}q_f^2 \quad (6.9)$$

$$\lim_{\tau \rightarrow 0} R_L^{f@p}(\tau) = \frac{2}{3}q_{f@p}^2 \quad (6.10)$$

$$\lim_{\tau \rightarrow 0} R_L^p(\tau) = \frac{2}{3}q_p^2 \quad (6.11)$$

These correlations were used in calculating the characteristic timescales of particles which are defined as:

$$T_L^f = \frac{1}{R_L^f(0)} \int_0^\infty R_L^f(\tau) d\tau \quad (6.12)$$

$$T_L^{f@p} = \frac{1}{R_L^{f@p}(0)} \int_0^\infty R_L^{f@p}(\tau) d\tau \quad (6.13)$$

$$T_L^p = \frac{1}{R_L^p(0)} \int_0^\infty R_L^p(\tau) d\tau \quad (6.14)$$

where  $T_L^f$  is the fluid Lagrangian timescale and it indicates the duration for which a fluid element stays in a large eddy.  $T_L^{f@p}$  is the Lagrangian timescale seen by the particles and it is a measure of fluid-particle interactions.  $T_L^p$  is the particle Lagrangian timescale which indicates a timerange for which particle has a memory of its past velocity.

Another statistical correlation can be added which is  $R_L^{fp}$  indicating the fluid-particle velocity correlation. With analogy to what has been written above, it can be written:

$$\lim_{\tau \rightarrow 0} R_L^{fp}(\tau) = \frac{1}{3}q_{fp} \quad (6.15)$$

where  $q_{fp}$  is the fluid-particle covariance. However, this correlation was never measured in this study.

## 6.4 Modulation of the turbulent kinetic energy and the dissipation rate

Two-way coupling mechanism is regarded in three major points (Clift et al., 1978, Peirano and Leckner, 1998). Dominant mechanisms in two-way coupled flows are first the work done by the turbulent eddies to transport the particles (dominant effect for point particles,  $d_p < \eta_K$ ),

vortex shedding caused by particles with high Reynolds number,  $Re_p$  and particle wake-turbulence interactions. In the flow fields without gravity and without external effects such as mean flow etc..., Squires and Eaton (1990), Elgobashi and Truesdell (1993) showed that point particles with small particle Reynolds numbers have tendency to reduce the turbulent kinetic energy due to the non-existence of a production mechanism.

Turbulent kinetic energy balance of the two-way coupled simulation (for  $St_0 = 12$  and  $\phi = 0.16$ ) is presented in figure 6.3. As remarked, the production term  $P$ , calculated by the relation 2.38, is sensibly constant after the addition of the particles to the reference field at  $t = 100$ . Two-way coupling term  $\Pi_{q_f^2}$  and the dissipation rate  $\epsilon$  descend to the equilibrium values. Kinetic energy balance equation can be written, for isotropic homogeneous turbulence, briefly as:

$$\frac{dq_f^2}{dt} = P - \epsilon - \Pi_{q_f^2} \quad (6.16)$$

As seen, production term  $P$  balances the  $\epsilon + \Pi_{q_f^2}$  to an acceptable accuracy. The difference, which counts to 7%, should be due to the interpolation of the back force onto the Eulerian grid by the interpolation scheme, explained in section 2.2.1.6.

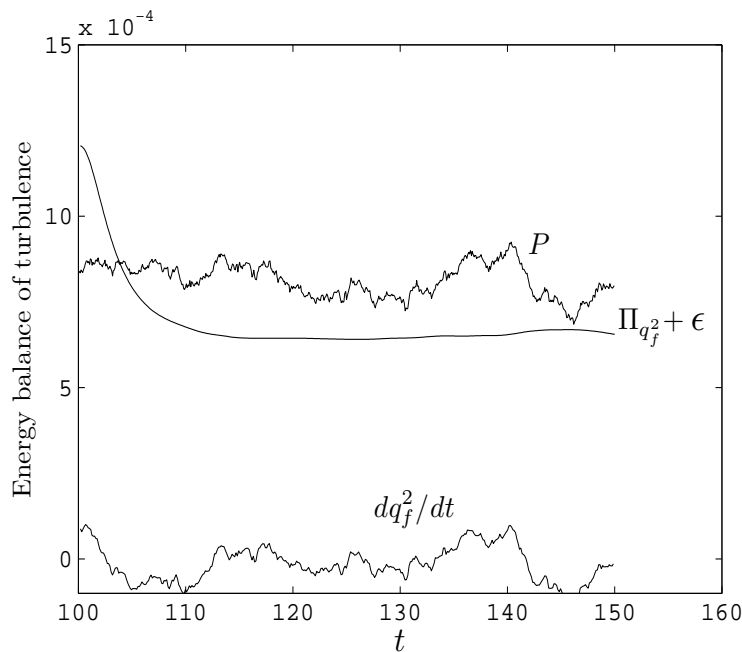


FIGURE 6.3: Turbulent kinetic energy balance in presence of particles (Simulation  $\phi = 0.16$  and  $St_0 = 2.0$ ,  $Re_L = 96$ )

The evolution of the turbulent kinetic energy for different mass loadings and particle inertia is presented in figure 6.4. Coherently with the works mentioned above, it is observed

that the turbulent kinetic energy decreases.

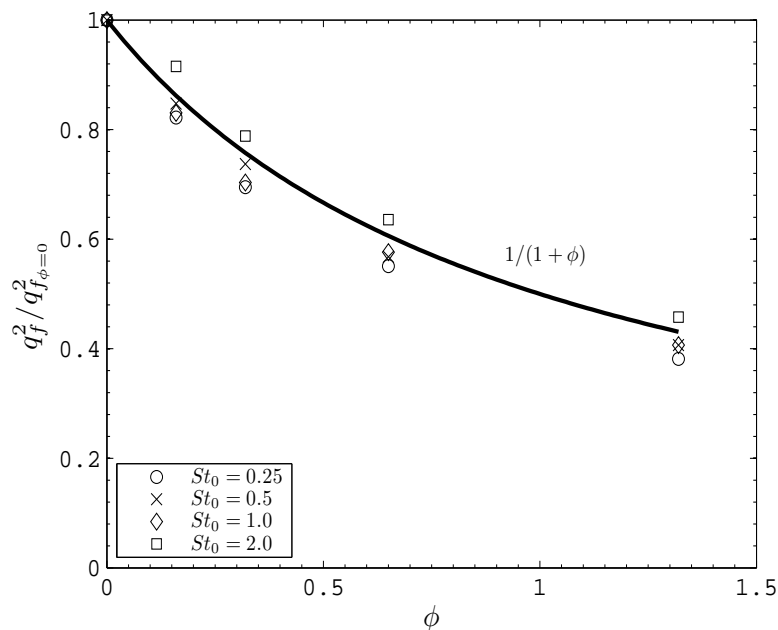


FIGURE 6.4: Modification of the turbulent kinetic energy with reference to the reference flow's kinetic energy (see table 2.2)

Modulation of the turbulent kinetic energy seems weakly dependent on the particle inertia which is in coherence with the works of Squires and Eaton (1994), Boivin (1996). Coherently with the work of Boivin (1996), the modulation follows the line  $1/(1+\phi)$ . It is remarked that for the same mass loading, different Stokes numbers do not result in the same fluid kinetic energy. This is due to the interaction of the particles with different scales of turbulence according to their inertia. For the smallest inertia particles ( $St_0 = 0.25$ ) used in this study, particles preferentially concentrate on the peripheries of the large scales (subject will be investigated in the next chapter). According to this, the reduction in the turbulent kinetic energy is slightly more significant for the flows with small-inertia particles which interact more with the turbulence (Ferrand et al., 2003).

Modulation of the dissipation rate is presented in figure 6.5. It is marked that the descent does not follow the  $1/(1+\phi)$  line. Instead, the line  $1/(1+\phi)^2$  seems more satisfactory to define the decrease. Moreover, it can be noted that the decrease is more dependent on the inertia and the mass loading of particles. Indeed, the smallest inertia causes the minimum reduction in the dissipation rate (here around %60). As noted by Squires and Eaton (1991b), this is due to the preferential concentration of small-inertia particles which results in the increase of the fluid velocity fluctuations on the small scales due to the local perturbation of particles. This

in turn increases the viscous dissipation of the turbulent flow and therefore the reductions in the both quantities  $q_f^2$  and  $\epsilon$  are not of the same order.

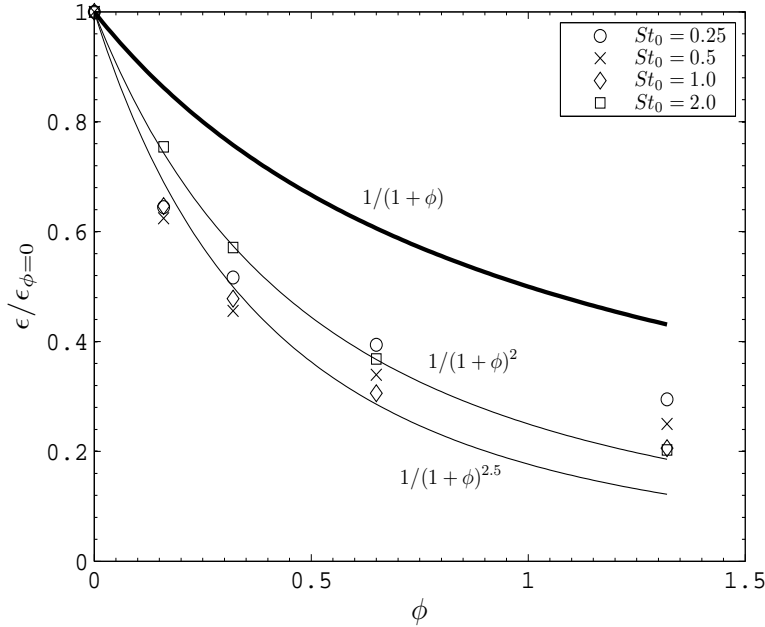


FIGURE 6.5: Modification of the turbulent dissipation rate with reference to the reference flow's dissipation rate (see table 2.2)

As a complementary figure, the modification of the turbulent characteristic timescale  $q_f^2/\epsilon$  with reference to the uncharged flow is presented in figure 6.6. It can be noted that for small inertia particles  $St_0 = 0.25$ , the modification is constant for each mass-loading and indicates to a %20 of increase with reference to the uncharged flow. On the other hand, inertial particles  $St_0 = 2.0$  results in increasing  $q_f^2/\epsilon$  ratio with the mass-loading.

The reduction in the turbulent and Taylor scale Reynolds numbers of each simulation is presented in figures 6.7 and 6.8. It is seen that for each simulation turbulent Reynolds number is modified between 20 and 30% whereas  $Re_\lambda$  is practically not modified for the highest inertia particles and for all loadings. For small inertia particles, there is up to 30% of descent in the  $Re_\lambda$ . Considering the definition of turbulent Reynolds number, this behavior should be due to the modulation in the turbulent kinetic energy levels presented above, therefore the modulation in the characteristic velocity  $u'$  of turbulence. Modification in the Taylor scale Reynolds number will be useful for the discussion in the section for the Lagrangian structure function at the end of this chapter.

As shown in figure 6.9, the large scales, after the two-way coupling is turned on, are fairly similar in length, e.g., they are almost one tenth of the length of the domain,  $L_b$ . It should

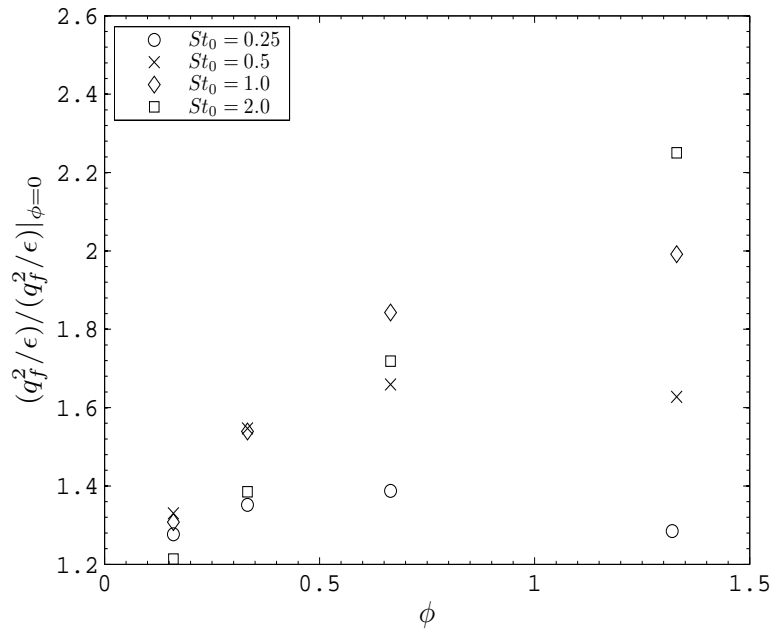


FIGURE 6.6: Modification of the characteristic timescale of turbulence  $q_f^2/\epsilon$  with reference to the uncharged flow.

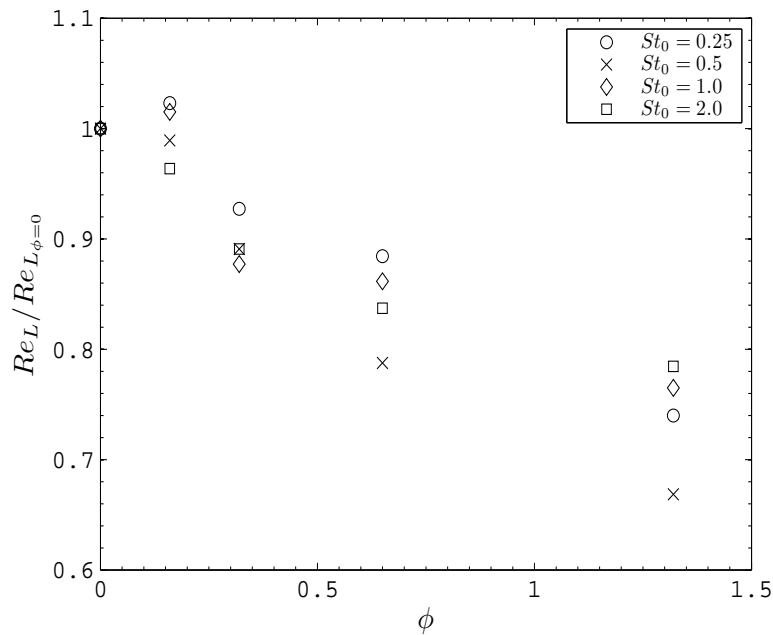


FIGURE 6.7: Modification of the turbulent Reynolds number,  $Re_L$

be noted that the large scales' length is imposed by the stochastic forcing scheme used (see chapter 2).

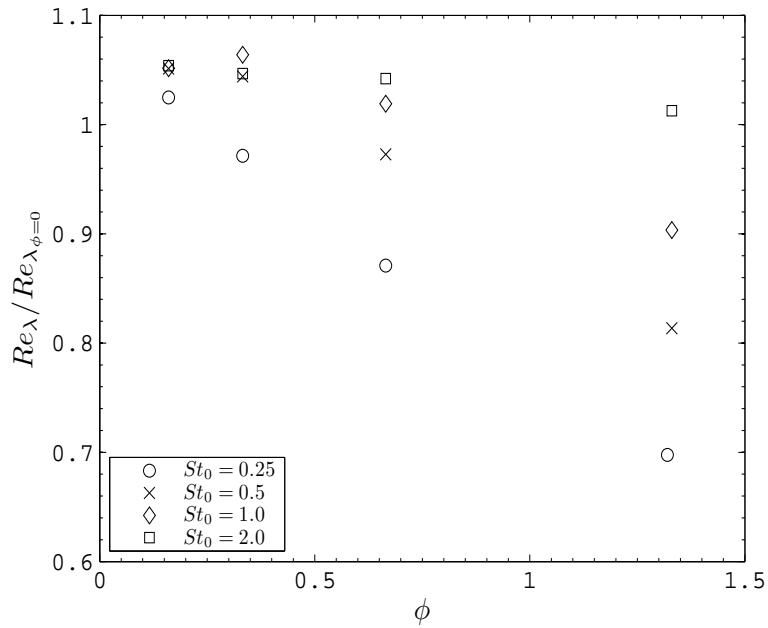
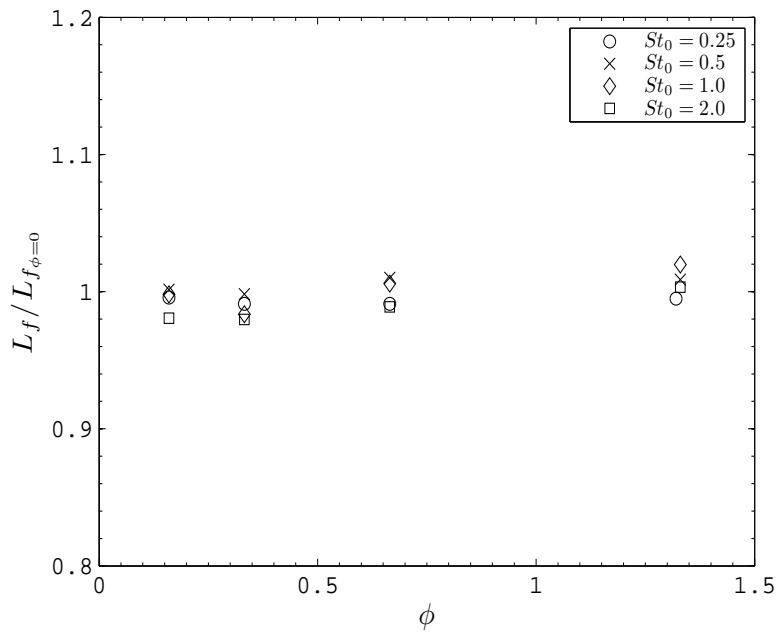
FIGURE 6.8: Modification of the Taylor scale Reynolds number,  $Re_\lambda$ 

FIGURE 6.9: Modification of the integral scales of turbulence

Considering the eddy turnover time defined as  $T_e = L_f/u'$ , the decrease in the turbulent characteristic velocity  $u'$  causes the eddy turnover time to increase. Therefore after the coupling, the large eddies have similar lengths with reference to the one-way coupled flow

but they turn with more slower velocity.

The modification of the Taylor length scales are presented in figure 6.10. In contrast to the integral scales, Taylor length scale is modified by the effect of particles. More clearly, for the smallest inertia particles, not very significant modification has been observed which is not true for the highest inertia particles. For highest inertia particles, increase in mass-loading results in increase in the Taylor length scale. However, considering the modulation of the turbulent kinetic energy,  $q_f^2$ , the decrease in the turbulent kinetic energy is compensated by the increase in the Taylor length scale for the highest inertia particles  $St_0 = 2.0$ , hence the Reynolds number based on the Taylor scale is not modified significantly with reference to the uncharged flow. On the other hand, for smallest inertia, interestingly, Taylor length scale is not significantly modified by the two-way coupling mechanism, therefore the  $Re_\lambda$  values decrease.

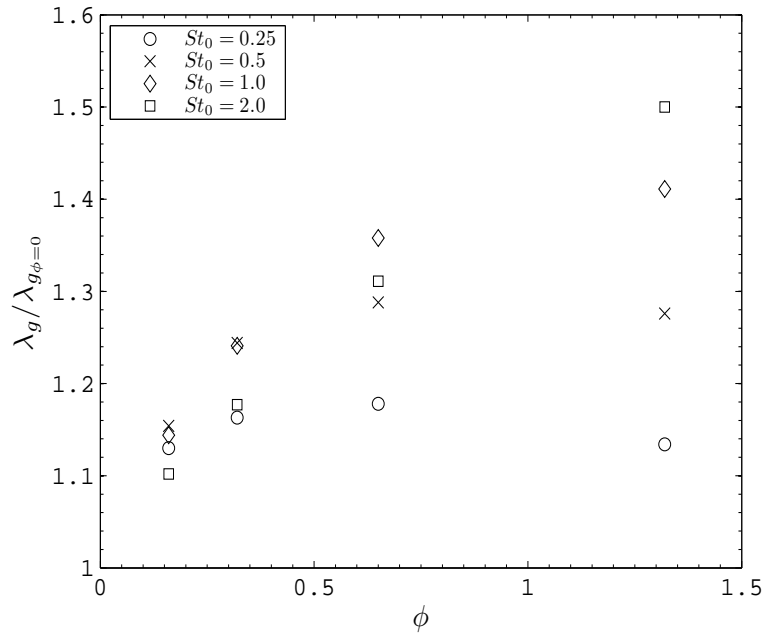


FIGURE 6.10: Modification of the Taylor length scale

## 6.5 Modulation of 3D turbulent energy spectrum

It is fundamental to investigate the effect of the particles on different scales of turbulence. In the work of Elgobashi and Truesdell (1993), it has been observed that for large inertia particles, the modulation of spectrum of turbulence is more uniform whereas for the small inertia particles, the modulation is non-uniform, e.g, different scales of turbulence respond

differently to the particles. Turbulent energy spectra after the two-way coupling is turned on are presented in figures 6.11 and 6.12 for the smallest and the largest inertia, respectively, and for all mass loadings. Net decrease in the kinetic energy is marked immediately but the energy budget, the distribution among different scales of turbulence, significantly changed.

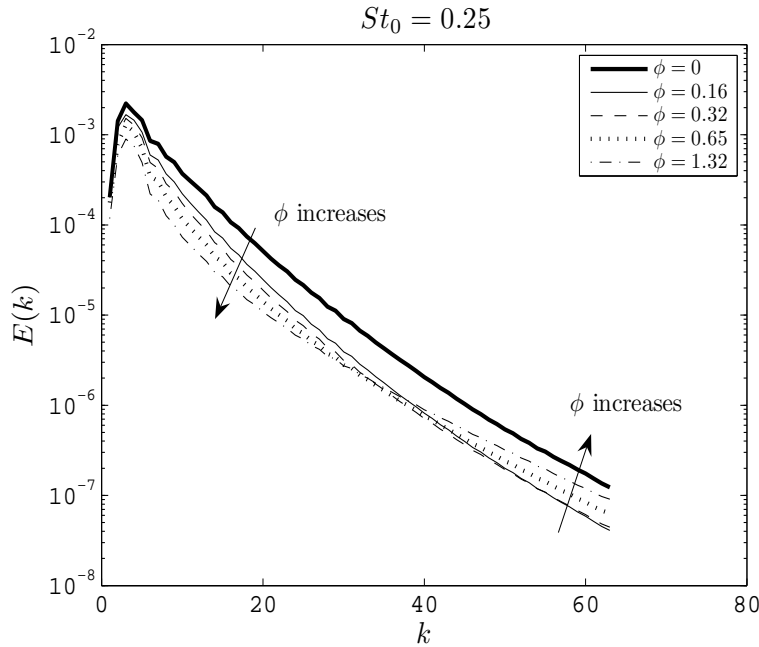


FIGURE 6.11: Modification of the turbulent 3D spectrum of the reference flow by the addition of particles, for small inertia particles

Coherently with the literature, for small inertia particles (figure 6.11), the modification of the spectrum is non-uniform. It is observed a net decrease in the low wavenumber range, however, small scales seem more and more active with the increase in mass loading of particles after an initial immediate descent for  $\phi = 0.16$ . This results in a net change in the rate of energy transfer between the scales (slope of the spectrum). Boivin (1996) showed that the small scales could even be more energetic than they were in one-way coupled flows with high turbulent Reynolds number (one-way coupled simulation is shown by dashed lines). These results are in coherence with the work of Elgobashi and Truesdell (1993) and Squires and Eaton (1994) where they showed that the increase in energy for the large wavenumbers is recompensated by the decrease in the low wavenumber scales. Therefore, globally, the modification depends on both the mass loading  $\phi$  and also the inertia of the particles  $\tau_p$ .

For large inertia particles (presented in figure 6.12), modification seems more uniform. Interestingly, the modification at the very low wavenumber end of the spectrum is less significant than the flows charged with low inertia particles (presented in figure 6.11).

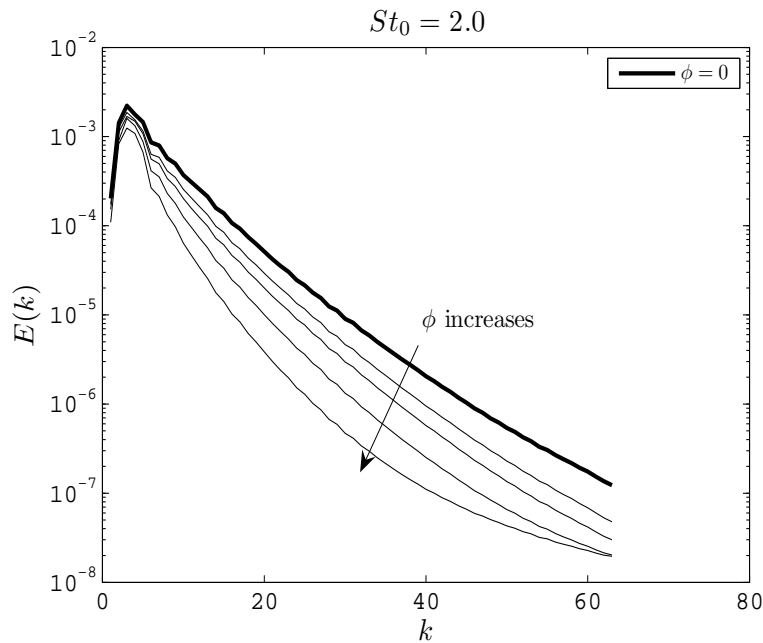


FIGURE 6.12: Modification of the turbulent 3D spectrum of the reference flow by the addition of particles, for large inertia particles

These movements of the spectra clearly shows that the particles with low inertia extracts collectively kinetic energy from some of the scales of turbulence and reinject it to the preferential scales of turbulence. As noted by Février (2000), this reinjection of kinetic energy to certain scales of turbulence could be possible with the collective motion of particles which is a correlated motion and could be described by the mesoscopic velocity  $\tilde{u}_p$  of the particles (see section 5.7.2). Therefore the energy transferred to the uncorrelated motion of particles would be dissipated by the action of viscosity. Then the model proposed in section 5.7.2, should cover these movements of the spectra.

## 6.6 Modulation of the Eulerian and Lagrangian temporal correlations of turbulence

In previous sections, it has been seen that the decrease in the kinetic energy level of turbulence leads to the increase in the eddy turnover time,  $T_e$ . Parallel to this, the temporal correlations and timescales of turbulence with two-way coupling will be investigated in this section. The definition and the method of calculation of these correlations are already mentioned in section 2.3.4.3, so will not be discussed here, any further.

Eulerian one-point correlations are presented in figures 6.13 and 6.14. As seen, for each

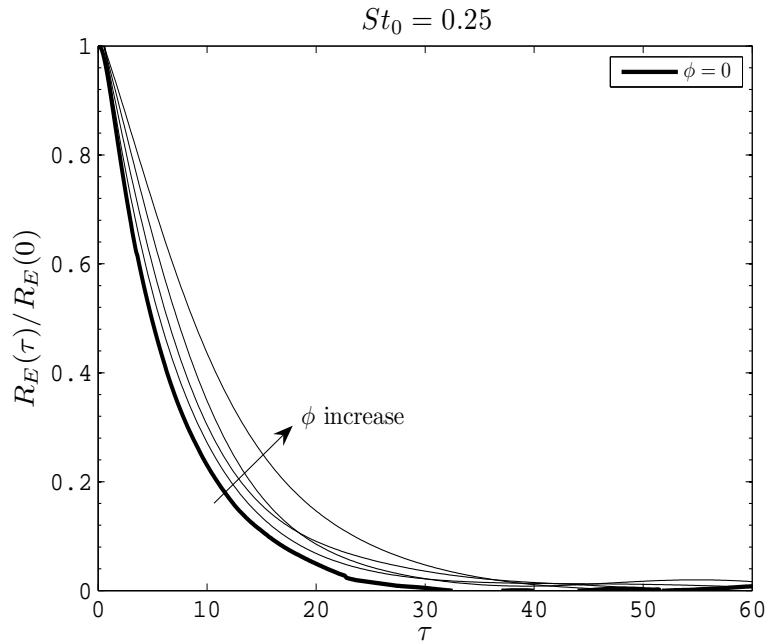


FIGURE 6.13: Modification of the Eulerian one-point correlation of the fluid fluctuation velocity, for small inertia particles

inertia and all the mass-loadings, correlations increase for a fixed time separation. This is in consistence with the increase in  $T_e$  e.g., eddies turning more slowly results in larger decorrelation time according to an immobile observer. The modulation of the Lagrangian timescales are shown in figure 6.15. The dependence of the Eulerian decorrelation timescale on the particle inertia and mass-loading is complicated, as can be noted from the figure. It seems that with increasing mass-loading and particle inertia, Eulerian timescale gets larger.

The ratio  $T_E/T_e$  is presented in figure 6.16. As seen, the ratio reaches at the values around 1.25 for high inertia particles. This should be acceptable due to the stochastic forcing that generates high levels of oscillations from one timestep to another. This in turn can cause some inprecise calculation of the correlations and finally the Eulerian timescale  $T_E$ . Therefore the fluid turbulent field keeps its homogeneity and isotropy after the two-way coupling is turned on.

Note on stochastic forcing scheme:

It should be mentioned in passing that the parameters of stochastic forcing calibrated in second chapter (see table 2.1) are not modified after the two-way coupling is turned on. Therefore the equality  $T_F = T_E = T_e$  is verified for the one-way coupled simulations but for the two-way coupled simulations, it is  $T_F < T_E \approx T_e$ .

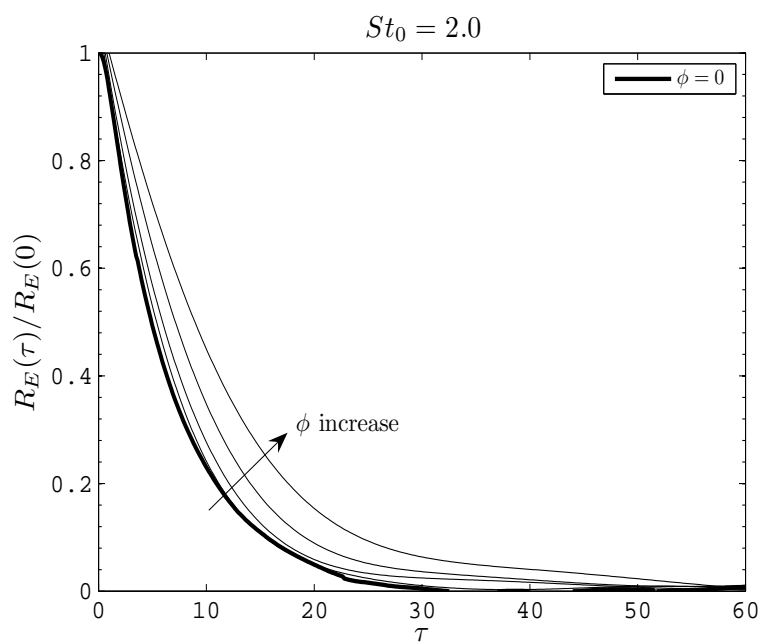


FIGURE 6.14: Modification of the Eulerian one-point correlation of the fluid fluctuation velocity, for large inertia particles.

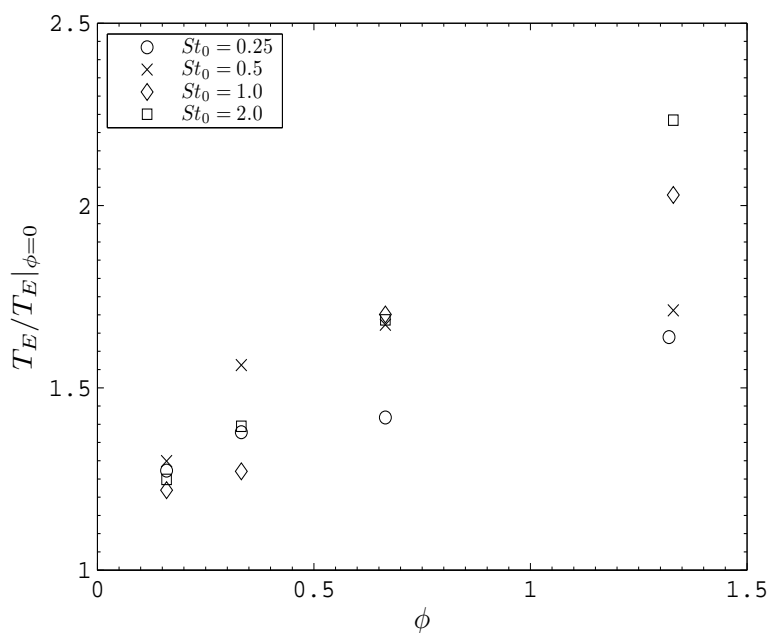


FIGURE 6.15: Modulation of the Eulerian timescale calculated from the one-point correlations

Lagrangian temporal correlations are presented in figures 6.17 and 6.18. For small inertia particles, it is seen that the correlations increase with increasing mass loading whereas,

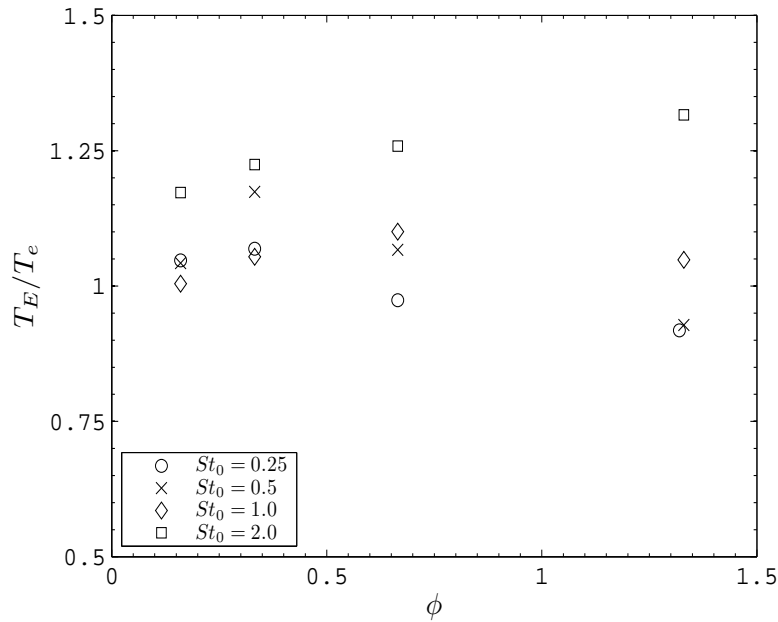


FIGURE 6.16: Ratio of the characteristic timescales with the effect of two-way coupling,  $T_E/T_e = 1$  for the reference flow field (see table 2.2).

for the high inertia particles, the correlations seem weakly dependent on the mass loading. The variation of the Lagrangian timescale with the mass-loading and the particle inertia is presented in figure 6.19. More step increase is remarked for small inertia particles where the value is up to 1.9 times the uncharged flow value.

The motivation in Lagrangian stochastic models is to write down the trajectorial equation of motion of discrete elements, of which the statistics must be predicted out of this equation. This behavior of the Lagrangian correlations presented above has to be taken into account by the stochastic model equation 5.17 for the fluid element trajectories.

### 6.6.1 Classical stochastic modeling for single phase flows

As shown in section 5.4.1, stochastic modeling leads to the Lagrangian timescale,  $T_L^f$ , written as:

$$T_L^f = \frac{4}{3C_0} \frac{q_f^2}{\epsilon} \quad (6.17)$$

where  $C_0$  is the Kolmogorov constant usually taken equal to 2.1. Therefore here the Lagrangian timescale is written in terms of turbulent quantities which are of practical importance in terms of turbulence modeling.

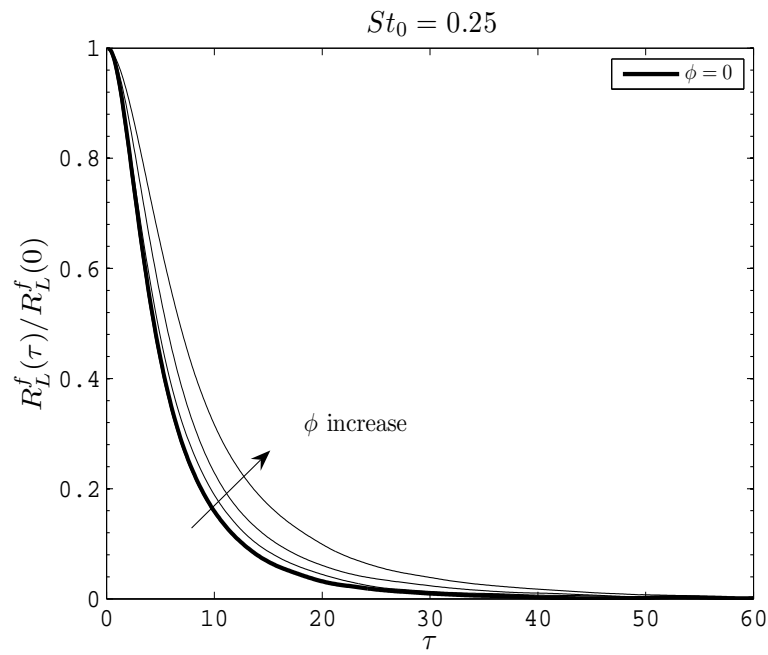


FIGURE 6.17: Modification of the Lagrangian one-point correlations, for small inertia particles

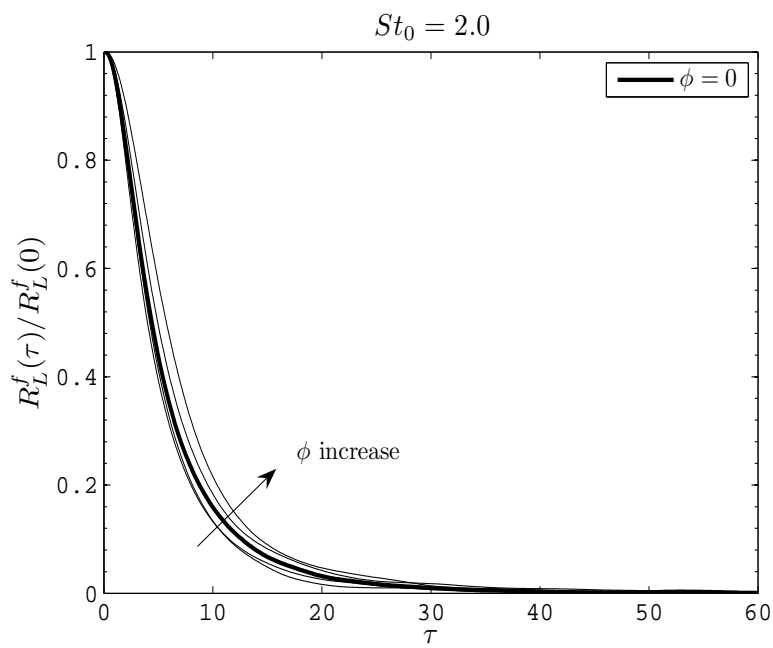


FIGURE 6.18: Modification of the Lagrangian one-point correlations, for large inertia particles

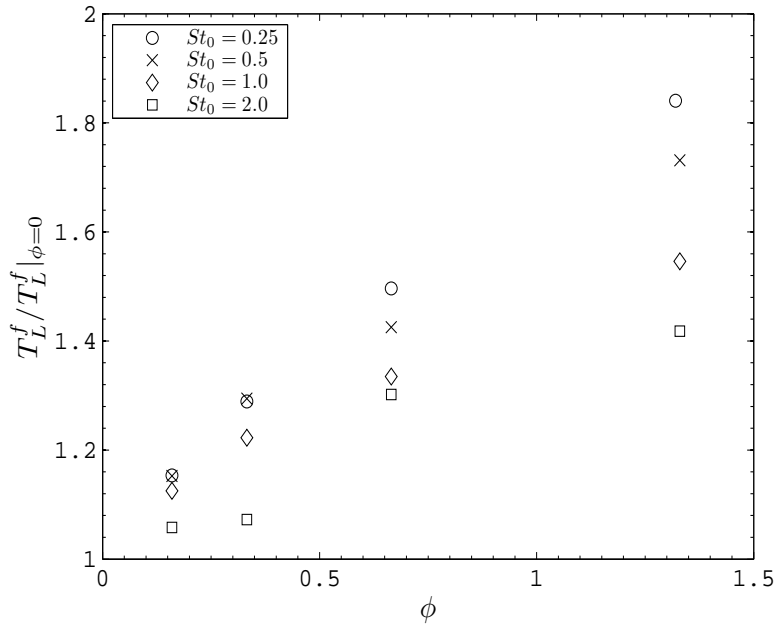


FIGURE 6.19: Modification of the Lagrangian timescale of the fluid elements

### 6.6.2 Extension to the two-way coupled gas-solid flows

The Langevin equation for single phase flows was extended to the two-way coupled gas-solid flows with an additional term  $\Pi_{u_f,i}^*$  to account for the effect of the particles on the fluid element trajectories. The additional term  $\Pi_{u_f,i}^*$  was defined with two different models, namely: mean and instantaneous models.

#### Mean model:

Using the mean model given by relation 5.66, due to the statistical operator, the Lagrangian structure function derived from the Langevin equation 5.17 is written as:

$$D_L^*(s) = B_f^2 s \quad (6.18)$$

with  $B_f = \sqrt{-\frac{4}{3}A_f q_f^2}$ . The \* symbol represents the quantity of a stochastic particle governed by the Langevin equation.

If the consistency with the Kolmogorov hypothesis is used for the coefficient  $B_f$ , then it will be written as  $B_f = \sqrt{C_0 \langle \epsilon \rangle}$  and the relation for Lagrangian timescale  $T_L^f$  will be written as 6.17. According to the relation 6.17, the Lagrangian timescale is linearly proportional to the  $q_f^2/\epsilon$ . Presented Lagrangian correlations of the fluid element velocities show variations in presence of two-way coupling mechanism as presented in figure 6.20.

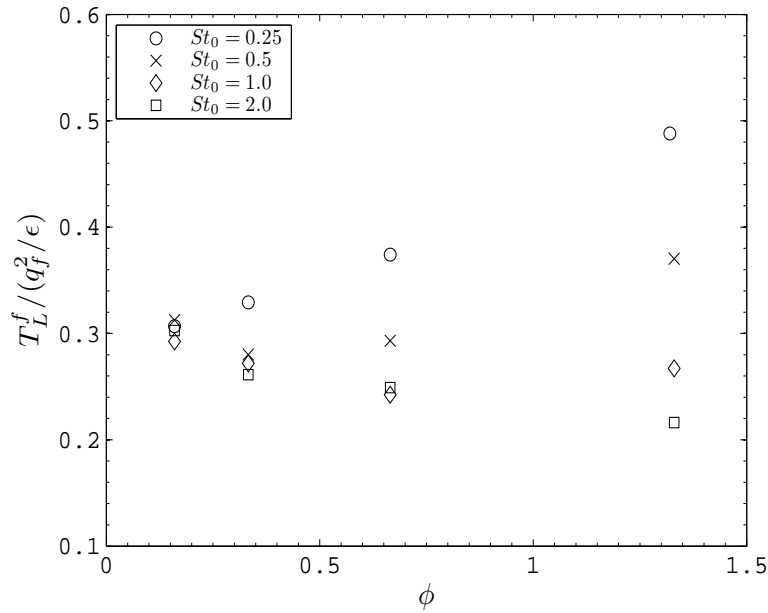


FIGURE 6.20: Ratio of the Lagrangian timescale  $T_L^f$  to the characteristic turbulence timescale  $q_f^2/\epsilon$ , see relation 6.17

As shown in the figure, the ratio  $T_L^f/(q_f^2/\epsilon)$  does not have a constant value, but, it is a coefficient changing according to the mass loading and particle inertia which is due to the variations in the Kolmogorov constant  $C_0$ . The value of this parameter is largely discussed in the literature and it has been shown already by Yeung et al. (2006) that increasing turbulent Reynolds number,  $Re_L$ ,  $C_0$  approaches to the asymptotic limit of 7.0. For small Reynolds numbers,  $Re_L$ , a value of 3.0 is seen to produce good results (Sawford and Tivendale, 1992). It is significantly important in stochastic models because it controls the Lagrangian timescale of the fluid  $T_L^f$  and significantly difficult to measure in low Reynolds number turbulent flows such as used in this thesis.

#### Instantaneous model:

Using the instantaneous model 5.87, the Lagrangian structure function is derived as:

$$D_L^*(s) = B_f^2 s + \frac{\phi^2}{\tau_p^2} [2\tilde{q}_p^2 - 2q_{fp} + 2q_{f@p}^2] s^2 + 2A_f \frac{\phi}{\tau_p} [q_{fp} - 2q_{f@p}^2] s^2 \quad (6.19)$$

where  $B_f$  and  $A_f$  could be determined from the relations 5.129 and 5.121, respectively. The determination of these coefficients should be useful in order to calculate the magnitude of the second and third terms in 6.19 but requires an hypothesis because the relations hold the fluid statistics viewed by the particles and the fluid elements. From the other part, the solution of 5.121 seems not possible analytically.

To investigate the behavior of  $C_0$  precisely, Lagrangian structure function must be studied which is the subject of the next section.

## 6.7 Modulation of the Lagrangian structure function

To examine the fluid element velocities on different scales of turbulence, the best method is to use the Lagrangian structure function  $D_L(s)$ . Second-order Lagrangian structure function carries great importance to the research on small scales of turbulence due to its superiority to precisely characterize a turbulent flow (Kolmogorov scale similarity) than an Eulerian scaling law. However, in high Reynolds number turbulent flows, Lagrangian statistics are extremely difficult to be obtained, even in numerical environment (no need to mention on laboratory experiments). From the other part, this function is also important to stochastic modeling because these models try to predict it to satisfy the coherence with the scale similarity law of Kolmogorov. Detailed explanation of this function and its utility can be found in the book of Monin and Yaglom (1975).

Measurements of  $D_L$  for the two-way coupled simulations performed are presented in figures 6.21 and 6.22.

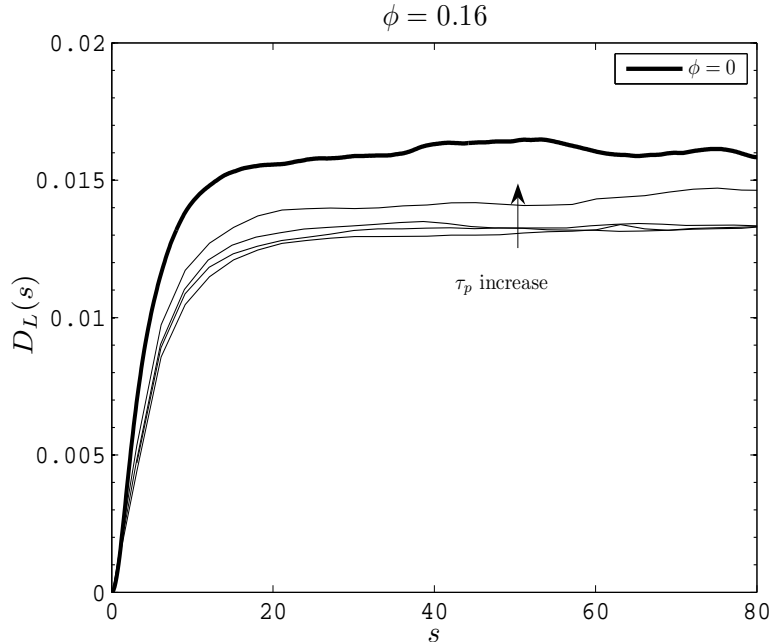


FIGURE 6.21: Modification of the Lagrangian structure function, for low mass loading

As seen, with increasing particle inertia, high mass loading of particles modifies the structure function of fluid elements more significantly than the low mass loadings. After initial

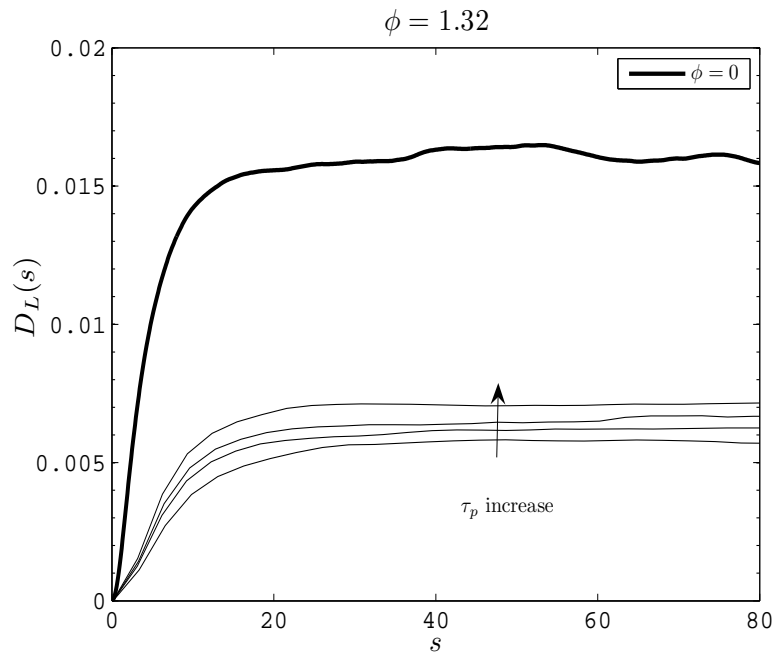


FIGURE 6.22: Modification of the Lagrangian structure function, for high mass loading

increase, all the curves approach to a stationary value which is larger for small loading  $\phi = 0.16$  (comparing the figures). However, both mass loading shows an initial sudden decrease and then following increase with the particle inertia which should be an effect due to the turbulent dissipation-rate.

As noted by Yeung et al. (2006),  $D_L(s)$  has a rise and a fall when normalized by  $\epsilon s$  due to its limiting behaviors. Normalized curves are presented in figures 6.23 and 6.24.

Coherently, a peak is obtained in the normalized structure function curves where the peak corresponds to the Kolmogorov constant  $C_0$ . In fact, for large Reynolds number turbulent flows, instead of very short peak value, sufficiently large range of constant value is obtained where a scaling could be applied (Yeung et al., 2006). However, the Reynolds numbers considered in this thesis are fairly low due to the restrictions imposed by DNS. Considering the modification in the Reynolds number  $Re_\lambda$  based on the Taylor length scale,  $\lambda$ , figure 6.8 shows that there is not much variation in the normalized  $D_L$  curves with increasing relaxation times,  $\tau_p$ , for  $\phi = 0.16$ . This is in coherence with the  $Re_\lambda$  which does not show much variation for increasing  $\tau_p$  and  $\phi = 0.16$ , either.

For high mass loading,  $\phi = 1.32$ , figure 6.24 shows that increasing  $\tau_p$ , the peak value ( $C_0$ ) increases and for the highest value of  $\tau_p$ , it arrives at the level of  $C_0$  values of flows with mass loading  $\phi = 0.16$ . Figure 6.23 is in coherence with the figure 6.8 of modification of  $Re_\lambda$  in that for highest particle relaxation time,  $Re_\lambda$  of the flow does not vary with reference to

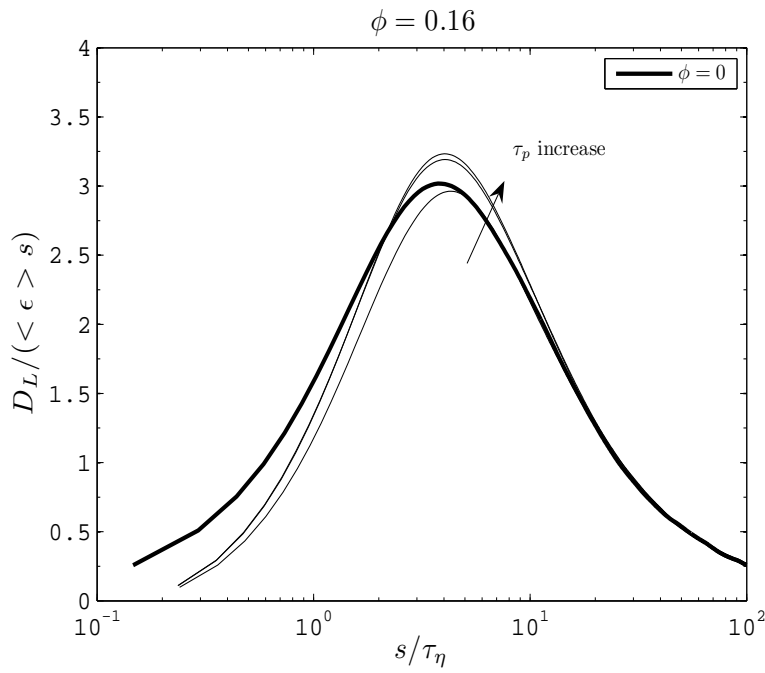


FIGURE 6.23: Modification of the normalized Lagrangian structure function, for low mass loading

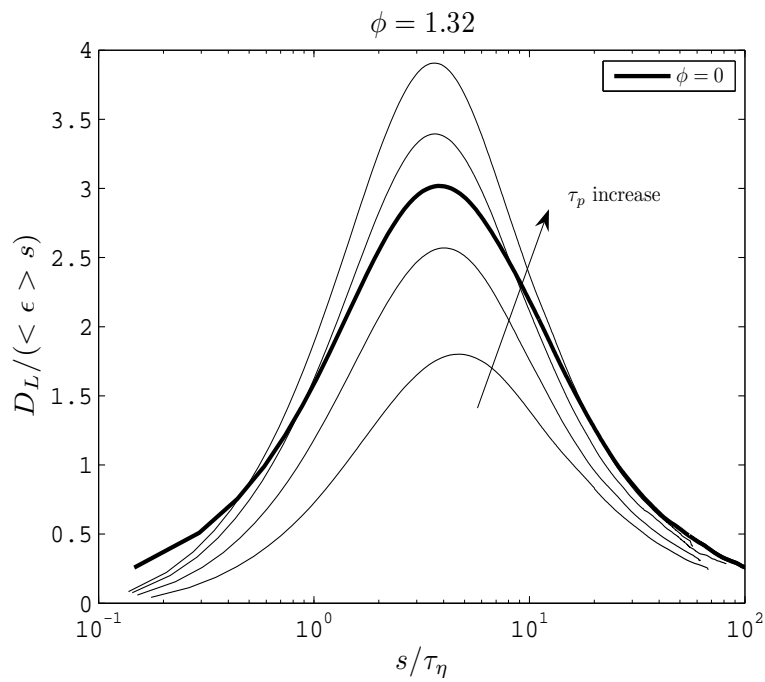


FIGURE 6.24: Modification of the normalized Lagrangian structure function, for high mass loading

the uncharged flows. Therefore, obtained value of  $C_0$  is similar to the values of obtained in flows with  $\phi = 0.16$ . For smallest  $\tau_p$  and  $\phi = 1.32$ , figure 6.24 shows that the  $Re_\lambda$  is reduced

up to 30% of the uncharged flow value.  $C_0$  accordingly diminishes and the minimum value obtained 1.80 is clearly below the results obtained by (Yeung et al., 2006). This could be attributed to the two-way coupling mechanism which has large effect on the small scales (see the section 6.5 for the turbulent spectra).

Therefore, Lagrangian structure function curves show dependency on both the  $\phi$  and  $\tau_p$  for small Reynolds number flows. From the other part, for the low Reynolds numbers considered in this study (even lower values are obtained with the effect of particles), determination of the precise value of  $C_0$  is difficult and strictly it is not a constant. For a summary, the evolution of the  $C_0$  values as a function of the Reynolds number based on the Taylor length scale  $Re_\lambda$  is presented in figure 6.25 where the measured values are compared to the literature. In the range of Reynolds numbers considered in this thesis, the values seem to agree with the values reported by Yeung et al. (2006).

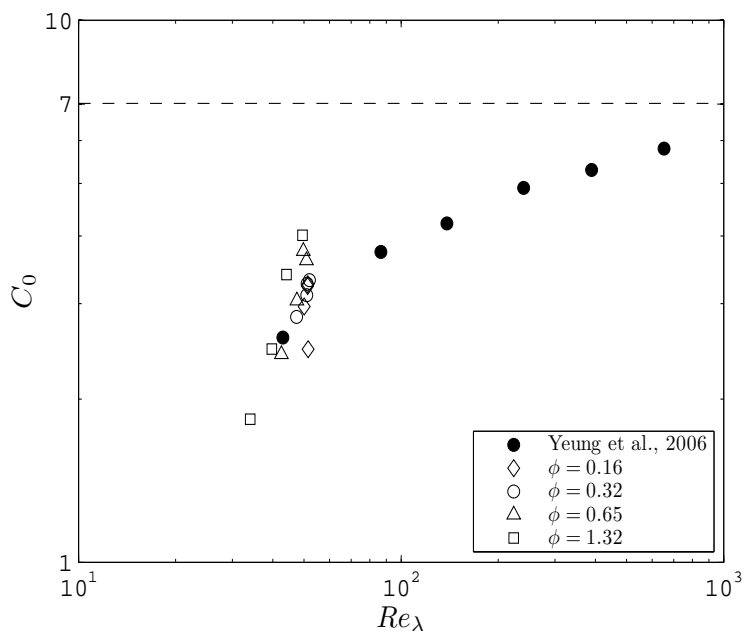


FIGURE 6.25:  $C_0$  values measured from DNS+DPS for two-way coupled flows.

Based on these findings, the modeling approach of Pope (2002) is more adequate due to the low Reynolds numbers used in this study. Therefore in the methodology presented in section 5.5, first the coefficient  $A_f$  is determined using the correlation function and then once knowing  $A_f$ , the coefficient  $B_f$  can be determined from the  $q_f^2$  transport equation instead of considering the Lagrangian structure function.

## 6.8 Conclusion

In this chapter, basically, measurements of the effect of particles with finite inertia on the turbulence are reported. Measurements correspond to the DNS for the fluid phase and DPS for the particle phase. The interphase momentum transfer term in the Navier-Stokes equation is modeled using the point source approach (see chapter 2). It has been found that the inertial point particles decrease the turbulent kinetic energy in absence of external effects such as gravity, mean flow etc... also the turbulent kinetic energy spectrum is modified more non-uniformly by the effect of small inertia particles which highly interacts with turbulent scales. This findings are coherent with the literature reported.

An important point in this chapter is that the Lagrangian structure function is modified in a complex manner by the effect of high and small inertia particle resulting in different behavior of the Lagrangian timescale,  $T_L^f$ . This results in dependence of the Kolmogorov constant  $C_0$  on particle inertia  $\tau_p$ , particle loading  $\phi$  and Taylor scale Reynolds number  $Re_\lambda$ . Due to this restriction, the diffusion term in stochastic Langevin equation is modeled using the second order Reynolds tensor (see section 5.5.3) instead of using the Lagrangian structure function in the context of Kolmogorov scale similarity hypothesis.

The next chapter will talk about the comparison of the stochastic modeling results to the DNS+DPS results obtained in this section.

## Chapter 7

# Simulation and modeling of fluid-particle correlations

### 7.1 Introduction

In this chapter, the Lagrangian stochastic modeling presented in chapter 5 is going to be compared to the results of DNS+DPS. Indeed, in the previous chapter, it was shown that point particles can effect the turbulence structure and the cascade of kinetic energy to a large extent according to the particle inertia  $\tau_p$  and mass loading  $\phi$ . Therefore it is essential that the stochastic modeling of fluid element trajectories and the fluid velocity viewed by the solid particles must well predict the dispersion of particles in a turbulent flow modified by the presence of particles, fluid phase statistics viewed by the particles and fluid elements.

The chapter is written in the following order:

First, particle dispersion is going to be analyzed in terms of the autocorrelation functions of particle velocities and fluid velocity viewed by the particles. Autocorrelation function of the fluid viewed is once measured from the DNS+DPS and once derived from the Langevin model proposed. It is going to be clear that in low Reynolds number flows considered in this thesis, the Langevin modeling poorly predicts this correlation due to its infinite Reynolds number hypothesis. However, it is going to be shown that the low Reynolds number effects can be taken into account by the proposition of Sawford (1991) when mean drag model is used. Then the particle dispersion coefficient will be reported.

Second, particle statistics will be analyzed to validate the models. The practical relations derived in chapter 5 are going to be used to this purpose. It is going to be seen that the statistics viewed by the particles can be fairly different than the statistics viewed by the fluid

elements. This can cause in reduction in the dispersion coefficient for certain mass loadings. The nature of this statistical difference will be explored in the preferential concentration of particles.

As a final point, to complete the particle dispersion study, the fluid-turbulent drift velocity will be analyzed in a colored particle number density gradient configuration. It will be seen that both models are able to predict with some errors the particle fluxes due to the drift velocity which corresponds to the transport of particles due to the large turbulent scales. For more detailed explanation of drift velocity see the section 5.6.5. The instantaneous model results in more complicated relation for this flux's expression and it is difficult to measure and to model. Results than lets think that the mean drag model has more advantages than the instantaneous model.

## 7.2 Analysis of solid particle dispersion in turbulent flow field

### 7.2.1 Fluid element diffusion

It is known that turbulence diffuses scalar quantities better than a laminar flow. Diffusion of fluid elements in a turbulent flow has been studied initially by Taylor (1921) who gave a general relation for the fluid element displacement tensor using Lagrangian reference frame following the fluid element in 2D formalism. As also verified by the work of Corrsin (1961), the problem of turbulent diffusion is more suitably analyzed in Lagrangian reference frame than in Eulerian frame. However, the Lagrangian studies, being very costly to perform, Eulerian studies are known to be much more practical and therefore are the focal point of researchers in academy and in industry.

In Eulerian study of diffusion, generally, a transport equation for the spatial concentration  $c$  of scalar is considered. Ignoring the details of the flow and transport of scalars, a mean transport equation for the scalar concentration is written as:

$$\frac{\partial \langle c \rangle}{\partial t} + \langle u_{f,i} \rangle \cdot \nabla \langle c \rangle = (D_{f,ij}^t + D_m) \nabla^2 \langle c \rangle \quad (7.1)$$

where  $D_m$  is the molecular diffusion coefficient and  $D_{f,ij}^t$  is the diffusion coefficient corresponding to the turbulent mixing due to the large scales. Major drawback in Eulerian formulation is the lack of a consistent model for the flux of the scalar due to the turbulent velocity fluctuations,  $\langle u'_{f,i} c' \rangle$ . In general, a gradient diffusion model is used for this turbulent flux as  $\langle c' u'_{f,i} \rangle = D_{f,ij}^t \frac{\partial \langle c \rangle}{\partial x_j}$ .

To determine the diffusion coefficient, Taylor (1921) expresses the displacement tensor of a fluid element in a turbulent flow field in terms of Lagrangian correlations as:

$$\frac{d}{dt} \langle [x_{f,i}(t) - x_{f,i}(0)][x_{f,i}(t) - x_{f,i}(0)] \rangle = \int_0^t (R_{L,ij}^f(\tau) + R_{L,ji}^f(\tau)) d\tau \quad (7.2)$$

Using the fluid element displacement tensor, Batchelor (1949) defines the diffusion coefficient of a fluid element,  $D_f^t$ , as:

$$D_{f,ij}^t = \frac{1}{2} \frac{d}{dt} \langle [x_{f,i}(t) - x_{f,i}(0)][x_{f,j}(t) - x_{f,j}(0)] \rangle \quad (7.3)$$

For long time separations, the diffusion coefficient is written in its general form as:

$$\lim_{t \rightarrow \infty} D_{f,ij}^t = \frac{1}{2} \sqrt{\langle u_{f,i}'^2 \rangle \langle u_{f,j}'^2 \rangle} (T_{L,ij}^f + T_{L,ji}^f) \quad (7.4)$$

For homogeneous isotropic stationary turbulence, only the trace of the tensor needs to be calculated and the dispersion coefficient is written as:

$$D_f^t = \frac{2}{3} q_f^2 T_L^f \quad (7.5)$$

According to this relation, it can be said that the dispersion of fluid elements are controlled by the large scales of turbulence.

## 7.2.2 Solid particle dispersion

The extension of the formalism presented for the fluid element diffusion to the dispersion of solid particles in a turbulent flow is performed initially by Tchen (1947) and following researchers are Hinze (1975), Gouesbet et al. (1984), Squires and Eaton (1991a) etc... The particle dispersion coefficient is written in terms of the displacement tensor, according to these studies, as:

$$D_{p,ij}^t = \frac{1}{2} \frac{d}{dt} \langle [x_{p,i}(t) - x_{p,i}(0)][x_{p,j}(t) - x_{p,j}(0)] \rangle \quad (7.6)$$

$$D_{p,ij}^t = \frac{1}{2} \sqrt{\langle u_{p,i}'^2 \rangle \langle u_{p,j}'^2 \rangle} (T_{L,ij}^p + T_{L,ji}^p) \quad (7.7)$$

where  $u_{p,i}'$  is the fluctuating particle velocity in  $i^{th}$  direction,  $T_L^p$  is the Lagrangian timescale of particles (see relation 6.12).

In the long time limit, long time particle dispersion coefficient  $D_p^t$  is written, similarly in isotropic homogeneous stationary turbulence, as:

$$D_p^t = \frac{2}{3} q_p^2 T_L^p \quad (7.8)$$

In the context of this relation, according to the inertia  $\tau_p$  of particles, two different mechanisms are thought:

- Large agitation  $q_p^2$  (see figure 7.1) of particles which have very short memory (small  $T_L^p$ , small  $\tau_p$ )
- Small agitation of particles but with long memory (see figure 7.2) of the preceding velocity, leading to the same dispersion coefficient Gouesbet et al. (1984)

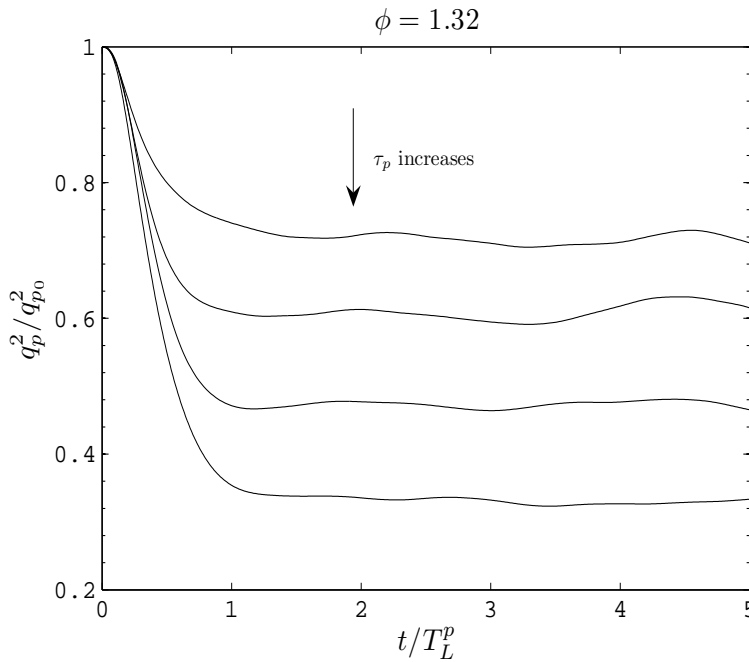


FIGURE 7.1: Behaviour of particle agitation,  $q_p^2$ , with the particle inertia  $\tau_p$  (see the relation 7.8)

As seen in figure 7.3, the dispersion coefficient is well verified, up to an error of 5%, by the particle phase statistical quantities. The imprecisions in the small particle inertia (right hand side of the graph) part should be due to the particles which are in interaction with the small scales of turbulence.

The physical effects explained above are consisted in the drag term of the particle equation of motion 2.7. For many gas-solid flow configurations, particle equation of motion can be

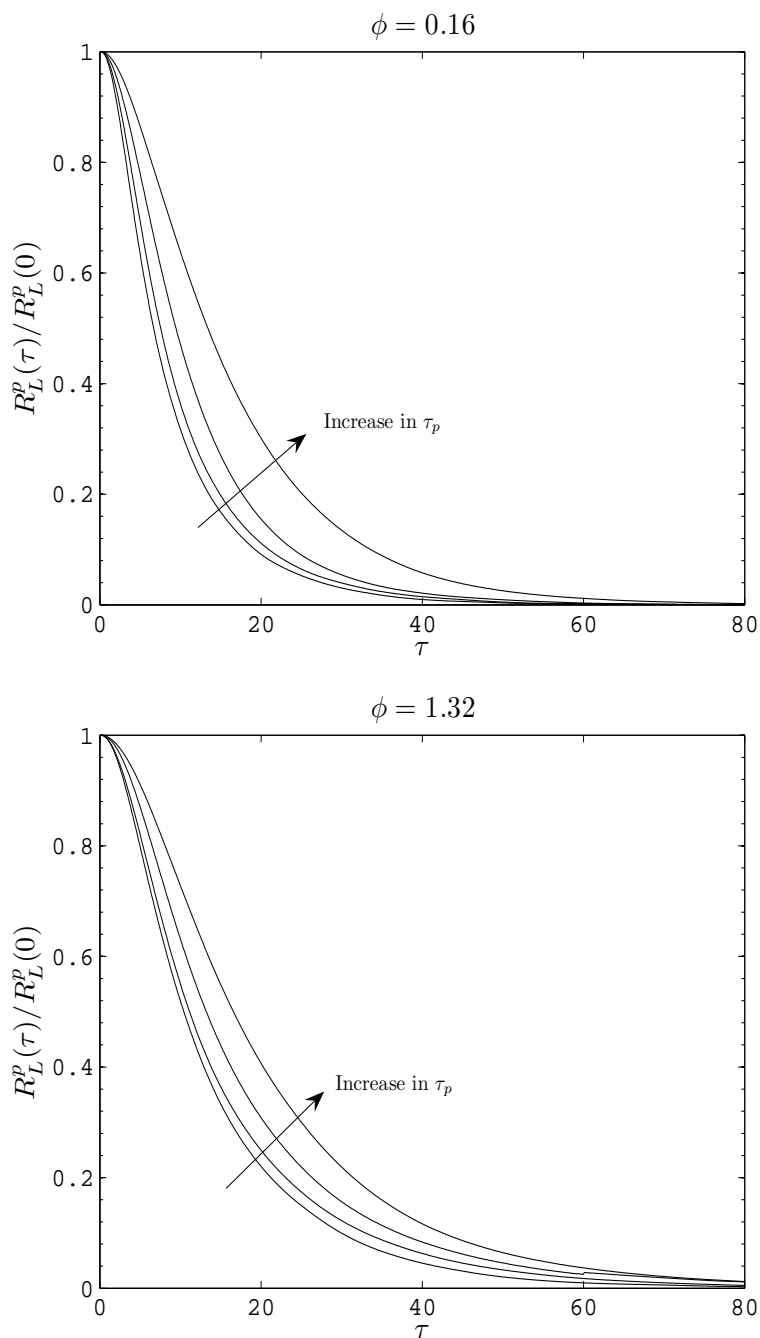


FIGURE 7.2: Modification of the Lagrangian correlations of particle fluctuation velocity for lowest and highest mass loadings.

greatly simplified. For example, if the density of the particle's is much larger than the fluid density, many of the forces in the equation of motion is negligible with reference to the drag term. When the particles obey the Stokes law, the drag term becomes linear in the relative velocity  $\mathbf{v}_r$ . Therefore typically, there are two mechanisms playing role in the dispersion of particles, namely:

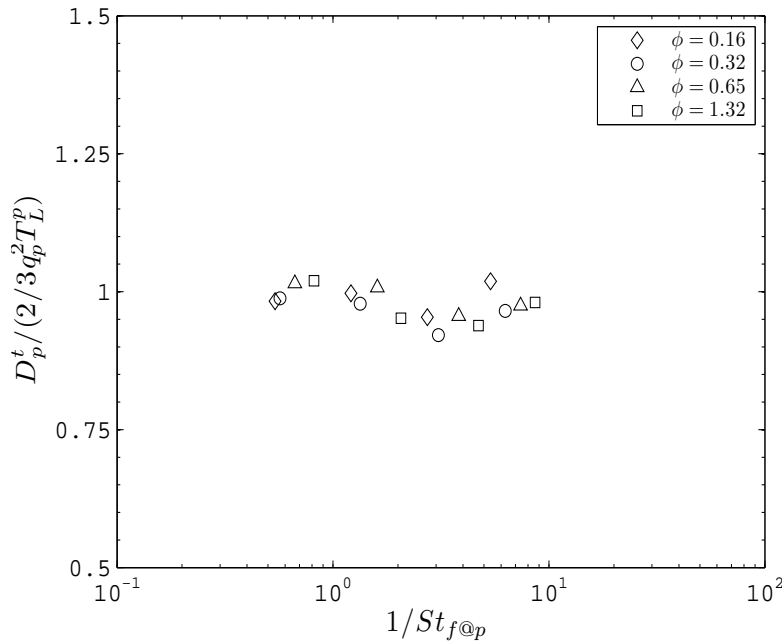


FIGURE 7.3: Dispersion coefficient calculated using the particle statistics, see relation 7.8

- Particle inertia (memory effect)
- Drift (in presence of a body force such as gravity.)

For the point particles (see chapter 2) considered in this thesis, these forces are the significant ones. The gravity is not taken into account for further simplification to the problem. However, the last section of this chapter has the intention to start such a study.

## 7.3 Theory of Tchen-Hinze for the particle dispersion

### 7.3.1 Classical theory of Tchen-Hinze

First analytical study on the relation between the fluctuating motion of particles and the one of fluid was done by Hinze (1975). Tchen (1947) linearized the equation of motion for a spherical particle in a turbulent flow and obtained expressions for the diffusion coefficient of fluid elements and the dispersion coefficient of particles. The turbulence used in the study is homogeneous isotropic and stationary. Most restrictive assumption is that the particle interacts with the same fluid element during its motion. However, as is well documented in literature, in turbulence, fluid elements are continuously stretched and distorted, therefore, this assumption is not widely applicable and saw many objections.

For small time separations, Tchen (1947) obtains:

$$\frac{D_p^t}{D_f^t} = \frac{u_p'^2}{u_f'^2} \quad (7.9)$$

where  $u_p$  is the velocity of the particle and  $u_f$  is the velocity of the fluid in the vicinity of the particle.

For long time separations, this relation becomes:

$$\frac{D_p^t}{D_f^t} = 1 \quad (7.10)$$

implying that for long time separations, the dispersion of particles and fluid elements are the same, e.g., they disperse in the same rate.

Hinze (1975) analyses the hypotheses of Tchen and put the one mentioned above in question. Performing a spectral analysis, Hinze (1975) refinds the results of Tchen and assuming an exponential form  $e^{-t/T_L^f}$  for the Lagrangian correlations for the intermediate time separations, he relates the spatial spectrum of fluid elements to the one of particles as:

$$E_{p,ij}(\omega) = Q(\omega)E_{f@p,ij}(\omega) \quad (7.11)$$

where the transfer function  $Q(\omega)$  is written as:

$$Q(\omega) = \frac{1}{1 + \omega^2 \tau_p^2} \quad (7.12)$$

where  $\omega$  is the frequency. Function  $Q(\omega)$  indicates an effect that the particles with increasing inertia are more and more independent of the high frequency oscillations of the turbulence and have trajectories more rectilinear. On the other hand, for very small inertia, particles behave like the fluid elements following the oscillations of the smallest scales.

After some algebra, Hinze (1975) derives famous relation for the agitation of the particles in terms of the fluid kinetic energy as:

$$2q_p^2 = q_{fp} = 2q_f^2 \frac{T_L^f}{T_L^f + \tau_p} \quad (7.13)$$

### 7.3.2 Extension of the theory of Tchen-Hinze

Deutsch and Simonin (1991), Deutsch (1992) extends the theory of Tchen-Hinze by putting the certain hypotheses of Tchen in question. They first replace the fluid-particle relative

instantaneous velocity in the expression of drag term by the mean relative velocity to linearize the particle relaxation time  $\tau_p$  appearing in equations of mean motion.

The second extension includes the independence of the particle of its fluid environment. Therefore, it is not obligatory that particle will follow the same fluid element during its motion, instead, it changes its fluid environment. This effect is largely enhanced by drift velocity (due to the gravity, for example) which is not taken into account in this work.

Basically, Deutsch and Simonin (1991) introduces the notion of fluid viewed by the particle  $u_{f@p}$  during its motion and a priori, the statistics of the fluid viewed by the particles are not the same with the statistics viewed by the fluid elements. By redoing the analysis of Tchen, they derive the dispersion coefficient of particles as:

$$D_p^t = \frac{2}{3} q_{f@p}^2 T_L^{f@p} \quad (7.14)$$

for isotropic homogeneous stationary turbulence.

Fluid velocity correlations along particle trajectories are presented in figure 7.4. It is remarked that for increasing inertia, whatever the mass loading is, particle-turbulence interaction time  $T_L^{f@p}$  decreases coherently with the particle dispersion mechanism explained above. Indeed, inertial particles interact less with the turbulent scales and the timescale is smaller with reference to the non-inertial particles. The figures also verify that the definition of Stokes number  $St_{f@p} = \tau_p / T_L^{f@p}$  is more convenient with  $T_L^{f@p}$  because the particle's effects are more pronounced on this timescale (see the figures 6.17 and 6.18 for the modulation of Lagrangian correlations of fluid element velocities).

Presented in figure 7.5, the particle dispersion coefficient is calculated using the fluid statistics seen by the particles and it is shown that the fluid statistics are well capable of defining the dispersion whatever the mass loading and the inertia. It is worth noting that the expression 7.14 is independent of the two-way coupling mechanism and of any assumption of the correlation curve. Therefore these results are not surprising.

By assuming an exponential form for the Lagrangian correlations of the fluid velocity during the particle trajectories, they derive the particle agitation in terms of the fluid kinetic energy viewed as:

$$2q_p^2 = q_{fp} = 2q_{f@p}^2 \frac{T_L^{f@p}}{T_L^{f@p} + \tau_p} \quad (7.15)$$

and a fundamental relation for the Lagrangian timescale  $T_L^p$  is derived as:

$$T_L^p = T_L^{f@p} + \tau_p \quad (7.16)$$

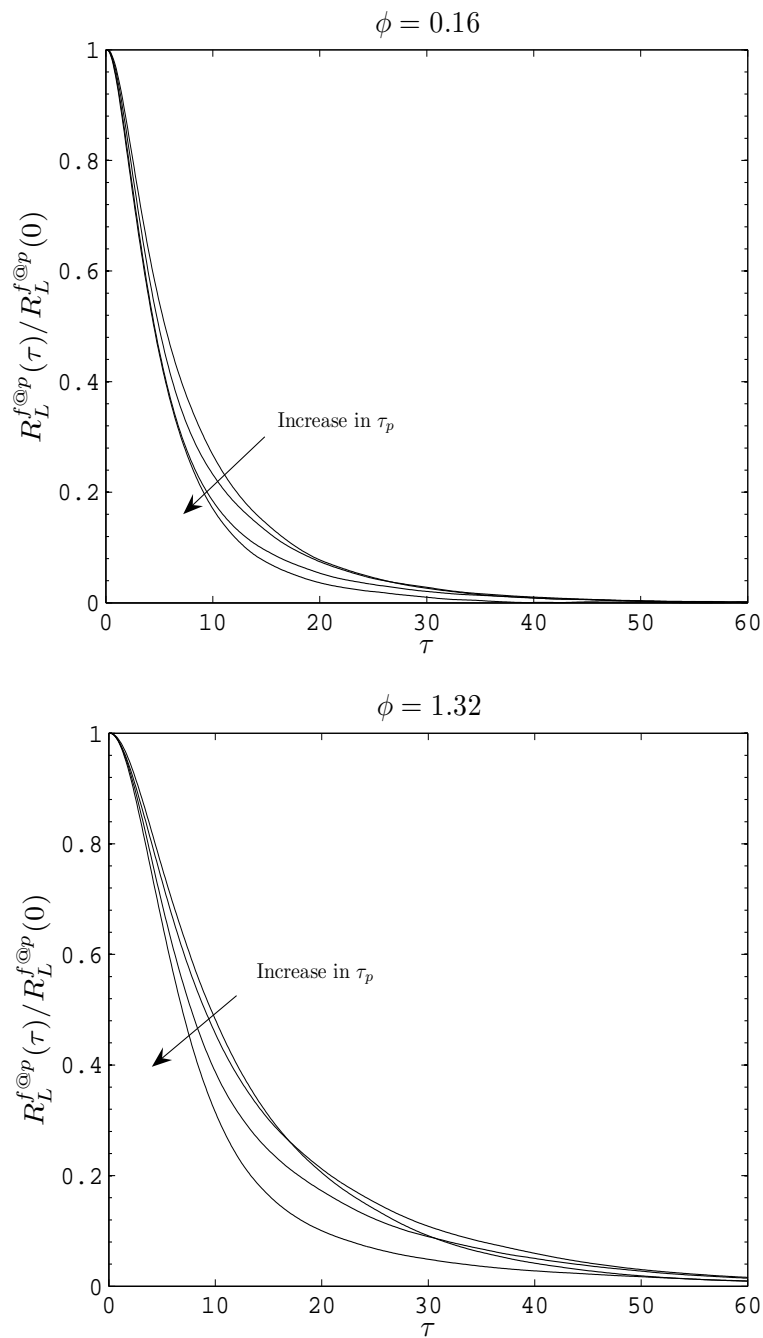


FIGURE 7.4: Modification of the Lagrangian correlations of fluid velocity correlation viewed by the particles for lowest and highest mass loadings

Figure 7.6 presents the evolution of the fluid-particle velocity covariance  $q_{fp}$  in terms of the particle inertia for each mass loading  $\phi$  with comparison to the one-way coupled flows. It is remarked that the Tchen-Hinze relation 7.15 works very well as in the one-way coupled flows. For very small inertia particles (right hand side), particles are correlated with the fluid scales (fluid-particle covariance is high) which in coherence with the Lagrangian analyses of particle

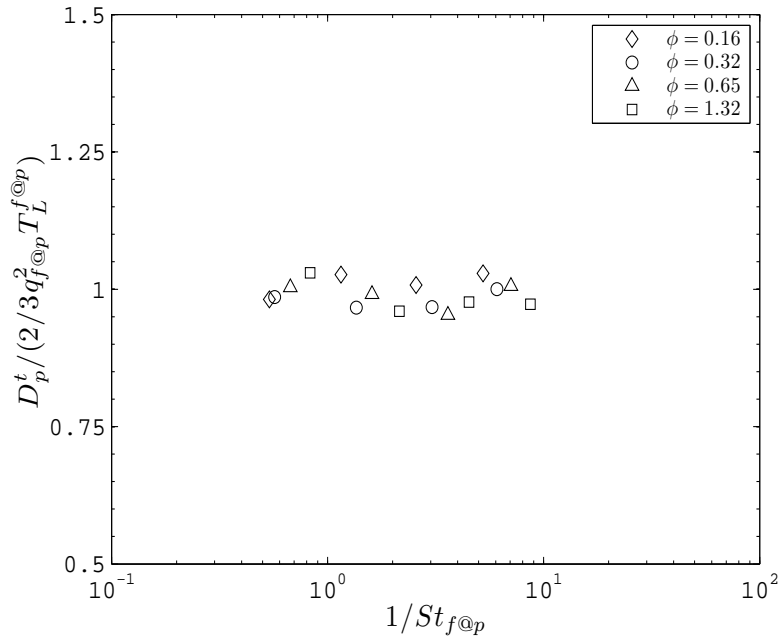


FIGURE 7.5: Dispersion coefficient calculated using the fluid statistics viewed by the particles, see relation 7.14

motion by the theory initial of Tchen (1947). Highly inertial particles are less correlated to the turbulent fluctuations and their covariances is relatively small (left hand side). Two mechanisms are clear on the figure:

First: as the mass loading increases, for a fixed  $\tau_p$ , the data points move right and upwards on the graph. This is primarily due to the increase of the Lagrangian timescale  $T_L^{f@p}$  due to the modulation of turbulence. For a fixed  $\tau_p$ , this results in the reduction of the Stokes number of particles and the data points move rightwards. Upward movement of the points is related to the increase in the ratio  $q_{fp}/(2q_{f@p}^2)$  due to the interaction of the small inertia particles with the turbulent scales. This could be, on one hand, due to the increase of the fluid-particle correlations due to the interactions of particles with smaller scales of turbulence, and on the other, due to the decrease in the fluid kinetic energy viewed by the particles.

Second: as the  $\tau_p$  increases, for a fixed  $\phi$ , the data points move to the left and downwards on the graph. This is due to the particles becoming more inertial with reference to the turbulent large scales. Therefore particles interact less with the turbulent scales and covariance decreases.

As remarked on the graph, the theory of Tchen-Hinze correctly defines the evolution of the covariance as a function of Stokes number for large inertia particles (left hand side of the graph). However, the theory has tendency to underestimate the ratio,  $q_{fp}/2q_{f@p}^2$ , for small

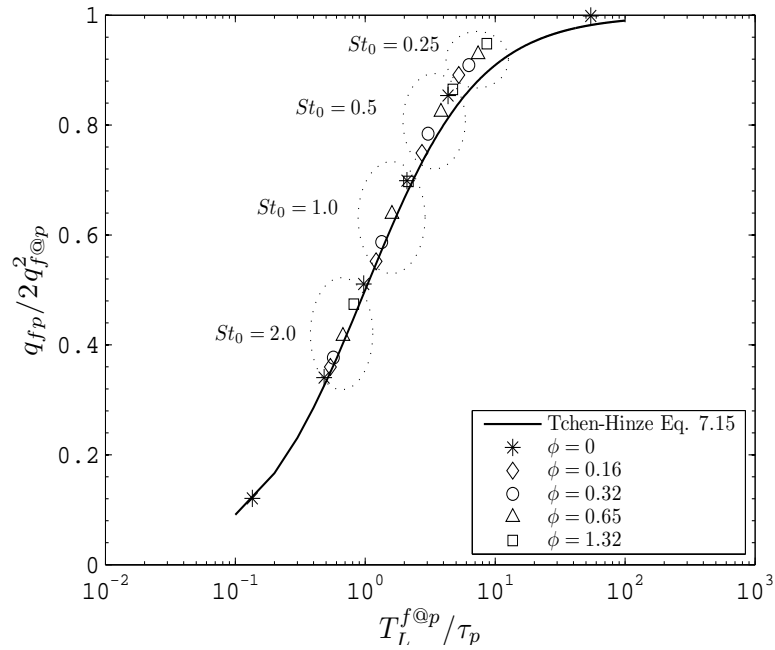


FIGURE 7.6: Tchen-Hinze relation 7.15 verified for two-way coupled flows compared to the one-way coupled flows,  $\phi = 0$

inertia. Therefore, deviations are observed for the small inertia (right hand side) part of the graph.

### 7.3.2.1 Low Reynolds number effects

As explained in the preceding section, the relation of Tchen-Hinze depends on the closure of the fluid Lagrangian correlation function. As noted by Hinze (1975), exponential form for these correlations is accurate only for the flows with infinite Reynolds number. For finite Reynolds numbers, the relation does not work due to the correlations deviating sensibly from the exponential curve. Specially, significant deviations are observed in the small time separations, as will be seen, in the next paragraph.

Sawford (1991) develops a stochastic model for the acceleration of the fluid elements taking into account the low Reynolds number effects. Hierarchically, this model is a second order process requiring two timescales as input for the memory effects of fluid elements, namely: Lagrangian timescale at the energetic scales' level, and Kolmogorov scale at the dissipative level. By the means of these timescales, Sawford (1991) achieves to take the Reynolds number into account in the model which is written as:

$$\frac{3 R_L^f(\tau)}{2 q_f^2} = \frac{1}{1 - \sqrt{Re^*}} \left[ \exp\left(-\frac{\sqrt{Re^*}}{T_L^{f*}} \tau\right) - \sqrt{Re^*} \exp\left(-\frac{\tau}{T_L^{f*}}\right) \right] \quad (7.17)$$

where  $Re^*$  is a Lagrangian Reynolds number defined as:

$$Re^* = \frac{16a_0^2 Re_\lambda^2}{C_0^4 15} \quad (7.18)$$

where  $C_0$  is the Kolmogorov constant measured from DNS,  $a_0$  is the acceleration constant which may be given as:

$$a_0 = 0.13Re_\lambda^{0.64} \quad (7.19)$$

$T_L^{f*}$  is the Lagrangian timescale corresponding to the flow with infinite Reynolds number and given as:

$$T_L^{f*} = \frac{T_L^f}{(1 + Re^{*-0.5})} \quad (7.20)$$

The correlations for the small time separations can be taken into account using this model, as seen on figure 7.7 for one of the simulations (not all presented for convenience).

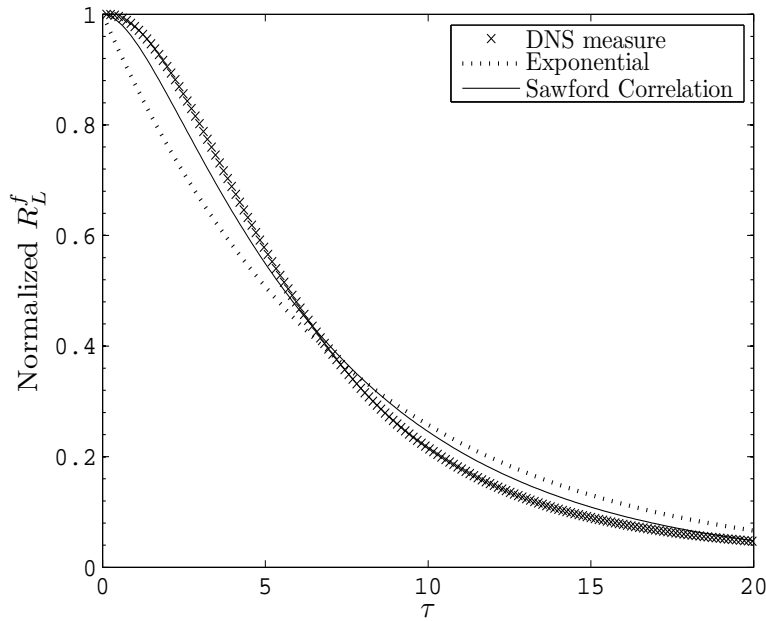


FIGURE 7.7: Sawford correlation 7.17 presented for the simulation  $St_0 = 0.25$  and  $\phi = 1.32$ ,  $Re_L = 65$

As seen on the figure 7.8, the expression 7.17 seems to work also for the correlation of the fluid velocity viewed by the particles.

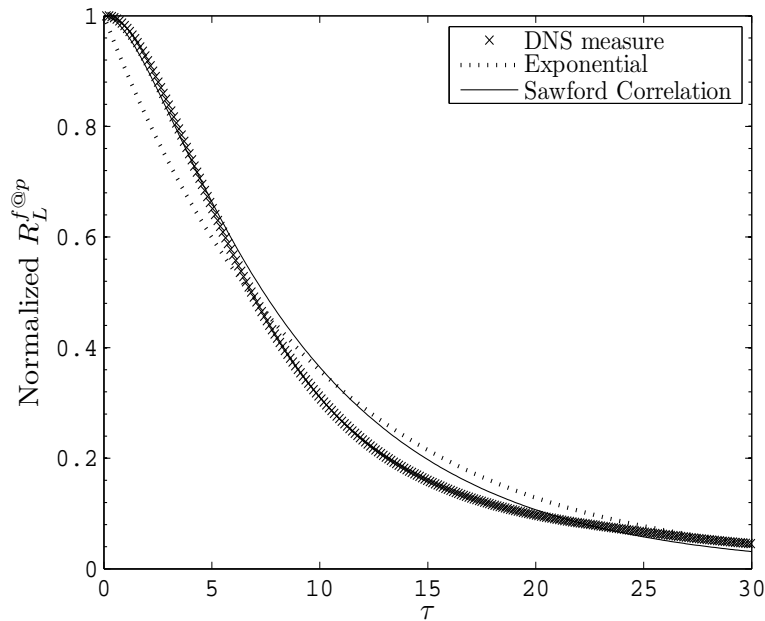


FIGURE 7.8: Sawford correlation 7.17 used for the Lagrangian correlation of fluid velocity viewed by the particles, presented for the simulation  $St_0 = 0.25$  and  $\phi = 1.32$ ,  $Re_L = 65$

Tchen-Hinze relation can then be rewritten in the form:

$$2q_p^2 = q_{fp} = 2q_{f@p}^2 \eta \frac{1 + \sqrt{Re^*} + \eta}{\sqrt{Re^*} + (1 + \sqrt{Re^*})\eta + \eta^2} \quad (7.21)$$

where  $\eta = \frac{T_L^{f@p}}{\tau_p}$ .

As seen on figure 7.9, using the same relation for the correlations  $R_L^{f@p}$ , a very good agreement is obtained.

### 7.3.3 Modification of the dispersion coefficient by the two-way coupling

In the classical theory of Tchen-Hinze, it is obtained that the long time diffusion coefficients of fluid elements and solid particles are equal,  $D_p^t = D_f^t$ . However, it has been found by analytical analysis by Reeks (1977), that this is not the case and particle dispersion is generally higher than the diffusion of fluid elements. This result is then confirmed by the results of Pismen and Nir (1978). Both these researchers have investigated the gas-solid flows in homogeneous isotropic turbulence without the effect of gravity (no drift). More recently Fung and Perkins (1989) analyzed the particle motion and found the same results.

The increase in the dispersion coefficient has also been observed in the experimental and numerical works (Crowe et al., 1985, Lazaro and Lasheras, 1992, Longmire and Eaton, 1992).

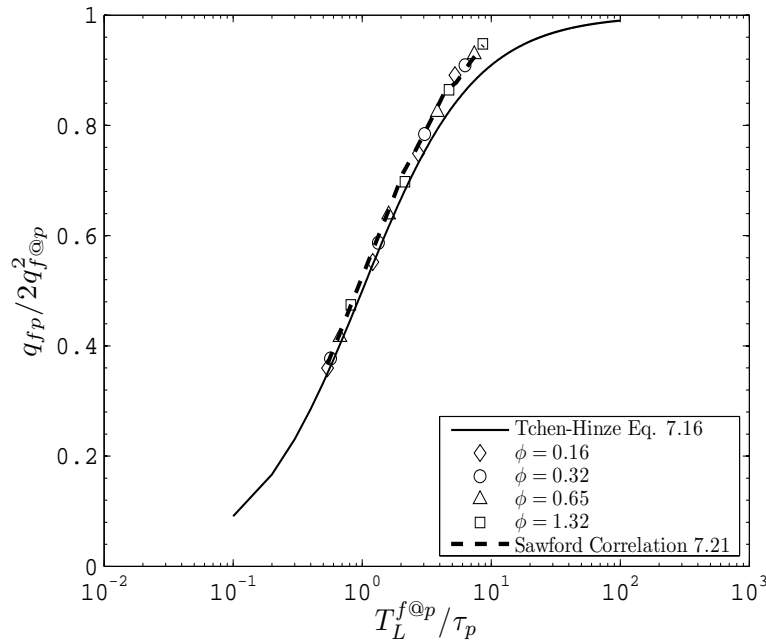


FIGURE 7.9: Tchen-Hinze relation 7.21 using the Sawford correction 7.17

According to the work of Reeks (1977), the modification of the dispersion coefficient is due to the inertia of the particles, with the hypothesis that the statistics seen by the particles and fluid elements are the same. In one-way coupled simulations of Février (2000), this hypothesis is well verified for different Stokes numbers and varying turbulent Reynolds numbers. Therefore, in the frame of the analysis of Reeks (1977), it was shown that Lagrangian correlation seen by the particles  $R_L^{f@p}$  tends to the Lagrangian correlations of fluid elements,  $R_L^f$ , in the scalar limit, and tends to  $R_E$  in high inertia limit and  $T_L^f < T_L^{f@p} < T_E$ . Wang and Stock (1993) gives the semi-empirical relation out of the experimental measurements for the evolution of the Lagrangian timescale viewed by the particles as:

$$\frac{T_L^{f@p}}{T_E} = 1 - \left(1 - T_L^f/T_E\right) \left(1 + \tau_p/T_E\right)^{-0.4(1+0.01\tau_p/T_E)} \quad (7.22)$$

This relation will be tested later on. For the time being, representative Lagrangian correlation of the fluid velocity viewed by the particles are seen in figures 7.10 and 7.11. It seems that the correlations  $R_L^{f@p}$  is between the Lagrangian correlation of fluid elements and Eulerian one-point correlations for the largest and smallest inertia particles.

Figure 7.12 presents the dispersion coefficients calculated by the relations 7.3 and 7.6 with comparison to the results of Deutsch and Simonin (1991) and theoretical relation of Pismen and Nir (1978). It is clear that in the range  $T_L^f/\tau_p = [1, 10]$  the dispersion coefficient of particles reaches up to 20% higher values of the diffusion of fluid elements. It is interesting

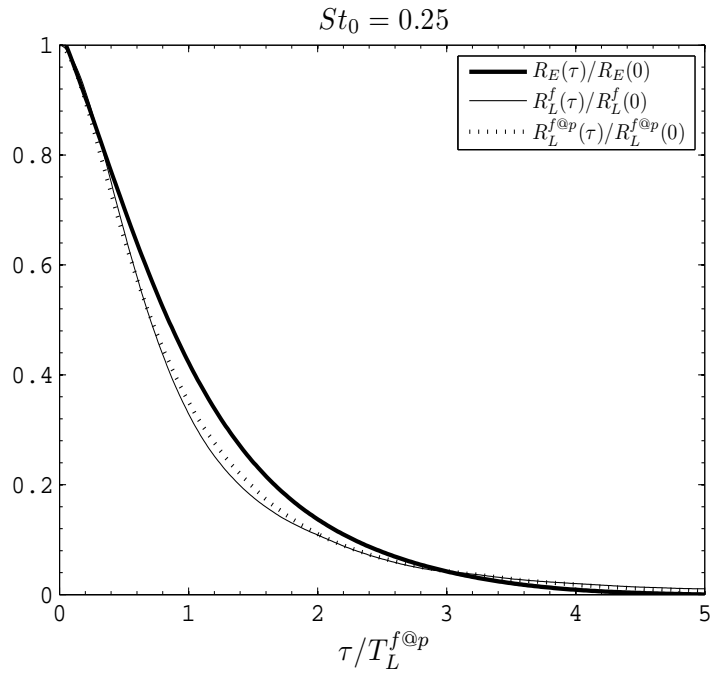


FIGURE 7.10: Comparison of the Eulerian and Lagrangian correlations of fluid velocity for  $St_0 = 0.25$  and  $\phi = 1.32$ ,  $Re_L = 65$

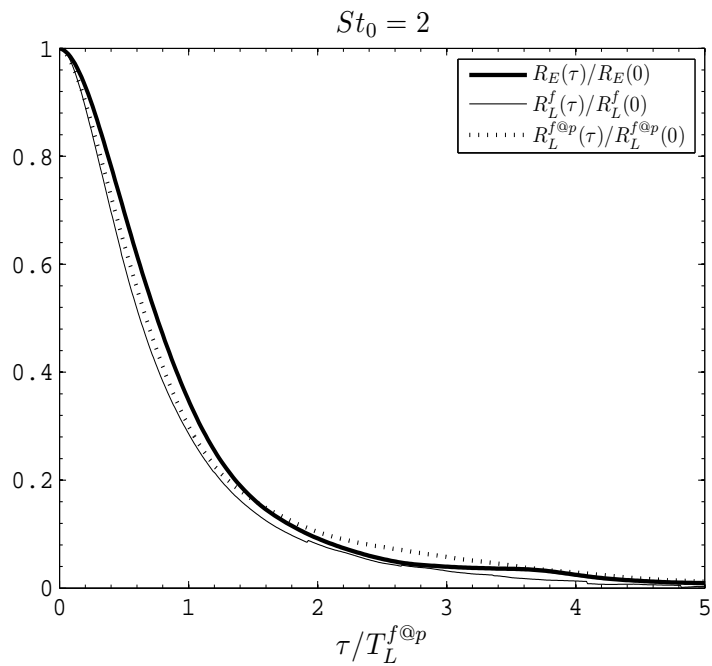


FIGURE 7.11: Comparison of the Eulerian and Lagrangian correlations of fluid velocity for  $St_0 = 2.0$  and  $\phi = 1.32$ ,  $Re_L = 76$ .

to note that this increase is not predicted by the relation of Pismen and Nir (1978). As in the work of Février (2000) and many others cited above, the general idea is that the particle

dispersion phenomenon is controlled at the macroscopic level of the flow. It has been shown by Deutsch and Simonin (1991) that this increase is due to the collection of the particles to the preferential zones in the flow due its finite inertia (an augmentation in the  $T_L^{f@p}$ ) therefore particles interact more with the turbulent scales. However, in the results reported here, this point is not clear due to the fact that two-way coupling mechanism affects both  $q_{f@p}^2$  and  $T_L^{f@p}$ .

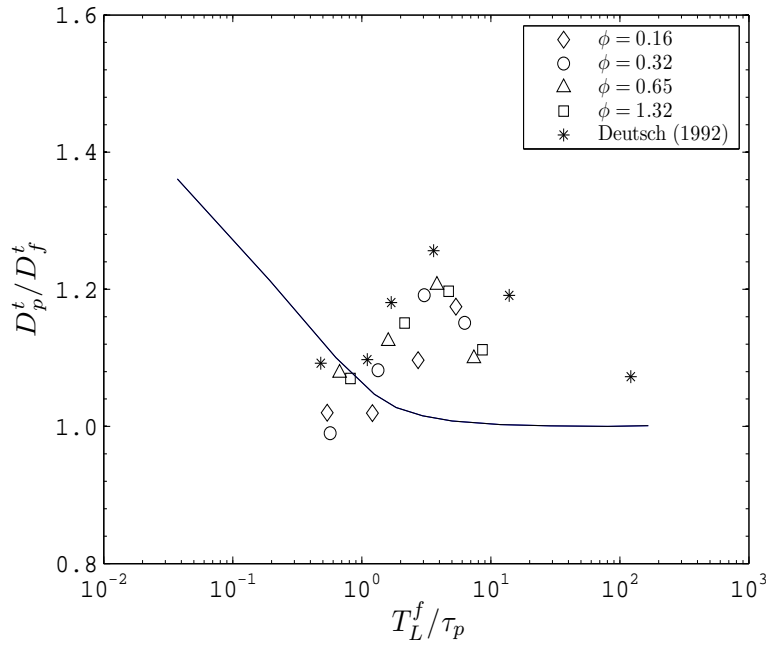


FIGURE 7.12: Modification of the dispersion coefficient with reference to the diffusion coefficient of fluid elements due to the two-way coupling, solid line corresponds to the theory of Pismen and Nir (1978).

In passing, it can be noted that Février (2000) also showed that this augmentation is not due to the stochastic forcing scheme.

For a last step, the modification of the values of the dispersion coefficient with reference to the uncharged flows are presented in figure 7.13 for all of the simulations. It is clear that the increasing mass loading reduces the dispersion of the particles. Particle Stokes number also plays a role on the dispersion but it is weaker than the effect of mass-loading and for the mass loading of 0.16, it practically has very small effect. Therefore it can be concluded that due to the decrease in turbulent Reynolds number of the flows, with increasing mass loading, particles disperse less.

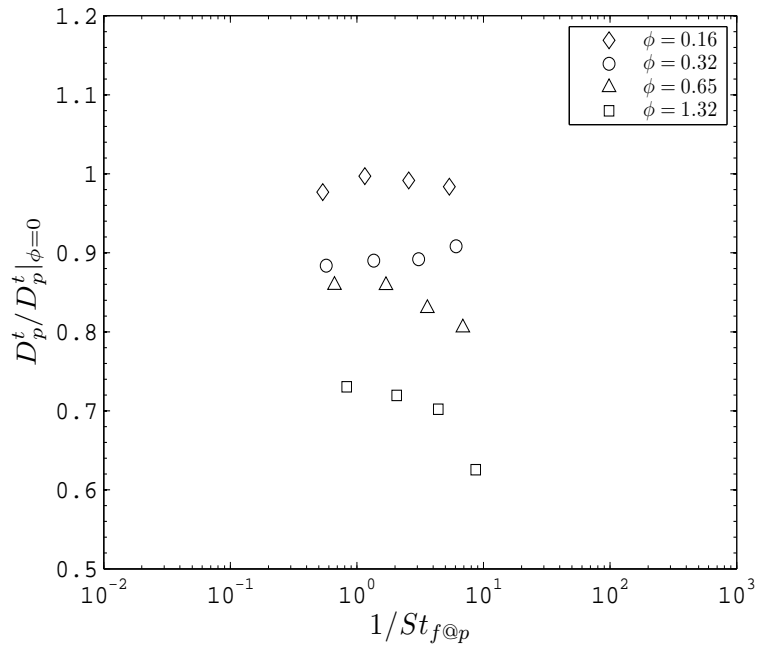


FIGURE 7.13: Modification of the dispersion coefficient with reference to the uncharged flows due to the two-way coupling.

### 7.3.4 Effect of two-way coupling on the fluid statistics viewed by the particles

In one way coupled flows, the fluid kinetic energy is shown to be sensibly the same as the one seen by the solid particles, therefore the Lagrangian timescale  $T_L^{f@p}$  is the one effecting the dispersion of particles. In this section, this phenomenon will be studied in two-way coupled flows.

Fluid kinetic energy seen by the particles is presented in figure 7.14 for all of the simulations with one-way coupled simulations and the results of Deutsch and Simonin (1991). It is immediately remarked that one-way coupled simulations,  $q_{f@p}^2$  is considerably constant for each particle inertia. The results of simulations of present thesis are in coherence with the results of Deutsch and Simonin (1991). However, in two-way coupled simulations, increasing mass loading leads to the reduction of the kinetic energy  $q_{f@p}^2$  up to 25% of the fluid kinetic energy  $q_f^2$  (for modification of the fluid kinetic energy from the one-way coupled flows, see figure 6.4) which should be accounted in stochastic modeling.

Evolution of the Lagrangian timescale seen by the particles  $T_L^{f@p}$  is presented in figure 7.15 with comparison to the semi-empirical relation of Wang and Stock (1993) (for the modification of the Lagrangian timescale with reference to the one-way coupled flow, see figure 6.19). Clearly, the one-way coupled simulation results are totally in coherence with

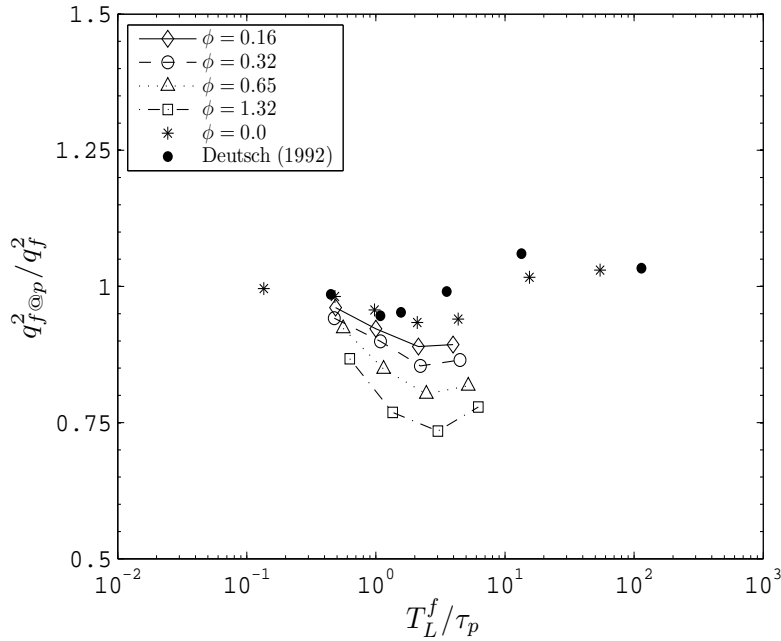


FIGURE 7.14: Modification of the fluid kinetic energy  $q_{f@p}^2$  viewed by the particles,  $q_f^2$  corresponds to the fluid kinetic energy of the two-way coupled flow.

the results of Deutsch and Simonin (1991) and they are partially in coherence with the results of the theoretical relation 7.22 for the highest and lowest inertia particles. However, the relation 7.22 does not predict the increase in the range  $T_L^f/\tau_p = [1, 20]$ . For two-way coupled flow simulations, increasing deviations are observed in this range with the increasing mass-loadings that the highest value is probably larger than the Eulerian timescale,  $T_E$ , of the turbulence indicating that the analysis of Reeks (1977) is not satisfied in all the flow simulations performed. This increase in  $T_L^{f@p}$  is an indication to the particles interacting longer with the large turbulent scales than the fluid elements with increasing mass loading.

The differences between  $q_f^2$  and  $q_{f@p}^2$  could be due to the preferential concentration mechanism. Indeed, the increase in  $T_L^{f@p}$  is associated to this mechanism in which particles collect to the peripheries of the turbulent large scales due to the centrifugal effect (Squires and Eaton, 1991b, Deutsch and Simonin, 1991). Effect of preferential concentration makes the subject of the next section.

### 7.3.5 Effect of preferential concentration on the statistics viewed by the particles

In the scalar limit, particles have very small inertia and they follow all the fluctuations of the fluid scales perfectly leading to the intuition that the particles should be homogeneously

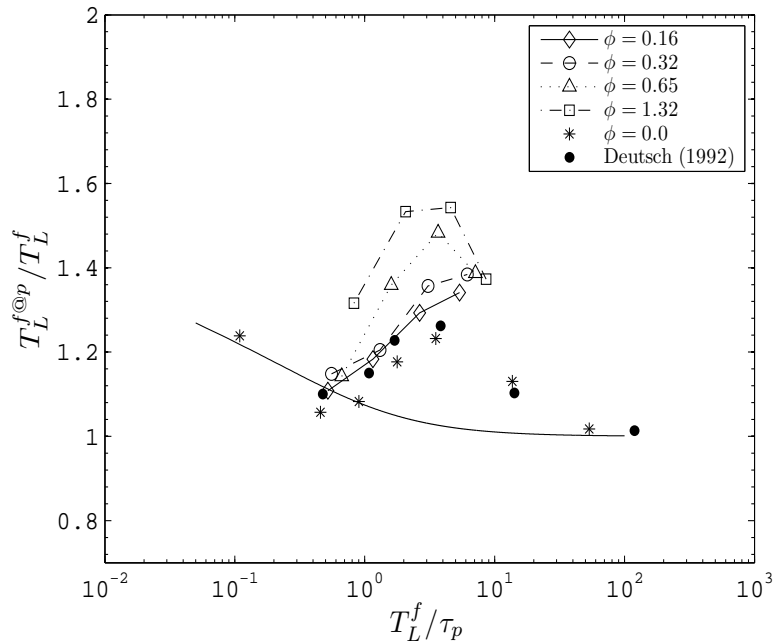


FIGURE 7.15: Modification of the Lagrangian timescale  $T_L^{f@p}$  viewed by the particles due to the particles,  $T_L^f$  corresponds to the Lagrangian timescale of the two-way coupled flow, solid line is the relation 7.22 for the  $T_L^f/T_E = 0.727$  (mean value over the ensemble of simulations)

distributed throughout the domain (note the flow is incompressible meaning that two fluid elements exponentially move away from each other (Falkovich et al., 2001)). In the opposite case, particles, due to their inertia, do not follow any of the fluctuations of the turbulent scales and therefore they have more rectilinear trajectories. The particles are not then correlated to the turbulent velocity field and therefore they should be randomly distributed, as well. In between these two limits, particles respond to more or less different scales of turbulence and they preferentially collect to the zones of weak vorticity and strong shear.

Maxey (1987), Squires and Eaton (1991b), Eaton and Fessler (1994) explains the collection of particles in terms of the centrifugal force tending to throw the particles from the centers of the turbulent scales to the peripheries due to maximum vorticity. The mechanism of preferential concentration is still an open question in that the mechanism depends either on the small or on the large scales is not well understood. Works of Wang and Maxey (1993), Wang et al. (2000) show that the mechanism is controlled by the small scales of turbulence. However, there are other works, such as the one of Wang and Squires (1996), showing that the mechanism is not only related to the small but also large scales. Finally, Février (2000) refinds the results reported in the literature and effects extensive study on different turbulent Reynolds numbers. The method of Février (2000) seems more realistic in terms of characterizing the preferential concentration, therefore it will be used in this study. The next section is about this method and its application.

### 7.3.5.1 Methodology

A widely used practical method of characterizing the preferential concentration is to calculate the probability distribution  $P(C)$  of having  $C$  number of particles in an elementary cubical volume. In perfect homogeneous distribution of particles, this function is equal to the Poisson distribution which is written as:

$$P(C) = \frac{e^{-\lambda} \lambda^C}{C!} \quad (7.23)$$

where  $\lambda$  is the mean number of particles per elementary volume and  $C!$  is the factorial of  $C$ .  $\lambda$  can also be written for homogeneous distribution as:

$$\lambda = \frac{N_p}{N_d} \quad (7.24)$$

where  $N_p$  is the number of particles and  $N_d$  is the number of elementary volumes covering the whole domain. It should be noted that  $P(C)$  becomes equal to the homogeneous distribution of Poisson in condition that the number of particles is large.

In non-homogeneous distribution of particles, a quantifying parameter can be defined as:

$$\Sigma_p = \frac{1}{\lambda} (\sigma - \sigma_{Poisson}) \quad (7.25)$$

where

$$\sigma^2 = \sum_C (C - \lambda)^2 P(C) \quad (7.26)$$

$$\sigma_{Poisson}^2 = \lambda \quad (7.27)$$

Large values of  $\Sigma_p$  corresponds to a more and more non-homogeneous distribution of particles.

### 7.3.5.2 Results

As seen on figure 7.16, the parameter  $\Sigma_p$  depends on the number of elementary volumes  $\Delta_{d,x}$  in one direction. Specifically, for increasingly smaller volumes (large  $\Delta_{d,x}$ ), the parameter  $\Sigma_p$  decreases after making a peak value for a fixed inertia. Indeed, Février (2000) notes that there is an optimum value for the largest  $\Sigma_p$  and this value should be considered to more precisely characterize the preferential concentration. Therefore, the maximum value out of all possible  $N_{d,x}$ s is chosen in this study, following the advices of Février (2000).

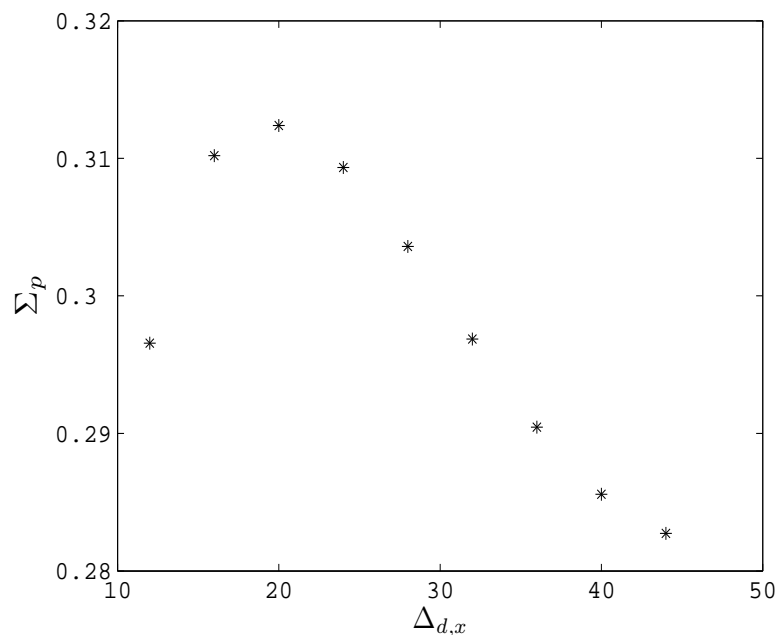


FIGURE 7.16: Representative presentation of evolution of  $\Sigma_p$  as a function of the number of elementary volumes ( $= \Delta_{d,x}^3$ ) covering the domain.

From the other part,  $\Sigma_p$  will also depend on the inertia of the particles as explained in the introductory paragraph of this section.

The parameter  $\Sigma_p$  is quantified in all the simulations considering 260000 particles. Results in one-way coupled and two-way coupled simulations are plotted in figures 7.17 and 7.18 with comparison to the results of Février (2000). First of all, either in simulations performed in this thesis or the simulations of Février (2000) put in evidence of more homogeneous particle distribution when the inertia approaches the limit values. In between, due to the particles' behavior of following different oscillations of different scales, the concentration increases.

It is remarked a maximum value around  $St \approx 0.2$  after which particles again forms a more homogeneous distribution. The values obtained in this thesis around the maximum  $St$  number are slightly higher than the results of Février (2000) which can be attributed to the low turbulent Reynolds numbers considered in this thesis due to the restrictions of DNS. Indeed, as observed by Février (2000), increasing turbulent Reynolds numbers decrease the preferential concentration and it is explained by the small scales losing their effects on the mechanism of preferential concentration. This argument goes face to face with the longtime open question of which scales control the preferential concentration.

More related to the two-way coupling mechanism, the figures show that Increasing mass

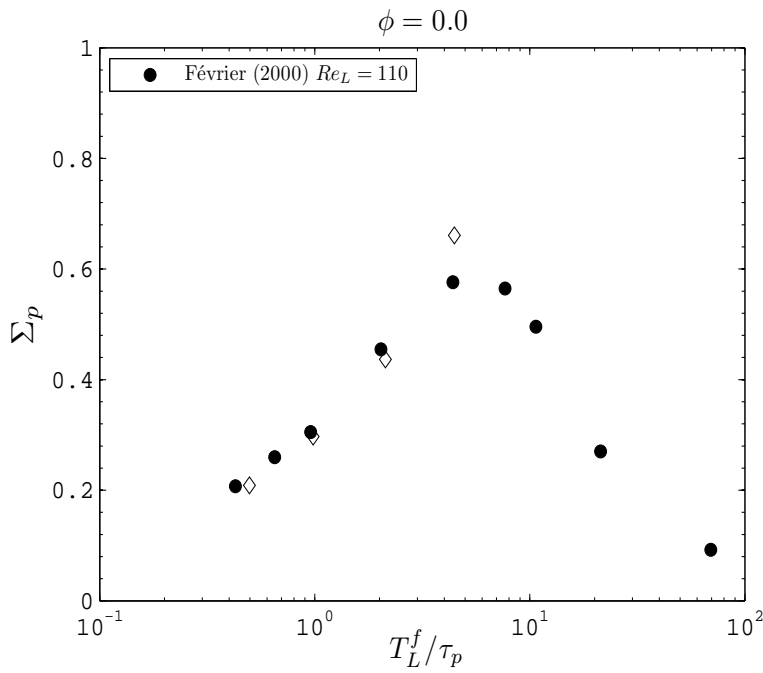


FIGURE 7.17: Preferential concentration measured in one-way coupled flows.

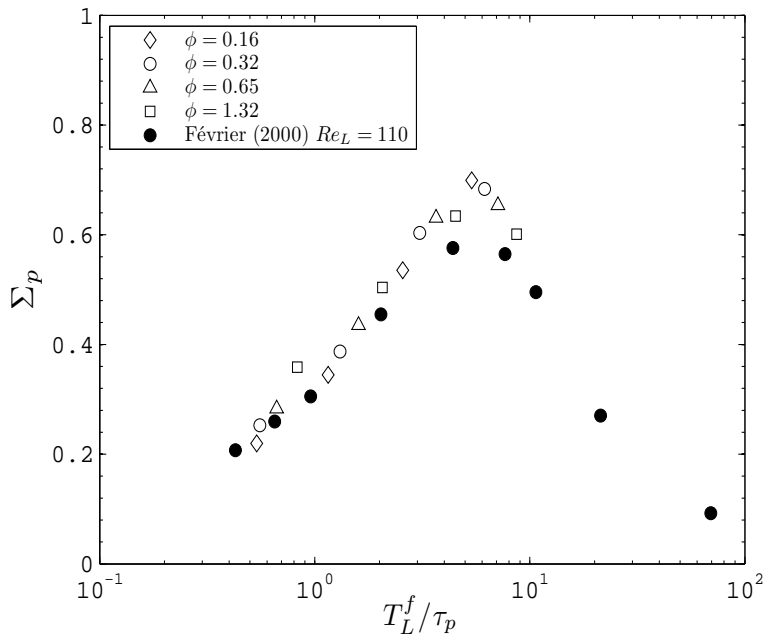


FIGURE 7.18: Preferential concentration measured in two-way coupled flows.

loadings  $\phi$  do not have an indirect effect on the concentration of particles by just to reduce their Stokes numbers by reducing the turbulence levels, and therefore increasing  $T_L^{f@p}$ .

Therefore, as also seen in the figures of Tchen-Hinze (figures 7.6), data points move rightwards by the effect of two-way coupling. It is to be noted that a maximum value of  $\Sigma_p$  is also obtained at the same range as in the one-way coupled simulations of Février (2000).

In conclusion, two-way coupling mechanism does not seem to affect the particles' spatial concentration in some special way. It only effects throughout the physical effect on the turbulence levels by reducing the turbulent Reynolds number. This lets think that the statistical differences observed in  $q_{f@p}^2$  and  $q_f^2$  are not due to the preferential concentration and this should be treated more using the transport equation 5.55 for  $q_{f@p}^2$ .

## 7.4 Lagrangian stochastic modeling results

In this section, Lagrangian stochastic modeling results are going to be compared to the results of DNS+DPS reported in the previous and this chapter.

### 7.4.1 Mean drag model

As largely discussed in chapter 5, the mean model neglects the effect of two-way coupling on the second order quantities. For homogeneous isotropic stationary turbulence, transport equation for the fluid-particle covariance  $q_{fp}$  results in simple relation:

$$q_{fp} = \left( \frac{1}{1 - A_{f@p}\tau_p} \right) 2q_{f@p}^2 \quad (7.28)$$

where  $A_{f@p}$  is derived from the Lagrangian correlation function of the fluid velocity along the particle trajectories as:

$$A_{f@p} = -\frac{1}{T_L^{f@p}} \quad (7.29)$$

After some algebra, the relation takes the form:

$$q_{fp} = 2q_{f@p}^2 \frac{T_L^{f@p}}{T_L^{f@p} + \tau_p} = 2q_{f@p}^2 \frac{1}{1 + St_{f@p}} \quad (7.30)$$

As seen, the mean drag model results in the same relation as the relation of Tchen-Hinze 7.15. This similarity is coherent with the condition that the models should satisfy the theory of dispersion of Tchen-Hinze given in section 5.7. The relation 7.30 is plotted (figure 7.19) again for convenience in order to do comparison with the figures that will follow. Taking the low Reynolds number effects using the model proposed by Sawford (1991), the results

seem promising. Therefore the mean drag model is in coherence with the particle dispersion mechanism explained in previous sections. Then the question is how to calculate the fluid statistics  $T_L^f$  and  $q_f^2$  in a practical way in terms of the fluid statistics viewed by the particles.

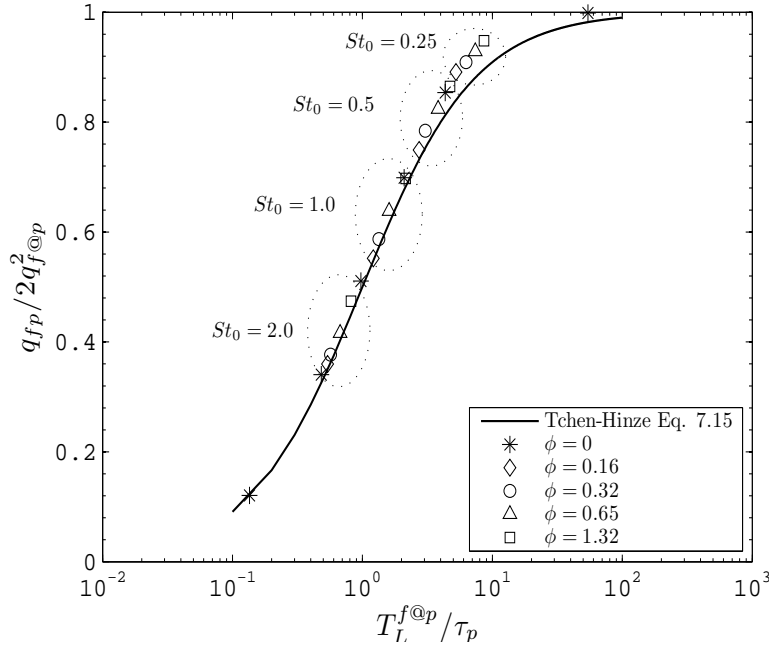


FIGURE 7.19: Tchen-Hinze relation obtained using the mean drag model, relation 7.30

Classical closures in one-way coupled flows for the fluid statistics seen by the particles are written as:

$$\begin{aligned} T_L^{f@p} &= T_L^f \\ q_{f@p}^2 &= q_f^2 \end{aligned} \quad (7.31)$$

These closures lead to the classical theory of Tchen-Hinze given by relation 7.13. As seen on figure 7.20, the classical theory overestimates the ratio  $q_{fp}/2q_f^2$ , especially for small inertia and high mass loading cases which shows that the fluid statistics seen by the fluid elements and the solid particles are different. Figure 7.21 plot the Tchen-Hinze relation using the closure  $q_{f@p}^2$ . The results indicate that the differences between the fluid kinetic energy seen by the particles and by the fluid elements are significant cause of deviations from the Tchen-Hinze curve, evidently, the comparison of the figures 7.19, 7.13 and 7.21 shows that the difference between  $T_L^f$  and  $T_L^{f@p}$  is not that significant because the  $x$  coordinate is plotted on log-scale for all three figures. The next sections will explore the differences between these statistics and the causes.

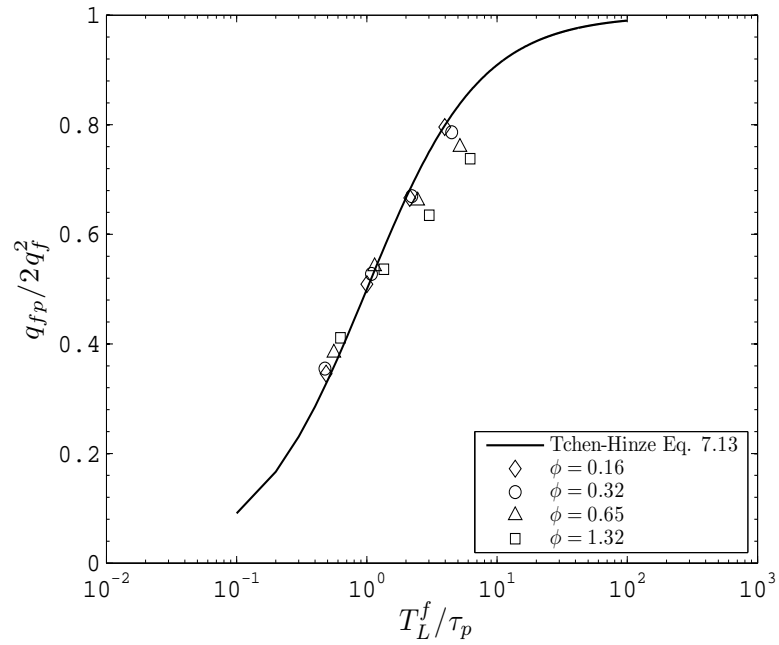


FIGURE 7.20: Tchen-Hinze relation using the closures 7.31 leading to the classical relation of Tchen-Hinze 7.13

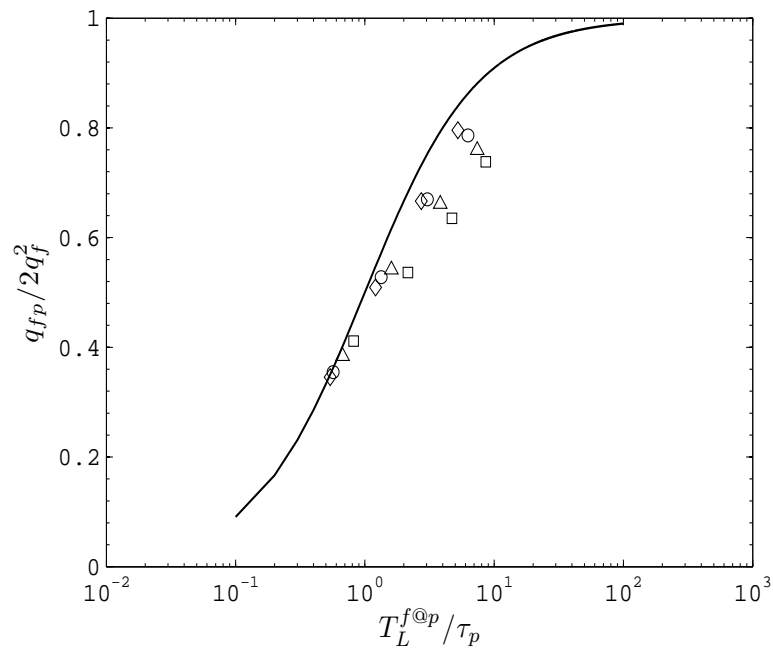


FIGURE 7.21: Fluid-particle covariance model 7.30 using only the closure  $q_{f@p}^2 = q_f^2$

To conclude, the modification of  $q_{f@p}^2$  causes more significant deviation from the theoretical Tchen-Hinze curve than the modification of  $T_L^{f@p}$ . Therefore the transport equation 5.55

for  $q_{f@p}^2$  should help improve the modeling approach with both mean and instantaneous drag models.

#### 7.4.1.1 A practical closure

A practical closure can be derived for the  $q_f^2-\epsilon$  models by plotting the fluid-particle covariance model 7.30 by taking instead of Lagrangian timescale, more applicable parameter,  $q_f^2/\epsilon$  which represents a characteristic turbulent eddy turnover time. It can be written as:

$$\begin{aligned} T_L^{f@p} &= \lambda \frac{q_f^2}{\epsilon} \\ q_{f@p}^2 &= q_f^2 \end{aligned} \quad (7.32)$$

These variables are more convenient in terms of modeling for industrial applications because they are readily present. Tchen-Hinze relation can be rewritten as:

$$q_{fp} = 2q_f^2 \frac{\lambda(q_f^2/\epsilon)}{\lambda(q_f^2/\epsilon) + \tau_p} \quad (7.33)$$

where  $\lambda$  is a constant. In forced homogeneous isotropic turbulence, the  $\lambda$  can be derived as:

$$\lambda = \frac{4}{3C_0} \quad (7.34)$$

where  $C_0$  is the Kolmogorov constant intended to be universal. In section 6.7, it has been shown that the value of this number measured from DNS+DPS for two-way coupled simulations is not constant, but, dependent on the mass-loading of the particles (see figure 6.25). In the simulations performed, the range of measured  $C_0$  values and corresponding range of  $\lambda$  are:

$$C_0 = [1.8, 4.0] \quad \lambda = [0.33, 0.72] \quad (7.35)$$

The relation 7.33 is plotted in figure 7.22 along with the range of values of  $\lambda$  measured from the simulations. Empirical value  $\lambda = 0.25$  seems to predict correctly the evolution of the covariance as a function of particle inertia. This implies in turn that a value of  $C_0$  around 4.0 seems correct so that the model gives good prediction of the covariance. This result is in coherence with the work of Boivin (1996).

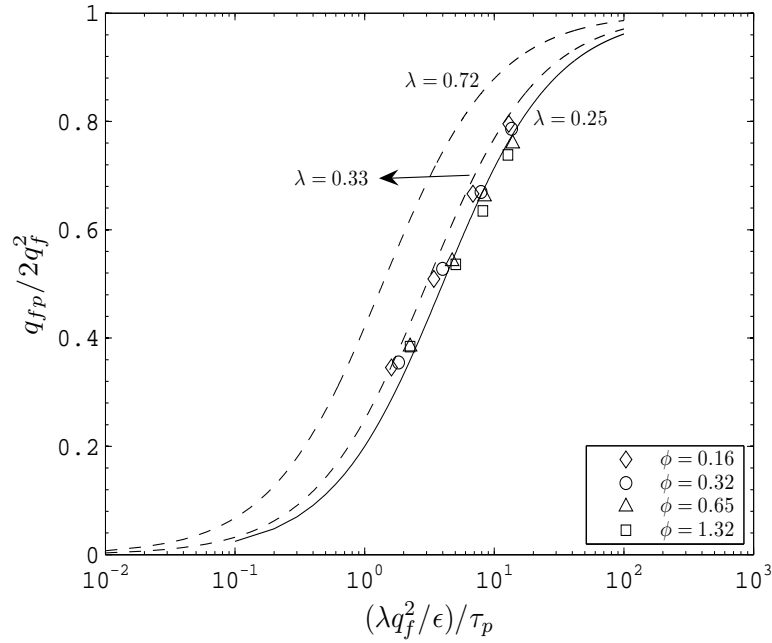


FIGURE 7.22: Practical closure 7.33 for  $q_{fp}$ . Lines correspond to the values of  $\lambda$  given in 7.35.

#### 7.4.2 Instantaneous drag model

Using the instantaneous drag model written with the help of the mesoscopic approach, the fluid-particle covariance transport equation results:

$$q_{fp} = 2 (q_{f@p}^2 + \phi \tilde{q}_p^2) \frac{1}{1 + \phi - A_{f@p} \tau_p} \quad (7.36)$$

where  $A_{f@p}$  is derived from the consistence condition of the Langevin model with the Lagrangian correlations and it is written as:

$$A_{f@p} = -\frac{1}{T_L^{f@p}} \left[ 1 + \phi \frac{q_{fp}}{2q_{f@p}^2} \right] \quad (7.37)$$

The model 7.36 includes the dependence on the mass loading  $\phi$ . For  $\phi = 0$ , the extension of the theory of Tchen-Hinze is obtained.

In the relation, mesoscopic particle kinetic energy  $\tilde{q}_p^2$  is also to be modeled. Février (2000) gives a practical model using the DNS simulation results. The model is written as:

$$\tilde{q}_p^2 = q_{f@p}^2 \left( \frac{q_p^2}{q_{f@p}^2} \right)^{1.5} \quad (7.38)$$

In figure 5.12, it has been already remarked that the mesoscopic particle energy  $\tilde{q}_p^2$  obeys the relation 7.38. Using this relation in equation 7.36 along with the relation for  $A_{f@p}$ , a second-order polynomial can be derived for the ratio  $q_{fp}/2q_{f@p}^2$  as:

$$\phi x^2 - \phi \kappa x^{1.5} + (1 + \kappa \phi + \kappa)x - \kappa = 0 \quad (7.39)$$

where  $x = \frac{q_{fp}}{2q_{f@p}^2}$  and  $\kappa = \frac{T_L^{f@p}}{\tau_p}$ .

This equation has not analytical solution therefore it has been solved by numerical methods using the software MATLAB. The solution is plotted in figure 7.23. In contrast to the mean model which is in coherence with the theory of Tchen-Hinze, the instantaneous model shows increasing deviation with increasing mass loading from the curve for  $\phi = 0$  whatever the inertia of the particles, therefore quantitatively it gives incorrect prediction of the fluid-particle covariance.

Using the practical closures for the statistics viewed by the particles given in relation 7.32 with  $\lambda = 0.25$  which works very well in the mean drag model, the resulting relation is plotted in figure 7.24. The closures for the  $\kappa$  and  $x$  in equation 7.39 are written as:

$$x = \frac{q_{fp}}{2q_{f@p}^2} \quad \kappa = \lambda \frac{q_f^2/\epsilon}{\tau_p} \quad (7.40)$$

As seen the instantaneous model does not take into account the evolution of the fluid-particle covariance, especially, for increasing mass-loadings. In contrast to the relation 7.36, quantitatively, it underestimates the ratio  $q_{fp}/2q_f^2$  for increasing mass-loadings.

It is clear that the closure of the mesoscopic particle kinetic energy leads to the incorrect prediction of the fluid-particle covariance. If the fluid-particle covariance  $q_{fp}$  is desired to satisfy the Tchen-Hinze condition, then it is written as:

$$q_{fp} = 2q_{f@p}^2 \frac{T_L^{f@p}}{T_L^{f@p} + \tau_p} \quad (7.41)$$

Equating the two expressions (equation 7.36 and equation 7.41 using the relation 7.37 for  $A_{f@p}$ ), a relation is obtained for the mesoscopic particle kinetic energy as:

$$\frac{\tilde{q}_p^2}{q_{f@p}^2} = \frac{q_p^2}{q_{f@p}^2} \left( 2 - \frac{q_p^2}{q_{f@p}^2} \right) \quad (7.42)$$

This expression is plotted in figure 7.25 along with the relation 7.38. It is clear that the relation overpredicts the measurement values which is not physical. Indeed, a quick analysis

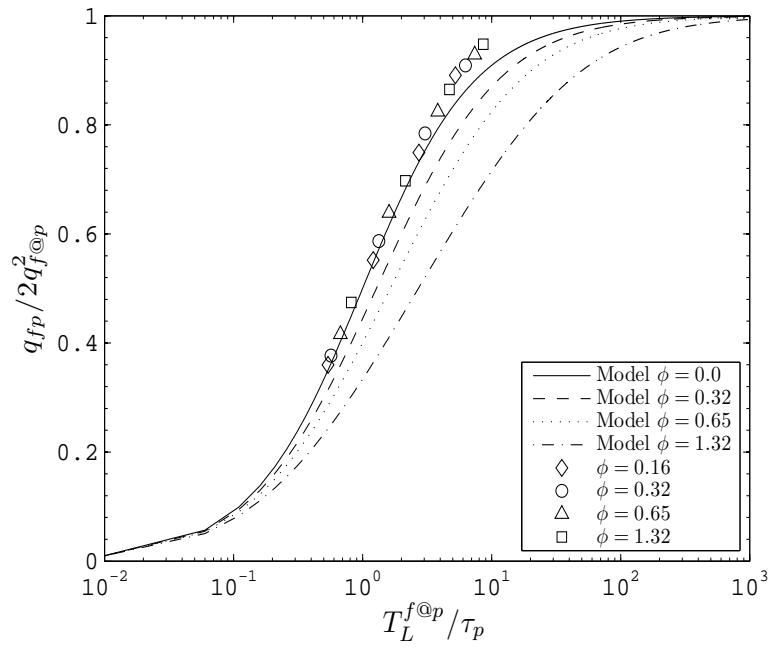


FIGURE 7.23: Fluid-particle covariance model 7.36 obtained using the instantaneous drag model and mesoscopic kinetic energy model 7.38.

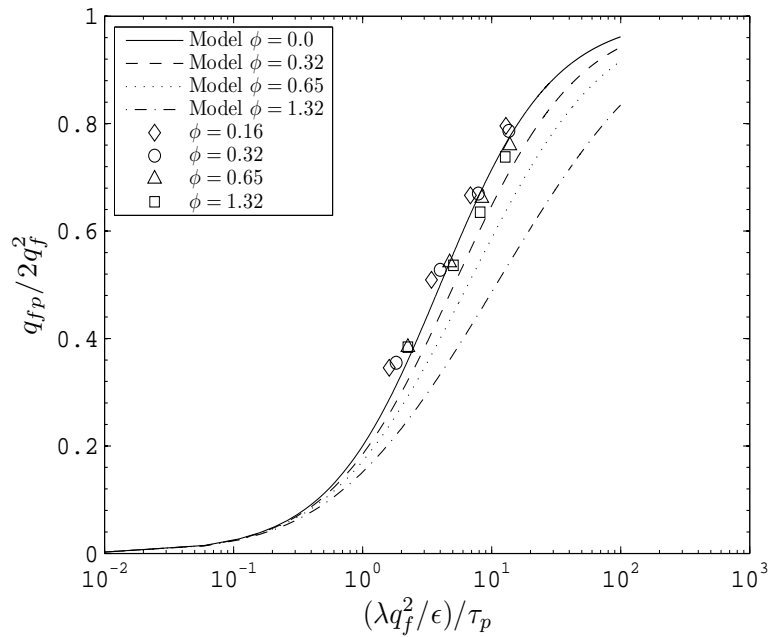


FIGURE 7.24: Fluid-particle covariance model 7.36 using the closures 7.31 with  $\lambda = 0.25$ .

of the figure implies that the mesoscopic particle kinetic energy is always larger than the

total agitation of the particles:

$$\tilde{q}_p^2 > q_p^2 \quad (7.43)$$

which is not physical. According to the figure 5.5 where the Eulerian two-point correlations of the particle velocities are presented, the field of the mesoscopic particle velocity should satisfy the relation:

$$\tilde{q}_p^2 \leq q_p^2 \quad (7.44)$$

for all inertia.

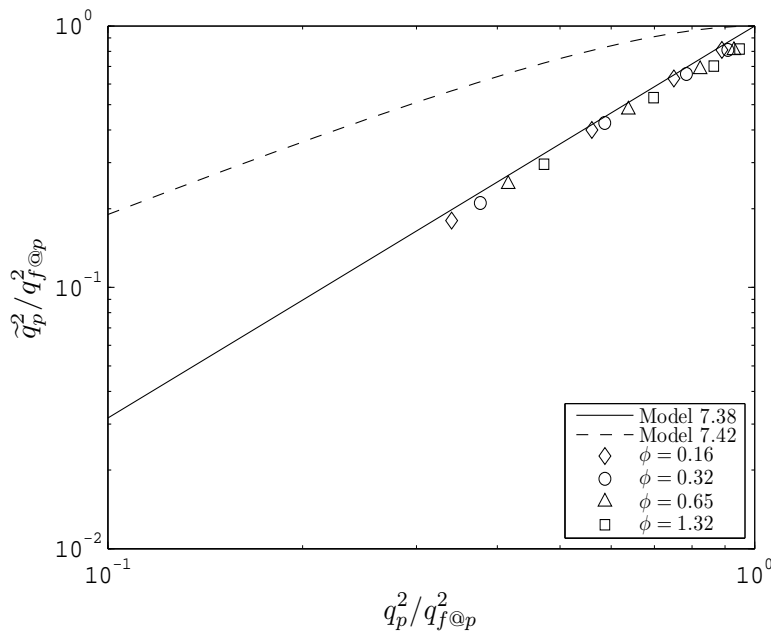


FIGURE 7.25: Comparison of the relation 7.42 to the relation in one-way coupled flows 7.38.

As a conclusion, it can be noted that the relation 7.36 can not predict the evolution of the fluid-particle covariance as a function of the particle inertia and mass-loading. The analysis of the mesoscopic particle energy given in figure 7.25 shows that for the model to satisfy the Tchen-Hinze relation (as observed from the DNS+DPS measurements), the mesoscopic particle energy should be higher than the particle total kinetic energy  $q_p^2$  which is physically inconsistent.

## 7.5 Analysis of fluid-particle turbulent drift velocity

In this section, the fluid-particle turbulent drift velocity contributing to the spatial dispersion of particles will be studied. As noted in section 7.2.2, for the particle motion in Stokes regime, the only important mechanisms effecting the dispersion of particles are inertia and drift. Inertia is already largely discussed in previous sections. This leaves the rest of the chapter to the work of drift velocity.

It is known that the drift velocity due to an external force such as gravity causes the famous 'crossing trajectories effect', first recognized by Yudine (1959) and Csanady (1963). This effect in turn reduces the particle dispersion. Many works were done on the effect of the drift velocity on the dispersion of particles, among many, the works of Meek and Jones (1973), Reeks (1977), Wells and Stock (1983), Maxey (1987), Koch (1989), Pozorski and Minier (1998) can be cited. Despite these studies, in presence of gravity, the effect of the drift velocity on the dispersion of particles is still an open question. Therefore in this section, as before, the gravity will not be considered to simplify the problem. Nevertheless, the results of this section is important in the sense that the models proposed would be applicable to a two-way coupled gas-solid flow where the gravity is important.

### 7.5.1 Methodology

In the configuration used in this thesis, due to the absence of the gravity, the drift velocity is negligibly small. Therefore, a method should be constructed to obtain a drift velocity without adding the gravity. The effect of drift can be artificially generated in a configuration where a group of particles colored differently from the totality of all the other particles. These two groups of particles can then be distributed non-homogeneously throughout the domain by controlling the boundary conditions of the particles.

Two groups of particles, red and blue, are introduced to the domain at the non-dimensional time  $t = 100$  (see the figure 6.2). After the transient regions, the final equilibrium flow field between the particles and the fluid is shown in figure 7.26 as a 2D cut-section. Indeed, at the top side of the domain, if a red particle arrives, it is converted to blue, however, if a blue particle arrives, nothing is performed on the color of particles. The procedure is the same for the down side of the domain, but, for red particles. At the end, particle number density gradients  $\partial n_p^r / \partial y$  and  $\partial n_p^b / \partial y$  are obtained where the indices  $r$  and  $b$  correspond to red and blue, respectively. Such a gradient is enough to create an artificial drift and mean particle velocity as seen on figure 7.27. The particle distribution is uniform in  $z$  direction.

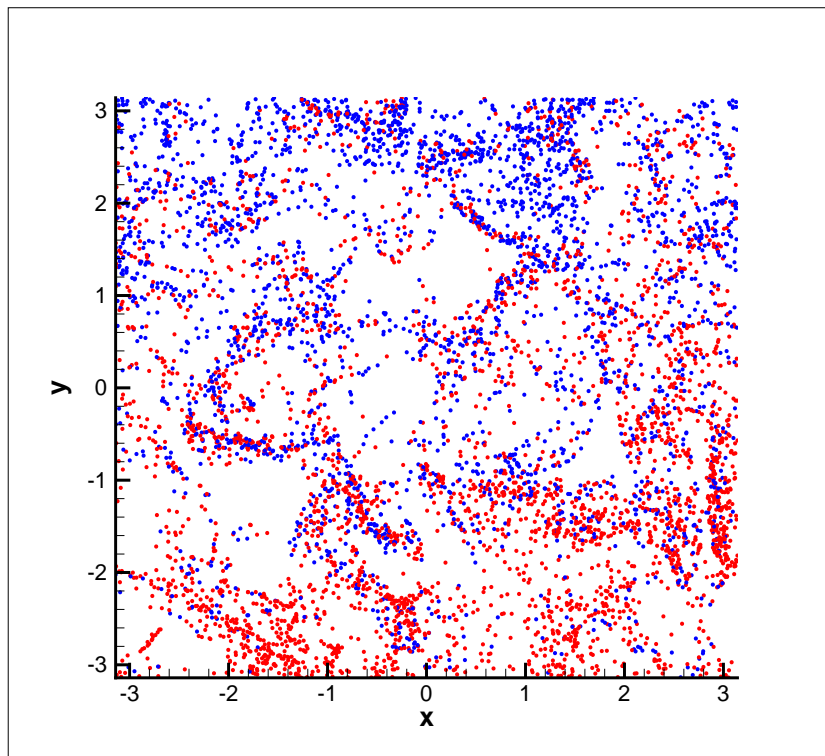


FIGURE 7.26: Example 2D spatial distribution of red and blue particles.

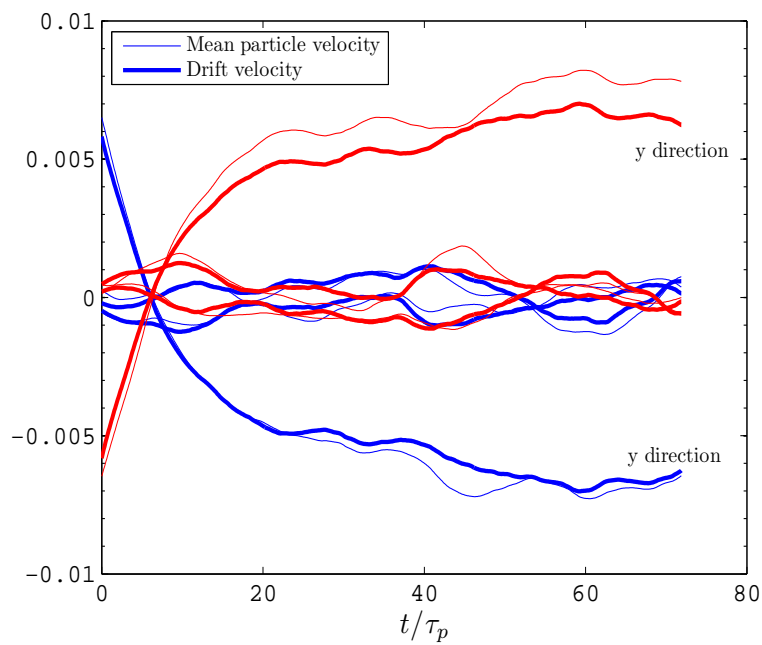


FIGURE 7.27: Time evolution of turbulent drift and mean particle velocity for red and blue particles.

### 7.5.2 Theoretical study

In such a configuration, mean particle number density  $n_p$  is constant. Then it can be written:

$$n_p = n_p^r + n_p^b = \text{constant} \quad (7.45)$$

The continuity equation for the red particles can be written as:

$$\frac{\partial n_p^r}{\partial t} + \frac{\partial}{\partial x_j} n_p^r U_{p,j}^r = 0 \quad (7.46)$$

The mean red particle velocity can be written as:

$$\frac{\partial n_p^r U_{p,i}^r}{\partial t} + \frac{\partial}{\partial x_j} n_p^r U_{p,i}^r U_{p,j}^r = -\frac{\partial}{\partial x_j} n_p^r \langle u'_{p,i} u'_{p,j} \rangle_p^r - \frac{n_p^r}{\tau_p} (U_{p,i}^r - U_{f,i} - V_{d,i}^r) \quad (7.47)$$

where  $u'_{p,i} = u_{p,i}^r - U_{p,i}$  is the fluctuation velocity of a red particle with reference to the mean total particle velocity  $U_{p,i}$ .

Precise calculation of the drift velocity carries importance in the exact formulation of the mean particle velocity equation. The mean fluid velocity and the mean total particle velocities are written as:

$$U_{f,i} = 0 \quad (7.48)$$

$$U_{p,i} = 0 \quad (7.49)$$

due to the construction of the flow configuration. The only hypothesis required is then the assumption for the turbulent dispersion term on the right hand side of the equation 7.47 which, in homogeneous isotropic turbulence, is:

$$q_p^{r2} = q_p^2 \quad (7.50)$$

e.g., the agitation of the red particles is equal to the agitation of the total particles. The hypothesis is well verified in the simulations performed in this thesis, as shown in figure 7.28. As seen, the agitations are equal up to 5% error for each mass loading and each particle inertia.

Performing the necessary simplifications on the equation 7.47 for stationary homogeneous isotropic turbulence, it can be written as:

$$0 = -\frac{\partial}{\partial x_i} n_p^r \langle u'_{p,i} u'_{p,i} \rangle_p^r - \frac{n_p^r}{\tau_p} (U_{p,i}^r - V_{d,i}^r) \quad (7.51)$$

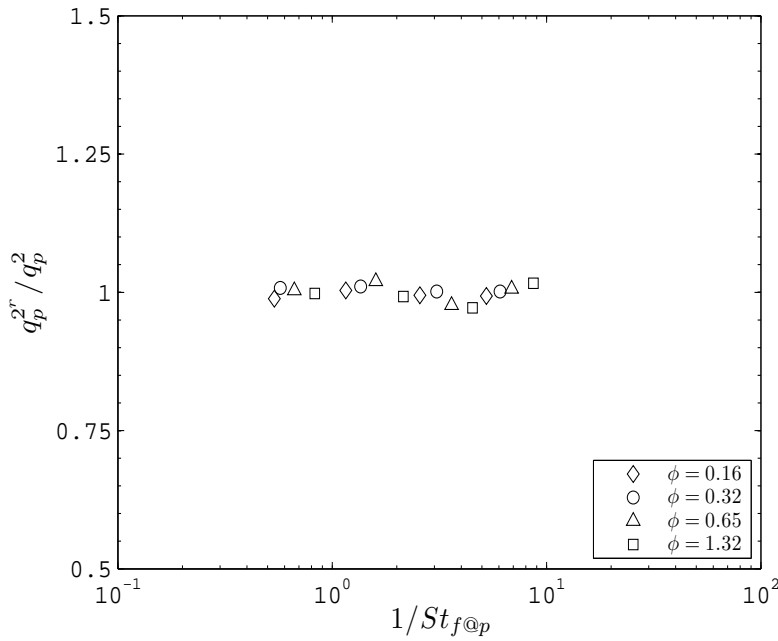


FIGURE 7.28: Comparison of the particle agitation of the red particles to the total particle agitation, hypothesis 7.50.

According to this last relation, it is clear that the particle dispersion due to the agitation is balanced with the transport of the red particles via their mean velocities and the drift velocity. Red particle flux due to the drift velocity can be written as:

$$n_p^r V_{d,i}^r = n_p^r U_{p,i}^r + \frac{2}{3} \tau_p q_p^2 \frac{\partial n_p^r}{\partial x_i} \quad (7.52)$$

According to the relation derived, mean particle transport of particles due to the drift velocity is composed of two contributions; one is the mean flux due to the mean red particle velocity and particle agitation. In case of inertia tending to zero, the second term tends to zero and the particle flux due to drift velocity becomes equal the flux due to the mean velocity.

### 7.5.3 Modeling of the flux due to the mean red particle motion

As imposed by the relation 7.52, to model the mean red particle flux due to the drift velocity, the flux due to the mean red particle velocity should be modeled. Hinze (1975) notes that the general gradient transport model for these fluxes can be written as:

$$n_p^r U_{p,i}^r = -D_p^t \frac{\partial n_p^r}{\partial x_i} \quad (7.53)$$

where  $D_p^t$  is the particle dispersion coefficient which is written, as a recapitulation of particle dispersion studied in previous sections, as:

$$D_{p,ij}^t = \frac{1}{2} \frac{d}{dt} Y_{ij}(t) \quad (7.54)$$

where  $Y_{ij}$  is the particle displacement tensor in the Lagrangian dispersion theory of Taylor (1921).

In the section for particle dispersion, it has been seen that the long time particle dispersion is written in the fluid statistics viewed by the particles as:

$$D_p^t = \frac{2}{3} q_{f@p}^2 T_L^{f@p} \quad (7.55)$$

(see Deutsch and Simonin, 1993). In figure 7.5, it was shown that this relation works well for the two-way coupled gas-solid flows.

To close the equation 7.52, the flux due to the drift velocity has also to be modeled. Because the intention is to lay the justification of the mean transport equation for the particles, turbulent drift velocity, being an unknown, must be modeled in proper physical bases and its transport equation should help in the purpose. In chapter 5, transport equation was already derived for  $V_d$  using the Langevin equation 5.49 with the proposed models for the two-way coupling term  $\Pi_{u_{f@p,i}}^*$ . The next section talks about the modeling of the drift fluxes.

#### 7.5.4 Modeling of the flux due to the fluid-particle turbulent drift velocity

For a recapitulation, the drift velocity transport equation derived from the Langevin model equation is written as:

$$\begin{aligned} n_p^r \frac{\partial V_{d,i}^r}{\partial t} + n_p^r U_{p,j} \frac{\partial V_{d,i}^r}{\partial x_j} &= -n_p^r \frac{\partial \langle u'_{f@p,i} u'_{p,j} \rangle_p^r}{\partial x_j} + n_p^r \frac{\partial \langle u'_{f,i} u'_{f,j} \rangle}{\partial x_j} \\ - \langle u'_{f@p,i} u'_{p,j} \rangle_p^r \frac{\partial n_p^r}{\partial x_j} - n_p^r V_{d,j}^r \frac{\partial U_{f,i}}{\partial x_j} &+ n_p^r A_{f@p,ij} V_{d,j}^r - n_p^r \langle \Pi_{u_{f@p,i}}^* \rangle_p \\ &- n_p^r \langle f_{u_i} \rangle \end{aligned} \quad (7.56)$$

For homogeneous isotropic stationary turbulent gas-solid flow, many of the terms will be canceled and the equation takes the form:

$$0 = - \langle u'_{f@p,i} u'_{p,i} \rangle_p^r \frac{\partial n_p^r}{\partial x_i} + n_p^r A_{f@p} V_{d,i}^r - n_p^r \langle \Pi_{u_{f@p,i}}^* \rangle_p - n_p^r \langle f_{u_i} \rangle \quad (7.57)$$

As noted, the relation is now written only for the red particles for which the finite value of drift velocity can be measured from the configuration.

#### 7.5.4.1 Mean drag model

Using the mean drag model 5.66, for the two-way coupling term  $\Pi_{u_{f@p,i}}^*$  in above equation, the fluid-particle momentum transfer terms (the last two terms on the right hand side of equation 5.61) are equal to each other but with an opposite sign. This leaves the relation as:

$$n_p^r V_{d,i}^r = -D_{fp}^t \frac{\partial n_p^r}{\partial x_i} \quad (7.58)$$

where  $D_{fp}^t$  is called fluid-particle dispersion coefficient written as:

$$D_{fp}^t = \frac{1}{3} q_{fp} T_L^{f@p} \quad (7.59)$$

where  $q_{fp}$  is the fluid-particle covariance.

Most important result of this analysis is that according to this modeling, the drift velocity is not directly effected by the two-way coupling mechanism.

Relation 7.58 is measured term by term from the DNS+DPS measurements. The results are plotted in figure 7.29. As seen, the mean model results seems to agree with the DNS+DPS measurements for each mass-loading (not all shown not to complicate the figure) and for all the particle inertia. This implies that the mean model correctly predicts the flux of particles due to the turbulent drift velocity in simple configuration. For high mass-loadings and small inertia particles, some deviations are visible and this is basically due to the small inertia particles which are sensitive to the high-frequency oscillations of the turbulence. From the other part, insufficient particle numbers considered are also in the source of error in the configuration considered.

#### 7.5.4.2 Instantaneous drag model

Using the instantaneous drag model given by relation 5.87, in the relation 7.57, the two-way coupling terms do not cancel each other, and the following relation is obtained:

$$n_p^r V_{d,i}^r = \frac{\langle u_{p,i}' u_{f@p,i}' \rangle_p^r}{A_{f@p}} \frac{\partial n_p^r}{\partial x_i} + \frac{m_p}{A_{f@p} \rho_f \tau_p} \left( \langle \tilde{n}_p' \tilde{n}_p' \tilde{u}_{p,i} \rangle_p^r - \langle \tilde{n}_p' \tilde{n}_p' u_{f@p,i} \rangle_p^r \right) \quad (7.60)$$

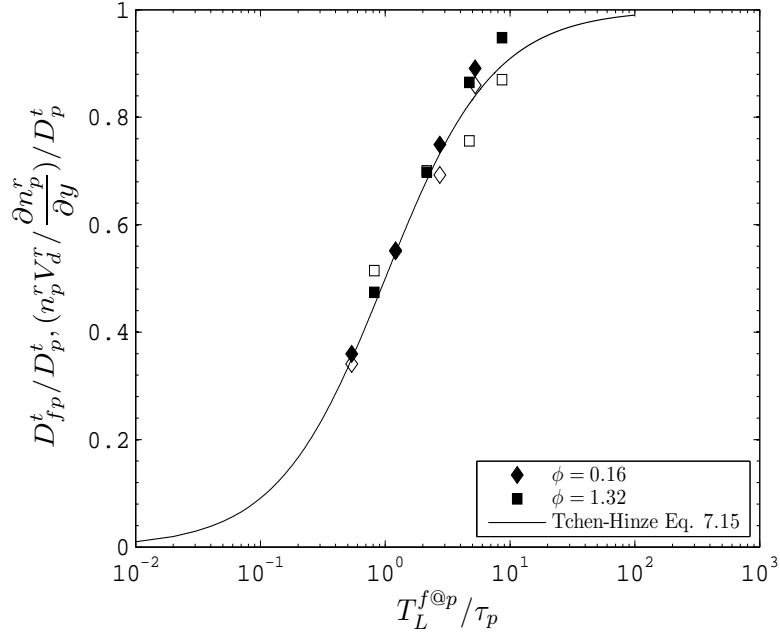


FIGURE 7.29: Verification of the relation 7.58 obtained using the mean drag model (measurements from DNS, blank symbols:  $n_p^r V_d^r / (\partial n_p^r / \partial y)$ , full symbols:  $D_{fp}^t$ ).

Inserting the relation 7.37 for  $A_{f@p}$  obtained from the Langevin equation by deriving the Lagrangian correlations, the relation can be rewritten as:

$$n_p^r V_{d,i}^r = -\kappa D_{fp}^t \frac{\partial n_p^r}{\partial x_i} - \kappa \frac{T_L^{f@p} m_p}{\rho_f \tau_p} \left( \left\langle \tilde{n}_p' \tilde{n}_p \tilde{u}_{p,i} \right\rangle_p^r - \left\langle \tilde{n}_p' \tilde{n}_p u_{f@p,i} \right\rangle_p^r \right) \quad (7.61)$$

where  $\kappa$  is:

$$\kappa = \frac{1}{\left[ 1 + \phi \frac{q_{fp}}{2q_{f@p}^2} \right]} \quad (7.62)$$

As can be noted, the flux due to the turbulent drift velocity has a second term which is unknown a priori. This term derives basically from the subtraction of the two-way coupling terms in the Navier-Stokes equation and in the Langevin equation for fluid element trajectories and represents the spatial segregation of particles due to their low inertia. The relation 7.61 has to be closed by modeling this term of which direct measurement is difficult in DNS due to the insufficient particle numbers  $N_p$  (see the table 6.1 for parametrization of simulations). Indeed, mesoscopic quantities require high number of particles for the precision which is pretty costly, especially for the simulations with very high number of particles.

Considering the relation 7.52, there is no choice but the last term in relation 7.61 must

be proportional to the gradient of the red particle number density with a proportionality constant as:

$$\kappa \frac{T_L^{f@p} m_p}{\rho_f \tau_p} \left( \left\langle \tilde{n}'_p \tilde{n}_p \tilde{u}_{p,i} \right\rangle_p^r - \left\langle \tilde{n}'_p \tilde{n}_p u_{f@p,i} \right\rangle_p^r \right) = C_f \frac{\partial n_p^r}{\partial x_i} \quad (7.63)$$

From relations 7.52 and 7.61, then the coefficient  $C_f$  can be written as:

$$C_f = \frac{2}{3} q_{f@p}^2 T_L^{f@p} - \frac{2}{3} q_p^2 \tau_p - \kappa \frac{1}{3} q_{fp} T_L^{f@p} \quad (7.64)$$

This coefficient is measured from the DNS experiments and plotted in figure 7.30. First thing to remark is that the ratio  $C_f/D_{fp}^t$  increases with increasing mass loading reaching up to values of 50%. The ratio increases with decreasing inertia but the increase is weaker with reference to the decrease due to mass loading. Especially, the small inertia particles give slightly higher ratio due to their increased interactions with the turbulent scales. For inertial particles, they do not respond much of the turbulent scales therefore practically, the drift velocity is relatively much smaller. Despite these facts, for high mass loadings, the ratio is significant which means that the second term in relation 7.61 should be modeled. Intuitively, figure 7.30 is in coherence with the reduction in the turbulent  $Re_L$  of the flows for increasing mass-loadings which in turn increases the preferential concentration (segregation) mechanism, as already noted in section 7.3.5 and seen in figures 7.17 and 7.18. More rigorous calculation of this term is to measure from the DNS experiments, however, this is very difficult due to the fact that mesoscopic variables requires high number of particles which surely can not be satisfied in the work presented here.

To conclude, the instantaneous model in Langevin equation is not in coherence with the transport equation of particle mean velocity due to the additional terms.

## 7.6 Conclusion

In this chapter, the measurements of the particle statistics from the DNS+DPS are presented. Models proposed in chapter 5 are tested against the DNS+DPS measurements in terms of fluid-particle velocity covariance and turbulent drift velocity. These statistics are significantly important in Eulerian modeling gas-solid flows in terms of particle dispersion.

In the modeling part, it has been shown that the mean drag model predicts well the evolution of the fluid-particle covariance with the particle inertia. Same set of equations are obtained as in the case of one-way coupling and this significantly makes the mean model easy to implement. Instantaneous drag model written with the help of Mesoscopic Eulerian

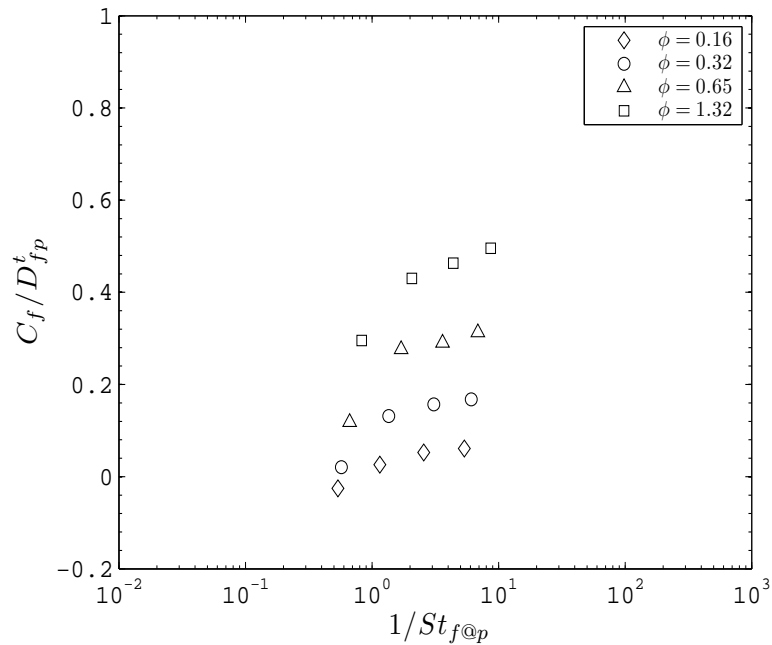


FIGURE 7.30: Behavior of the coefficient  $C_f$  measured from DNS to determine the order of magnitude of  $C_f$  with reference to  $D_{fp}^t$ .

Approach results in relations including the mass-loading of the particle phase, therefore, containing dependency on the two-way coupling mechanism. The results show that the classical closures help instantaneous drag model to take into account the evolution of the fluid-particle covariance with the realistic flow variables,  $q_f^2$  and  $T_L^f$ . However, the classical closures are in contradiction with the DNS+DPS results due to the observed differences between the fluid statistics viewed by the particles and fluid elements. It is shown in the modeling part that the difference in the fluid kinetic energy is much more important than in the Lagrangian timescale therefore the transport equations derived in chapter 5 should help improving the modeling approach.

In the last part, the modeling of the particle fluxes due to the fluid-particle turbulent drift velocity is studied. The transport equations derived from the Langevin models using the mean model do not contain two-way coupling term therefore an important result (in coherence with the work of Vermorel et al., 2003) is obtained, e.g., there is no direct effect of two-way coupling on the drift velocity. Instantaneous drag model results in more complicated relations. An extra term is derived to the drift flux expression which seems to be of important order magnitude as the mass-loading increases.



## Chapter 8

# Conclusion

The principal objective of this thesis was to extend the Lagrangian stochastic approach to the gas-solid flows where the carrier continuum phase is modified by the perturbations in the vicinity of the point particles. The basic purpose of the approach is to predict the fluid statistics encountered by the solid particles and fluid elements. Indeed, velocity of a fluid element and therefore of the fluid statistics viewed by the particles are modified due to the existence of particles. This should be represented by an additional term in the trajectorial equations which were not being considered in the past to treat gas-solid flows due to the consideration of flows in dilute regimes. It is known, at least in one-way coupled flows, that the statistics seen by the particles are capable of well predicting the dispersion of solid particles. Therefore the same approach could hold in two-way coupled flows, as well.

To arrive these aims, first a turbulent flow field was considered with proper statistical characteristics, e.g., homogeneous isotropic stationary turbulence. Stochastic forcing scheme, which is already largely used in the turbulence community, was verified to obtain proper characteristics of which the most important one in this work was the stationarity. In fact, stationarity allows statistical analyzes easily. It has been observed that stochastic forcing was very costly, even in parallel environment, therefore different configuration was installed in which an additional processor performing the inverse FFT and sending the data to the processors solving the flow velocity was conceived. From the other part, the stochastic forcing was seen to have a large effect on the large scales of turbulence, in coherence with the past works, nonetheless the effect on the small scales were absent.

As a possible alternative to the problem of stochastic forcing configuration, the linear forcing scheme was implemented on the flow field obtained by stochastic forcing. It is known that this scheme is very fast and very easy to be embedded into a numerical code. Nevertheless, the obtained turbulence characteristics were pretty far from the homogeneity and

isotropy, therefore, this scheme is thought to require further consideration. Especially, the scheme seems to be poor in the sense of the statistical calculations due to the large oscillations generated in the consecutive timesteps.

After preparing a turbulent flow field with proper statistics, the Euler-Euler models are briefly summarized and the advantages of the probabilistic approach of Simonin (1996) were explained. Indeed, it is known that the Euler-Euler models are not capable of proposing closures for the particle dispersion quantities; turbulent drift velocity,  $V_d$ , and the fluid-particle covariance,  $q_{fp}$  which depend strongly on the fluid statistics viewed by the particles. In stochastic approach, these quantities are closed using the Lagrangian way which, in coherence with what has been said in the first paragraph, requires to be extended to the two-way coupled gas-solid flows. The theory of Lagrangian stochastic modeling was studied next. A methodology was then proposed to obtain the drift and diffusion coefficients in the Langevin equations. The hypothesis that the Langevin equation for the fluid element trajectory has:

- The same Lagrangian timescale of the fluid elements,  $T_L^f$
- The same mean momentum equation ( $U_{f,i}$ )
- The same turbulent kinetic energy ( $q_f^2$ ) transport equation

as the ones derived from the Navier-Stokes equations.

Langevin equation for the gas velocity viewed by the particles was imposed only one condition which is:

- Theory of Tchen-Hinze on the particle dispersion

which was verified in the DNS+DPS simulations performed. However, the models are not known a priori, whether they satisfy this condition or not.

The steps to obtain the stochastic equation coefficients were then proposed as:

- Proposition of a model for the two-way coupling terms in Langevin equations which is consistent with the mean flow transport equation
- Derivation of the Lagrangian correlations of the fluctuating gas velocity and fluid kinetic energy transport equation
- Determination of the stochastic equation coefficients using the hypotheses

For the modeling of the two-way coupling term, the problem is that the deterministic and stochastic terms in the Langevin equation model the low wavenumber and inertial zone of the kinetic energy spectrum, respectively. However the additional term for two-way coupling effect is to be properly defined due to the interaction of particles with different scales of turbulence according to their inertia and mass-loadings which is well observed in DNS+DPS results of this study. According to these interactions, particles can extract energy from the turbulent scales and they can inject it to the preferential scales of turbulence. Two models were then proposed to take into account these effects, namely: mean and instantaneous drag models. The instantaneous model was seemed to be more adequate for the complex interactions between the particles and preferential scales of turbulence but the model is more complicated than the mean model.

After the modeling of the two-way coupling term, a database was constructed out of the DNS+DPS results of flows with different mass-loading and different particle inertia. Flow characteristics, especially the fluid phase, were analysed using the one-point and two-point correlations in order to observe how the flow responds to the variations in the particle characteristics. The results obtained were in accord with the literature. It has been observed that the point particles decrease the turbulence level,  $Re_L$  number, in relation with their inertia and with their mass-loading, but the dependence on the particle inertia seems to be weak. The decrease in  $Re_L$  was basically due to the reduction in the characteristic velocity of the turbulence because the turbulence is seen to keep its isotropy and homogeneity after it is coupled with the particles. Large scales' length did not change after the coupling. In relation with the reduction in the turbulence levels, larges scales were less rapid therefore increasing the eddy turnover and Eulerian decorrelation timescales. Analyzing the modifications in the Lagrangian structure functions, it has been also verified that the methodology proposed to obtain the stochastic equation coefficients is more proper because it includes to write the transport equations including all the related phenomena. The classical use of the Kolmogorov similarity hypothesis to justify the stochastic coefficient is not used in coherence with the proposition of Pope (2002) which reveals that this term can be highly anisotropic, in contrast to the Kolmogorov hypothesis, in shear flows.

Using the DNS+DPS results, the statistics concerning the particle phase were exploited next. Particle dispersion mechanism which includes the agitation and the relaxation time of particles is verified showing that a particle with high agitation has a small correlation time and this results in the same rate of dispersion as a particle with low agitation but with a long correlation time due to its large inertia. Particle dispersion mechanism is further extended to the fluid statistics viewed by the particles and it has been observed that in two-way coupled simulations, as in the one-way coupled flows, the theory of Tchen-Hinze is well capable of

predicting of the fluid-particle covariance as a function of the particle inertia and the mass-loading. Very significant results obtained in this study are that the fluid statistics viewed by the fluid elements and the solid particles are different and the difference increase with the mass-loading. It was direct that the modifications in the Lagrangian timescale  $T_L^{f@p}$  were due to the particles spending more time in the peripheries of the large fluid scales, an effect known as preferential concentration. This was shown to be due to the reduction in the turbulence levels which increases all the characteristic timescales and therefore reduces the particle Stokes number. However, the differences in the fluid turbulent kinetic energy viewed by the particles and fluid elements is less clear. No strange effect was observed in the preferential concentration mechanism to explain this difference. As in the one-way coupled simulations, particles were seen to collect more to the preferential zones in the flow domain as the Stokes' number decreases. This statistical difference should then be more studied using the transport equations derived in the course of this thesis.

Lagrangian modeling results showed that the mean model has more advantageous than the instantaneous models. This was basically due to its practical use neglecting the effect of the two-way coupling on the second order statistics such as gas-particle covariance and gas turbulent kinetic energy. The mean model is in coherence with the Tchen-Hinze theory of dispersion which is also verified in the simulations. It is to be noted that there is no term in the Langevin equation to take into account the effect of the stochastic forcing, despite the corresponding term in Navier-Stokes equations. Therefore it can be said that the drift and diffusion terms take into account the forcing effect, as well.

Next logical step is to give practical closures for the fluid statistics viewed by the fluid elements, in terms of the fluid statistics viewed by the particles. For the mean drag model, the classical closures were seen not to give correct prediction of these statistics, significantly due to the statistical differences in the fluid kinetic energies viewed by the both phases. An even more practical model for the Lagrangian timescale viewed by the particles was proposed for the  $q_f^2 - \epsilon$  models which can take into account the evolution of the fluid-particle covariance as a function of the particle inertia and mass-loading. This model seemed to be in coherence with the measured values of Kolmogorov constants.

Instantaneous model requires more complicated treatment because the transport equations have additional terms which are to be modeled. At first glance, mesoscopic particle kinetic energy should be modeled in order to close the prediction of fluid-particle covariance. Measured values of the mesoscopic energy was seen to lead to incorrect prediction of the fluid-particle covariance. Surprisingly, the classical closures were seen to correct qualitative prediction of the fluid-particle covariance whereas the classical closures are shown not to be valid in DNS+DPS measurements. Therefore, the theory of Tchen-Hinze was imposed on the model which leads to the unphysical behaviour of the mesoscopic particle energy.

---

As a final point, both models were tested on a configuration in which the colored particle gradient is generated where the particles are dispersed due to an artificially generated fluid-particle turbulent drift velocity. The mean model was seen to predict correctly, even though there are some errors due to the imprecisions in the calculations, which means that the two-way coupling has no direct effect on the turbulent drift velocity. The instantaneous model, on the other hand, does not neglect this effect and adds an additional term to the relation of particle flux due to the drift velocity which is pretty difficult to measure from DNS+DPS results. This term is basically due to the preferential segregation of low inertia particles and requires modeling. A dimensional analysis showed that this term has significant importance with the increase in mass-loadings due to the reduction in the Reynolds numbers leading to higher concentration of particles.



# Bibliography

- ABRAHAMSON, J., Collision rates of small particles in a vigorously turbulent fluid, *Chem. Eng. Sci.*, 30, 1371-1379., 1975
- AHMED, A.M. and ELGOBASHI, S., On the mechanisms of modifying the structure of turbulent homogeneous shear flows by dispersed particles, *Phys. Fluids*, 12, 2906-2930, 2000
- AYALA, O.F., AYALA, L.F. and AYALA, M.A., Multi-phase Flow Analysis in oil and gas engineering systems and its modeling, report, Universidad de Oriente, Pennsylvania State University, 2007
- BALACHANDAR, S. and MAXEY, M.R., Methods for evaluating fluid velocities in spectral simulations of turbulence, *J. Comput. Physics*, 83, 96-125, 1989
- BASSET, A.B., *Treatise on hydrodynamics*, Bell, London, 1888
- BATCHELOR, G.K., Diffusion in a field of homogeneous turbulence, *Austral. J. Sci. Res.* 2, 437-450, 1949
- BATCHELOR, G.K., *An introduction to fluid mechanics*, Cambridge University Press, 1968
- BAUM, M, Etude de l'allumage et de la structure des flammes turbulentes, Thèse de l'Ecole Centrale de Paris, 1994
- BENAVIDES, A. and VAN WACHEM, B., Numerical simulation and validation of dilute turbulent gas-particle flow with inelastic collisions and turbulence modulation, *Powder Technology*, 182, 294-306, 2008
- BOIVIN, M., Etude de l'influence des particules sur la turbulence à partir de simulations directes et de simulations des grandes échelles d'écoulements diphasiques gaz-solides homogènes isotropes stationnaires, Thèse de l'Université de Rouen, Rouen, France, 1996
- BOIVIN, M., SIMONIN, O. and SQUIRES, K.D., Direct numerical simulation of turbulence modulation by particles in isotropic turbulence, *J. Fluid Mech.*, 375, 235-263, 1998
- BOIVIN, M., SIMONIN, O. and SQUIRES, K.D., On the prediction of gas-solid flows with two-way coupling using large eddy simulation, *Phys. Fluids*, 12, 2080-2090, 2000

- BORGAS, M.S. and SAWFORD, B.L., Stochastic equations with multifractal random increments for modeling turbulent dispersion, *Phys. Fluids*, 6, 618-633, 1994
- BOUGHANEM, H. and TROUVÉ, A. Validation du code de simulation directe NTMIX3D pour le calcul des écoulements turbulents réactifs, Technical Report 42907, Institut Français du Pétrole, 1996.
- BOUSSINESQ, J., Sur la résistance qu'oppose un liquide indéfini en repos, *Compte rendu Acad. Sci*, 100, Paris, France, 1885
- BUYEVICH, Y.A., Motion resistance of a particle suspended in a turbulent medium, *Fluid Dynamcis, Physics and Astronomy*, 1, p119, 1966
- BUYEVICH, Y.A., Statistical hydromechanics of disperse systems Part 1. Physical background and general equations, *J. Fluid Mech.*, 49, 489-507, 1971
- CHAN, C.K., GUO, Y.C. and LAU, K.S., Numerical modeling of gas-particle flow using a comprehensive kinetic theory with turbulence modulation, *Powder Technology*, 150, 42-55, 2005
- CHAPMAN, S. and COWLING, T.G., *The mathematical theory of non-uniform gases*, Cambridge University Press, 1970
- CLIFT, R., GRACE, J.R. and WEBER, M.E., *Bubbles, Drops and Particles*, Academic Press, New York, 1978
- CLIMENT, E. and MAXEY, M.R., *The Force Coupling Method: A flexible approach for the simulation of particulate flows*, *Theoretical Methods for Micro Scale Viscous Flows*. Ressign Press, 2009
- COMTE-BELLOT, G. and CORRISIN, S., Simple Eulerian time correlation of full- and narrow-band velocity signals in grid-generated 'isotropic' turbulence, *J. Fluid Mech.*, 48, 273-337, 1971
- CORRSIN, S., Theories of turbulent dispersion, *Mécanique de la Turbulence*, no 108. Editions du CNRS, 27-52, 1961
- CROWE, C.T., SHARMA, M.P., STOCK, D.E., The particle source in cell (psi-cell) model for gas-droplet flows, *J. of Fluids Eng.*, 325-332, 1977
- CROWE, C.T., GORE, R. and TROUTT, T.R., Particle dispersion by coherent structures in free shear flows, *Particulate Sci. Tech.*, 3, 149-158, 1985
- CROWE, C.T., SOMMERFELD, M. and TSUJI, Y., *Multiphase Flow with Droplets and Particles*, CRC Press, New York, 1998

- CSANADY, G.T., Turbulent diffusion of heavy particles in the atmosphere, *J. Atmos. Sci.*, 20, 201-208, 1963
- DELHAYE, J.M., Thermohydrolics of two-phase systems for industrial design and nuclear engineering, ed. J.M. Delhaye, 1981
- DEREVICH, I.V. and ZAICHIK, L.I., Precipitation of particles from a turbulent flow, *Izvestiya Akademii Nauk SSSR, Mekhanika Zhidkosti i Gaza*, 5, 96-104, 1988
- DESJONQUERES, P., GOUESBET, G., BERLEMONT, A. and PICART, A., Dispersion of discrete particles by continuous turbulent motions: new results and discussions, *Phys. Fluids*, 29, 2147-2151, 1986
- DEUTSCH, E. and SIMONIN, O., Large eddy simulation applied to the motion of particles in stationary homogeneous fluid turbulence, *ASME-FED*, Vol. 110, 35-42, 1992
- DEUTSCH, E., Dispersion de particules dans une turbulence homogène isotrope calculée par simulation numérique directe des grandes échelles, Thèse de l'Ecole centrale de Lyon, Collection des notes internes de la DER, EDF, 1992
- DRUZHININ, O.A. and ELGOBASHI, S., On the decay rate of isotropic turbulence laden with microparticles, *Phys. Fluids*, 11, 602-610, 1999
- DURLOFSKY, L., BRADY, J.F. and BOSSIS, G., Dynamic simulation of hydrodynamically interacting particles, *J. Fluid Mech.*, 180, p21, 1987
- EARLS, C., *Fundamentals of Multiphase Flow*, Cambridge University Press, 2005
- EATON, J.K. and FESSLER, J.R., Preferential concentration of particles by turbulence, *International Journal of Multiphase Flow*, 20, 169-209, 1994
- ELGOBASHI, S.E. and TRUESDELL, G.C., On the two-way interaction between homogeneous turbulence and dispersed solid particles: I. turbulence modification, *Phys. Fluids, A* 5, 1790-1801, 1993
- ELGOBASHI, S.E., On predicting particle-laden turbulent flows, *Proc. 7<sup>th</sup> workshop on two-phase flow predictions*, 1994
- ENSKOG, D. and SVEN, K., *Vetenskapakad, Handl 4.*, page 63, 1922
- ESWARAN, V. and POPE, S.B., An examination of forcing in direct numerical simulations of turbulence, *Computers and Fluids*, 16(3), 257-278, 1988
- EVANS, L.E., *An Introduction to Stochastic Differential Equations Version 1.2*, Course in University of Berkeley, 2006

- FALKOVICH, G., GAWEDZKI, K. and VERGASSOLA, M., Particles and fields in fluid turbulence, *Rev. Mod. Phys.*, 73, p913, 2001
- FAXEN, H., Der Widerstand gegen die Bewegung einer Istarren Kugel in einer ziihen Flüssigkeit, die zwischen zwei parallelen, ebener Wänden eigeschlossen ist. *Arkiv Mat. Aston. Pya.* 18 (29), 3., 1924
- FERRAND, V., BAZILE, R., BORÉE, J. and CHARNAY, G., Gas-droplet turbulent velocity correlations and two-phase interaction in an axisymmetric jet laden with partly responsive droplets, *International Journal of Multiphase Flow*, 29, 195-217, 2003
- FERZIGER, J.H. and PÉRIC, M., *Computational Methods for Fluid Dynamics*, Springer, 2000
- FESSLER, J.R., KULICK, J.D. and EATON, J.K., Preferential concentration of heavy particles in a turbulent channel flow, *Phys. Fluids*, 6, 3742-3749, 1994
- FÉVRIER, P., Etude numérique des effets de concentration préférentielle et de corrélation spatiale entre vitesses de particules solides en turbulence homogène isotrope stationnaire, Thèse de Doctorat, INP Toulouse, 2000
- FÉVRIER, P., SIMONIN, O and SQUIRES, K.D., Partitioning of particle velocities in gas-solid turbulent flows into a continuous field and a spatially uncorrelated random distribution: theoretical formalism and numerical study, *Journal of Fluid Mechanics*, 533, 1-46, 2005
- FOX, D.G. and LILLY, D.K., Numerical simulation of turbulent flows, *Rev. Geophys. Space Phys.*, 10, 51-72, 1972
- FUNG, J.C.H. and PERKINS, R.J., Particle trajectories in turbulent flow generated by true-varying random Fourier modes, *Adv. Turbulence 2*, pp. 322328, 1989
- GARCÍA, J., Study of the turbulence modulation in particle-laden flows using LES, CTR, Annual Research Briefs, 177-184, 2001
- GATIGNOL, R., The Faxen formulae for a rigid particle in an unsteady non-uniform Stokes flow, *Journal de Mécanique Théorique et Appliquée*, 1, 143-160, 1983
- GIBSON, M. and LAUNDER, B., Ground effects on pressure fluctuations in the atmospheric boundary layer. *Journal of Fluid Mechanics* , 86, 491511, 1978
- GORE, R.A. and CROWE, C.T., Effect of particle size on modulating turbulence intensity, *Int. J. of Multiphase Flow* 15:279-85, 1989
- GOUESBET, G., BERLEMONT, A. and PICART, A., Dispersion of discrete particles by continuous turbulent motions. Extensive discussion of the Tchen's theory, using a two-parameter family of Lagrangian correlation functions, *Phys. Fluids*, 27, 827-837, 1984

- HAWORTH, D.C. and POPE, S.B., A generalized Langevin model for turbulent flows, *Phys. Fluids*, 29(2), 387-405, 1986
- HE, J. and SIMONIN, O., Etude de l'influence des collisions entre particules et de l'anisotropie de leur mouvement fluctuant sur la modélisation des écoulements gas-solides en regime dilue, Collection des notes internes de l'EDF, 1994
- HINZE, J.O., Turbulence, New York, McGraw-Hill, 1975
- HOFFMAN, J.D., Numerical methods for engineers and scientists, 2002
- HWANG, W. and EATON, J.K., Homogeneous and isotropic turbulence modulation by small heavy ( $St \sim 50$ ) particles, *Journal of Fluid Mechanics*, 564, 361-393, 2006a
- HWANG, W. and EATON, J.K., Turbulence attenuation by small particles in the absence of gravity, *International Journal of Multiphase Flow*, 32, 1386-1396, 2006b
- HYLAND, K.E., The modeling of particle dispersion in turbulent flows, Ph.D. Thesis, University of Strathclyde, 1995
- ISHII, M., Thermo-Fluid dynamic theory of two-phase flow, Eyrolles, Paris, 1975
- JEANS, J.H., An introduction to the kinetic theory of gases, Cambridge University Press, New York, 1946
- KENNING, V.M. and CROWE, C.T., On the effect of particles on carrier phase turbulence in gas-particle flows, *International Journal of Multiphase Flow*, 23, 403-408, 1997
- KERR, R.M., Theoretical investigation o a passive scalar such as temperature in isotropic turbulence, PhD thesis, Cornell University, 1981
- KIM, J., MOIN, P. and MOSER, R., Turbulence statistics in fully developed channel flow at low Reynolds number, *J. Fluid Mech.*, 177, 133-166, 1981
- KOCH, D., On hydrodynamic diffusion and drift in sheared suspensions, *Phys. Fluids A*, 1, 1742-1745, 1989
- KOCH, D., Kinetic theory for a monodisperse gas-solid suspension, *Phys. Fluids*, 2 (10), 1711-1723, 1990
- KRAICHNAN, R.H., Lagrangian-history closure approximation for turbulence, *Phys. Fluids*, 8, 574-598, 1965
- KULICK, J.D., FESSLER, J.R. and EATON, J.K., Particle response and turbulence modification in fully developed channel flow, *J. of Fluid Mech.*, 277, 109-134, 1994

- LAVIÉVILLE, J., Simulations numériques et modélisation des interactions entre l'entraînement par la turbulence et les collisions interparticulaires en écoulements gaz-solides, Thèse de Doctorat, Université de Rouen, 1997
- LAZARO, B.J. and LASHERAS, J.C., Particle dispersion in a developing free shear layer, Part 2: Forced flows, *J. Fluid Mech.*, 235, 179-221, 1992
- LELE, S., Compact finite difference schemes with spectral-like resolution, *J. Comput. Phys.*, 103, 16-42, 1992
- LEMONS, D.S., *An Introduction to Stochastic Processes in Physics*. The Johns Hopkins University Press., 2003
- LONGMIRE, E.K. and EATON, J.K., Structure of a particle-laden round jet, *J. Fluid Mech.*, 236, 217-257, 1992
- LUNDGREN, T.S., Linearly forced isotropic turbulence, *Annual Research Briefs (CTR)*, 461-473, 2003
- MAGNAUDET, J., RIVERO, M. and FABRE, J., Accelerated flows past a solid sphere or a spherical bubble, Part I. Steady straining flow, *J. Fluid Mech.*, 284, 97-135, 1995
- MAXEY, M.R. and RILEY, J.J., Equation of motion for a small rigid sphere in a nonuniform flow, *Phys. Fluids*, 26, 883-889, 1983
- MAXEY, M.R., The gravitational settling of aerosol particles in homogeneous turbulence and random flow fields, *J. Fluid Mech.*, 174, 441-465, 1987
- MAXEY, M.R., PATEL, B.K., CHANG, E.J. and WANG, L.P., Simulations of dispersed turbulent multiphase flow, *Fluid Dynamics Research.*, 20, 143-156, 1997
- MEEK, C.C. and JONES, B.G., Studies of the behavior of heavy particles in a turbulent fluid flow, *J. Atmos. Sci.*, 30, 239-244, 1973
- MIGDAL, D. and AGOSTA, D.V., A source flow model for continuum gas-particle flow, *Trans. ASME, J. Appl. Mech.*, 34E, p860, 1967
- MINIER, J.P., Construction de la trajectoire d'une particule dans un écoulement turbulent, *Rapport EDF, EDF*, 1988
- MINIER, J.P. and PEIRANO, E., The pdf approach to turbulent polydispersed two-phase flows, *Physics Reports* 352(1-3), 1-214, 2001
- MIZUKAMI, M., PARTHARASATY, R. N. and FAETH, G. M., Particle-generated turbulence in homogeneous dilute dispersed flows, *International Journal of Multiphase Flow*. 18, 397-412, 1992

- MOIN, P. and MAHESH, K., Direct Numerical Simulation: A tool in turbulence research, *Annu. Rev. Fluid Mech.*, 30, 539-578, 1998
- MONIN, A.S. and YAGLOM, A.M., *Statistical Fluid Mechanics*, MIT Press, 2, 1975
- MORIZE, C., MOISY, F., RABAUD, M. and SOMMERIA, J., Dynamics of the anisotropy in decaying rotating turbulence with confinement effects, 18<sup>ème</sup> Congrès Français de Mécanique, Grenoble, 2007
- NASR, H. and AHMADI, G., The effect of two-way coupling and inter-particle collisions on turbulence modulation in a vertical channel flow, *International Journal of Heat and Fluid Flow*, 28, 1507-1517, 2007
- OKSENDAL, B., *Stochastic Differential Equations: An Introduction with Applications*, 2003
- ORSZAG, S.A. and PATTERSON, G.S., Numerical simulation of three-dimensional homogeneous isotropic turbulence. *Physical Review Letters*, 28(2), 7679, 1972
- OSEEN, C.W., *Hydrodynamik*, Leipzig, 1927
- PARTHARASATY, R. N. and FAETH, G. M., Turbulence modulation in homogeneous dilute particle-laden flows, *J. Fluid Mech.*, 220, 485-514, 1990
- PASSOT, T. and POUQUET, A., Numerical simulation of homogeneous flows in the turbulent regime, *J. Fluid Mech.*, 101, 104-129, 1992
- PEIRANO, E. and LECKNER, B., Fundamentals of turbulent gas-solid flows applied to circulating fluidized bed combustion, *Progress in Energy and Combustion Science*, 24, 259-296, 1998
- PISMEN, L.M. and NIR, A., On the motion of suspended particles in stationary homogeneous turbulence, 84, 193-206, 1978
- POPE, S.B., Transport equation for the joint probability density function of velocity and scalars in turbulent flow, *Phys. Fluids*, 24, 588-596, 1981
- POPE, S.B., Lagrangian pdf methods for turbulent flows, *Annu. Rev. Fluid Mech.* 26, 23-63, 1994
- POPE, S.B., Stochastic Lagrangian models of velocity in homogeneous turbulent shear flow, *Phys. Fluids* 14(5), 1696-1702, 2002
- PORTELA, L. and OLIEMANS, R.V.A., Eulerian-Lagrangian DNS/LES of particle-turbulence interactions in Wall-Bounded flows. *International journal for numerical methods in fluids*, 43(9), 1045-1065, 2003

- POZORSKI, J. and MINIER, J.P., On the Lagrangian turbulent dispersion models based on the Langevin equation, *International Journal of Multiphase Flow*, 24, 913-945, 1998
- PRESS, W.H., TEUKOLSKY, S.A., VETTERLING, W.T. and FLANNERY, B.P., *Numerical Recipes in Fortran 77*, Cambridge University Press, 2001
- PRIGOGINE, I., HERMAN, R., *Kinetic Theory of Vehicular Traffic*, American Elsevier Publishing Co., New York, 1971
- RANI, S.L., WINKLER, C.M. and VANKA, S.P., Numerical simulations of turbulence modulation by dense particles in a fully developed pipe flow, *Powder Technology*, 141, 80-99, 2004
- REEKS, M., On the dispersion of small particles suspended in an isotropic turbulent field, *J. Fluid Mech.*, 83, 529-546, 1977
- REEKS, M., Eulerian direct interaction applied to the statistical motion of particles in a turbulent fluid, *J. Fluid Mech.*, 97, 569, 1980
- REEKS, M., On a kinetic equation for the transport of particles in turbulent flows, *Phys. Fluids A.*, 3, 446-456, 1991
- REEKS, M., On the continuum equations for dispersed particles in nonuniform flows, *Phys. Fluids A*, 4, 1290-1303, 1992
- REEKS, M., On the constitutive relations for dispersed particles in nonuniform flows. I: Dispersion in a simple shear flow, *Phys. Fluids A*, 5, 750-761, 1993
- RILEY, J.J., Ph.D. Thesis, The Johns Hopkins University, Baltimore, MD, 1971
- RISSO, F. and FABRE, J., Diffusive turbulence in a confined jet experiment, *J. Fluid Mech.*, 337, 233-261, 1997
- RIVERO, M., Etude par simulation numérique des force exercées sur une inclusion sphérique par un écoulement accéléré, *These de Doctorat*, INP Toulouse, 1991
- ROGALLO, R., Numerical experiments in homogeneous turbulence, *NASA technical Memorandum 81315*, NASA, Ames Research Center, 1981
- ROSALES, C. and MENEVEAU, C., Linear forcing in numerical simulations of isotropic turbulence: Physical space implementations and convergence properties, *Phys. Fluids*, 17, 1-8, 2005
- SAFFMAN, P.G., The lift on a small sphere in a slow shear flow, *J. Fluid Mech.*, 22, 385-400, 1965

- SAFFMAN, P.G., On the settling speed of free and fixed suspension, *J. Fluid Mech.*, 1, 16-30, 1973
- SAWFORD, B.L., Reynolds number effects in Lagrangian stochastic models of turbulent dispersion, *Phys. Fluids A* 3 (6), 1577-1588, 1991
- SAWFORD, B.L. and TIVENDALE, C.M., Measurements of concentration statistics downstream of a line source in grid turbulence. In *Proc. 11<sup>th</sup> Australasian Fluid Mechanics Conf.*, 945-948, University of Tasmania, Hobart, 1992
- SCHILLER, L., NAUMAN, A., A drag coefficient correlation, *V.D.I. Zeitung*, 77, 318-320, 1935
- SIGGIA, E.D., PATTERSON, G., Intermittency effects in a numerical simulation of stationary three-dimensional turbulence, *J. Fluid Mech.*, 86, 567-592, 1978
- SIGGIA, E.D., Numerical study of small-scale intermittency in three-dimensional turbulence, *J. Fluid Mech.*, 107, 375-406, 1981
- SIMONIN, O. and VIOLLET, P.L., Modeling of turbulent two-phase jets loaded with discrete particles, *Proc. Int. Conf. Phase-Interphase Phenomenon in Multiphase Flow*, Dubrovnik, Yugoslavia, 1990
- SIMONIN, O., Second-moment prediction of dispersed phase turbulence in particle-laden flows, *Eighth Symposium on turbulent shear flows*, Munich, 1991
- SIMONIN, O., DEUTSCH, E. and MINIER, J.P., Eulerian prediction of the fluid/particle correlated motion in turbulent two-phase flows, *Applied Scientific Research* 51, 275-283, 1993
- SIMONIN, O., DEUTSCH, E. and BOIVIN, M., Comparison of large-eddy simulation and second-order moment closure of particle fluctuating motion in two-phase turbulent shear flows, *Turbulent Shear Flows* 9, ed. by F. Durst et al., Springer-Verlag, 1995
- SIMONIN, O., *Combustion and turbulence in two-phase flows*, VKI for Fluid Dynamics, Lecture Series, 1996
- SIMONIN, O., *Statistical and continuum modeling of turbulent reactive particulate flows. Part I: Theoretical derivation of dispersed phase modeling from probability density function kinetic equation*, VKI for Fluid Dynamics, Lecture Series, 2000
- SIMONIN, O. and SQUIRES, K.D., On two-way coupling in gas-solid turbulent flows, in *Proceedings of FEDSM03*, 2003
- SKURTYS, O. and AGUILERA, J.M., Applications of microfluidic devices in food engineering, *Food Biophysics*, 3, 1-15, 2008

- SQUIRES, K.D. and EATON, J.K., Particle response and turbulence modification in isotropic turbulence, *Phys. Fluids* 2, 1191-1203, 1990
- SQUIRES, K.D. and EATON, J.K., Measurements of particle dispersion from direct numerical simulations of isotropic turbulence, *J. Fluid Mech.*, 226, 1-35, 1991
- SQUIRES, K.D. and EATON, J.K., Preferential concentration of particles by turbulence, *Phys. Fluids A*, 3, 1169-1178, 1991
- SQUIRES, K.D. and EATON, J.K., Effect of Selective Modification of Turbulence on Two-Equation Models for Particle-Laden Turbulent Flows, *J. Fluids Eng.*, 116, 778-784, 1994
- SOO, S.L., Pneumatic transport. Chap. 29 in *Handbook of fluids in motion*, 1983
- STOKES, G.G., On the effect of the inertial friction of fluids on the motion of pendulums, *Trans. Cambridge Phil. Soc.* 9, 8-23, 1851
- SUNDARAM, S. and COLLINS, L.R., A numerical study of the modulation of isotropic turbulence by suspended particles, *Journal of Fluid Mechanics*, 379, 105-143, 2000
- TAYLOR, G.I., Diffusion by continuous movements, *Proc. London Math. Soc.*, 20, 196-211, 1921
- TCHEN, C.M., Mean value and correlation problems connected with the motion of small particles suspended in a turbulent fluid, PhD thesis, University of Delft, The Hague, 1947
- TENNEKES, H., Eulerian and Lagrangian time microscales in isotropic turbulence, *J. Fluid Mech.*, 67, 561-567, 1975
- TOUTANT, A., Modélisation physique des interactions entre interfaces et turbulence , These de Doctorat, INP Toulouse, 2006
- TOWNSEND, A.A., *The structure of turbulent shear flow*, Cambridge University Press, 1956
- UIJTTEWAAL, W. S. J. and OLIEMANS, R. V. A., Particle dispersion and deposition in direct numerical and large eddy simulations of vertical pipe flows. *Phys. Fluids* 8(10), 2590-2604, 1996
- YARIN, L.P. and HETSRONI, G., Turbulence intensity in dilute two-phase flows-3: the particles-turbulence interaction in dilute two-phase flow, *Int. J. Multiphase Flow*, 20, 27-44, 1994
- YEUNG, P.K. and POPE, S.B., Lagrangian statistics from direct numerical simulations of isotropic turbulence, *J. Fluid Mech.*, 207, 531, 1989

- YEUNG, P.K., POPE, S.B. and SAWFORD, B.L., Reynolds number dependence of Lagrangian statistics in large numerical simulations of isotropic turbulence, *Journal of Turbulence*, 7, p58, 2006
- YUAN, Z. and MICHAELIDES, E.E., Turbulence modulation in particulate flows - a theoretical approach, *Int. J. Multiphase Flows*, 18, 779-785, 1992
- YUDINE, M.I., Physical considerations on heavy-particle dispersion, *Adv. Geophys.*, 6, 185-191, 1959
- VERMOREL, O., BÉDAT, B., SIMONIN, O., POINSOT, T., Numerical study and modeling of turbulence modulation in a particle laden slab flow, *Journal of Turbulence*, Vol. 4, 2003
- VICHNEVETSKY, R. and BOWLES, J.B., Fourier analysis of numerical approximations of hyperbolic equations, *SIAM studies in applied mathematics*, Soc. Indust. Appl. Math., p140, 1982
- WANG, L.P. and MAXEY, M.R., Settling velocity and concentration distribution of heavy particles in homogeneous isotropic turbulence, *J. Fluid Mech.* 256, 27-68, 1993
- WANG, L.P. and SQUIRES, K.D., Large eddy simulation of particle-laden turbulent channel flow, *Phys. Fluids*, 8, 1207-1223, 1996
- WANG, L.P. and STOCK, D.E., Dispersion of heavy particles by turbulent motion, *J. Atmos. Sci.* 50(13), 1897-1913, 1993
- WANG, L.P., WEXLER, A.S. and ZHOU, Y., Statistical mechanical description and modeling of turbulent collision of inertial particles, *J. Fluid Mech.*, 415, 117-153, 2000
- WELLS, M.R. and STOCK, D.E., The effects of crossing trajectories on the dispersion of particles in a turbulent flow, *J. Fluid Mech.*, 136, 31-62, 1983
- ZHANG, J. and ROCO, M.C., A probabilistic method for field solutions in two-phase flows, *Numerical Methods in Fluids*, 16, 65-81, 1993